BIOPHYSICAL AND BIOCHEMICAL CONTROL OF THREE-DIMENSIONAL EMBRYONIC STEM CELL DIFFERENTIATION AND MORPHOGENESIS

A Dissertation
Presented to
The Academic Faculty

by

Melissa A. Kinney

In Partial Fulfillment
of the Requirements for the Degree
Doctor of Philosophy in Biomedical Engineering in the
Wallace H. Coulter Department of Biomedical Engineering

Georgia Institute of Technology
May 2014

BIOPHYSICAL AND BIOCHEMICAL CONTROL OF THREE-DIMENSIONAL EMBRYONIC STEM CELL DIFFERENTIATION AND MORPHOGENESIS

Approved by:

Dr. Todd C. McDevitt, Advisor
Department of Biomedical Engineering
Georgia Institute of Technology

Dr. J. Brandon Dixon
School of Mechanical Engineering
Georgia Institute of Technology

Dr. Ari Glezer
School of Mechanical Engineering
Georgia Institute of Technology

Dr. Roger D. Kamm
Department of Mechanical Engineering
Massachusetts Institute of Technology

Dr. Manu O. Platt
Department of Biomedical Engineering
Georgia Institute of Technology

Date Approved: 7 March 2014

To my family - Robin, Scott and Adam - for their guidance and examples of tenacity, dedication, and ambition

To Phil, for his unwavering support, encouragement, and confidence

ACKNOWLEDGEMENTS

It is with much thanks to many who have supported me and contributed to various aspects of my project over the past 6 years that I can present the work detailed within this dissertation. To my mentors, labmates, friends, and family - I can not thank you enough.

First, and foremost, I would like to thank my advisor, Todd McDevitt. Todd has been a wonderful teacher and mentor and has provided an incredible amount of support on this project. I have been through a huge number of milestones with Todd - all the way from pre-tenure, assistant professor, to full professor and incredibly accomplished leader in stem cell engineering. It has been an amazing opportunity to work on early grants in the lab while also seeing incredible growth and success and I am so proud to have been part of this group. Despite all of the changes and the demands of the lab over the years, Todd has always been incredibly supportive. I am constantly impressed by Todd's conviction, passion for research, and willingness to unwaveringly stand up for his students, whenever necessary. I have learned so much about research design and interpretation from working with Todd; over many years of meeting with Todd, he has taught me that "negative" (or more appropriately described as "unexpected") data are opportunities to probe further and learn more about the system. Working closely with Todd on grants, fellowships, manuscripts, and presentations has taught me to envision and articulate the big picture in the context of our lab, the field, and future directions. I seem to have taken on many (or all?) of Todd's high standards (quirks), particularly in terms of presentation aesthetics and writing; however, I am always impressed by the presentations by Todd and our group and I know that we are all incredibly fortunate to have learned from

Todd.

My thesis committee - Roger Kamm, Brandon Dixon, Manu Platt, and Ari Glezer - has also provided valuable feedback and poignant questions which have been crucial in shaping the directions of this project and broadening my perspective outside of stem cell engineering. The expertise that Roger and Brandon have provided, each with extensive backgrounds in tangential fields applying fluidics to study and perturb biological phenomena, helped me to think about alternative design constraints and analyses in working to develop the perfusion bioreactor platform. Many of the questions, derived from their own practical personal experiences and expertise, enabled me to consider aspects of the system that may have been easily overlooked, due to many of the properties of our biological system being relatively undefined. Moreover, led by Manu, the group as a whole pushed me to develop more specific biological hypotheses and develop more sophisticated questions about my biological system in a larger scope, beyond the technical aspects of the technology development. Ari and his group have been a significant part of the project, well before his role as a formal committee member. Beginning with a grant written in 2009 - 6 months after starting graduate school - our groups have actively collaborated, thanks to the fluidic expertise of the Glezer lab, to develop the technologies described in this dissertation. I have worked closely with Ari and several members of his lab, including Jelena Vukasinovic, Boris Zakharin, and Pablo Hidalgo, to brainstorm, design, and test various iterations, leading up to the prototype described here.

I am incredibly lucky to have worked, through the course of my PhD, with the best group of colleagues, including fellow graduate students, postdocs, undergrads, and research staff, who have made the lab a great place to be everyday. I had no idea when I started in the lab, but the point at which I joined the lab gave me the really unique opportunity to be the transition between two distinct phases of the McDevitt lab. I will be forever grateful to Carolyn Sargent, one of the founding McDevitt lab

members, who took me in and taught me everything about cell culture, stem cells, and research in general. Working closely with her during my first couple of years of grad school not only taught me technical skills, but also gave me insight into the analytical skills and advanced thought processes developed through years of training. The entire original group of McDevitt lab members pushed me to hold myself to a higher standard, even as a very early graduate student. Along with Carolyn, the other senior lab members, Rich Carpenedo and Rekha Nair, established the overall lab culture, including the open and honest communication that enables us to ask one another the really difficult questions and push each other to consider new ideas and approaches. I also worked closely with each of the other members of the original McDevitt lab group - Alyssa Ngangan, Andrés Bratt-leal, Barbara Nsiah, and Ken Sutha - each of whom brought their own unique character to the lab environment. In addition to each of their technical skills and rigor, I will always admire Alyssa's enthusiasm, Andrés' sense of humor, Barbara's ability to stay true to herself, and Ken's contagious happiness. While many of the current lab members have never met some (or any) of these people, I can say undoubtedly that the lab is the way it is today - including all of our standards, culture, and successes - because of the foundation that they all established for us. I had so many good times with the original lab group - in and out of lab - I would like to wholeheartedly thank each of them for everything that they contributed to me, my research, and to the lab.

In addition to all of those who have been incredible role models and mentors to me, I have also been fortunate to work every day for the past several years with a (continually growing) unbelievably talented group of people. I am so thankful for those who I am around and working with every day, especially those I sit nearby - Jenna Wilson, Anh Nguyen, Josh Zimmerman, and Denise Sullivan - with whom I have spent an extraordinary amount of time brainstorming ideas, troubleshooting, designing experiments, and generally procrastinating. I will always be glad that Todd

paired Jenna and I together when she first started in the lab - not because anything we did that summer worked out, but because we have become so close as a result of working together. Jenna has already achieved so much and has been an amazing leader and role model for the lab. I am so thankful to call her my friend, and I am excited to see what the future holds for her. I am also thankful to have had the opportunity to work with Doug White (co-advised with Melissa Kemp), as he is really making some groundbreaking and exciting paradigm shifts within the field, which have changed the way that I think about experimental design and contributed to my perspective on future directions of stem cell engineering. In addition, all of the co-advised students - Doug, Marian Hettiaratchi, Melissa Goude, Emily Jackson, Liane Tellier, and Chad Glen - have brought new dynamics into the lab, by bridging personal and professional collaborations between different labs nearby. Josh and Denise are two of my favorite people, and their interactions are always great for comic relief; however, I feel strongly that their relationship embodies all of the dynamics that make the McDevitt lab unique and successful. While I have not worked as closely with Marian, her happiness (or Canadian-ness) is truly contagious and is always great for general lab morale. Alex and Olivia continue the trend of incredibly talented, loyal, positive leaders and each bring their own unique character to the group (and extend the Josh-Denise dynamic). While Katy is now a first year graduate student, she started in the lab just a few months after I did, as an undergraduate student working with Andrés. It has been really exciting to see her progress through the years in the lab and after coming back from her Whitaker fellowship. I know that she will be a source of continuity for the lab, a natural leader, and a talented researcher, as the McDevitt lab brings in new generations of trainees. While I have spent much less time with the other new students - Jessie Butts, Liane, and Chad - I am constantly amazed by the caliber of new graduate students, in terms of experience, excitement, and ideas, and I know that this group will continue to elevate the McDevitt lab in

new, exciting directions.

Along with the graduate students, I am incredibly thankful to have worked with all of the postdocs who have come and gone in the McDevitt lab through the years - Priya Baraniak, Ankur Singh, Krista Fridley, Yun Wang, Tobias Miller, Tracy Hookway, Lindsay Fitzpatrick and Sarah Griffiths. I really love having postdocs as a part of the group, not only because they are extremely intelligent scientists and extend the scope of research in our lab, but also because each postdoc has brought their own unique backgrounds and perspectives, which pushes us all to question our processes and understandings. In particular, Priya was brave enough to join the group as the first, and only, postdoc and I really appreciate everything that she did for me and for the lab - scientifically and personally. Priya taught me to think critically, view my work from the perspective of reviewers, and anticipate questions, which are all invaluable skills that have allowed me to more fully think through the scope of my research story. She has also been an amazing mentor and I am glad to still call her a friend even years after she has moved on. Similarly, Tracy has pushed the bounds of our research projects to explore new avenues and integrate new expertise into our lab. She has taken the lead on countless projects and I am constantly impressed by her willingness to take on more. I have learned so much from working directly with Tracy and I can't wait to see what she does in the lab and in the future.

Most of the work presented herein would not be possible without the tireless work of talented undergraduate researchers. I have worked with two undergraduate students through my PhD - Rabbia Saeed and Lu Ling. The reason that I have worked with so few undergrads is because Rabbia was so talented and committed that she stayed with me for 3 years and through several different projects. Working with Rabbia was always fun because, not only was she technically skilled in the lab, but she always had such a positive attitude and contagious happiness, regardless of what she was doing (and how monotonous the task was). I would like to sincerely

thank her, not only for her direct work on these projects, but also for making the lab a fun and interesting place to work and for her friendship through the years.

In addition to my labmates, many colleagues in our lab, IBB and BME have provided immeasurable support on various aspects of this project. The research staff who have worked in the McDevitt lab over the years - Marissa Cooke, Jesse McClellan, Alex Ortiz, Megan Richards, Elizabeth Peijnenburg and Christian Mandrycky - have worked tirelessly to keep our lab running (no small job) and made our day-to-day lives much easier. Much of what they all do is lost in the background and thankless, but I want to thank each of them. I really appreciate all of their hard work. Similarly, the research staff in IBB cores - Aqua Asberry, Andrew Shaw, Steve Woodard, and Nadia Boguslavsky - enable us to have the high quality resources available and operational at all times, which makes Georgia Tech a great place to do research. The additional support staff within BME/IBB - Sally Gerrish, Shannon Sullivan, Steven Marzec, Jesus Mata-Acosta, Dewayne Roberson, Sandra Wilson, Meg McDevitt, and Colly Mitchell - have been essential for keeping our computers working, classes registered for, and countless other administrative responsibilities that we would be lost on without their help. In particular, I would really like to thank Meg for everything that she has done - for the lab, for me, and for my project. Meg not only supports Todd and his work (again, behind the scenes), but she has also done an immeasurable amount of work for the lab - everything from coordinating events to marketing and publicity (and feeding us!). Meg independently pushed me to pursue outside awards and recognition, such as the Suddath Award, and has always been such a huge supporter. I know that everything that I have accomplished, particularly in the past year, is not only thanks to Todd, but thanks, in large part, to everything Meg has done to support me, and I will never forget that.

I have also been very fortunate to have been given many exciting opportunities - many atypical for a graduate student - during the course of my PhD, which is thanks

to many of those who have supported me beyond the scope of my specific research project. In particular, Dr. Nerem has become an informal mentor to me over several years, and has supported me in countless ways, from writing letters to broadening my network. Dr. Nerem's advocacy of my talents and potential even led to my participation in a workshop at the National Academies of Sciences, which was an amazing opportunity professionally and a personal aspiration. Similarly, Bill Murphy (U. Wisconsin) has been a vocal proponent of my work and an extremely valuable collaborator who pushed me to explore new opportunities, such as the NextProf Workshop at Michigan. Both Bill and Dr. Nerem were amazingly supportive as I authored my first independent grant through the NIH and have been nothing but encouraging as I pursue new aspects of my future career. I am excited to continue to work with them in new collaborative capacities as I venture in new research directions. In addition, those who have supported my research by providing constructive feedback on manuscripts - Melissa Kemp, Andres Garcia, Todd Streelman, and Doug Lauffenburger (MIT) - have also helped to broaden my perspective and consider new avenues of research, which has been invaluable throughout this project. Linda Griffith (MIT) has also been a vocal proponent of my work through EBICS, and I look forward to continuing to work with her and Doug in the future as they both have very insightful perspectives on analytical research and biomedical engineering. I am thankful to have worked with everyone from MIT, UIUC and satellite schools through collaborative research ventures and I will be excited to see the new directions of EBICS as the field continues to shift perspectives.

In addition to those that I have worked with over the past 6 years of graduate school, I would be remiss to not mention those supporters who have been instrumental in my career path to this point. In particular, Lucy Treiman and Rick Ferguson at Barrow Neurological Institute (Phoenix, AZ) took me into their lab as a high school student in 2003. Despite my inexperience, they were both patient and enthusiastic

teachers and incited my passion for research. With Lucy and Rick as mentors, I made the decision that I would study biomedical engineering, obtain a PhD, and some day run my own lab. While I am not quite there yet, my passion for research is as strong as ever and I believe wholeheartedly that it would not be possible without the amazing mentorship that I was fortunate to gain so early in my career. All of this work is also thanks to many others who have supported me as mentors through the years - Charles DeLisi (BU), Tim Gardner (BU), Ken Lutchen (BU), Rafael Cordero (Aspect Medical), and Bob Harhen (Aspect Medical). While I have worked across a number of different (seemingly disparate) disciplines through the years, I believe that the knowledge and skills, both technical and practical, have made me a better investigator and will be invaluable in my future.

Finally, to my family - my parents, Robin and Scott, and my brother, Adam - who have been my light through this process, thank you for your constant guidance and encouragement. Looking back, it now seems obvious that I would someday become an engineer; however, even early on, my parents recognized and nurtured my skills and interests. They helped me to find opportunities and pursue my interests outside of the classroom, which inevitably led me to my love for research and pursuit of the career path that I am lucky to be on today. I have always admired my parents' strength, conviction and unwavering support of family. Adam has, through the years, become my best friend. Despite being younger, I have learned so much from him. I think being almost complete opposites has its advantages (including improving my writing skills!), as we make each other better. I am constantly impressed by Adam's professional successes and personal strengths and I am proud to call him my brother. Through the rough times, my family has helped me to maintain my perspective on the important things in life and has rejoiced with me in all of the successes. Thank you for all of your love and strength. In addition, I would like to thank my extended family - my grandparents, aunts, uncles, and cousins - who have each shaped my life in

their own unique way. I would also like to thank my extended Keegan family - Mike, Debbie, Brian, Ricarose - who have taken me in as one of their own and supported me in countless ways through this process. Everything I am and everything I have achieved is thanks to the values, ambition, and dedication that I have gained from my immediate and extended families.

Perhaps most importantly, this dissertation would not be possible without the love, support, and encouragement, Philip Keegan. Phil has been my rock through this process. Words cannot express how grateful I am to him for everything he has done (and put up with) in the past 6 years, through all of the challenges and successes, and in particular during the last several months as I have put together this dissertation. Phil has been by my side every single day (even via Skype from Africa) and I am beyond thankful to have him in my life. He is always willing to talk science, brainstorm, and teach me new things (see the Western blots in Appendix A!), with incredible patience and enthusiasm. I am constantly astounded by his love for teaching and eagerness for learning - he makes everyone around him a better person and I aspire to maintain and instill such a love of science in my future. Phil has taught me so much about science, life and love and I am excited to continue to grow and learn together.

TABLE OF CONTENTS

LIST OF TABLES

LIST OF FIGURES

LIST OF SYMBOLS OR ABBREVIATIONS

aβC	active (dephosphorylated) β-catenin.
α-MHC	α-myosin heavy chain.
APC	adenomatous polyposis coli.
AVE	anterior visceral endoderm.
B-T	brachyury-T.
BMP4	bone morphogenetic protein 4.
CFD	computational fluid dynamics.
EB	embryoid body.
ECM	extracellular matrix.
EMT	epithelial-mesenchymal transition.
ESC	embryonic stem cell.
GSK3β	glycogen synthase kinase 3 beta.
LIF	leukemia inhibitory factor.
LRP5/6	low-density lipoprotein receptor-related protein 5/6.
Mef-2c	myocyte enhancer factor-2c.
mESC	murine embryonic stem cell.
Mesp-1	mesoderm posterior-1.
MLC-2v	myosin light chain-2 ventricle.
MOI	multiplicity of infection.
MSC	mesenchymal stem cell.
PS	primitive streak.
ROCK	rho associated protein kinase.
VEGF	vascular endothelial growth factor.

SUMMARY

Stem cell differentiation is regulated by the complex interplay of multiple parameters, including adhesive intercellular interactions, cytoskeletal and extracellular matrix remodeling, and gradients of agonists and antagonists that individually and collectively vary as a function of spatial locale and temporal stages of development. Directed differentiation approaches have traditionally focused on the delivery of soluble morphogens and/or the manipulation of culture substrates in two-dimensional, monolayer cultures, with the objective of achieving large yields of homogeneously differentiated cells. However, a more complete understanding of stem cell niche complexity motivates tissue engineering approaches to inform the development of physiologically relevant, biomimetic models of stem cell differentiation. The capacity of pluripotent stem cells to simultaneously differentiate toward multiple tissue-specific cell lineages has prompted the development of new strategies to guide complex morphogenesis of functional tissue structures [164]. The *overall objective* of this project was to understand embryonic stem cell (ESC) interactions within the three dimensional microenvironment, in order to control spatial and temporal aspects of pluripotent cell fate and morphogenesis and ultimately enable the derivation of complex, functional microtissues amenable to the replacement or regeneration of damaged tissue.

The sensitivity of stem cells to environmental perturbations has prompted the study of the quantitative influences of three-dimensional embryonic stem cell, or "embryoid body" (EB), culture conditions on differentiation. Hydrodynamic suspension cultures, routinely employed for cell expansion and scalable bioprocessing

applications, impart complex fluid shear and transport profiles, and influence cell fate as a result of changes in the mixing conditions [111]. We have previously determined that hydrodynamic environments alter the endogenous ESC differentiation efficiency toward various lineages [282] and that simple hydrodynamic perturbation of spheroid formation alters the dynamics of cadherin assembly and reorganization, which impacts ESC cardiogenic differentiation via the β-catenin signaling pathway (Appendix A; [167]). The impact of hydrodynamics on stem cells, therefore, manifests via alterations in several key cellular processes, including aggregation (kinetics, size), metabolism (viability, transport, proliferation), and phenotype (differentiation, function), which are inter-related within the context of stem cell biology [166]. The aim, therefore, was to control the EB microenvironment in order to systematically decouple various parameters (EB size, formation, and differentiation) that are modulated in the context of complex hydrodynamic environments. Using micro-well technologies, EB size and formation kinetics can be reproducibly controlled and distinct populations of pre-formed EBs can be maintained in rotary orbital suspension cultures as a means to regulate and standardize EB size in scalable hydrodynamic cultures (Chapter 3; [165]). Controlling EB formation and resultant size is significant for bioprocessing applications to standardize EB morphogenesis; however, modulation of the fluid mixing environment also indicated that there are several subtle, yet significant changes induced by hydrodynamic parameters. The response of stem cells to hydrodynamic perturbations highlights important tissue engineering principles that should be considered for implementation in bioreactor design.

The more uniform and reproducible EB differentiation afforded through the combination of microwell and rotary orbital technologies provides a controlled platform amenable to better understanding three-dimensional stem cell morphogenesis. The secondary objective of this project was to characterize the physical changes (mechanical, transport) that accompany morphogenesis of the 3D EB microenvironment, in

order to inform engineering approaches for computational modeling [349] and controlling stem cell fate. The stiffness and viscoelastic properties of EBs were modulated during ESC differentiation, and in response to mesenchymal morphogenesis (Chapter 4). Additionally, mesenchymal stem cell spheroids exhibited increased stiffness in response to incorporation of microparticles composed of matrix-derived materials [15]. The stiffness of EBs was mediated largely by the actin cytoskeleton, as well as cell-cell and cell-matrix adhesions, all of which are dynamically modulated during tissue morphogenesis. Understanding the physical changes accompanying epithelial-to-mesenchymal transition of ESCs has broad implications which may be analogous to similar remodeling events during embryonic development, tissue morphogenesis and cancer metastasis. In parallel with mechanical changes, EB remodeling also limits the transport of soluble factors, including nutrients, waste and morphogens (Chapter 5). Together, the dynamic remodeling that occurs during 3D ESC differentiation motivates the development of engineering approaches for controlling spatiotemporal administration of physical and chemical cues. To more precisely control the EB microenvironment, a bioreactor platform was engineered in conjunction with a computational fluid dynamic (CFD) model, in order to inform the development of approaches to impart a pressure gradient across immobilized spheroids and drive convective transport throughout the interior of EBs (Chapter 6). The increased understanding of convection within EBs developed through this project is expected to inform novel approaches to more precisely control of parameters affecting ESC differentiation, such as temporal kinetics and spatial localization of morphogen delivery.

Understanding biochemical and physical tissue morphogenesis, including the relationships between remodeling of cytoskeletal elements and intercellular adhesions, associated developmentally relevant signaling pathways, and the physical properties of the EB structure together elucidate fundamental cellular interactions governing embryonic morphogenesis and cell specification. Ultimately, this project has established

a foundation for controlling, characterizing, and systematically perturbing aspects of stem cell microenvironments in order to guide the development of complex, functional tissue structures for regenerative therapies.

CHAPTER I

INTRODUCTION

Embryonic stem cells (ESCs) possess the unique capacity to differentiate into clinically relevant somatic cell types, making them a promising cell source for regenerative therapies. Moreover, the capacity of ESCs to simultaneously differentiate toward multiple tissue-specific cell lineages has prompted the development of strategies aimed to guide complex morphogenesis of functional tissue structures. Traditionally, directed differentiation methods have relied on the addition of morphogens to monolayer cultures of ESCs, which permits homogeneous delivery; however, this culture format is not easily amenable to the scalable production of differentiated cell yields necessary for therapeutic applications. In addition, culture of stem cells as three-dimensional aggregates is thought to more accurately recapitulate cellular adhesions and signaling exhibited by stem cells found in native tissues. Specifically, the differentiation of ESCs as multicellular aggregates enables the three-dimensional assembly and remodeling of intercellular adhesions, including cadherins, which are important for directing morphogenesis and spatial patterning. Therefore, opportunities remain to develop a more complete understanding of the interplay between biophysical and biochemical cues during such morphogenic processes, as well as the spatial and temporal dynamics of three-dimensional morphogenesis, particularly in the context of self-organization and tissue patterning in ESC spheroids. Moreover, approaches to achieve controlled spatial patterning of morphogenesis within microtissues remain largely unexplored. Engineering approaches aimed to characterize and control biophysical cues within the local stem cell microenvironment may ultimately enable the development of novel, functional microtissues for tissue regeneration and repair.

The long-term goal motivating this project was to develop methods for controlling spatial and temporal aspects the pluripotent microenvironment, to engineer three-dimensional ESC-derived microtissues. The objective of this project was to characterize the spatiotemporal dynamics of stem cell biophysical characteristics and morphogenesis, in order to engineer ESC culture technologies with defined and tunable biochemical temporal delivery within the three-dimensional spheroid microenvironment. The hypothesis was that the biophysical and biochemical cues present within the 3D microenvironment are altered in conjunction with morphogenesis as a function of stem cell differentiation stage. This hypothesis was based on principles of cell specification during embryonic development, whereby the presentation and organization of cell-cell adhesions, intra- and extracellular structural elements, and signaling factors, are precisely controlled spatially and temporally, in order to guide complex tissue patterning. The rationale for this work was that employing engineering principles to alter the biochemical context within three-dimensional multicellular assemblies would enable enhanced morphogen delivery to control the spatiotemporal dynamics of stem cell differentiation. The central hypothesis of the proposal was examined through the following specific aims:

Specific Aim 1. Control the uniformity of morphogenesis and differentiation in mixed suspension cultures. The *working hypothesis* was that upstream processing by formation of EBs in microwells would standardize EB size across culture conditions, in order to enable a more systematic understanding microenvironmental influences on ESCs. Hydrodynamic environments were imparted by maintaining EBs in rotary orbital suspension cultures across a range of mixing conditions and the effects were assessed via analysis of morphological changes within EBs, as well as through gene and protein expression based on markers of pluripotent and differentiated (endoderm, ectoderm, mesoderm) cell populations.

Specific Aim 2. Define the biophysical characteristics and phenotypic changes that arise simultaneously during 3D stem cell morphogenesis. The *working hypothesis* was that stem cell spheroids undergo changes to the biophysical microenvironment during three-dimensional cell fate determination and morphogenesis. The dynamic physical changes accompanying differentiation of ESCs were characterized in the context of an epithelial-to-mesenchymal (EMT) morphogenesis, characteristic of 3D mesoderm specification induced by bone morphogenetic protein 4 (BMP4). In addition, the role of the cytoskeleton was studied in the context of the mechanical properties of stem cell spheroids, and perturbation of the cytoskeleton enabled the analysis of the interrelated changes in biophysical and phenotypic characteristics during differentiation.

Specific Aim 3. Investigate and control the transport characteristics of stem cell spheroids. The *working hypothesis* was that EBs exhibit spatial limitations within diffusive transport platforms and that imparting convective transport within the culture would enable more efficient spatial and temporal delivery of soluble factors for directing differentiation of ESCs. A micro-bioreactor platform was developed is capable of immobilizing individual spheroids and imparting a pressure gradient to drive convective transport throughout the interior of EBs. The diffusive and convective environments were characterized by tracking of fluorescently labeled dyes and growth factor signaling, in order to understand the transport limitations that arise within EBs as a function of differentiation.

This project is *innovative* because it established a platform to systematically study the EB microenvironment, to inform approaches for engineering biophysical and biochemical cues in stem cell spheroids. The biological design principles established

within the context of stem cell spheroids are amenable to understanding and controlling morphogenesis and organoid development via physical and biochemical perturbations within the three-dimensional structure. The outcomes of this work yield insights regarding the biophysical properties and limitations in 3D tissues, which creates new opportunities for the scalable culture of multicellular assemblies and large tissue constructs for applications in tissue engineering and regenerative medicine.

CHAPTER II

BACKGROUND[1,2,3,4]

2.1 Cardiovascular tissue engineering

Differentiation of embryonic stem cells (ESCs) toward cardiac phenotypes is an attractive application within tissue engineering and regenerative medicine, due to the high mortality and morbidity rates related to cardiovascular disease worldwide [200]. Following cardiac infarction, few endogenous mechanisms exist to regenerate the damaged myocardium [6], which leads to the formation of a fibrous scar and impairment of conduction velocity, blood pressure, and cardiac output. Therefore, therapies aimed at delivering multi- and pluripotent stem cell populations have garnered attention in tissue engineering, due to the potential of exogenous cells to integrate into host tissue. Several types of multipotent stem cells, including skeletal myoblasts [320, 229], and mesenchymal progenitor cells [309, 326], have been successfully transplanted post-infarction, with many of the studies demonstrating enhancement in myocardial function. Additionally, clinical trials have recently demonstrated the feasibility, safety

---

[1]Modified from: Kinney MA and McDevitt TC. Pluripotent stem cells. The Biomedical Engineering Handbook, 4th Edition (eds. J. Fisher, A. Mikos, Tissue Engineering Section), CRC Press.

[2]Modified from: Kinney MA, Sargent CY, McDevitt TC. (2011). The multi-parametric effects of hydrodynamic environments on stem cell culture. Tissue Engineering Part B: Reviews. 17(4):249-62. doi:10.1089/ten.TEB.2011.0040

[3]Modified from: Kinney MA, McDevitt TC. (2013). Emerging strategies for spatiotemporal control of stem cell fate and morphogenesis. Trends in Biotechnology. 31(2):78-84. doi:10.1016/j.tibtech.2012.11.001

[4]Modified from: Kinney MA, Hookway TA, Wang Y, McDevitt TC. (2013). Engineering three-dimensional stem cell morphogenesis for the development of tissue Models and scalable regenerative therapeutics. Annals of Biomedical Engineering. doi:10.1007/s10439-013-0953-9

and efficacy of transplanting bone marrow-derived progenitor cells for microvascular repair in humans post-infarction [12, 94, 186]. Embryonic stem cells are a promising source for transplantation in cardiovascular defects, due to relative ease of expansion compared to multipotent progenitor cell types, as well as the promise of pluripotent cells for deriving many cell types necessary to regenerate the entire myocardium. ESC-derived cardiomyocytes retain the capacity to proliferate after injection, undergo angiogenesis, and electrically couple with the endogenous myocardium [155, 180]. In an infarct model, injection of ESC-derived cardiomyocytes resulted in increased injection fraction and wall thickness, more closely resembling the functional and geometric properties of the non-infarcted conditions [179]. However, the applicability of ESCs in regenerative medicine applications is currently limited by the inability to efficiently direct the differentiation of large yields of cells toward a desired lineage.

2.2 Embryonic stem cells

ESCs possess the unique capacity to proliferate indefinitely in culture and differentiate into all somatic cells, thereby serving as a promising cell source for tissue engineering applications, including the treatment of degenerative diseases, traumatic injuries and chronic wounds. ESCs, derived from the inner cell mass of blastocysts, were first isolated from mouse embryos [96, 209, 88], followed by the establishment of ESC lines from primate [324, 325] and eventually human [323, 273] sources. ESCs are characterized by unlimited self-renewal and pluripotent differentiation potential into all three germ layers mesoderm, endoderm, and ectoderm as well as into germ cells. One of the unique traits of ESCs is the capacity to generate any cell type, including cells which can not be easily isolated from primary sources, such as pancreatic β-cells [299, 28, 55], neurons [310, 284, 236], and cardiomyocytes [356, 204, 34, 99]. ESCs, therefore, are a promising cell source for tissue engineering, either for the direct

replacement of cells in degenerative diseases such as Parkinsons or heart disease, or through the use of paracrine actions of trophic factors secreted by stem cells to direct regeneration of endogenous tissue [16]. Additionally, stem cells serve as a flexible platform for drug screening, in which pharmaceutical companies can employ large quantities of differentiated cells for *in vitro* testing of cytotoxicity and for the creation of pathological tissue models [216]. Large-scale culture technologies are likely necessary for the bioprocessing of stem cells to produce the large cell yields required for such clinical and screening applications.

2.3 ESC differentiation

2.3.1 Approaches for directing differentiation

Differentiation approaches often rely upon understanding the changes during embryogenesis in order to define environmental parameters for the differentiation of ESCs. Many protocols rely on soluble delivery of factors in monolayer and exploit pathways known to be important in the context of early development. In the absence of anti-differentiation factors such as leukemia inhibitory factor LIF, murine ESCs (mESCs) spontaneously differentiate. Early specification of ESCs proceeds similarly to gastrulation, with the commitment of either neuroectoderm or a primitive streak-like population. Neuroectoderm specification is often referred to as the default pathway, because ESCs differentiate into neural precursors with high fidelity without the supplementation of serum of other exogenous growth factors [364]. Cells have been induced to enter the primitive streak lineage by bone morphogenetic protein-4 BMP4, which requires active signaling of the FGF and TGFβ/Nodal/Activin pathways [351, 245, 372]. Addition of primitive streak (PS)-inducing morphogens results in inhibition of neuroectoderm differentiation, which is consistent with the active signaling pathways during gastrulation [13, 173]. PS induction was initially accomplished

by the addition of serum; however, the components of serum are highly variable between lots and the identification of factors that actively promote differentiation has led to the creation of serum-free defined media. The levels of various factors are also important, as exemplified by the differential induction of mesoderm or endoderm, depending on the concentration of exogenous Activin A [173].

Delivery of exogenous small molecules and growth factors is most often accomplished via monolayer culture of ESCs in the absence of anti-differentiation factors. Culture of ESCs in monolayer format affords uniform application of external stimuli, including biochemical factors and mechanical forces, resulting in increased efficiency of directed differentiation compared to other formats [376]. Monolayer culture of ESCs also permits co-culture with stromal cells, as a method of directing differentiation via paracrine signaling [234]. For example, ESCs have been induced to differentiate into hematopoietic precursors by co-culture with OP9 bone marrow derived stromal cells [234, 61, 290], thereby elucidating possible mechanisms of hematopoietic differentiation *in vivo*. Co-culture methods do not require supplementation with exogenous growth factors; however, the signaling from stromal cells is often complex and poorly defined. Additionally, in monolayer, ESCs undergo uniform fluid flow, which has been employed as a method to alter the autocrine and paracrine signaling of ESCs [33] and may be amenable for improved homogeneity of directed differentiation.

2.3.2 ESC differentiation formats

Stem cells respond to a variety of environmental cues *in vitro* to either maintain potency or regulate differentiation; these cues include biochemical factors (both exogenous and endogenous), cell-cell interactions, cell-matrix interactions, and mechanical stimuli. Monolayer culture of stem cells provides a defined substrate for cellular attachment and uniform application of external stimuli (Fig. 2-1). However, from a

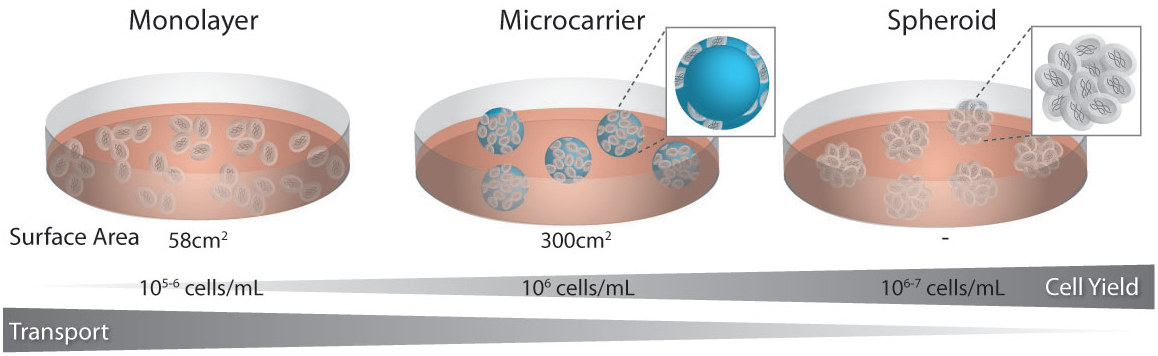

Figure 2-1: Stem cell differentiation formats. Stem cells can be cultured in monolayer or in suspension, either adherent to spherical microcarriers or as aggregates of cells. Suspension cultures generally increase the density of cells, and thus increase the overall cell yield per volume or media. Although suspension cultures are more scalable, the three-dimensional aggregate structure increases the diffusive distance between the media and cells at the center, which may result in decreased transport and the development of gradients of nutrients and metabolites throughout the spheroid.

bioprocessing standpoint, monolayer culture is not readily amenable to the production of increased cellular yields necessary for regenerative therapies (upwards of 10^9 cells, depending on the application) [333, 199, 149]. Alternatively, colonies can be enzymatically dissociated to obtain a single cell suspension, whereby ESCs spontaneously aggregate to form spheroids of pluripotent cells, known as embryoid bodies (EBs) [183, 80]. Culture of stem cells as three-dimensional aggregates is scalable, and thought to more accurately recapitulate cellular adhesions and signaling exhibited by stem cells found in native tissues [7, 56], including morphological changes similar to gastrulation during embryogenesis [228].

2.3.3 Mesoderm differentiation

Due to the promise of ESCs for repair and regeneration in myocardial infarction, cardiovascular specification of ESCs is a widely studied differentiation scheme. The initiation and progression embryonic cardiovascular development, including the signaling patterns necessary for cell specification, have been detailed in literature [308]. Expression patterns of agonists and inhibitors, which lead to primitive streak formation and

cell specification during embryogenesis, highlight several key genetic pathways which are likely responsible for the temporal and spatial regulation of various differentiation events in ESCs. The PS is associated with expression of transforming growth factor β (TGFβ) factors (Lefty 1, Nodal) and Wnt, whereas the anterior visceral endoderm (AVE) secretes Nodal and Wnt repressors (DKK1, Sfrp1 and Sfrp5) [100, 160, 275]. Cells traverse the PS to form the mesoderm and definitive endoderm lineages in a spatially and temporally controlled manner within the embryo [184].

When differentiated as EBs in the presence of serum, mESCs differentiate into cardiomyocytes, resulting in $\sim$8% of EBs exhibiting spontaneous contractility [154]. Cardiomyogenic differentiation of ESCs also results in functional cells that exhibit action potentials consistent with different regions of the heart and are capable of reacting to pharmacological treatments [204]. Additionally, the culture format alters the efficiency of spontaneous cardiomyocyte differentiation, with rotary orbital cultures resulting in $\sim$50% of EBs with contractile activity [283]. However, due to the heterogeneity of differentiation within EBs, the overall efficiency of differentiation in rotary orbital suspension is still less than 15% of the total cell yield. Several groups have successfully increased the efficiency of cardiomyocyte differentiation by co-culture with endothelial cells [224] or using soluble treatments, such as retinoic acid [355]. Two widely adopted protocols for cardiac differentiation of ESCs involve the temporal treatment with a series of morphogens, including activin A, BMP4, bFGF, DKK1, and VEGF, and result in approximately 30% efficiency of cardiomyocyte differentiation [179, 362], with purities of $> 80\%$ after density gradient centrifugation [179]. However, most current approaches for directing ESC differentiation rely on monolayer culture, which is not easily amenable to the production of clinically relevant cell yields, warranting the development of scalable directed differentiation approaches.

2.4 Microtissue formation and differentiation

2.4.1 Embryoid body differentiation

Spontaneous aggregation of ESCs is mediated by E-cadherin, a Ca^{2+} dependent homophilic adhesion molecule, which is also expressed in the morula and blastocyst stages of embryogenesis [183]. As aggregates of ESCs begin to differentiate, the first specification leads to a layer of primitive endoderm cells at the exterior of the EB. The formation of primitive endoderm is mediated largely by fibroblast growth factor (FGF) signaling and the downstream PI 3-kinase pathway [59, 95]. The primitive endoderm then differentiates to form the visceral and parietal endoderm, which deposit a basement membrane-like layer of ECM comprised largely of laminin and collagen IV [342, 193]. It is thought that cell survival within the EB is dependent upon contact with the basement membrane layer, and death of interior cells often results in the formation of cystic cavities within EBs [70, 305, 227]. After specification of the exterior endoderm cells, differentiation of the remaining cells within the EB proceeds to form the three germ lineages. The genetic regulation during differentiation demonstrates a temporal sequence of events similar to the processes of embryonic gastrulation and specification [146, 91].

PSCs exhibit striking examples of morphogenesis upon three-dimensional assembly and differentiation [286], thereby providing an intriguing model system amenable to studying and perturbing physiochemical elements mediating cell fate. For example, induction of Rx+ neuroepithelium in 3D PSC spheroids via supplementation with exogenous morphogens (Nodal) and matrix proteins (Matrigel) resulted in spatially distinct patterns of differentiation, with the resulting neo-tissues exhibiting phenotypic markers and architecture reminiscent of the native optic cup [92, 235]. Interestingly, the dynamic structural changes, including evagination of epithelial vesicles and subsequent invagination, yielded distinct layers of neural retinal and retinal pigment epithelial (RPE) cells that were directed solely by cell-intrinsic morphogenic processes

and self-organization of cells in 3D [92]. Similarly, simple biochemical induction of differentiation directed the morphogenesis of 3D microtissues comprised of organized enterocytes, goblet, Paneth and enteroendocrine cells, thereby establishing an *in vitro* organoid model of intestinal structure and function [307]. Another model exhibiting self-formation of complex cerebral structures [182] was developed to study the pathogenesis of human microcephaly using iPS cells. Moreover, similar approaches have yielded functional anterior pituitary [311], thyroid [11], and hepatic [318], structures which exhibit secretory functions when transplanted *in vivo*. Together, these studies highlight the capacity for pluripotent stem cells to direct self-organization and patterning to yield functional structures, with relatively minimal exogenous cues. Therefore, the 3D aggregation of stem cells provides opportunities to study tissue morphogenesis and develop *in vivo* therapeutics, thereby providing a valuable tool for developmental biology, drug discovery and regenerative medicine.

2.4.2 Enabling technologies for controlled EB formation

Several techniques have been developed to facilitate stem cell spheroid formation and differentiation (Fig. 2-2), including methods that physically separate individual aggregates, which yield homogeneous populations, and batch methods that result in larger yields of EBs but with increased heterogeneity. Hanging drop cultures are initiated by suspending small volumes of culture media (10-20 μL) containing a defined number of cells (200-1000 cells) from the lid of a Petri dish. Although hanging drops yield uniformly-sized aggregates, the number of spheroids formed per dish is limited by the need to physically separate individual drops ($\sim$ 100 per 10 cm plate); thus, hanging drops are not readily amenable to scale-up methods [204, 350, 366]. Larger EBs also cannot be easily formed because the media volume is usually limited to less than $\sim$ 50μL, due to the surface tension needed to keep the inverted

drops suspended from lid surface. It is also traditionally difficult to exchange media in the hanging drop format, necessitating transfer to suspension cultures after approximately 2-3 days of formation in hanging drops; however, this has recently been addressed through the development of a modified 384-well hanging drop plate, which contains access holes for manipulation of the media in individual drops [332]. Alternatively, larger yields of EBs (i.e. 1000s) can be produced simply by inoculation of a single cell population of ESCs ($10^3 - 10^6$ cells/ml) into suspension culture in bacteriological grade dishes or dishes coated with non-adhesive materials such as agar or hydrophilic polymers [88]. The EBs form via random aggregation of cells and are largely dependent on inoculation concentrations and local interactions between cells. After initial aggregation, individual spheroids often agglomerate to form larger masses, resulting in large, irregularly shaped EBs that are widely variable in size and shape. When comparing different EB formation and culture methods, it is apparent that there is an inherent tradeoff between the ability to control EB formation and the yield of cells produced [79, 176, 52]. Recently, new methods have been established which provide increased control of EB size and homogeneity, yet are amenable to higher throughput production. Such methods, including encapsulation of ESCs within beads, physical separation using micro-wells and growth of ESC colonies on micropatterned substrates, rely on physical separation of EBs to promote controlled formation [242, 219, 327, 217, 335].

The altered phenotype of differentiated ESCs in response to aggregation kinetics and spheroid size has been established through research on the enrichment of mesoderm and cardiogenic phenotypes when aggregates are formed using hanging drop culture [34, 366, 175, 283]. Recent studies have reported that changes in ESC differentiation as a function of EB size may be attributed to changes in cell signaling and polarity within the spheroid [23, 142, 220, 22]. Bauwens et al reported that modulation of EB size alters the proportion of endoderm on the exterior surface of the

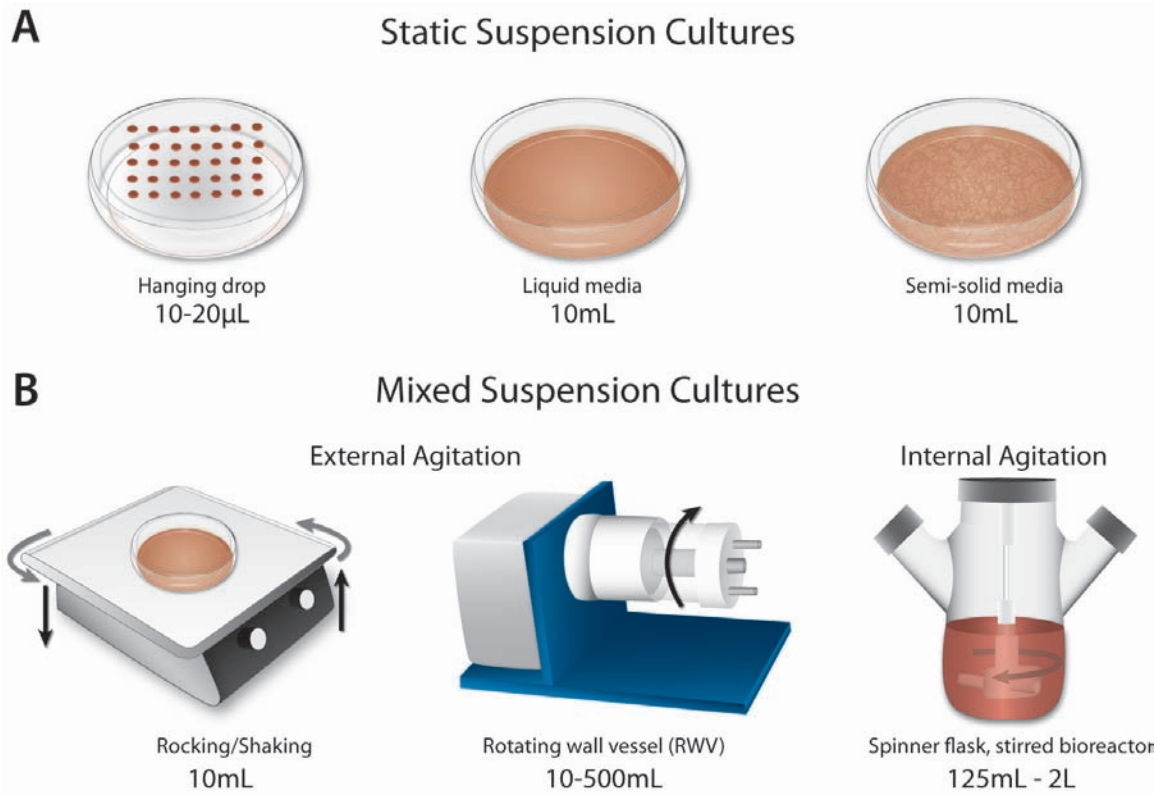

Figure 2-2: Methods of embryoid body formation and propagation. (A) Aggregates of stem cells can be formed and maintained statically by physically separating cells in small volume drops or by spontaneous aggregation of cells within bulk suspension cultures in liquid or semi- solid media. (B) Dynamic cultures are amenable to supporting increased culture volumes (1013 L) for the production of large cell yields in various formats, such as rotating wall vessels, or stirred bioreactors, which employ external or internal agitation, respectively.

EB, which results in increased mesoderm differentiation within EBs due to paracrine signaling [22]. Cell organization is also central to morphogenesis and differentiation through the expression of lineage specific cell adhesion molecules, such as E-cadherin, which mediates both initial spheroid formation as well as subsequent cellular organization and signaling. Binding and remodeling of adhesion receptors can alter differentiation through the activation of downstream signaling pathways such as the Wnt/β-catenin pathway [183, 80], thus highlighting the importance of the temporal aspect of cell aggregation and the implications for altering downstream signaling kinetics.

2.5 Biophysical pluripotent microenvironments

2.5.1 Microtissue mechanics

Three-dimensional morphogenesis, often associated with tumorigenesis and embryonic development, is a fundamentally biophysical process [359], as cellular migration and proliferation occur in conjunction with dynamic rearrangements of adhesions and the cytoskeleton. Mechanics have been directly implicated in mediating aspects of embryonic gastrulation [157], elongation [373], and dorsal and neural tube closure [107]. Moreover, the actomyosin cytoskeleton exhibits distinct dynamics during mesoderm migration accompanying gastrulation, whereby the stochastic assembly and disassembly of cortical actin in punctuated contractions mediates cell shape changes [161].

The three-dimensional remodeling of intercellular adhesions and ECM during morphogenesis modulates the intracellular cytoskeletal architecture (Fig. 2-3), which is responsible for transmitting forces within and between cells [144]. The mechanical structure of individual cells is often described by the tensegrity model [143], in which interior elements are maintained in compression by exterior elements in tension. The primary load-bearing structures within cells include cytoskeletal filaments, such as

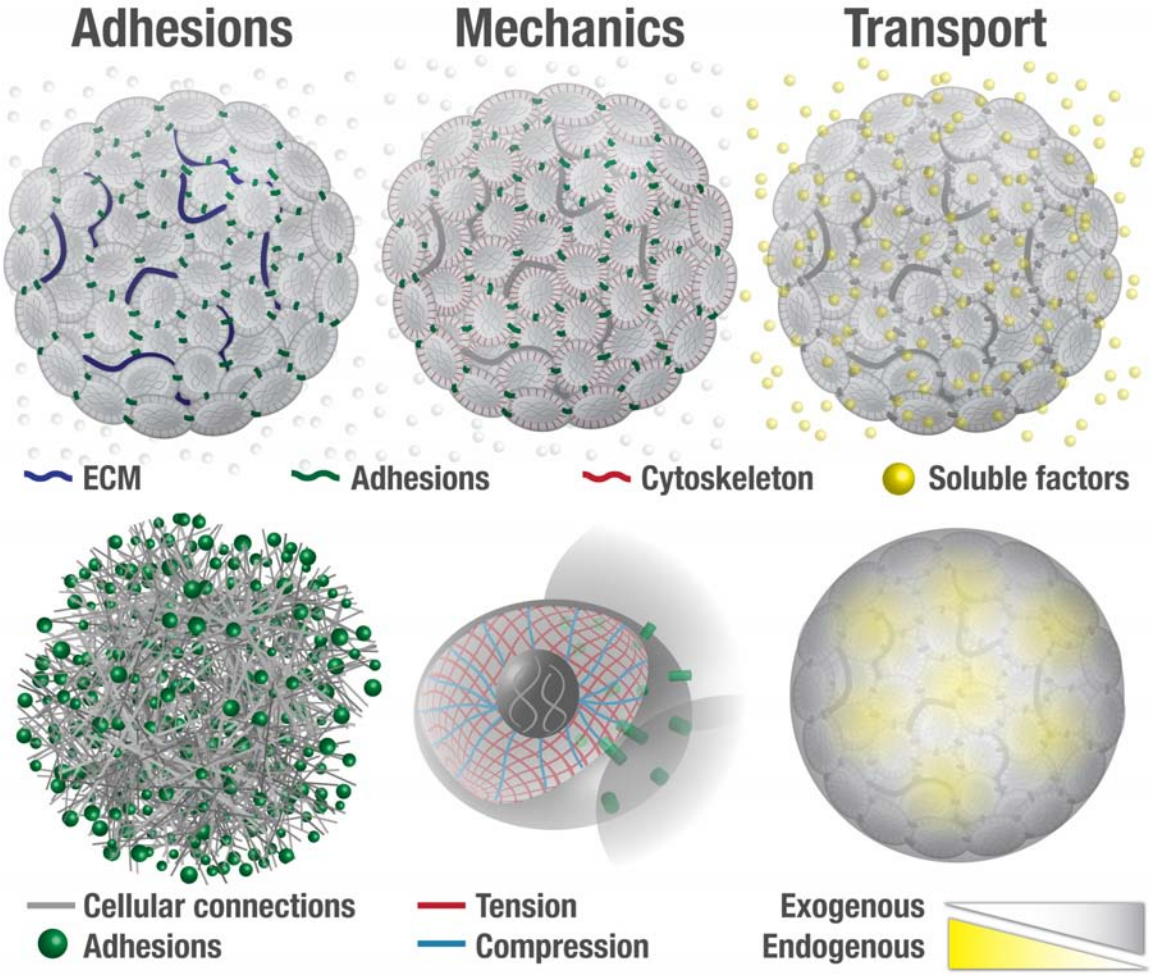

Figure 2-3: Physical parameters influenced by 3D assembly of stem cells. Multicellular assembly of stem cells alters the cell-cell and cell-matrix associations, the mechanical tension resulting from cytoskeletal rearrangements, and the distribution of exogenous and endogenous biochemical factors.

microtubules, microfilaments, and the actomyosin network [102]. Cellular forces are also opposed through extracellular factors [304], such as ECM, which impart dynamic feedback to mediate reorganization of the cytoskeleton [213] and associated cell-cell and cell-matrix adhesions [198], including integrins and cadherins.

Approaches to manipulate cell shape have been extensively explored in two-dimensional

cultures, as the regulation of inter- and intra-cellular tension mediates stem cell responses, including proliferation [237] and differentiation [215]. Such engineering approaches aim to control stem cell mechanics by changing adhesive ligand coating density [329] or through manipulation of substrate cross-linking [93], independent of ECM concentration [112]. Downstream signaling within the Rho associated protein kinase (ROCK) pathway is often implicated in mediating both cytoskeletal reorganization [202] and stiffness-mediated phenotypic changes [215]. For example, the epithelial-to-mesenchymal transition (EMT), a common phenotypic switch relevant to embryogenesis and pathophysiological processes [322], was patterned within regions of high cellular tension, and is abrogated by perturbation of the ROCK pathway [118]. Similarly, MSC differentiation was also patterned by controlling the geometry of multicellular sheets, with increased osteogenesis in regions of high tension [276]. In addition, defective mechanotransduction has been linked to decreases in the expression of nuclear proteins, such as nuclear lamins [181], which have also been implicated as markers of hESC differentiation [67]. Therefore, in addition to adhesive and cytoskeletal changes, nuclear shape may also play a key role in transducing extracellular forces and cellular tension to ultimately mediate cell signaling and transcription via changes in chromatin structure [78], thereby demonstrating multiparametric effects of the extracellular environment on cellular tension and stem cell fate.

The role of mechanics in mediating three-dimensional stem cell differentiation, however, remains less defined; given the dramatic changes in cellular organization and adhesive profiles when stem cells are assembled as spheroids [73], the cytoskeletal organization, and thereby biomechanics, are fundamentally distinct from properties measured in monolayer cultures. While integrin adhesions and ECM impart the primary forces opposing cytoskeletal tension in 2D, the cells themselves take on load bearing processes in 3D, with the network of cell-cell cadherin adhesions and actomyosin cytoskeletal associations regulating cellular tension. Moreover, the orientation

and composition of extracellular and pericellular matrices vary spatially and temporally during differentiation in 3D aggregates [230], and may play an active mechanical role in mediating changes in adhesive signature or clustering [255]. Therefore, due to the established role of biomechanics in mediating stem cell phenotype, opportunities remain to develop methods to monitor and perturb local tension in 3D aggregates as a novel approach to direct spatial patterns of differentiation and morphogenesis.

The dynamic regulation of cell morphology and migration associated with embryonic specification suggests an active role of biomechanics in gastrulation and analogous mesoderm differentiation. The stiffness of tissues has been linked to force generation [339], with mesodermal tissues, which actively migrate through the primitive streak, being 10 fold stiffer than endoderm in embryonic explants [373]. Computational simulations based upon mechanical models indicated that the homeostatic state of epithelial tissue structure is maintained by cellular tension, and accurately recapitulated cellular rearrangements upon laser ablation of individual cells [97]. Similar methods have elucidated the biomechanical basis underlying the regulation of wing size in the imaginal disc of drosophila embryos [140, 3]; despite the presence of biochemical signals, cell growth is inhibited by cell compression at the center of the disc, which ultimately dictates the final wing size. Similarly, non-uniform proliferation has been linked to geometrical regulation of mechanical tension in cells [301], with proliferation occurring in regions of increased local tension [237]. Together, the mechanical mechanisms underlying proliferation and differentiation enable the formation of distinct shapes and cellular patterning to direct divergent lineages and form complex tissues.

In addition, mechanical changes accompanying local cellular patterning are supported by the established role of ROCK signaling in mediating morphogenic processes *in vivo*. For example, RhoA signaling is induced by TGF-β in epithelial cells and

is implicated in mediating stress fiber formation during EMT [31]. Moreover, Rho-mediated contractility increases the stiffness of tumor cells, with the transformed phenotype being reversed through inhibition of ROCK signaling [256]. ROCK signaling has also been implicated as a mechanism underlying the dissociation of adherens junctions [280], thereby demonstrating the interplay between biochemical and biophysical processes mediating active cellular morphogenic processes. In addition to the synergistic effects mediating cell phenotype, mechanical and biochemical signals are transmitted across different length scales in tissues [90]. For example, in spheroids, tension is transmitted between cells through the structure via the actomyosin-cadherin network. In contrast, tissues comprised of large quantities of ECM or cells encapsulated in hydrogel materials tension is resisted via integrin adhesions to static extracellular structures, which may limit the range or dampen the force associated with extracellular mechanotransduction. Therefore, the dynamics of tissue remodeling during morphogenesis also dictate the local response to mechanical cues.

While ESCs, in particular, recapitulate many aspects of embryonic development on the biochemical level, opportunities remain to elucidate the biomechanical morphogenic processes in 3D stem cell spheroids, in order to draw from analogous *in vivo* events to direct cell fate by recapitulating physical extracellular and intracellular cues mediating cell migration and patterning in embryonic microenvironments.

2.5.2 Morphogen transport

Cell fate specification and tissue morphogenesis are orchestrated by precisely controlled spatial and temporal presentation of biochemical signals within the three-dimensional assemblies of cells. While current methods for directing ESC differentiation toward specific lineages have focused on the exposing cell monolayers to combinations of soluble factors, such culture techniques are limited in the temporal precision of morphogen delivery.

In addition to vascular flow, transport also occurs *in vivo* by mechanical or pressure driven convection through the extracellular space, known as interstitial transport. Interstitial flow has been most widely studied in the context of lymphatics [315], but occurs in many tissues, including flow through cartilage as a result of dynamic mechanical compression [223]. Interstitial flow is generally characterized by low velocity magnitudes, because the complexity and density of ECM leads to high resistance to transport. Measurements of interstitial flow *in vivo* have reported velocities ranging from 0.1 to 4.0 μm/s [57, 77], which is 10^2-10^5 times lower than flow in capillaries and the aorta, respectively. Several models exist for estimating hydraulic conductivity, diffusivity, and resultant solute gradients in tissues [316]; however, many of the parameters required for such calculations require knowledge of specific tissue properties (i.e. tissue geometry and composition, cell density, biochemical uptake rate). Currently, few studies have analyzed the composition of the EB microenvironment as a function of differentiation stage, thereby warranting studies to further quantify the physical parameters of EBs, in order to understand transport within 3D aggregates of ESCs.

The complexity of the three-dimensional structure of EBs leads to transport limitations (Fig. 2-4) stemming from size of aggregates and the formation of a non-permissive shell consisting of ECM (collagen I, collagen IV), and epithelial cells at the exterior of the EB [278, 51]. The inherent diffusional barriers of the spheroids arise as a function of differentiation state, which indicates that the EB microenvironment also changes over time [278, 51]. The transport properties of the EB microenvironment underscore the inability to efficiently deliver morphogens for directing ESC differentiation, which likely contributes to the heterogeneity in resulting cell types. However, the influence of morphological events on the transport of molecules with different properties (size, charge, uptake rate) has not been quantitatively assessed. The limited ability to deliver morphogens to scalable EB cultures therefore motivates

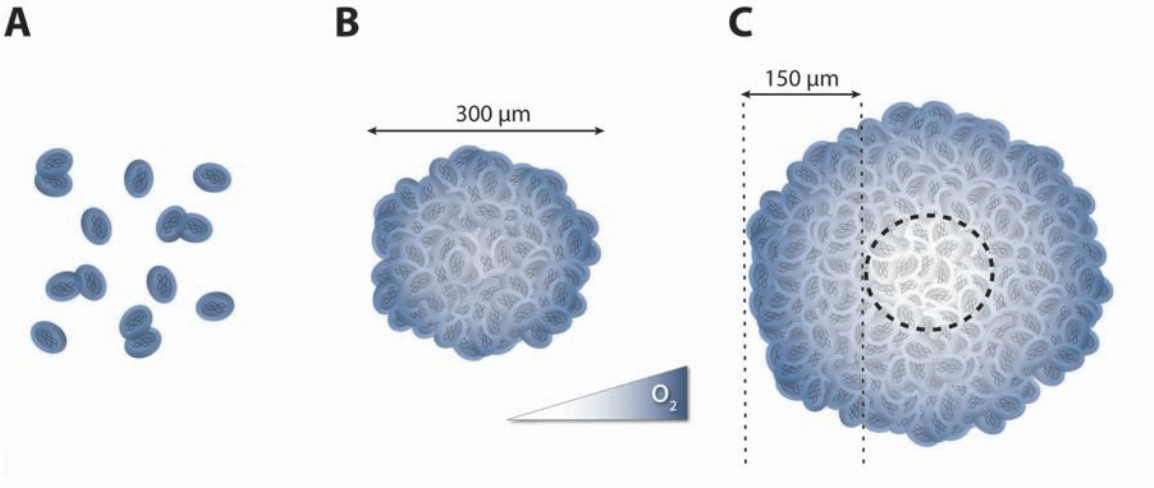

Figure 2-4: Transport in stem cell spheroids. (A) Macro-scale transport in various stem cell culture formats. Blue intensity represents relative concentrations of soluble morphogens and nutrients (such as O_2) within populations of single cells and (B, C) different-sized aggregates of stem cells. Concentration gradients arise in spheroid culture, with diffusive limitations in large aggregates.

the development of methods for eliminating gradients of nutrients within the interior of spheroids, in order to more homogeneously direct the differentiation of stem cell aggregates. The incorporation of microspheres within stem cell aggregates enables the delivery of morphogens more homogeneously throughout the multi-cellular microenvironment [203, 98, 51, 40, 53, 306]. However, many directed differentiation approaches rely on temporally controlled delivery of morphogens. Biomaterial-based microparticle delivery methods are limited in the control of release profiles, as well as the capacity for multi-factor release with varying kinetics. Additionally, the complex EB microenvironment, including the secretion of autocrine and paracrine factors, may modulate the local response of ESCs to factors delivered via microparticles, which could potentially inhibit the effects of the delivered morphogens. Ultimately, understanding and overcoming transport barriers in EBs may serve as a novel route to reduce gradient formation and enable homogeneous delivery of morphogens within the EB microenvironment.

The derivation and expansion of tissues *in vitro* is one of the central aims of

many tissue engineering technologies. Extensive research in the area of biomaterials has developed sophisticated scaffolds for the 3D culture of various cell types [201]. However, the size of tissue-engineered constructs is currently restricted by the limited ability to form functional vascular networks to provide adequate transport [187]. EB size also impacts the transport of nutrients and metabolites; in purely diffusive culture conditions, necrosis occurs in spheroids larger than approximately 300 μm in diameter [295, 104], presumably due to O_2 transport limitations, which indicates that the maximum diffusive distance is on the order of approximately 100-150 μm. The use of bioreactors for the culture of 3D tissues has been explored in order to increase transport throughout scalable culture volumes. However, standard bioreactor designs provide mass transfer throughout the bulk media, with media passing around, rather than through tissues. Therefore, current bioreactor designs largely rely on diffusion through tissues and do not provide adequate transport for large constructs *in vitro* [337]. The transport limitations that arise during *in vitro* culture of thick tissues have been addressed through the development of a bioreactor platform that employs forced convection of nutrients and morphogens through tissues, and has been shown to significantly enhance the the viability of cells within thick brain slices [74, 271]. Forced convection is expected to provide more uniform nutrient delivery, metabolite removal, and enable the more homogenous differentiation of 3D aggregates of ESCs *in vitro*.

CHAPTER III

SYSTEMATIC ANALYSIS OF EMBRYONIC STEM CELL DIFFERENTIATION IN HYDRODYNAMIC ENVIRONMENTS WITH CONTROLLED EMBRYOID BODY SIZE[1]

3.1 Introduction

New technologies at the interface of stem cell biology and bioprocessing are needed for the production of functional tissues for regeneration or replacement in novel therapeutic applications. The unique capacity of embryonic stem cells (ESCs) to differentiate into all somatic cells [96, 209, 323] makes them an attractive alternative to cell types for which primary cells are not easily isolated or derived. Strategies for the production of clinically relevant cell yields *in vitro* ($> 10^9$ cells) [199, 149, 333] often employ differentiation protocols based on principals of existing bioprocessing technologies which aim to scale traditional culture formats by producing batch cultures with increased volumes ($>$ 100 mL)[168]. However, stem cells are sensitive to environmental perturbations, including manipulation of cell adhesions [106, 172, 193], morphogen availability [84, 245], and mechanical forces [101, 9, 112, 93], all of which may be modulated due to the hydrodynamic environments created in large volume mixed/stirred culture systems. Fluid shear stress is a critical factor for establishing correct patterning and function during embryonic differentiation *in vivo* [2, 244, 138],

[1]Modified from: MA Kinney, R Saeed, and TC McDevitt. *Systematic analysis of embryonic stem cell differentiation in hydrodynamic environments with controlled embryoid body size.* Integr Biol., 2012, DOI: 10.1039/C21B00165A

and likewise impacts the differentiation of pluripotent and multipotent stem cells toward endothelial and hematopoietic lineages in two-dimensional, adherent monolayer cultures [211, 371, 345, 361, 5]. Although monolayer cultures permit control and manipulation of the substrate properties, as well as uniform application of fluid shear and soluble factors, ESC differentiation is commonly initiated by the formation of three-dimensional cell aggregates, termed embryoid bodies (EBs); the cell-cell adhesions and signaling within three-dimensional spheroid structure recapitulate many aspects of tissue morphogenesis, as well as several signaling pathways of embryogenesis. Additionally, the differentiation of ESCs as multicellular aggregates in suspension is not constrained by surface area (as in adherent cultures), and therefore is readily scalable to larger volume bioreactors. However, complexity arising from the three-dimensional structure of EBs confounds analysis of environmental perturbations in hydrodynamic cultures [166].

Although previous studies have noted that mixed cultures do not inhibit the pluripotent differentiation potential of ESCs [104, 47, 365, 117], several groups have reported changes in the relative efficiency of endogenous differentiation to various cell types, including cardiac and hematopoietic phenotypes, when EBs are cultured within hydrodynamic environments compared to those maintained in static suspension culture [283, 282, 197]. Additionally, various parameters of the hydrodynamic environment (such as mixing speed and bioreactor type) differentially impact ESC commitment [110, 282]. Scalable ESC cultures, however, generally rely on the spontaneous formation of cell aggregates within stirred bioreactors, which also results in changes in EB formation kinetics and size as a function of bioreactor geometry, configuration and mixing frequency [52, 47, 365, 117]. In rotary orbital cultures, slower rotation frequency (e.g. 25 rpm) resulted in accelerated EB formation and larger EBs, compared to aggregates formed at faster rotary orbital speeds (e.g. 40-55 rpm) [282].

Recent studies have reported that changes in EB size may influence ESC differentiation, which has been attributed to changes in cell signaling and polarity within the spheroid [220, 142, 23, 22]. Similarly, the kinetics of cell-cell association during EB formation may alter downstream signaling related to cadherin assembly [334, 321]. Overall, these studies indicate that hydrodynamic effects on differentiation may be confounded by changes in EB formation kinetics and size in different mixed bioreactor cultures, thus warranting a more systematic study of ESC differentiation in hydrodynamic environments.

Recently, new technologies have been developed which are capable of reproducibly forming large yields of uniform-sized EBs by forcing aggregation of the cells in micro-wells or on micro-patterned substrates [253, 23, 219, 142, 335]. Such technologies enable the study of EB differentiation in different hydrodynamic environments, because forced aggregation techniques can standardize the kinetics of EB formation, independent of hydrodynamics. Additionally, pre-forming EBs prior to introduction into mixed environments permits the maintenance of uniform populations throughout the culture period and across different conditions. The objective of this study was to analyze the impact of hydrodynamic environments on differentiation of ESCs, independent of EB size, by developing a method for maintaining uniform EB populations in different mixed suspension cultures. EBs were formed via forced aggregation in polydimethylsiloxane (PDMS) micro-wells, and maintained through the course of differentiation in rotary orbital suspension cultures [52, 283, 282]. The impact of mixing conditions on size-controlled EBs was analyzed by morphometric, morphological, and phenotypic metrics. The results from this study demonstrate that maintaining uniform populations of pre-formed EBs in different hydrodynamic environments overall increases the uniformity of morphogenesis and differentiation within hydrodynamic cultures, with relatively subtle changes in the differentiation toward certain lineages.

The differentiation format developed in this study enables a more systematic understanding of the modulation of ESC differentiation within hydrodynamic environments and provides an alternative technique for the standardization of scalable ESC cultures.

3.2 Materials and Methods

3.2.1 Embryonic stem cell culture

Murine ESCs (D3 cell line) were expanded on tissue culture treated polystyrene dishes (Corning Inc., Corning, NY) adsorbed with 0.1% gelatin (Mediatech, Manassas, VA). Undifferentiated ESC media consisted of Dulbeccos Modified Eagles Medium (DMEM; Mediatech) containing 15% fetal bovine serum (Hyclone, Logan, UT), 100 U/mL penicillin (Mediatech), 100 μg/mL streptomycin (Mediatech), 0.25 μg/mL amphotericin (Mediatech), 2 mM L-glutamine (Mediatech), 1x MEM non-essential amino acid solution (Mediatech), 0.1 mM 2-mercaptoethanol (Fisher Scientific, Fairlawn, NJ), and 10^3 U/mL leukemia inhibitory factor (LIF; ESGRO, Millipore, Billerica, MA). The media was exchanged every other day, and cells were passaged at approximately 70% confluence.

3.2.2 Embryoid body formation

A single cell suspension of undifferentiated ESCs was obtained by dissociating monolayer cultures using 0.05% trypsin-EDTA (Mediatech). Forced aggregation of ESCs was accomplished by centrifugation (200 rcf) of ESCs into 400 μm diameter polydimethylsiloxane (PDMS) micro-wells (AggrewellTM, Stem Cell Technologies, Vancouver, Canada) as previously reported [335]. The cell inoculation concentration was modulated to seed wells with approximately 500, 1000 and 2000 cells each in differentiation medium, consisting of undifferentiated ESC media without LIF. After incubation for 24 hours to allow formation, the resultant EBs were transferred to suspension culture (approximately 2000 EBs in 10 mL of media) in sterile 100 x 15 mm

bacteriological grade polystyrene Petri dishes (BD, Franklin Lakes, NJ) and maintained on rotary orbital shakers [52] at rotational frequencies of approximately 25, 45, and 65 rpm. For static cultures, EBs were transferred from the micro-wells to dishes coated with sterile 2% agar, which is used to prevent cell attachment to the dish. 90% of the media was exchanged every other day by gravity-induced sedimentation in a 15 mL conical tube. Suspension cultures were maintained through 14 days of differentiation.

3.2.3 Morphometric analysis

Phase images were acquired at days 1, 2, 7, 10 and 14 of differentiation using a Nikon TE 2000 inverted microscope (Nikon Inc., Melville, NY), equipped with a SpotFlex camera (Diagnostic Instruments, Sterling Heights, MI). The cross sectional area of EBs was measured by using a custom-written computational macro in ImageJ software (NIH), which delineates EB boundaries through a combination of thresholding, edge detection, and smoothing, as described previously [282]. At least 100 EBs were analyzed for each sample (n=3 independent samples per experimental condition), and the distribution of EBs was visualized by frequency histograms.

3.2.4 EB yield analysis

The total yield of EBs in each culture at days 1, 2, and 7 was manually counted by dilution of the total population and visual inspection using a Nikon Eclipse TS100 inverted phase microscope, which resulted in approximately 20-50 EBs per well of a 24 well non-tissue culture treated polystyrene plate. 3 separate counts were recorded for each sample (n=3 independent samples per experimental condition).

3.2.5 Histology and immunohistochemistry

EBs were sampled from rotary cultures at days 7, 10 and 14 of differentiation, rinsed in PBS and fixed in 10% formalin (4% formaldehyde) for 45 minutes with rotation at

room temperature. Fixed EBs were rinsed 3 times in PBS and embedded in Histogel (Richard-Allen Scientific, Kalamazoo, MI) at 4 °C overnight. Samples were processed via a series of graded ethanol and xylene rinses and embedded in paraffin. Paraffin-embedded samples were sectioned with a thickness of 5 μm, using a rotary microtome (Microtom HM310). For histological analysis, samples were de-paraffinized by rinsing in a series of xylene and graded ethanol concentrations, followed by staining with hematoxylin and eosin (H&E). H&E stained sections were imaged using a Nikon Eclipse 80i microscope (Nikon, Inc.) equipped with a SpotFlex digital camera (Diagnostic Instruments).

3.2.6 PCR array and quantitative real time PCR

EBs were sampled at days 7, 10, and 14 of differentiation for PCR gene expression analysis. For real time (RT)-PCR, total RNA was isolated from EBs using the RNeasy Mini kit (Qiagen Inc, Valencia, CA), followed by synthesis of cDNA from 1 μg of RNA using the iScript cDNA synthesis kit (Bio-Rad, Hercules, CA). To prepare cDNA for use in PCR Arrays, the RT2 First Strand Kit (SABiosciences, Frederick, MD) was used with 1 μg of total RNA. RT-PCR was performed with SYBR Green technology and the MyIQiCycler (Bio-Rad), using primers that were designed with Beacon Designer software (Invitrogen) and validated against cell-specific controls. Primers for both pluripotency (*Oct-4*) and differentiated cell phenotypes (*Nkx2.5*, *AFP*, *Pax-6*) were analyzed by RT-PCR. The relative concentration of each gene transcript was calculated based on a standard curve, and normalized with respect to expression of the housekeeping gene *18s* [262].

Global gene expression was analyzed using the Mouse Embryonic Stem Cell RT^2 Profiler^{TM} PCR Array (SABiosciences) which includes 84 genes related to pluripotency and markers of differentiation toward all lineages, as well as 5 housekeeping genes and several PCR controls. RT-PCR was performed on the arrays using a MyIQ

iCycler (Bio-Rad) with SYBR green based RT^2 qPCR Master Mix (SABiosciences). All sample data were visually inspected post-run, including both the amplification phases and melt curves, to ensure efficacy of the individual primers. To account for changes in PCR efficiency between PCR runs, data from individual runs were normalized with respect to the geometric average of 3 housekeeping genes. The PCR arrays included 5 housekeeping genes (*Gusb*, *Hprt1*, *Hsp90ab1*, *Gapdh*, *Actb*), and 3 were chosen based on the calculation of gene stability that yielded a combination with the least variability (*Gusb*, *Hsp90ab1*, *Actb*) [338]. The normalized Ct values were then used to calculate the relative fold changes in gene expression relative to the group of interest (45 rpm / ESCs, 65 rpm / ESCs, 45 rpm / 65 rpm) [262]. The Genesis software package was used to visualize heatmaps of gene expression, represented as the log2 transform of fold change, and to calculate two-dimensional hierarchical clustering between genes and experimental groups, based on Euclidean distance and average linkage clustering. Statistical differences were calculated using an independent samples t-test for each gene, and genes with $p<0.05$ were determined to be statistically significant.

3.2.7 Flow cytometry

EBs were rinsed with PBS and dissociated at 37 °C with rotation, using 0.25% trypsin-EDTA and triturating every 10 minutes for a total of 30 minutes in order to obtain a single cell suspension. Cell solutions were centrifuged at 1000 rcf for 5 minutes, and rinsed 3 times in PBS. Flow cytometry was conducted using an Accuri C6 cytometer (Accuri Cytometers, Ann Arbor, MI), with a minimum of 30,000events within the FSC/SSC gate collected per sample (n=3 independent samples experimental per condition). After obtaining a single cell suspension, a LIVE/DEAD kit (Invitrogen) was used to assess cell viability. Briefly, cells were resuspended in 1 mL of PBS and stained for 15 minutes using 2 μL of 50 μM calcein AM and 4 μL of 2 mM ethidium

homodimer-1 (EthD-1). Unstained and single stained populations were used for gating and compensation. Forward scatter (FSC) and side scatter (SSC) were analyzed within the live (calcein AM+, EthD-1-) cell populations.

D3 mESCs were transduced using plasmids encoding EGFP under the AFP (pAFPpHyg/EGFP; provided by Iwao Ikai, M.D., Ph.D., Kyoto University, Kyoto Japan) or Oct-4 (phOCT3-EGFP1; provided by Wei Cui, Ph.D., Imperial College, London, UK) promoters, and stable clones were established following geneticin (G-418) selection. AFP-GFP+ and Oct4-GFP+ cells were analyzed by flow cytometry prior to differentiation, and after 7, 10, and 14 days of differentiation. The dissociated cell population was initially identified by gating on the FSC/SSC plot. Within the FSC/SSC gate, polygonal gating was used on the FSC/FL-1 (480nm excitation; 530 ± 15 nm emission) plots, to include 2% of the untransduced (D3 mESCs; negative control) population using FlowJo software (Tree Star, Inc., Ashland, OR).

3.2.8 Analysis of spontaneous contractile activity

After 7 days of differentiation in rotary suspension, single EBs were transferred to individual wells of 0.1% gelatin-coated 48 well tissue culture dishes in a total volume of 500 μL of differentiation media, to promote adherence and spreading of cells (30 EBs per sample, n=3 independent samples per experimental condition). The development of contractile activity, indicative of cardiomyogenic differentiation, was monitored at days 10, 12, and 14 by visual inspection using a Nikon Eclipse TS100 inverted phase microscope. Blinded counts of contractile activity were conducted by scoring EBs with one or more beating foci were as contractile, and representing the contractile EBs relative to the total plated EB population.

3.2.9 Statistical analysis

All experiments were performed with triplicate samples with independent conditions and data is represented as the mean of independent replicates (n=3) $\pm$ standard error.

Statistical analysis was performed using an independent samples t-test between the conditions (45 and 65 rpm), assuming either equal or unequal variances, depending on the results from Levenes equality of variances test. Statistical analysis comparing changes over time was conducted using a one-way ANOVA, with a post-hoc Tukey or Mann-Whitney U test for comparison of individual samples, depending on the equality of variances.

3.3 Results

3.3.1 Control of EB formation and size by forced aggregation

In order to investigate the ability to control EB formation and size in scalable suspension cultures, EBs were formed via centrifugation of cells into 400 μm diameter PDMS micro-wells (Aggrewell^{TM}) prior to transfer into rotary orbital cultures [335]. Micro-well aggregation produced large, homogeneous yields of EBs of defined size after 24 hours of formation, which were subsequently transferred into bulk suspension cultures (Fig. 3-1 A). Additionally, the EB size was modulated by altering the seeding density of cells in each well (500, 1000, and 2000 cells per well), which produced uniform populations that could be distinguished by morphometric image analysis of EB cross sectional area. Histograms of EB area demonstrated narrow distributions, indicating homogeneity of resulting EBs, as well as distinct peaks, which distinguish the populations formed with different cell seeding densities (Fig. 3-1 B).

EBs formed with different seeding densities were maintained in rotary orbital culture at 45 rpm, in order to analyze the changes in EB morphogenesis during differentiation in mixed suspension. During the first 7 days of differentiation, 500-, 1000-, and 2000-cell EBs increased in size; however, the relative size differences initially exhibited by EBs from different seeding densities were maintained, indicated by statistical differences ($p<0.05$) in EB cross sectional area immediately after formation

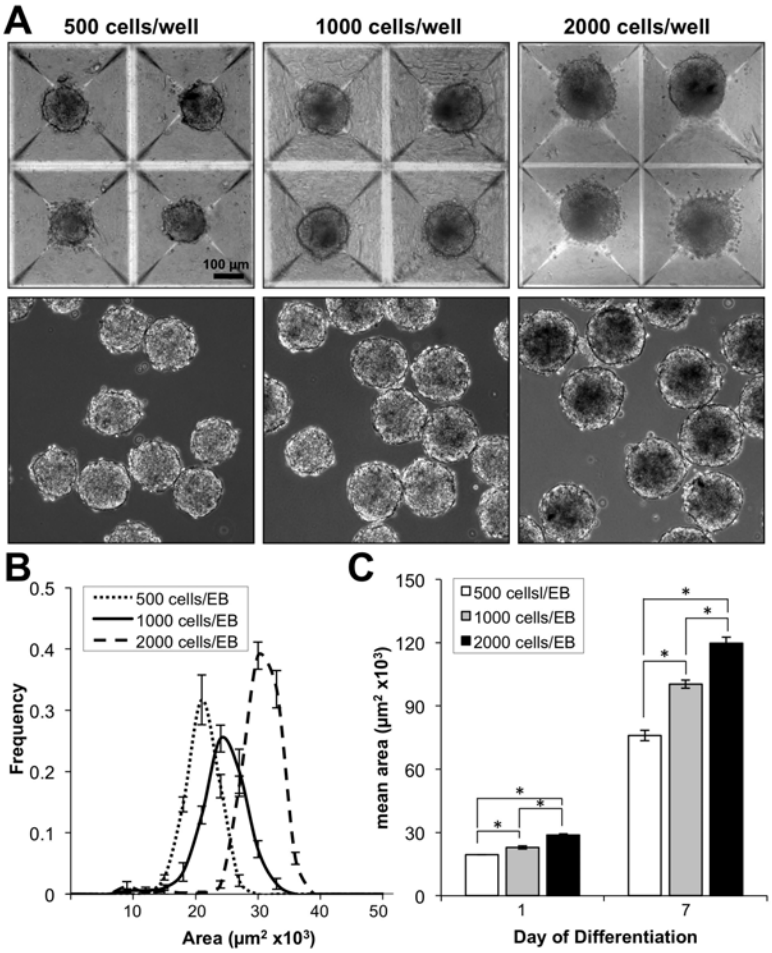

Figure 3-1: Micro-well formation and rotary maintenance of size-controlled EBs. Micro-well formation and rotary maintenance of size-controlled EBs. (A) Forced aggregation of ESCs into micro-wells to form size-controlled EBs was accomplished via centrifugation of single cells, followed by 24 hours of incubation in wells, and subsequent transfer to rotary orbital suspension (scale bar = 100 μm). (B) After 24 hours, the resulting EB populations exhibited narrow size distributions with distinct peaks modulated by ESC seeding density, and (C) relative size differences were maintained over 7 days of differentiation in rotary orbital suspension culture.

(day 1) and after 7 days of differentiation (Fig. 3-1 C). These results indicate that the size and formation kinetics of EBs can be reproducibly controlled using micro-well technologies, and that distinct populations of pre-formed EBs can be maintained in rotary orbital suspension cultures as a means to regulate and standardize EB size.

To further investigate the feasibility of maintaining pre-formed EBs in different hydrodynamic conditions, EBs formed with 1000 cells per aggregate in micro-wells were transferred to static or rotary orbital cultures at a range of speeds from 25 to 65 rpm. Visual analysis after 24 hours in suspension indicated that agglomeration of individual pre-formed EBs occurred in static cultures and at the lowest (25 rpm) rotary orbital speed (data not shown). In contrast, when maintained at 45 rpm and 65 rpm, EBs maintained uniform spherical populations, and did not exhibit evidence of substantial agglomeration. After 7 days of differentiation, EBs at 45 and 65 rpm remained homogeneous and appeared to be similar in size; however, agglomeration of individual EBs led to spherical, but substantially larger EBs at 25rpm and large, irregularly-sized EBs, in static cultures (Fig. 3-2 A). The visual observations regarding EB agglomeration were verified by quantification of EB size and yield over 14 days of differentiation (Fig. 3-2 B-C). In 45 and 65 rpm rotary orbital conditions, EB size significantly increased ($p<0.05$) at all time points compared to day 1, (immediately after micro-well formation), but did not exhibit size differences between the hydrodynamic culture conditions at 45 and 65 rpm. Additionally, similar EB yield was maintained in both 45 and 65 rpm rotary conditions; the yield at day 7 of differentiation was not statistically different compared to day 1, and was not different between rotary conditions. Taken together, these results indicate that the hydrodynamic conditions imposed at 45 rpm and 65 rpm prevent agglomeration of pre-formed EBs and enable the culture of uniform EBs in different mixed culture environments. The combination of micro-well formation with hydrodynamic cultures at 45 and 65 rpm was therefore chosen for the further analysis of ESC morphogenesis and differentiation of uniformly

sized EBs maintained in different hydrodynamic environments.

3.3.2 Impact of hydrodynamic cultures on ESC morphogenesis

Analyses of cell and EB morphology as well as cell viability after 14 days of differentiation suggested similarities between different populations of pre-formed EBs, despite differences in hydrodynamic culture conditions. Morphological features of EBs, examined following H&E staining of histological sections, indicated the appearance of differentiated cell populations, including cells exhibiting tightly packed epithelial-like morphologies, as well as more spread-out mesenchymal-like morphologies in all EB populations; however, no obvious differences were noted between EBs cultured in different hydrodynamic conditions (Fig. 3-3 A). Additionally, single cell analysis via flow cytometry indicated similar refractive properties of single cells, with respect to both forward and side scatter metrics, which are indicative of cell size and complexity respectively (Fig. 3-3 B). Moreover, there were no differences in the proportion of live and dead cells stained with calcein AM and ethidium homodimer-1, respectively, between EBs from different hydrodynamic conditions and the yield of cells per EB remained similar between hydrodynamic conditions (Fig. 3-3 C). Altogether, these results indicate that changes in the hydrodynamic environment did not globally alter the ability of ESCs to undergo morphogenesis within EBs through 14 days of differentiation.

3.3.3 Impact of hydrodynamic cultures on gene expression

Changes in gene expression over the course of differentiation were analyzed using an embryonic stem cell PCR array (SABiosciences), which included 84 genes commonly associated with the maintenance of pluripotency and differentiation to the three germ lineages. Heatmap visualization of the gene expression profiles indicated that there were distinct subsets of genes that exhibited increased (Fig. 3-4 A, red) or decreased (Fig. 3-4 A, green) expression in EB cultures compared to the starting population of

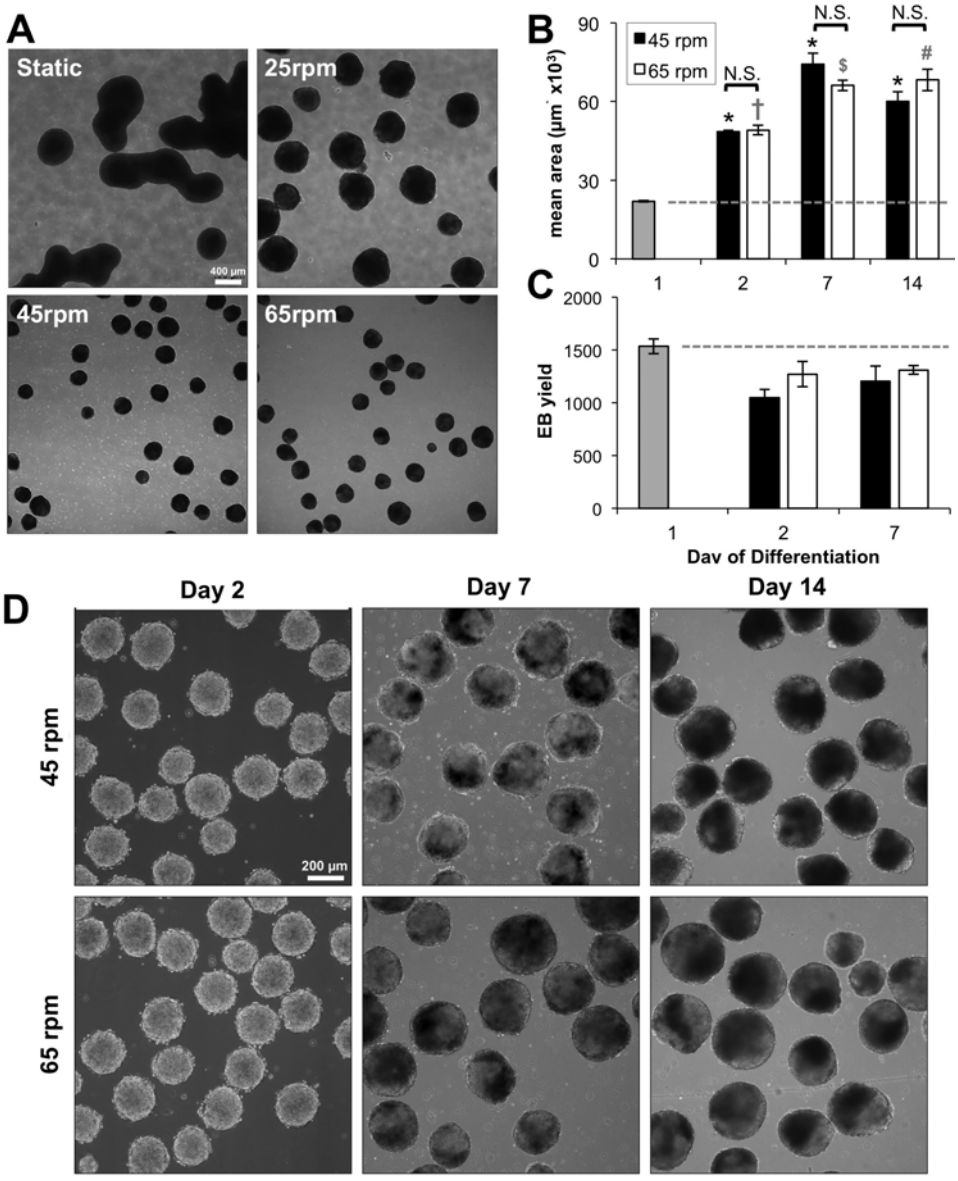

Figure 3-2: Maintenance of EB populations in different hydrodynamic environments. (A) EBs maintained in rotary orbital suspension exhibited changes in size and shape after 7 days of differentiation. The irregular shape and large size of EBs maintained in static and low rotary orbital speed (25 rpm) conditions indicated agglomeration of individual EBs (scale bar = 400 μm). (B) At 45 and 65 rpm, however, EBs maintained uniform, similarly-sized populations through 14 days (scale bar = 200 μm). (C) Although EB size increased during the course of differentiation, the EB area at 45 and 65 rpm was not significantly different. (D) Additionally, the total number of EBs did not change over time or between conditions, indicating minimal agglomeration of individual pre-formed EBs. * = $p<0.05$ (45 rpm) compared to all time points; + = $p<0.05$ (65 rpm) compared to all time points; \$ = $p<0.05$ (65 rpm) compared to all time points except day 14; # = $p<0.05$ (65 rpm) compared to all time points except day 7; N.S. = no statistical significance.

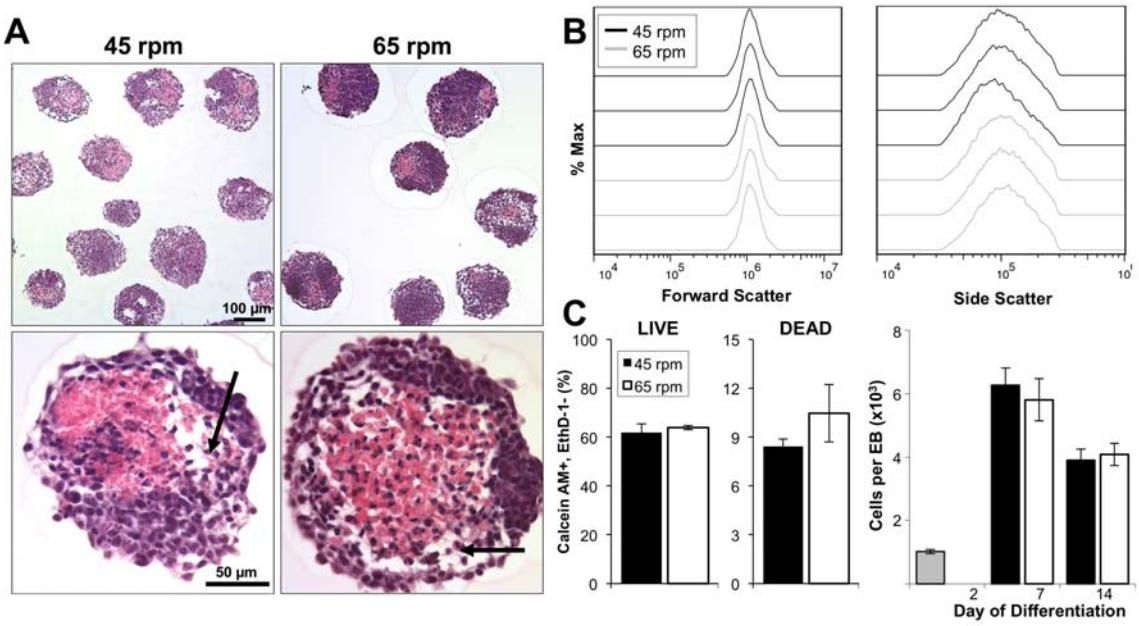

Figure 3-3: Morphological features of EBs and ESCs in hydrodynamic environments. (A) ESCs within EBs exhibited epithelial- and mesenchymal-like (arrows) morphologies; however, few distinct changes were apparent between rotary conditions (scale bars = 100 μm, 50 μm). (B) Overlays of Forward scatter (FSC) and side scatter (SSC) histograms from flow cytometry indicated similarities in cell properties between conditions. (C) viability and total cell yield per EB were not affected by hydrodynamics at the mixing speeds tested.

undifferentiated ESCs. After 7 days of differentiation, 20 genes exhibited a minimum of 3-fold increase compared to ESCs, whereas 15 genes were decreased greater than 3-fold compared to ESCs. Two-way hierarchical clustering of all genes and experimental groups separated the individual time points, reflecting distinct changes in gene expression that arose during the course of differentiation; however, within individual time points, the gene expression profiles of the experimental groups did not cluster separately, which suggested a lack of global distinction between the EB populations subjected to different hydrodynamic conditions.

Specific analysis of the subsets of genes that were differentially expressed compared to ESCs (minimum of 1.5 fold change, and $p<0.05$ compared to ESCs) indicated that ~93% of the genes (25/27) that were decreased compared to ESCs after 7 days of differentiation were common to both hydrodynamic conditions (Fig. 3-4 B). Of the genes that were significantly decreased compared to ESCs, many were transcription factors (*Oct-4, Nanog, Sox2*) and signaling molecules (*Fgf4, Lefty1, Lefty2, Nodal*) known to be associated with the undifferentiated, pluripotent state of ESCs (Fig. 3-5 A). Temporal gene expression analyzed using RT-PCR with independent primers verified the decrease in *Oct-4* over the time course of differentiation (Fig. 3-5 B) and stably transduced cells expressing GFP driven by the *Oct-4* promoter exhibited a decrease in the proportion of GFP+ cells (Fig. 3-5 C). Additionally, ~44% (12/27) of genes that were increased (minimum of 1.5 fold change, and $p<0.05$ compared to ESCs) during EB differentiation were commonly increased in both hydrodynamic conditions (Fig. 3-4 B), including markers of differentiated phenotypes related to epiblast (*fibroblast growth factor 5, Fgf5*), endoderm (*alpha fetoprotein, AFP; forkhead box A2, Foxa2; Sox17*), and mesoderm lineages (*Gata4, Podxl1; VE-cadherin, Cdh5; Flt1*), as well as signaling molecules, such as *Noggin* (*Nog*) and factors such as *Laminin* (*Lamb1-1*), which are related to the morphogenesis of ESCs in EB differentiation [260, 305]. Overall, compared to ESCs, the global patterns of gene expression in EBs

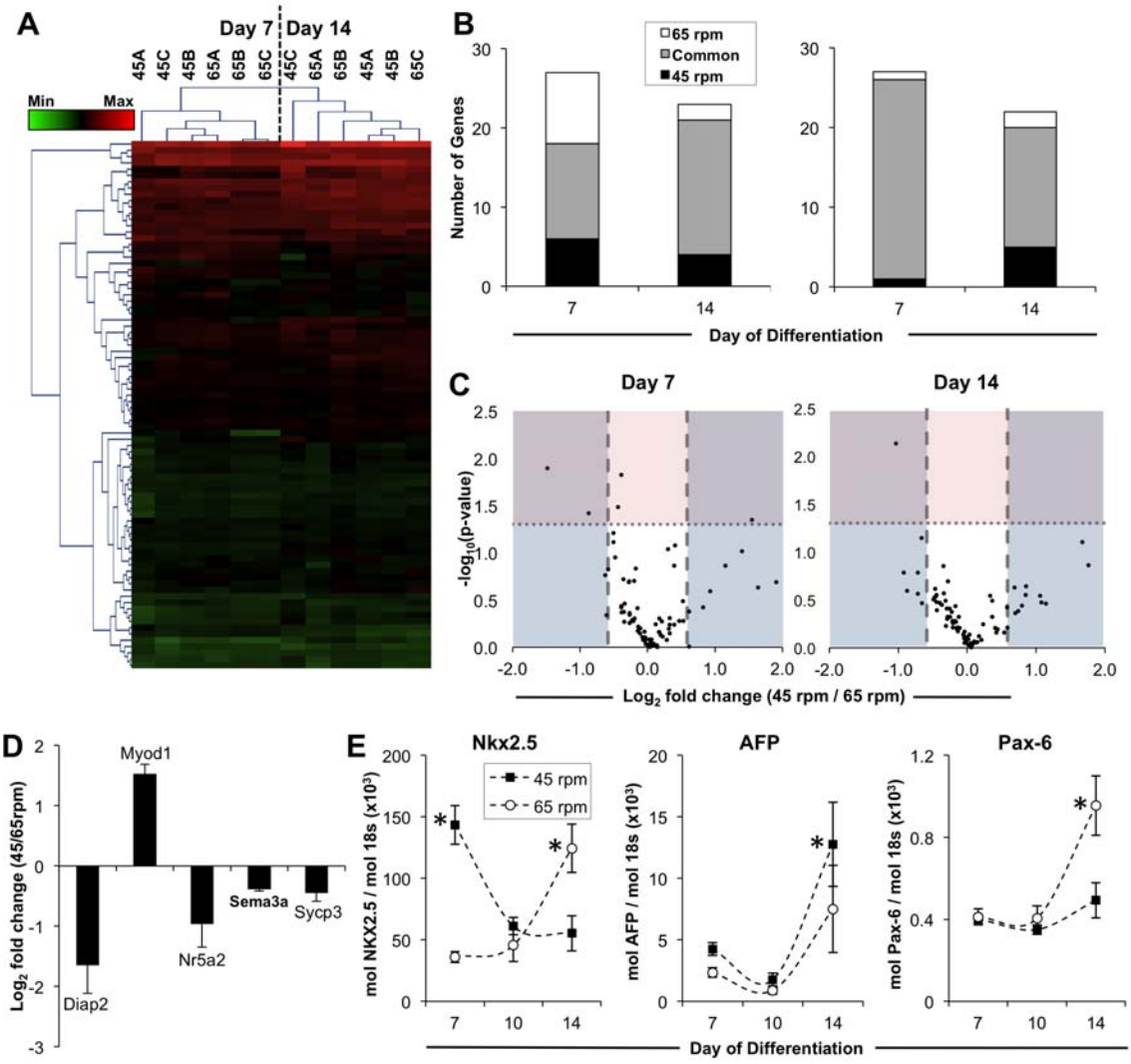

Figure 3-4: Gene expression profiles of size controlled EBs in hydrodynamic environments. Global gene expression of 84 genes related to ESC pluripotency and differentiation was assessed in EBs from 45 rpm and 65 rpm after 7 and 14 days of differentiation using PCR Arrays. (A) Heatmap visualization of gene expression demonstrated (B) distinct subsets of genes up- and down-regulated compared to ESCs, with (C) several significantly modulated genes being regulated differently between the 45 rpm and 65 rpm conditions. Although several genes exhibited differences in fold change (>1.5 fold, blue; represented as the fold change of 45 rpm / 65 rpm), few genes exhibited statistically significant differences ($p<0.05$, pink) between the hydrodynamic conditions, (D) including 4 genes increased in 65 rpm, and 1 gene increased in 45 rpm after 7 days of differentiation. (E) Rotary conditions also modulated the temporal expression of genes from the mesoderm (*Nkx2.5*), endoderm (*AFP*), and ectoderm (*Pax-6*) lineages. * $p<0.05$

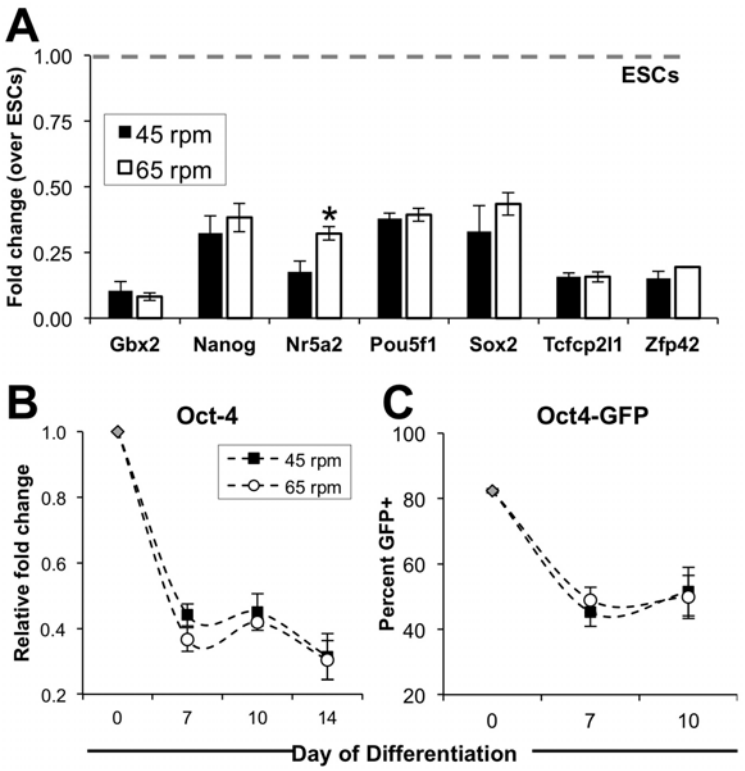

Figure 3-5: Pluripotency in EBs. Transcription factors related to maintaining pluripotency exhibited decreased expression compared to ESCs in (A) PCR array analysis, (B) RT-PCR for *Oct-4*, and (C) incidence of GFP+ cells in a cell line expressing GFP driven by the *Oct-4* promoter.

from both hydrodynamic conditions suggested the progressive loss of pluripotency, with an increase in markers related to differentiation of ESCs.

However, of the genes that were increased compared to ESCs, there were also several genes (45 rpm: 6/27; 65 rpm: 9/27) that were uniquely increased in the specific hydrodynamic conditions, including markers of endoderm (*Gata6, Ins2, Iapp, Serpina1a*) and mesoderm (*Kit, Grb7, Hba-x, Hba-y*) lineages, which warranted a direct comparison of the gene expression profiles in different hydrodynamic environments. Comparisons of the expression patterns between the hydrodynamic conditions indicated that the profiles were largely similar at both time points, as evidenced by a direct, positive correlation between data from 45 rpm and 65 rpm (R^2=0.95, day 7;

R^2=0.95, day 14). Fold changes in gene expression between hydrodynamic conditions (represented as 45 rpm / 65 rpm) indicated that a number of genes were modulated greater than 1.5 fold (14 genes at day 7; 19 genes at day 14) (Fig. 3-4 C; blue). However, only 5 genes exhibited statistically significant changes in gene expression between hydrodynamic conditions at day 7 of differentiation, and 1 gene (out of 84) was significantly modulated after 14 days (Fig. 3-4 C; pink). Of the 5 genes significantly changed after 7 days of differentiation, 4 were increased in 65 rpm (2 genes >1.5 fold change), whereas 1 gene was increased in 45 rpm (Fig. 3-4 D). Genes related to pluripotency and germ cell differentiation, *Nuclear receptor family 5, group A, member 2* (*Nr5a2*) [134] and *synaptonemal complex protein 3* (*Sycp3*) [328], respectively, exhibited overall decreased expression compared to ESCs, and both were significantly increased in 65 rpm compared to 45 rpm. *Diaphanous homologue 2* (*Diap2*), which encodes a downstream effector of the RhoA signaling pathway, and is implicated in cytoskeletal remodeling and stabilization of adherens junctions, was also increased in the 65 rpm rotary orbital condition [280]. Additionally, contrasting patterns of gene expression related to muscle (*Myod1*; increased in 45 rpm) and neural differentiation (*Sema3a*; increased in 65 rpm), supported the divergent differentiation, albeit modest based on the sub-set of genes examined, of size-controlled EBs cultured in different hydrodynamic conditions (Fig. 3-6).

Individual RT-PCR using independently designed primers also confirmed the temporal modulation of genes from all germ layers. *Nkx2.5*, a mesoderm marker which is increased during early cardiac differentiation, was significantly increased at day 7 in 45 rpm, and significantly increased in 65 rpm at day 14 (Fig. 3-4 E); the pattern of *Nkx2.5* expression indicates a possible temporal shift in the onset and progression of mesoderm differentiation within the hydrodynamic conditions. Further, the gene expression for *alpha fetoprotein* (*AFP*), indicative of endoderm differentiation, was significantly increased after 7 days of differentiation in 45 rpm EBs, whereas *Pax-6*,

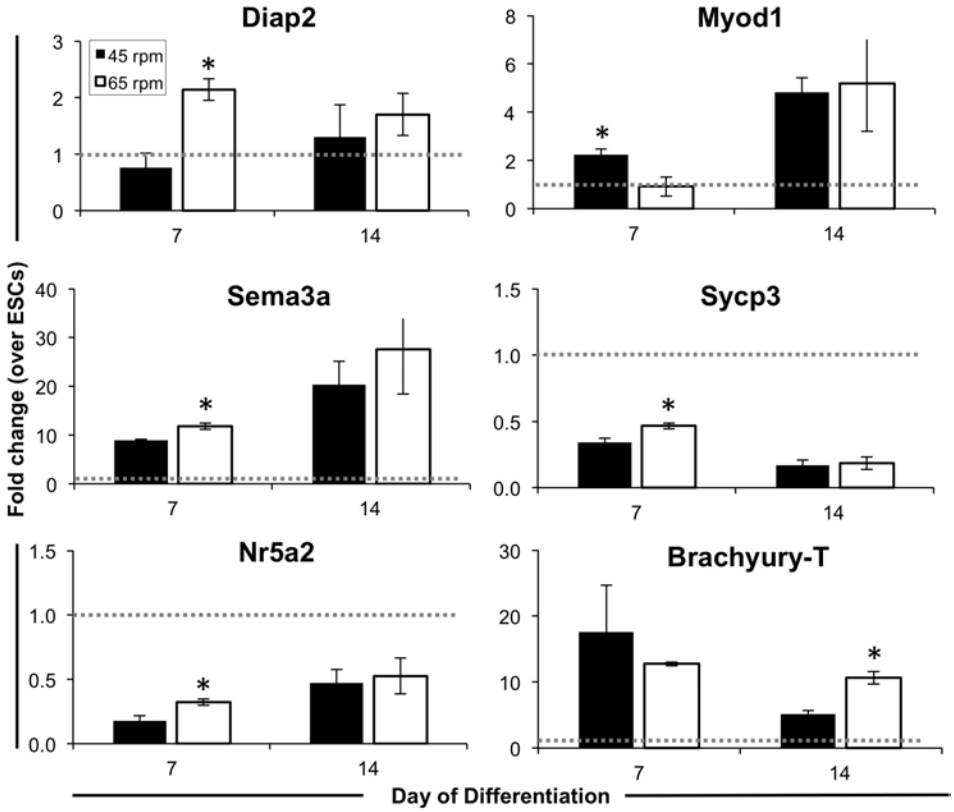

Figure 3-6: Genes differentially regulated between hydrodynamic conditions. Several genes exhibited statistically significant changes in gene expression between the rotary orbital conditions, after 7 (*Diap2, Myod1, Nr5a2, Sema3a, Sycp3*) and 14 (*Brachyury-T*) days of differentiation. Differences were apparent in genes that were both increased and decreased compared to ESCs (dotted line). *$p<0.05$

an ectoderm marker, was increased in 65 rpm rotary conditions after 14 days (Fig. 3-4 E). Overall, gene expression patterns suggested that size-controlled EBs undergo similar changes related to loss of pluripotency and differentiation, with a subset of genes exhibiting subtle changes in temporal kinetics and relative expression levels due to culture in distinct hydrodynamic environments.

3.3.4 Impact of hydrodynamics on visceral endoderm and cardiomyogenic differentiation

EB morphogenesis commonly occurs through the differentiation of the cells at the exterior of the spheroid toward the visceral endoderm lineage [193]. Although altered efficiency of ESC differentiation toward visceral endoderm in hydrodynamic environments has been reported [282], the exterior endoderm has also been suggested as a mechanism for changes in differentiation as a result of EB size [22]. Therefore, flow cytometry and immunostaining were used to analyze the proportion and localization of visceral endoderm cells within EBs from the hydrodynamic conditions at 45 and 65 rpm. Flow cytometry was performed using cells transduced to express GFP under control of the AFP promoter. Prior to EB formation and differentiation, ESCs expressed low levels of GFP; however, after a week of EB differentiation, increased proportions of cells expressed GFP (>30% GFP+ by day 7 of differentiation), indicating differentiation of ESCs toward the visceral endoderm lineage. Cytometry data from the different hydrodynamic conditions demonstrated both differences in the total number of cells within the gate (45.5 ± 1.6% at 45 rpm compared to 37.6 ± 0.9% at 65 rpm after 7 days of differentiation), as well as differences in the intensity and distribution of expression of GFP expression (geometric mean relative fluorescence values of 956.5 ± 11.6 at 45 rpm compared to 897.0 9.5 at 65 rpm; coefficient of variation of 58.7 ± 1.0 at 45 rpm and compared to 64.7 ± 0.6 at 65 rpm) (Fig. 3-7 A). Quantification of the proportion of GFP+ cells over time also demonstrated a greater number of GFP+ cells after 7, 10 and 14 days of differentiation in the 45

rpm rotary condition compared to 65 rpm (Fig. 3-7 C). Additionally, as the exterior visceral endoderm cells have been reported to direct mesoderm differentiation via paracrine signaling [225], the development of spontaneous contractile foci, indicative of cardiomyocyte differentiation, was quantified (Fig. 3-7 D). Consistent with the increase in visceral endoderm, there was a significant increase in the proportion of EBs maintained at 45 rpm that exhibited contractile foci after 10, 12, and 14 days of differentiation (46.8% at 45 rpm compared to 2.4% at 65 rpm after 10 days of differentiation). Overall, the relative efficiencies of differentiation toward visceral endoderm and cardiomyogenic phenotypes were altered due to perturbations in the hydrodynamic culture environment.

3.4 Discussion

The results of this study demonstrate the ability to systematically decouple various parameters (EB size, formation, and differentiation) which can be modulated by complex hydrodynamic environments, in order to examine the impact on ESC differentiation. This study and others establish the ability to reproducibly control the initial size of EBs by forced aggregation methods in scalable formats [243, 253, 23, 219, 142, 335]. The combination of micro-well formation of EBs with maintenance in rotary orbital suspension permits the prolonged culture of uniform EBs within a range of hydrodynamic environments, enabling increased standardization of scalable differentiation protocols. Recent studies discuss the modulation of ESC differentiation as a function of EB size [220, 142, 23, 22], and are consistent with similar reports demonstrating changes in stem and progenitor cell differentiation as a result of cytoskeletal organization and localization of cells within 3D aggregates [276, 331]. Bauwens et al reported that modulation of EB size alters the proportion of endoderm on the exterior surface of the EB, which results in increased mesoderm differentiation within EBs due

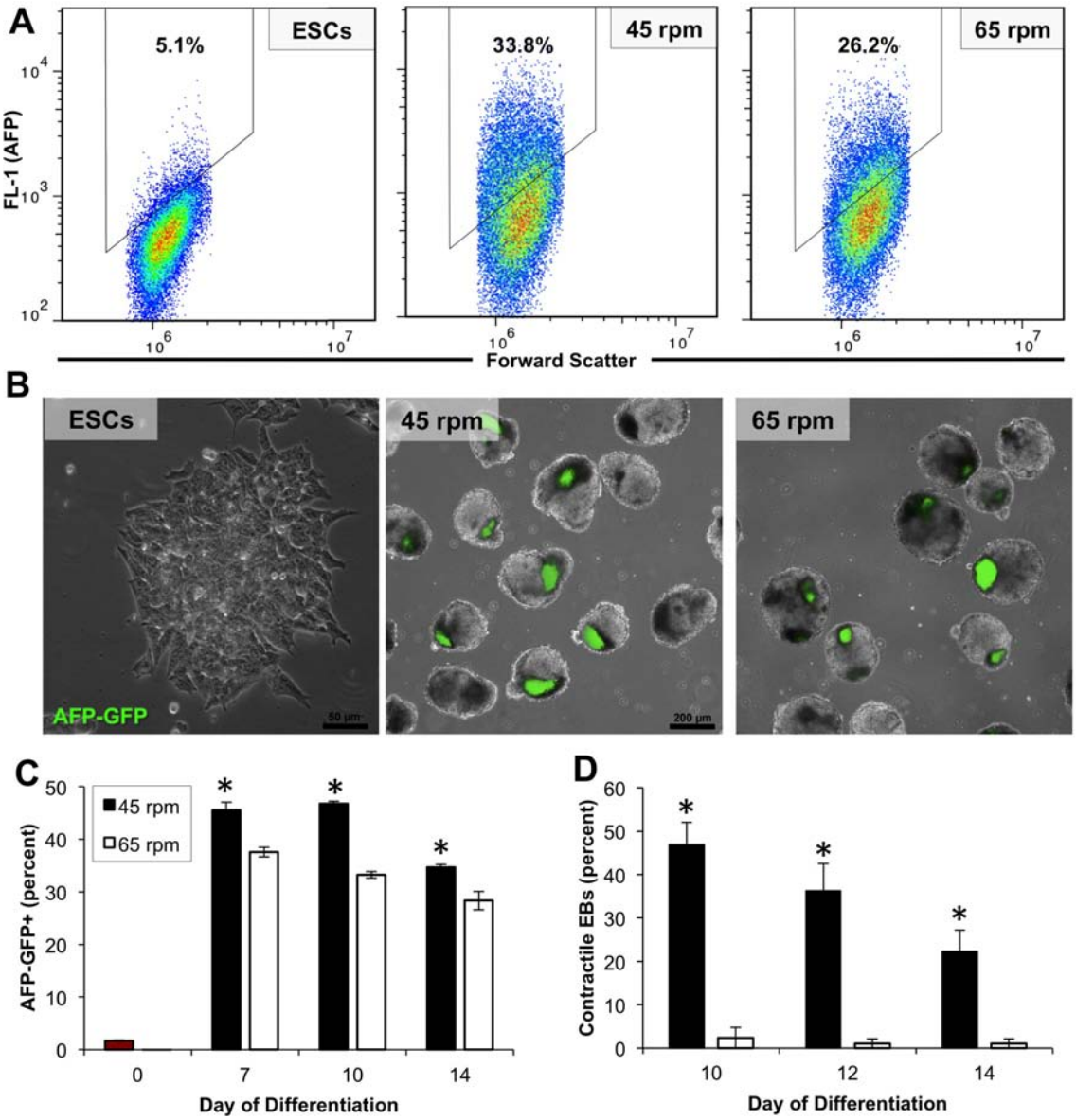

Figure 3-7: Modulation of visceral endoderm and cardiac mesoderm differentiation in response to rotary orbital culture. (A) AFP-GFP transduced ESCs exhibited few GFP+ cells when maintained as an undifferentiated monolayer; however after 14 days of differentiation, EBs from rotary orbital cultures increased expression of GFP (AFP), with (B) EBs cultured at 45 rpm consistently exhibiting increased expression of GFP+ cells after 7, 10 and 14 days of differentiation. (C) Within EBs, the GFP+ cells appeared to cluster in distinct areas, which co-localized with dark regions visualized under phase (overlay) (scale bars = 50 μm, 200 μm). (D) The proportion of EBs exhibiting spontaneous contractile activity was increased following culture 45 rpm compared to 65 rpm after 10, 12, and 14 days of differentiation. * $p<0.05$.

to paracrine signaling [22]. The system developed and discussed in this study permits the formation of EBs with a desired initial size, and maintenance of relative EB size over time, which may be an important factor capable of aiding or hindering differentiation toward distinct cell lineages.

Computational fluid dynamic modeling to determine the shear profiles within rotary orbital cultures previously demonstrated that between cultures at 40 rpm and 55 rpm, there is an increase of approximately $1 dyn/cm^2$ within the central region of the plate traversed by EBs during the rotation, indicating changes in the fluid shear environment due to modulation of rotary orbital speed [282]. The data presented here demonstrate that pre-formed EBs can be maintained at higher rotational frequencies, up to 65 rpm, which were previously reported to not support spheroid formation from single cells [282]. Consistent with previous reports, decreased rotary speeds result in larger EBs, due to the agglomeration of individual pre-formed EBs [282, 52], indicating that a hydrodynamic threshold (apparently near 45 rpm) may be necessary to maintain homogeneous populations of individual EBs. Similarly, studies have demonstrated decreased size of multicellular aggregates at higher mixing speeds [282, 52, 68, 291], presumably due to modulation of cell collision frequencies, as well as by perturbation of the kinetics of E-cadherin binding [166]. Although it remains possible that hydrodynamics may modulate the growth kinetics of ESCs within EBs, the lack of observed differences in EB size and the average number of cells per EBs over 14 days of differentiation suggest that homogeneous populations of EBs can be maintained within different hydrodynamic conditions.

In the context of the present and past experiments, it is difficult to separate the effects of fluid shear and transport on EBs within hydrodynamic environments. In monolayer culture of ESCs, fluid shear has been reported to impact hematopoietic and endothelial differentiation [211, 371, 345, 361, 5]. However, the response to fluid shear in 3D cultures is more complex and much less defined. The work herein

demonstrates that the modulation of hydrodynamic environments in size-controlled, three-dimensional cultures do not appear to dramatically impact overall morphogenesis or the gene expression profile of differentiating ESCs within EBs. It is important to note that, within the context of this study, a relatively small set of genes and phenotypes were analyzed, and it remains possible that there may be differences in other phenotypes that were not directly examined. Additionally, although dramatic changes in global expression patterns were not apparent, the subtle changes in gene expression exhibited due to hydrodynamic conditions may significantly impact cell specification. Interestingly, there was a change in the relative quantities of visceral endoderm cells, with 45 rpm conditions exhibiting an overall increase in visceral endoderm differentiation compared to 65 rpm. As fluid shear is expected to more directly impact the exterior of EBs, it is likely that visceral endoderm differentiation may be responsive to fluid shear mechanotransduction at the EB surface. Additionally, EBs cultured at 65 rpm exhibit significantly increased expression of diaphanous homolog 2 (Diap2), which is involved in microtubule organization and cell-cell contacts, thus indicating changes in cytoskeletal organization, which is a characteristic response to fluid shear in other cell types [108, 188].

This work also highlights shifts in the temporal kinetics of differentiation in hydrodynamic environments. The mixing conditions in bioreactors may have implications for paracrine signaling and for the delivery of exogenous soluble factors, due to changes in transport and receptor-ligand binding kinetics in hydrodynamic environments. Mixing may potentially impact the transport of nutrients, metabolites, and exogenous factors within the EB microenvironment. It is possible, therefore, that the influence of hydrodynamic cultures may be altered by using chemically defined media formulations, or by the addition of soluble factors to promote the endogenous differentiation of ESCs. Additionally, gradients of oxygen may arise as EBs reach a

critical size limit (∼300 μm in diameter) [295]. Hypoxic conditions have been associated with modulation in β-catenin signaling and cardiomyogenesis [303], as well as with expansion of pluripotent cell populations [214]. Although there may be changes in fluid transport due to modulation of the mixing speeds, the normalization of multicellular aggregate size may attenuate some of the effects of transport seen in previous experiments where EBs were significantly larger at low mixing speeds [52, 282]. In the studies presented, EBs were approximately 300 μm in diameter by day 14 of culture, which indicates that few transport limitations likely arose within the system under the experimental conditions used. The decrease in both EB size and cell yield between days 7 and 14 of differentiation may be in part regulated by such transport limitations, indicating that cellular remodeling may dynamically alter transport within EBs. It is, however, difficult to quantitatively assess changes in transport gradients and availability of soluble factors in the EB microenvironment using traditional bioprocessing technologies. As many protocols rely on tightly controlled signaling of factors at different stages in differentiation, shifts in the temporal kinetics of differentiation may alter the efficacy of some directed differentiation approaches. Ultimately, the control of EB size prior to introduction into large scale hydrodynamic cultures may enable increased standardization, which is necessary for the efficacy and reproducibility of directed differentiation protocols in the context of scalable bioprocessing.

3.5 Conclusions

We have developed a novel culture platform which enables the study of ESC differentiation as 3D multicellular aggregates in hydrodynamic environments, independent of the effects of mixed cultures on EB formation kinetics and size. The results of this study indicate that, despite subtle changes in temporal differentiation toward certain lineages, EBs maintained under different hydrodynamic conditions exhibit similarities in morphogenesis and the overall differentiation profiles of ESCs. These data suggest

that controlling EB formation upstream of hydrodynamic cultures may be amenable to standardization of ESC cultures in scalable suspension formats for bioprocessing applications.

CHAPTER IV

MESENCHYMAL MORPHOGENESIS OF EMBRYONIC STEM CELLS DYNAMICALLY MODULATES THE BIOPHYSICAL MICROTISSUE NICHE[1]

4.1 Introduction

The biochemical composition and physical structure of tissue microenvironments are critical regulators responsible for maintaining and directing stem cell fate and function [288, 222]. *in vivo*, native stem cell niches maintain the self-renewing state through short range soluble signaling[113] and extracellular signals [58], such as direct anchorage via intercellular or matrix adhesions. Conversely, dysregulation of niche elements leads to differentiation and migration of resident stem cell populations [192]. Therefore, the synergy of biophysical and biochemical signals and the complexity of the local microenvironment have been increasingly recognized as critical mediators of the delicate balance between self-renewal and differentiation. However, while engineering approaches often aim to dissect the relative influence of individual stimuli, the signals regulating stem cell differentiation are interrelated, motivating the multiparametric analysis of stem cell structure and phenotype accompanying dynamic cell fate decisions.

The pre-implantation embryo is one of the most dynamic tissue microenvironments, whereby the patterning of structurally and functionally distinct tissue structures, such as liver, skin, and heart arise from adjacent, yet spatially defined, regions during development [319]. In particular, embryonic gastrulation mediates the first

[1]Modified from: MA Kinney, R Saeed, and TC McDevitt. *Mesenchymal morphogenesis of embryonic stem cells dynamically modulates the biophysical microtissue niche.* In press.

somatic cell fate decisions, and results in spatially distinct localization of the three germ lineages endoderm, ectoderm, and mesoderm. During gastrulation, the cells of the epiblast that will comprise the mesoderm lineage undergo a rapid and concerted morphogenesis [43, 64] through which the tightly adherent, epithelial cells become less adhesive mesenchymal cells, in a process known as the epithelial-to-mesenchymal transition (EMT) [322]. The dynamics and patterning of EMT is tightly regulated by the biophysical and biochemical tissue microenvironment, through signals that maintain or abrogate the apical-basal polarity of epithelial cells. While biochemical signals are often implicated in the induction of EMT, the changes in cell shape that occur during gastrulation are a fundamentally biomechanical process, through which forces arising as a result of adhesion remodeling are transmitted via changes in cytoskeletal tension [157].

While the phenotypic and mechanical changes arising during embryonic development have been characterized through orthogonal approaches and in various species, several questions remain regarding the role of cellular biomechanics in determining cell fate, particularly during mammalian embryogenesis. The differentiation of pluripotent embryonic stem cells (ESCs), the *in vitro* analog to the inner cell mass of pre-implantation embryos, parallels many of the cell fate transitions *in vivo*, which highlights the utility of ESCs as a model for systematically studying mammalian embryonic development. ESC differentiation has also traditionally been studied through orthogonal approaches aimed to recapitulate the biochemical and biophysical milieu of the gastrulating embryo, including the perturbation of developmentally relevant signaling pathways [228] and the manipulation of the composition and mechanical properties of adherent substrates [87, 93]. However, when assembled as three-dimensional aggregates, ESCs undergo morphogenic processes, including EMT [302], which establishes a dynamic, cell intrinsic, developmentally relevant system through which to study biomechanics in parallel with changes in cell fate and morphogenesis.

The objective of this study, therefore, was to define the intrinsic cell biophysical characteristics and phenotypic changes that arise simultaneously during the morphogenesis of three-dimensional pluripotent stem cell microenvironments and cell fate specification. An interdisciplinary approach was employed to assess the dynamics of morphogenesis and differentiation via gene expression and histological analyses, as well as biomechanical characterization of 3D microtissue properties, paired with multivariate data modeling to distinguish correlations between the structure and phenotype of EBs. Overall, this study demonstrates that microtissue morphogenesis arises via EMT during mesoderm differentiation and that the dynamic temporal changes in phenotype are highly predicted by biomechanical characteristics. Ultimately, understanding the biophysical changes accompanying epithelial-to-mesenchymal transition of ESCs has broad implications that may inform mammalian embryonic development, as well as physical processes underlying tissue homoeostasis, pathological remodeling and cancer metastasis.

4.2 Materials and Methods

4.2.1 Embryonic stem cell expansion

Pluripotent murine ESCs (D3 cell line) were expanded on 0.1% gelatin coated polystyrene tissue culture treated dishes in Dulbeccos Modified Eagles Medium (DMEM) containing 15% fetal bovine serum (FBS) and supplemented with penicillin (100 U/mL), streptomycin (100 mg), amphotericin (0.25 mg/mL), L-glutamine (2 mM), MEM non-essential amino acid solution (1x), 2-mercaptoethanol (0.1 mM), and leukemia inhibitory factor (LIF; 103 U/mL). Media was exchanged every other day and ESCs were passaged prior to 70% confluence.

4.2.2 Embryoid body formation and culture

A single cell suspension of ESCs was obtained by treatment of monolayer cultures with 0.05% trypsin/0.53 mM EDTA solution. EBs were formed by centrifugation (200 rcf) of ESCs into 400 μm diameter polydimethylsiloxane (PDMS) microwells (AggrewellTM; Stem Cell Technologies), with approximately 1000 cells per well. After 20 hours of microwell formation in serum containing ESC media without LIF, EBs were transferred to suspension culture ($\sim$2000 EBs per dish) and maintained on a rotary orbital shaker platform at 65 rpm, as described previously (Chapter 3). EBs were differentiated in basal serum-free media (N2B27) composed of DMEM/F12 supplemented with N2 (5 μg/ml insulin, 100 μg/ml transferrin, 6 ng/ml progesterone, 16 μg/ml putrescine, 30 nM sodium selenite) and 50 μg/mL bovine serum albumin (BSA), combined 1:1 with NeurobasalTM media supplemented with B27 [364]. Antibiotics and L-glutamine were supplemented at the same concentrations as the undifferentiated ESC media. 90% of EB media, including growth factor supplements, was exchanged every other day by gravity-induced sedimentation of EBs. Mesoderm induction was accomplished, as detailed in the results, by supplementation with 10 ng/mL BMP-4 (R&D Technologies) [266]. Perturbation of the cytoskeleton was accomplished by 1-hour treatment with inhibitor of the Rho-associated protein kinase (ROCK) pathway (Y27632; 10 μM) [145] or by supplementation of the media between days 4-7 of differentiation with Y27632, Jasplakinolide (Jas, 50 nM) [358], or Latrunculin B (LatB, 100 nM) [340]. DMSO ($\leq$0.1%) was also included as a vehicle control.

4.2.3 Parallel plate mechanical compression

The bulk mechanical properties of microtissues were measured using a micron-scale mechanical testing system (Microsquisher; CellScale), which calculates force via measurement of beam deflection in response to user-defined displacements (Fig. 4-4 A).

All samples were tested in a PBS fluid bath (pH 7.4, containing 0.90 mM Ca^{2+} and 0.49 mM Mg^{2+}). The cantilever beams were composed of Tungsten (modulus = 411 GPa), and beams of diameters from 76.2 μm to 152.4 μm were employed, depending on the stiffness and sensitivity required for each aggregate.

To determine the bulk physical characteristics of EBs, a viscoelastic creep method was employed, which exerts a constant force while measuring the changes in displacement over time (Fig. 4-4 B). The magnitude of force was chosen as the average force corresponding to approximately 40% strain, determined based upon constant strain rate analysis of stress versus strain in n=3 samples. The time to relaxation was determined to be less than two minutes, which was established based upon empirical testing. The creep parameter was calculated as the percent increase in displacement during constant force interval (Fig. 4-4 C). Relevant physical characteristics, including moduli (instantaneous modulus, E_o; relaxed modulus E_∞), time constants (creep time constant, τ_σ; stress relaxation time constant, τ_ϵ), and apparent viscosity (μ) were calculated based upon a linear viscoelastic model of creep displacement (u) behavior over time, described in equations 1 - 3, where R_o is the initial EB diameter, the stress (σ) is calculated as the constant force normalized to relaxed cross sectional EB area, and H(t) is a unit step function [247].

$$u(t) = \frac{4\sigma R_o}{3E_\infty}\left[1 + \left(\frac{\tau_\epsilon}{\tau_\sigma} - 1\right)e^{\frac{-t}{\tau_\sigma}}\right]H(t) \tag{1}$$

$$E_o = \frac{\tau_\sigma}{\tau_\epsilon}E_\infty \tag{2}$$

$$\mu = \tau\left(E_o - E_\infty\right) \tag{3}$$

4.2.4 Quantitative real time PCR

RNA was extracted from EBs using the RNeasy Mini kit (Qiagen Inc, Valencia, CA) and cDNA was synthesized using the RT2 First Strand Kit (SABiosciences, Frederick, MD) with 900 ng of total RNA. To assess gene expression, a custom RT^2 Profiler^{TM} PCR Array (SABiosciences) was used in conjunction with a MyIQ iCycler (Bio-rad) and SYBR green master mix (information). The array consists of 26 genes relevant to pluripotency and differentiation toward all three germ lineages, as well as 3 house-keeping genes (*Actb*, *GAPDH*, *Hsp90ab1*) and PCR efficiency controls. Alternatively, quantitative real time PCR was performed using primers for the hyaluronan synthase isoforms (*HAS-1*, *HAS-2*, and *HAS-3*), which were designed using Beacon Designer software [302]. PCR data were normalized to geometric average of the three house-keeping genes and fold changes in expression were calculated from normalized Ct values, relative to expression in ESCs [262]. The Genesis software package was used to generate heatmap visualizations of the gene expression data.

4.2.5 Histology and immunohistochemistry

EBs sampled from rotary orbital culture were rinsed in PBS and fixed with 10% formalin (4% paraformaldehyde) for 45 minutes with rotation at room temperature. Fixed EBs were embedded within Histogel (Richard Allen Scientific), and processed through a series of ethanol and xylene rinses prior to paraffin embedding. Paraffin embedded EBs were sectioned with a thickness of 5 μm using a rotary microtome (Microtom HM310) and mounted on slides. Sections were deparaffinized prior to staining via ethanol and xylene rinses and subsequently stained with hematoxylin and eosin, alcian blue (pH 2.5; nuclear fast red counterstain) or safranin-O (fast green counterstain).

Alternatively, for immunohistochemistry, slides were blocked in 1.5% normal goat

serum (NGS) for 1 hour at room temperature, incubated in mouse monoclonal anti-human smooth muscle actin (α-SMA) primary antibody (Dako; clone 1A4) for 1 hour, and subsequently incubated in biotinylated donkey anti-mouse IgG (1:400, Vector Labs). Slides were then incubated with avidin and biotin-based horseradish peroxidase, based on manufacturer instructions (Elite Vectastain Kit, Vector Labs) and developed using a 3, 3-diaminobenzidine (DAB) substrate (Vector Labs). Nuclei were counterstained with hematoxylin. After staining, slides, were cover slipped and imaged using a Nikon 80i upright microscope. Sections of mouse intestine, cartilage, and heart, were included as positive control for alcian blue, safranin-O, and α-SMA, respectively.

4.2.6 Whole mount immunostaining

For whole mount immunostaining, formalin fixed EBs were blocked and permeabilized in 2% BSA/0.1% Tween-20, containing 1-1.5% Triton X-100 for 30 minutes at 4°C with rotation, re-fixed in formalin for 15 minutes and blocked for an additional 3 hours. EBs were then stained with Alexa Fluor 546 phalloidin (1:40, Molecular Probes), counterstained with Hoechst (10 μg/mL) and imaged using a Zeiss LSM 710 Confocal microscope.

4.2.7 Scanning electron microscopy

For ultrastructural analysis, EBs were fixed in 2.5% glutaraldehyde in cacodylate buffer (pH 7.2) for 1-2 hours, followed by rinses in buffer. The samples were subsequently incubated in 1% osmium tetroxide for 1 hour, followed by rinses in water and dehydrated through a series of graded acetone rinses (60 min each) from 25-100%. Prior to imaging, EBs were dried using a Polaron E3000 critical point dryer, adhered to an aluminum stub using double sided carbon adhesive tape and gold coated using a Polaron range sputter coater (120 s at 2.2 kV). Scanning electron microscopy (SEM) was conduced using a Hitachi S-800 microscope.

4.2.8 Multivariate partial least squares regression (PLSR) modeling

A data matrix (MxN) was constructed with M culture conditions (Jas, LatB, etc), and N experimental parameters (*Oct-4*, *Nanog*, modulus, etc), where each column of the independent X (input) matrix represents a unique gene expression signal and the dependent variables in the Y (output) matrix represent mechanical properties. All data were mean-centered and scaled to unit variance and SIMCA-P (Umetrics) was employed to construct the PLSR model using a nonlinear iterative partial least squares (NIPALS) algorithm [116]. Predictions were determined based on cross-validation, with standard error of predicted values determined via jack-knifing, and the predictability was calculated from the root mean squared error of estimation (RMSEE) [254].

4.2.9 Statistical analysis

All experiments were conducted with replicate data are represented as the mean of n=3-6 independent replicates +/- standard error. Prior to statistical analysis, all data were pre-processed using a box-cox power transform, in order to normalize data according to a Gaussian distribution. Statistical tests were conducted between groups and time points using one-way or two-way ANOVA, combined with either a post-hoc Tukey or Mann-Whitney U test for comparison of individual samples, depending on the results from Levenes equality of variances test.

4.3 Results

4.3.1 Biochemical induction of mesoderm differentiation in ESC microtissues

Homogeneous populations of EBs were formed via forced aggregation and maintained in controlled hydrodynamic suspension culture, as described previously (Chapter 3), in order to systematically examine three-dimensional stem cell morphogenesis. EBs

remained uniform in size and homogeneous across populations through the initial 4 days of differentiation (Fig. 4-1 A); however, EBs cultured in basal, serum-free culture conditions lost the characteristic uniform, spherical structure and adopted EB morphologies with less smooth exterior appearances by 7 days of differentiation. Moreover, supplementation with BMP4 (10 ng/mL) led to the appearance of distinctly polarized regions exhibiting different opacities within individual EBs after 14 days of differentiation. In addition, supplementation with BMP4 altered the overall gene expression profile, resulting in increased expression genes related to mesoderm lineages at days 4 and 7 of differentiation compared to those maintained in basal, serum-free culture conditions (Fig. 4-1 B). Although, the pluripotency markers *Sox2* and *Oct-4* were not significantly different between the two culture conditions, markers of hematopoietic mesoderm (*Gata2*, *Hba-x*) were increased by BMP4 treatment (*Gata2* p=0.07; Hba-x p=0.03), and genes related to endoderm (*Foxa2*) and ectoderm (*Fgf5*) were significantly increased (*Foxa2* p=0.04; *Fgf5* p=0.004) in basal conditions, thereby illustrating the morphogenic influence of BMP4 in directing mesoderm differentiation in 3D cultures, analogous to previous reports using monolayer differentiation techniques [150, 191].

4.3.2 Mesenchymal morphogenesis of ESCs during 3D mesoderm differentiation

Consistent with the gross changes in EB morphology, distinct differences in cellular morphology and organization within EBs were observed during the course of differentiation, in a soluble factor-dependent manner (Fig. 4-2). While EBs within both conditions exhibited similarly homogenous epithelial populations initially, biochemical-mediated differentiation led to changes in cellular organization and morphogenesis, with basal EBs continuing to exhibit tightly packed, epithelial cell morphologies, in contrast to BMP4-treated EBs, in which populations of elongated, mesenchymal-like cells were apparent by 7 days of differentiation (Fig. 4-3 A). In addition, BMP4 treated

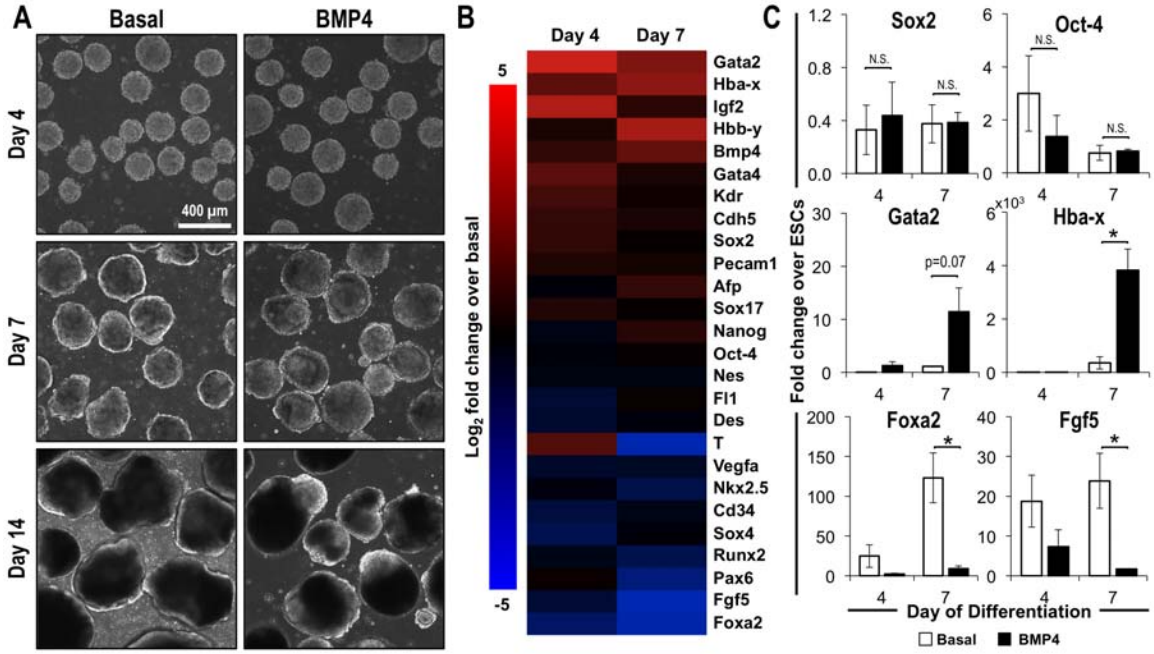

Figure 4-1: Induction of mesoderm differentiation within EBs via BMP4 treatment. (A) Phase contrast images demonstrate similar gross morphology of EBs cultured in basal, serum-free media or media supplemented with BMP4 after 4 days of differentiation, with differences apparent at 7 and 14 days of differentiation. (B) Gene expression profiles also differed between EBs cultured in different soluble culture environments after 4 and 7 days of differentiation, resulting in similar levels of pluripotency factors, with divergent expression of markers for hematopoietic mesoderm (*Gata2*, *Hba-x*), endoderm (*Foxa2*), and ectoderm (*Fgf5*). Scale bar = 200 μm; n = 3; * = p$\leq$0.05

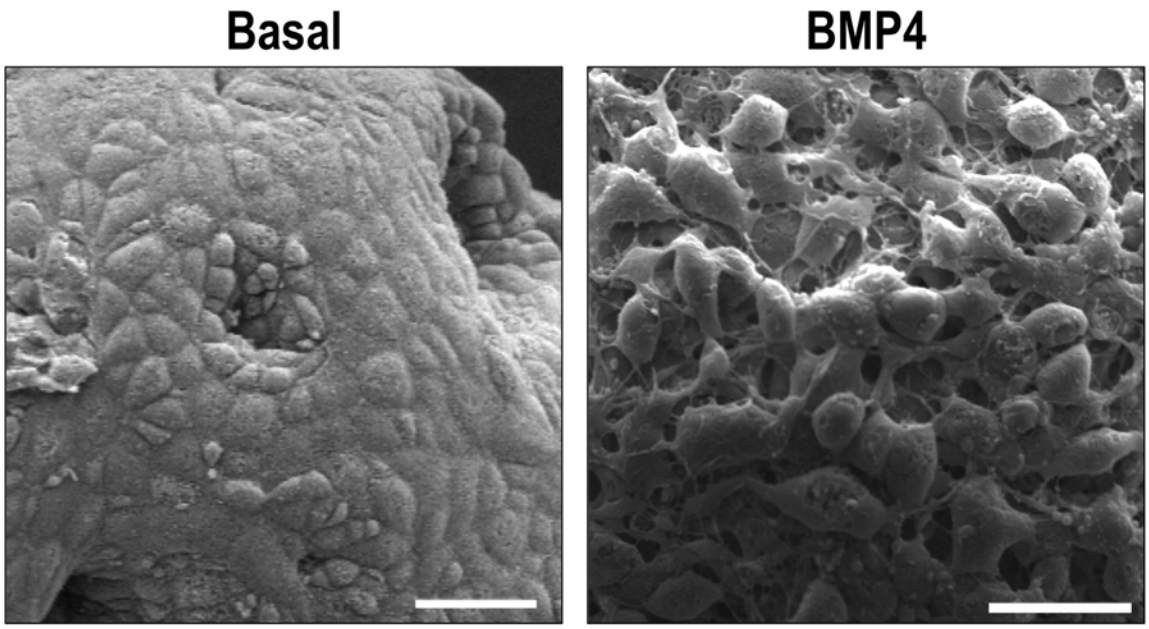

Figure 4-2: Mesenchymal EB ultrastructure. Cells at the exterior of EBs exhibited dramatically different morphologies, with basal EBs exhibiting more tightly packed, epithelial-like cells, in contrast to the mesenchymal morphology of cells at the exterior of BMP4-treated EBs. Scale bars = 20 μm.

EBs exhibited deposition of a non-sulfated glycosaminoglycan (GAG) rich matrix, as evidenced by positive alcian blue (pH 2.5) and negative safranin-O staining within the interstitial space between cells exhibiting mesenchymal morphologies (Fig. 4-3 B). The putative mesenchymal cells also expressed α-smooth muscle actin (α-SMA), a hallmark of EMT. In addition to the increased deposition of non-sulfated GAGs, EBs also exhibited increased expression of the hyaluronan synthetase (HAS) isoforms during the course of differentiation, with significantly increased expression of *HAS-2* (day 4 p=0.001; day 7 p=0.003) in BMP4-treated EBs (Fig. 4-3 C). Taken together, EBs differentiated toward mesoderm lineages via BMP4 treatment undergo EMT-like morphogenic processes to yield characteristic mesenchymal cell populations.

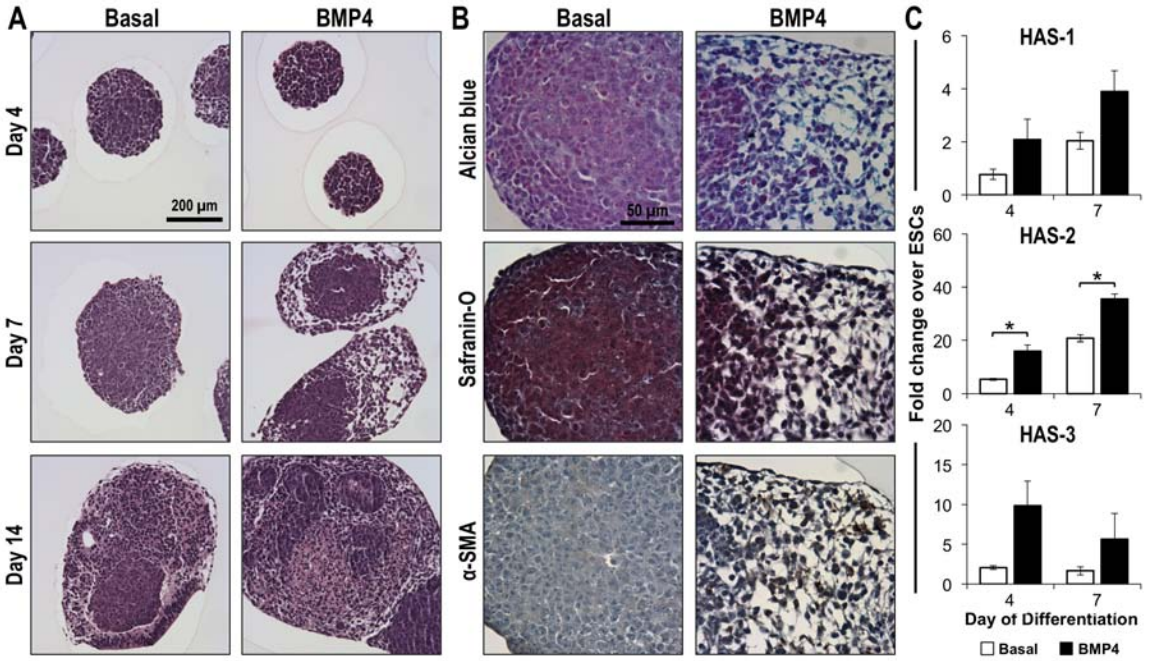

Figure 4-3: Mesenchymal morphogenesis of ESCs within EBs. (A) EBs exhibited dynamic remodeling of the microenvironment through 14 days of differentiation, with distinct differences apparent between EBs in different soluble media formulations. (B) After 7 days of differentiation, mesenchymal-like regions within EBs exhibited positive staining for alcian blue and α-SMA, whereas safranin-O stained positively within epithelial-like regions and was largely absent within the mesenchymal-like regions of BMP4-treated EBs. (C) EBs also exhibit increasing expression of genes related to hyaluronan synthetase isoforms, with increased expression in BMP4-treated EBs. Scale bars (A) = 200 μm, (B) = 50 μm; n = 3; * = p$\leq$0.05.

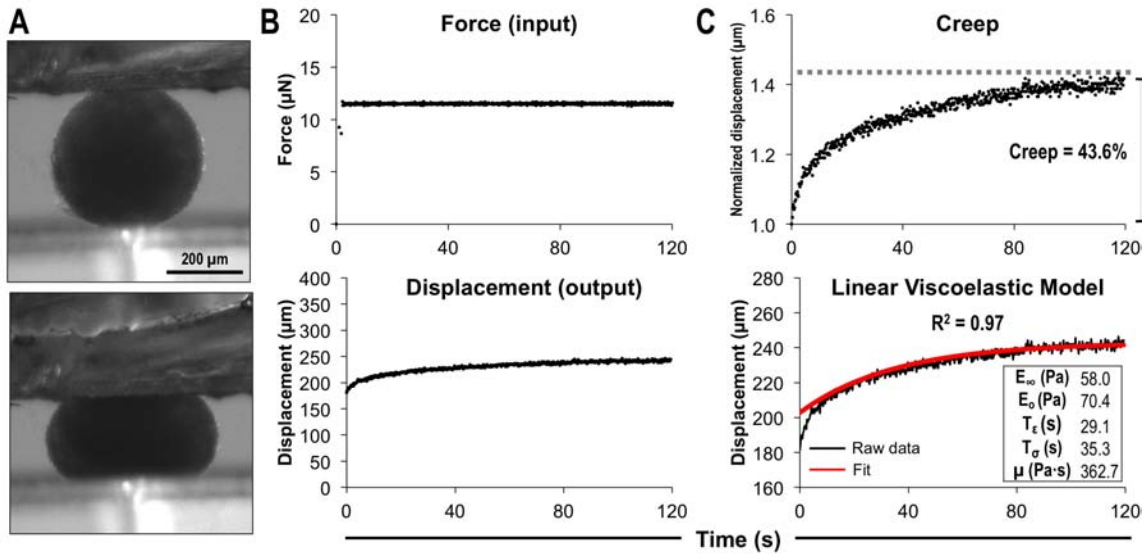

Figure 4-4: Mechanical testing methods. (A) Mechanical testing of EBs was accomplished through parallel plate compression, in which (B) the displacement was measured over time under constant force. (C) The resultant creep curves enable calculation of viscoelastic properties, including characteristic creep displacement, as well as parameters determined from the fit to a linear viscoelastic model. Scale bar = 200 μm.

4.3.3 Dynamic changes in biophysical microtissue characteristics during ESC differentiation

To characterize the physical remodeling of the microenvironment during the ESC differentiation, the biomechanical microtissue properties were measured via micron-scale parallel plate compression (Fig. 4-4 A). Descriptive physical characteristics, including moduli, were calculated by measuring the viscoelastic creep (change in deformation under constant force), which was well described by a linear viscoelastic model (average $R^2 = 0.97$; Fig. 4-4 B&C).

EBs treated with BMP4 exhibited increased viscous responses (p=0.0003), or an increased resistance to deformation, as evidenced by decreased creep deformation compared to those differentiated in basal conditions at day 7 of differentiation (Fig. 4-5 A). In addition, BMP4-treated EBs were significantly stiffer than basal EBs, with a 1.5 fold increase in modulus (p=0.004) after 7 days of differentiation (Fig. 4-5 B).

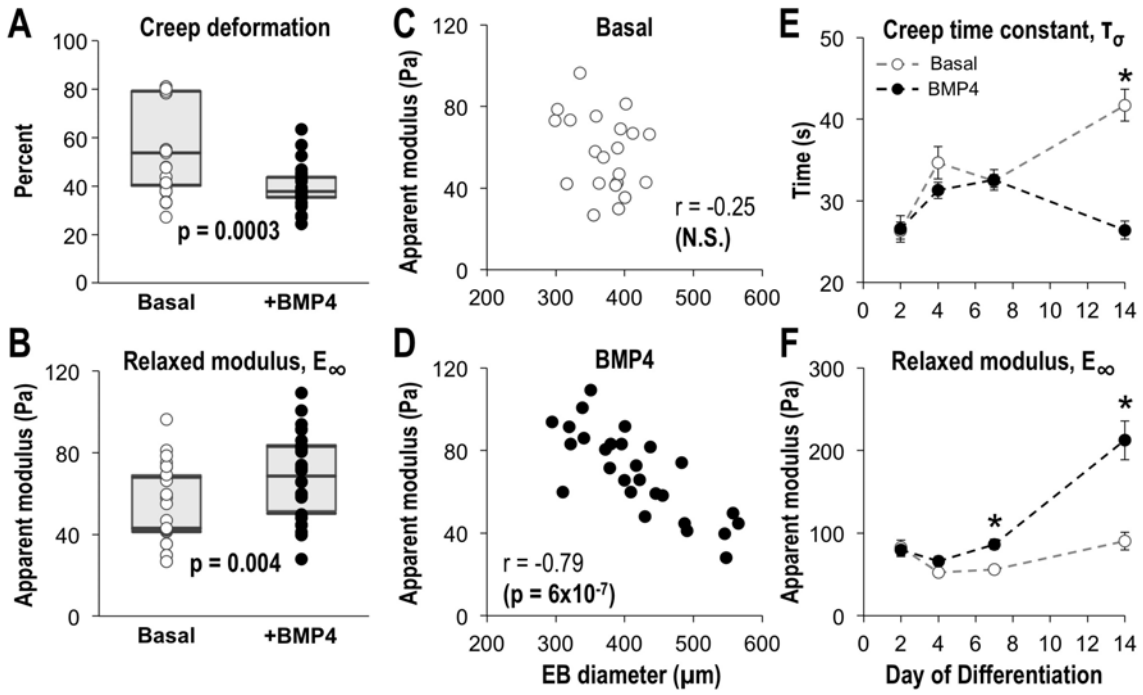

Figure 4-5: Dynamic modulation of EB mechanical properties. (A) EBs exhibit differences in viscoelastic creep and modulus after 7 days of differentiation, including (B) a significant correlation between modulus and EB diameter within BMP4-treated EBs. In addition, modulus and viscoelastic time constant characteristics were modulated as a function of time, with differences between culture conditions after 14 of differentiation. n=6; * = $p \leq 0.05$.

Therefore, EBs exhibiting distinct morphological characteristics also exhibited distinct biomechanical changes, both in terms of viscoelasticity and microtissue stiffness. Interestingly, while the stiffness and size of basal EBs were not correlated (Fig. 4-5 C), those differentiated with BMP4 demonstrated an inverse relationship ($p \leq 0.001$), with smaller BMP4 treated EBs exhibiting increased stiffness (Fig. 4-5 D). In addition to the increased population stiffness of BMP4 treated EBs, the correlation between size and stiffness suggests a relationship between the extent of morphogenesis and biomechanical characteristics, thereby providing single EB metrics to assess population heterogeneity.

Moreover, the biomechanical characteristics of EBs were dynamically modulated during the course of differentiation, whereby significant differences in the stiffness and

viscosity were observed over time, both within and between individual biochemical differentiation conditions (Fig. 4-5 E&F and Fig. 4-6). Specifically, basal conditions exhibited decreased stiffness between days 2 and 4 of differentiation ($p=0.04$), whereas BMP4-treated EBs exhibited similar stiffness through day 7 of differentiation; the stiffness of EBs both conditions was significantly increased at day 14 compared to day 4 (basal $p=0.01$; BMP4 $p\leq0.001$), thus indicating an overall increase in stiffness during differentiation in both conditions. Both conditions also exhibited similar initial viscosity dynamics, whereby the viscous response decreased (increasing deformation time, or creep time constant) during the initial 7 days of differentiation (basal $p=0.04$; BMP4 $p=0.04$); however, the viscosity of basal conditions continued to decrease through day 14 of differentiation, whereas the viscosity of BMP4-treated EBs increased over the same time frame, resulting in significantly increased viscosity of BMP4-treated EBs compared to basal EBs ($p\leq0.001$). Overall, the biomechanical ESC microenvironment is dynamically modulated during differentiation, whereby BMP4-treated EBs stiffen and increase viscosity as cells commit toward mesoderm lineages and undergo EMT.

4.3.4 Cytoskeletal regulation of biophysical microtissue environments

The actomyosin cytoskeleton is one of the main structural components of cells, and is particularly important in mediating cell shape, force generation, and stiffness in embryonic tissues [374]. However, the role of cytoskeletal tension in cell fate specification during three-dimensional morphogenesis and differentiation remains unclear. The actin filament organization of basal serum-free EBs appeared largely cortical in structure at all stages of differentiation, consistent with the epithelial cellular morphology; however, BMP4-treated EBs exhibited decreased assembly of F-actin, with the cortical structures being less continuous after 4 days of differentiation (Fig. 4-7). Moreover, consistent with the mesenchymal morphology, cells within BMP4-treated

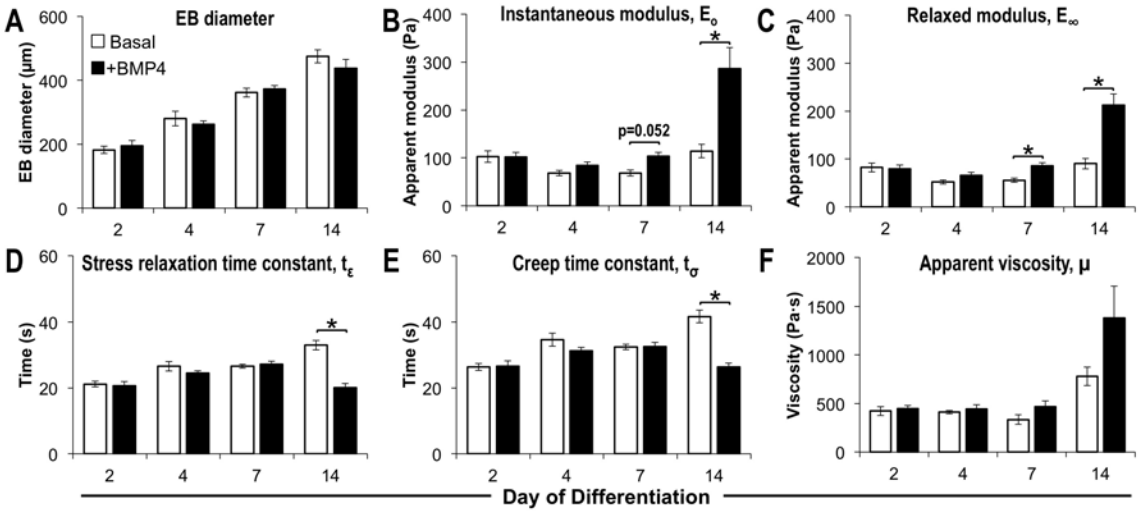

Figure 4-6: Mechanical characterization. (A) Although EB diameter was not significantly modulated by culture environment, treatment with BMP4 resulted in increased (B) instantaneous and (C) relaxed moduli after 7 and 14 days of differentiation, as well as decreased (D) stress relaxation and (E) creep time constant. (F) The apparent viscosity increased over time, but was not modulated by culture condition. n=6; * = $p \leq 0.05$.

EBs exhibited thicker stress fibers with localization throughout the cytoplasm by day 7 of differentiation. The observed modulation of cytoskeletal architecture during three-dimensional ESC differentiation, therefore, motivates a more systematic analysis of the role of cytoskeleton in mediating tissue stiffness during EB morphogenesis (Fig. 4-8 A). Disruption of the Rho associated protein kinase (ROCK) pathway with a small molecule inhibitor (Y27632; 10 μM; 1 hour) [145] decreased the stiffness of EBs from both differentiation conditions and across all time points ($p \leq 0.03$ in all conditions), indicating that active cytoskeletal elements significantly contribute to the stiffness of EBs ($\sim$50%) (Fig. 4-8 B&C). In addition, despite similar overall stiffness, the active cytoskeleton of BMP4-treated was stiffer compared to basal EBs after 2 days of differentiation ($p \leq 0.001$), demonstrating unique biophysical characteristics at early stages of differentiation, even before morphological or phenotypic changes were

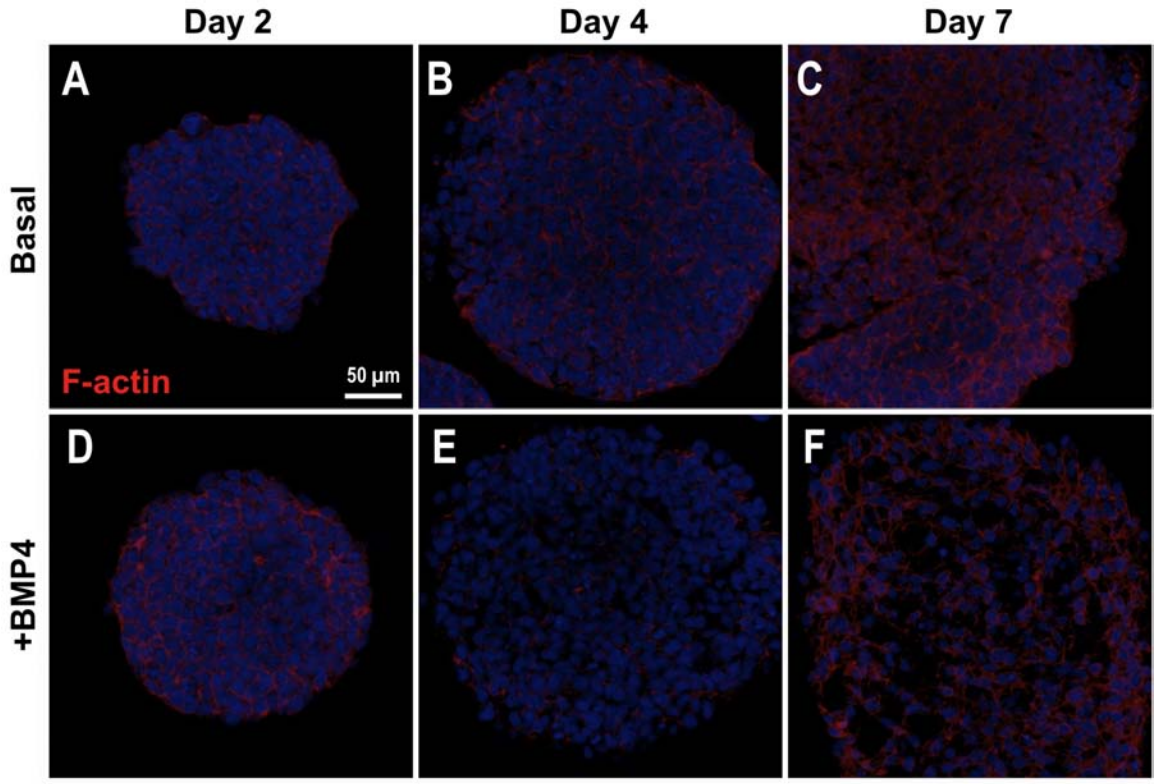

Figure 4-7: F-actin localization within EBs during differentiation. EBs displayed largely cortical F-actin structures, which were dynamically remodeled during the course of differentiation after 2 (A&D), 4 (B&E), and 7 (C&F) days of differentiation in basal, serum free cultures (A-C) or upon soluble treatment with BMP4 (D-F). Scale bar = 50 μm.

observed (Fig. 4-8 D). Moreover, the relative contribution of active cytoskeletal tension to the overall modulus decreased during the differentiation of BMP4-treated EBs, suggesting the decreasing influence of the cytoskeleton at later stages of mesenchymal morphogenesis. Together, the filamentous actin cytoskeletal structure is remodeled during mesenchymal morphogenesis and active cytoskeletal tension significantly contributes to ESC microtissue stiffness, which suggests a role for the cytoskeleton in mediating the observed changes in biomechanical characteristics during mesoderm differentiation and mesenchymal morphogenesis.

While the static cytoskeletal structure directly mediates tissue stiffness, the dynamics of actin polymerization has also been implicated in morphogenic processes,

such as EMT [118]. Therefore, the cytoskeletal dynamics were perturbed via treatment with an agonist (Jasplakinoide, Jas) [358] or antagonists (latrunculin B, LatB; Y27632) [340] during ESC morphogenesis in order to assess the impact on biomechanics, morphogenesis, and cell phenotype (Fig. 4-8 E). BMP4-treated EBs exhibited decreased viscosity in response to the cytoskeletal mediators, whereby treatment with Jas and Y27632 significantly increased creep deformation, compared to both untreated (Jas $p \leq 0.001$; Y27632 $p=0.01$) and basal (Jas $p \leq 0.001$; Y27632 $p=0.003$) EBs (Fig. 4-8 E); in contrast, the viscous response of basal EBs remained similar across all conditions. The kinetics of the viscous response, in terms of the creep time constant, was increased by treatment with Y27632 in both conditions (Fig. 4-8 F), which suggests differences in the magnitude and kinetics of the viscous response upon cytoskeletal perturbation. In addition, Jas increased the stiffness of EBs cultured in basal, serum-free media compared to untreated EBs, consistent with its known role in mediating actin polymerization ($p \leq 0.001$); however, the stiffness of BMP4-treated EBs was not affected by Jas (Fig. 4-8 F). In contrast, Y27632 significantly decreased the stiffness of BMP4 EBs compared to untreated conditions ($p \leq 0.001$), but did not affect EBs differentiated in basal conditions. Interestingly, although LatB has been reported to decrease actin polymerization, BMP4-treated EBs were significantly stiffer when cultured in LatB compared to untreated EBs ($p \leq 0.001$). Together, compounds implicated in altering the dynamics of cytoskeletal tension and actin polymerization significantly altered the biomechanical characteristics of microtissues during differentiation and morphogenesis of ESCs.

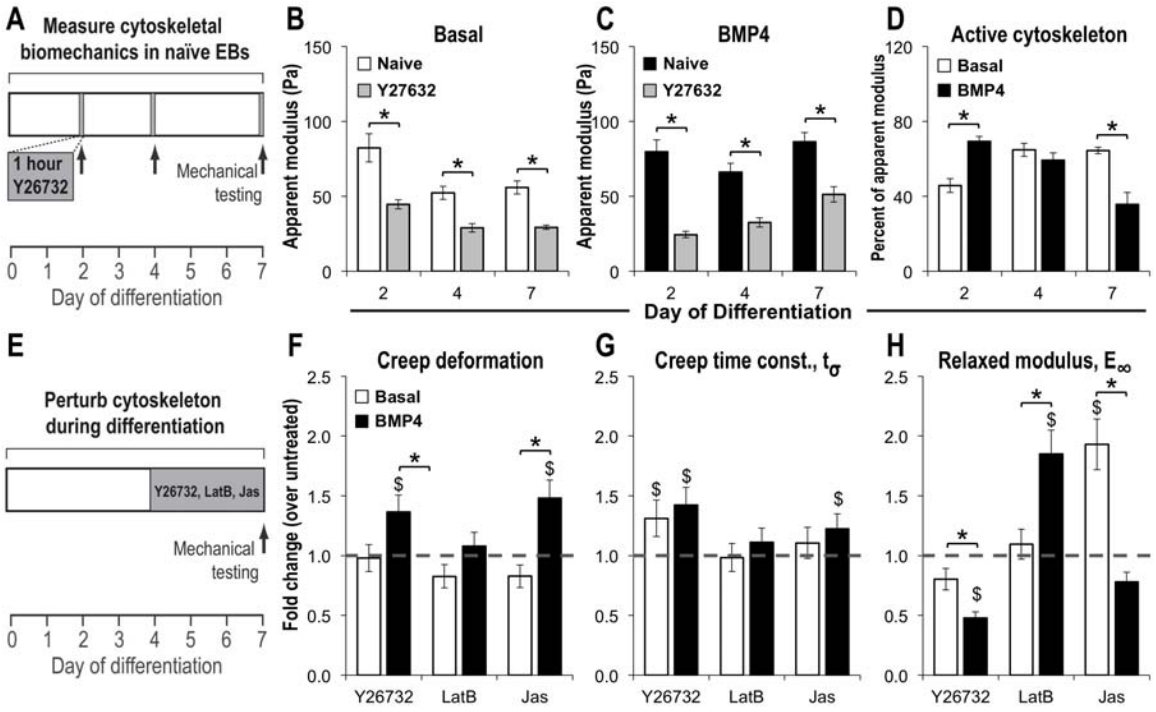

Figure 4-8: Influence of cytoskeletal tension on EB mechanical properties. Treatment of EBs with the ROCK inhibitor Y27632 for 1 hour significantly decreased the modulus of (A) basal and (B) BMP4-treated EBs and (C) demonstrated differences in the relative contribution to the overall naive EB modulus at 2 and 7 days of differentiation. In addition, EBs were differentiated in the presence of (D) cytoskeletal agonists and antagonists, and exhibited changes in the (E) viscoelastic creep response and (F) modulus after 7 days of differentiation. n = 6; * = p≤0.05 compared to basal; $ = p≤0.05 compared to untreated.

4.3.5 Biomechanics predict microtissue phenotypic profiles

The impact of biomechanical forces on stem cell phenotype has been increasingly appreciated as an exogenous means to direct cell fate [93, 279, 215]; however, a quantitative relationship between ESC phenotype and biophysical properties of three-dimensional microtissues has not been established. Therefore, the morphology and phenotype of ESCs were assessed in parallel with the changes in microtissue stiffness upon treatment with small molecules. The cytoskeletal agonist and antagonists did not induce marked morphological changes, based on gross histology (Fig. 4-9); however, subtle differences were noted, as LatB-treated BMP4 EBs exhibited more epithelial-like cells, similar to basal EBs (Fig. 4-9 S), whereas Jas and Y27632 treatment induced more mesenchymal morphogenesis within BMP4 EBs (Fig. 4-9 Q,R).

In addition, treatment with the small molecules altered the gene expression profiles of both basal and BMP4 EB populations after 7 days of differentiation; hierarchical clustering indicated marked phenotypic differences for Jas treated EBs from both conditions relative to untreated EBs (Fig. 4-10). Similarly, a PLS model (R^2Y=0.70, Q^2=0.10; 3 significant PCs) illustrated the variance in gene expression signatures due to BMP4 treatment and cytoskeletal perturbations, which were distinctly separated along the first and second principal components, respectively (Fig. 4-10); although the biochemical morphogen treatment in the presence or absence of BMP4 dominated the phenotypic gene expression, subtle variations in the phenotypic profile were induced by cytoskeletal perturbations, thereby indicating the utility of PLS modeling for capturing variations not detectable through traditional analytical methods, such as hierarchical clustering. Consistent with the histological observations, LatB-treated EBs exhibited phenotypic profiles indicative of decreased EMT, similar to basal EBs, whereas Jas-treated BMP4 EBs exhibited increased mesoderm differentiation and mesenchymal morphogenesis, as evidenced by the position along the first principal component. Increased expression of pluripotency genes such as *Nanog*, *Sox-2*, and

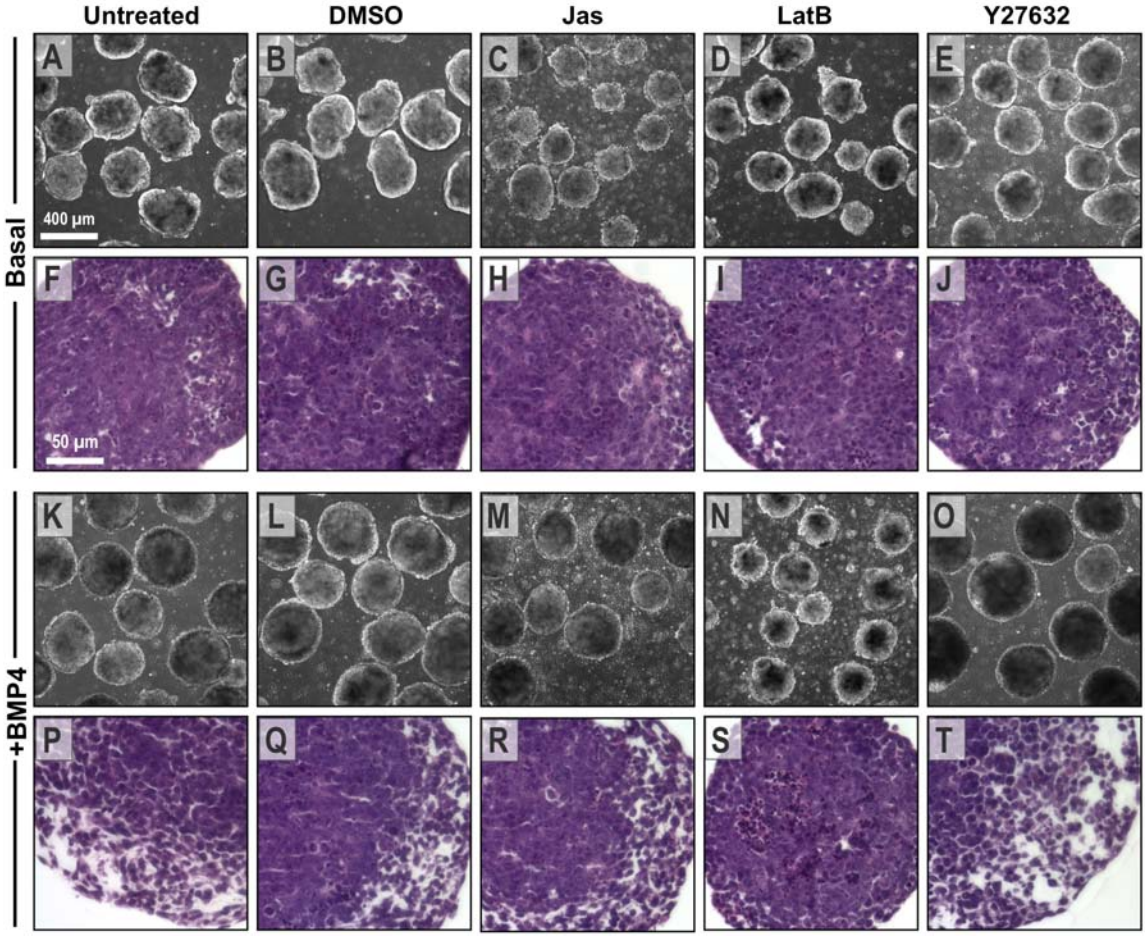

Figure 4-9: Morphology of EBs cultured with cytoskeletal agonists and antagonists. Phase images (A-E, K-O) and H&E staining (F-J, P-T) of EBs cultured in basal, serum free media (A-J) or upon supplementation with BMP4 (K-T) exhibit changes largely consistent with the soluble growth factor treatment, with few subtle changes due to cytoskeletal perturbation with Jas (C, H, M & R), LatB (D, I, N & S), and Y27632 (E, J, O & T). Scale bar (A) = 200 μm, (F) = 50 μm.

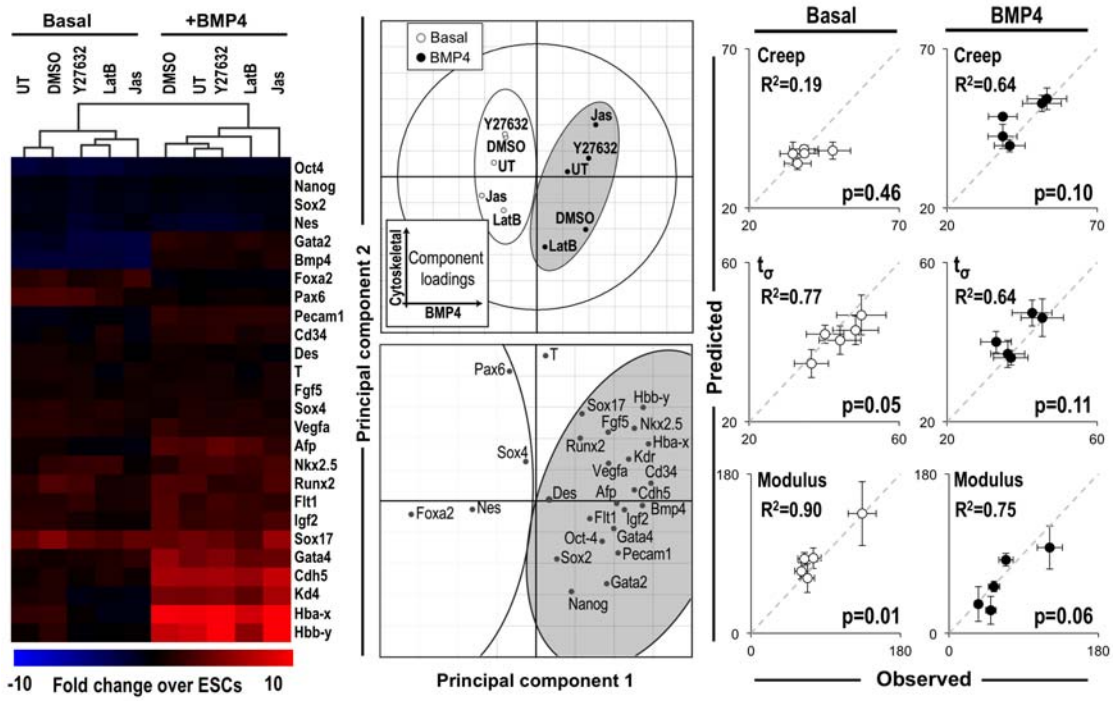

Figure 4-10: Multivariate association between phenotypic characteristics in response to biophysical perturbations. PCR array analysis of gene expression suggested differences in cell fate after 7 days of differentiation due to small molecule-mediated perturbation of the cytoskeleton from days 4-7. In addition, the score plot demonstrates distinctions between culture conditions across the first and second principal components, based upon gene expression profiles, shown in the loadings plot. Separate PLS with gene expression as inputs and mechanical properties as outputs demonstrated a high degree of predictability of mechanical properties based upon phenotypic traits.

Oct-4, indicated that LatB treatment delayed the differentiation kinetics of ESCs for both culture media conditions. Interestingly, the same mesendoderm genes (*Hbb-y*, *Sox17*, *Nkx2.5*, *Fgf5*) increased by Jas treatment of BMP4 EBs were decreased by Jas in basal EBs, thus demonstrating that actin polymerization was not sufficient to induce a mesendoderm gene expression profile within basal EBs (Fig. 4-10).

Based on the biochemical-mediated variability between experimental groups captured by the first principal component, separate PLS models were constructed based

upon the gene expression (input, X) and mechanical properties (output, Y) to distinguish the cellular responses to cytoskeletal perturbations for EBs differentiated in basal, serum-free media (R^2Y=0.70, Q^2=0.10; 1 significant PC) and in the presence of BMP4 (R^2Y=0.65, Q^2=0.30; 1 significant PC) (Fig. 4-10). The models reflect changes in biomechanical properties as a function of the gene expression profile, thus enabling a quantitative relationship between biophysical microtissue environments and ESC differentiated phenotypes. Overall, the gene expression profile was highly correlated with several of the mechanical characteristics; however, the strength of correlations varied between individual biomechanical parameters and across differentiation conditions. The model theoretically predicted the EB stiffness, with R2 coefficients of 0.90 and 0.75 in the basal and BMP4 conditions, respectively. In contrast, the viscous creep response of EBs did not correlate as highly with the phenotype of EBs in either condition, indicating that the changes in individual mechanical properties, such as viscosity, could not be fully explained through phenotypic changes and may also be influenced by extracellular factors, such as ECM deposition. To illustrate the complex relationship between biophysical characteristics and ESC phenotype, the model was instead constructed using the biomechanical parameters to predict gene expression profiles (Fig. 4-11). Overall, the biomechanical profile significantly (background $Q^2Y < 0.05$) predicted the responses of 61.5 and 65.4% of the genes, respectively, which established subsets of genes responsive to biophysical perturbations. Moreover, the upper quartile of genes (Basal: *Pax-6*, *Oct-4*, *Bmp4*, *Hba-x*; BMP4: *Hba-x*, *Hbb-y*, *Bmp4*, *Gata4*) within each condition were predicted by the models with >70% accuracy. Interestingly, *Bmp4* and *Hba-x*, which were highly predicted by both models, exhibited divergent responses to small molecule treatments within basal- and BMP4-treated EBs, thereby demonstrating the capacity for multivariate analytics to identify putative markers highly correlated with biomechanics across different environmental conditions. In addition, the genes most highly predicted in basal EBs included those

that exhibited decreased (*Hba-x*, *Hbb-y*), increased (*Gata4*), and unchanged (*Bmp4*) expression patterns in response to cytoskeletal perturbations, indicating that the mechanical model captured an array of different phenotypic responses. In contrast, while the mechanical model largely recapitulated the phenotypic profile of BMP4-treated EBs, several individual genes were not as highly correlated, which may be due to diverse responses arising within less uniform microtissues. The data together indicate that distinct phenotype profiles could be accurately described by multivariate analyses based upon multiple viscoelastic parameters. In summary, these results collectively suggest that ESC differentiated phenotypes are directly related through complex, multiparametric changes in the stiffness and viscoelastic characteristics of EBs.

4.4 Discussion

Taken together, the studies presented employ a novel approach which enables a more mechanistic understanding of embryonic-derived microtissue properties, including changes in morphogenesis, remodeling of cytoskeletal elements and modulation of biophysical characteristics during three-dimensional ESC differentiation. The biochemical-mediated differentiation of ESCs toward mesoderm lineages via BMP4 highlights parallels between three-dimensional ESC differentiation and embryonic development, particularly in terms of remodeling and morphogenesis leading to regions comprised of mesenchymal-like populations, similar to primitive streak migration during gastrulation [43]. Overall, the insight regarding biophysical dynamics accompanying ESC differentiation provides distinctions from adult tissue models and highlights important principles for establishing relevant microenvironments to direct early fate decisions.

Much previous work has aimed to recapitulate the mechanical microenvironment of stem cell niches through the development of substrates with elasticity comparable

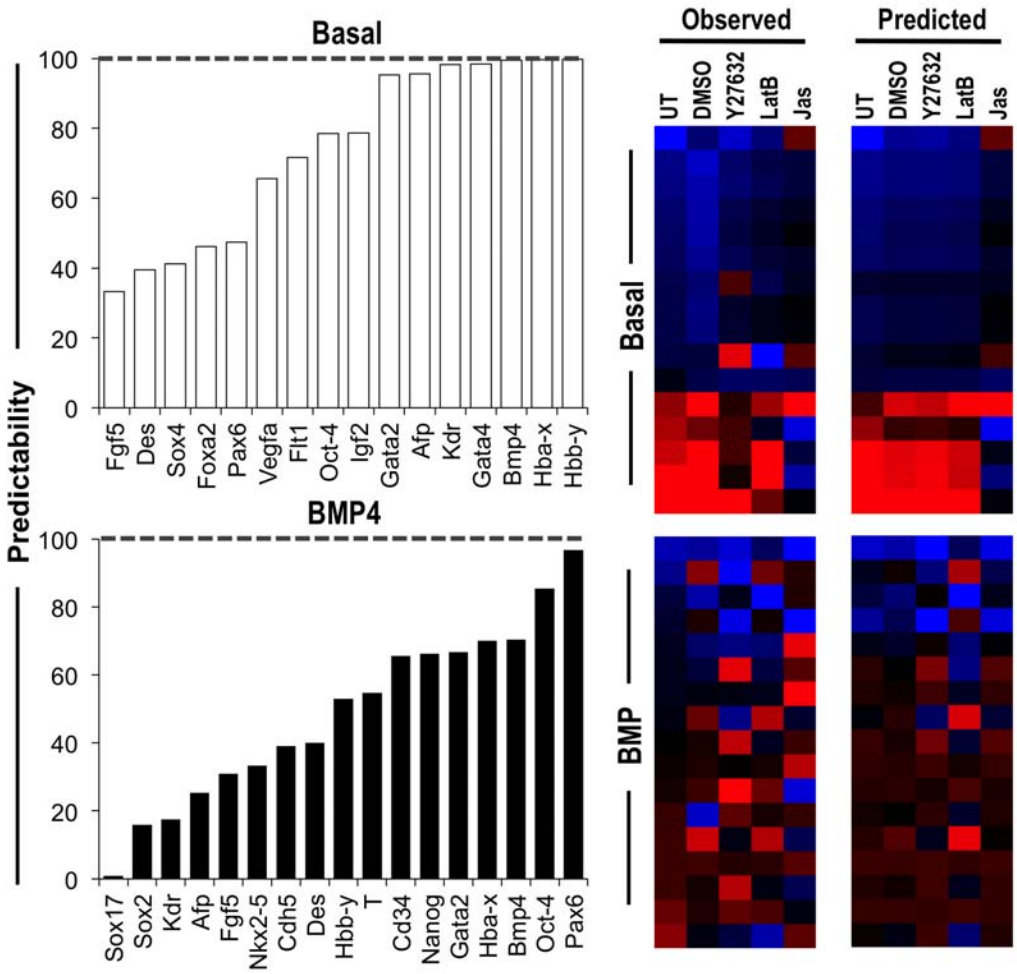

Figure 4-11: Prediction of microtissue stiffness and ESC phenotypes by multivariate modeling. PLS models based upon mechanical characteristics demonstrated different degrees of predictability for the associated gene expression profiles when trained with the full biomechanical profiles.

to the range of adult tissues (1 kPa - 100 kPa) [93, 363], which is a $>10^4$ fold decrease compared to standard polystyrene culture dishes. In contrast, the modulus of the ESC microenvironment appears to be substantially decreased compared to that of native tissues ($\leq$0.1 kPa). Such biophysical observations, however, are consistent with dramatic differences in tissue structure and composition between adult- and embryonic-derived tissues. The mechanical properties herein were measured between days 2-14 of differentiation, with most of the emphasis prior to day 7; previous characterization of the EB microenvironment at such stages of differentiation has indicated minimal ECM deposition [230]. Moreover, the high nuclear density evidenced by histological staining (Fig. 4-3 A&B) is distinct from the structure of adult tissues; therefore, the principal structural elements within EBs are likely the cells themselves (cytoskeletal elements), and the adhesions between cells, which is supported by the loss of EB structure upon simple removal of calcium. Consistent with such hypotheses, the EB modulus appears to be more comparable with the moduli of single cells, which is substantially decreased compared to that of tissues, with the cytoplasmic regions often measured in the range of $\sim$1 kPa [212]. Moreover, the modulus of embryonic tissues has been measured in the range of 10-100 Pa [373], consistent with the reported data, thereby highlighting the unique characteristics of embryonic microenvironments.

The single cell modulus of hESCs has been measured as approximately 0.5 kPa, and the cells exhibited a >3 fold increase in modulus upon differentiation toward chondrogenic lineages [247]. thereby indicating that undifferentiated, pluripotent cells may be inherently less stiff compared to more mature cell phenotypes. Moreover, the mechanical properties of adipose stem cells (ASCs) have been correlated with differentiation potential [119]. which highlights the interrelationship between biophysical cell characteristics and phenotype. In addition, the modulation of MSC morphology via changes in cell spreading [215] or substrate stiffness [93] has been linked to altered differentiation trajectories. PLSR modeling of the mechanical response to

changes in gene expression (Fig. 4-10) suggests a similar relationship between morphology, phenotype, and mechanical properties of pluripotent stem cell aggregates. The data presented collectively suggest that three-dimensional mesoderm differentiation and associated mesenchymal morphogenesis are correlated with increasing microtissue stiffness.

The mechanism for increased stiffness upon differentiation has been suggested to be largely a result of cytoskeletal mediated changes in the morphology [247, 86]. The measurement of EB biophysical characteristics enables quantitative analysis of the mechanisms underlying biophysical tissue properties via systematic perturbation of cellular elements; in ESC microenvironments, the cytoskeleton provides significant contributions (>50% of modulus) to the overall modulus during all stages of differentiation (Fig. 4-8 A-C). In addition, changes in relative cytoskeletal contributions provide insight into the physical mechanisms contributing to morphogenesis and remodeling. Interestingly, very early changes in cytoskeletal organization have been previously used to successfully predict the differentiated phenotypes of MSCs [331]. Therefore, the measured modulation of cytoskeletal tension between basal and BMP4-treated EBs as early as day 2 of differentiation may be indicative of such dynamic processes occurring prior to observing changes using standard biochemical or histological approaches. In addition, cytoskeletal tension exhibited a decreasing contribution over time to overall microtissue modulus over time in BMP4-treated EBs (Fig. 4-8 C), despite increases in the bulk EB modulus compared to basal conditions. One hypothesis to explain the decreasing cytoskeletal contribution over time is due to the loss of E-cadherin during EMT [49]. which has been shown to directly affect actin assembly dynamics through Arp2/3 [171]. However, the studies presented also establish that the increased modulus in BMP4-treated EBs is not a result of increased cytoskeletal tension, thereby implicating extracellular factors, such as cell-cell and cell-matrix adhesions as mediators of the biophysical mesenchymal microenvironment. Together, we

describe a complex and unique scaffold-free biophysical multicellular model in which the cytoskeletal tension is transmitted between cells via ESC intercellular adhesions and dynamically remodeled during differentiation and EB remodeling.

Cytoskeletal remodeling is a dynamic process, particularly during EMT [210] and embryonic development [103, 19], whereby cytoskeletal treadmilling causes the polymerization of actin at the leading edge of migration with reciprocal actin depolymerization at the opposite end of the cell.[314] Previous studies have demonstrated the role of jasplakinolide or latrunculin in increasing or decreasing motility, respectively [127]. In addition, EMT has been shown to occur in regions of increased cytoskeletal tension, and is inhibited by decreasing tension with agonists of ROCK or myosin II via transcriptional activation of serum response factor and myocardin related transcription factor [118]. Consistent with such previous observations, polymerization of actin via Jas treatment appeared to act synergistically with BMP4 to increase EMT and mesoderm differentiation. Interestingly, while Jas increased the stiffness of basal EBs, those treated with BMP4 and Jas did not exhibit statistical differences compared to untreated conditions. It appears, however, that polymerization of actin was not sufficient, in this case, to initiate EMT within basal, serum-free culture conditions in the absence of BMP4. Similarly, inhibition of actin polymerization via LatB decreased the BMP4-induced mesenchymal transition and mesoderm differentiation (Fig. 4-10, Supplemental Fig. 4-8). However, despite its known role in depolymerizing actin, LatB treated BMP4 EBs exhibited increased stiffness, suggesting the possibility role of redundant or compensatory mechanisms, including those within the Rho/ROCK pathways, in maintaining the structure of the epithelial-like aggregates. Finally, BMP4 EBs treated with Y27632 exhibited decreased stiffness, consistent with decreasing cytoskeletal tension; however, PLSR modeling suggested a slight increase in EMT and mesoderm differentiation upon inhibition of ROCK.

The likely mechanism for such observations, however, is through the known association of ROCK signaling with maintaining E-cadherin [38], without which cells are free to undergo EMT and migrate. Together, the dynamics of cytoskeletal changes and the insight provided through biophysical and phenotypic changes in response to cytoskeletal perturbations highlights important factors governing the morphogenesis of ESCs during cell fate specification.

Overall, the understanding of dynamic changes in embryonic tissue microenvironments during ESC differentiation highlights important principles for the design of tissue engineering strategies aimed to direct differentiation and patterning of complex, functional tissues amenable to modeling embryogenesis, screening pharmaceutical compounds, and developing molecular therapeutics.

CHAPTER V

SPATIOTEMPORAL DYNAMICS OF DIFFUSIVE SMALL MOLECULE AND GROWTH FACTOR SIGNALING IN STEM CELL AGGREGATES

5.1 Introduction

Cell specification during embryonic development is orchestrated by precisely controlled spatial and temporal signaling arising from the establishment of morphogen gradients via paracrine signaling. Such gradients have been extensively explored over the past 40 years, with the earliest reports identifying biochemical diffusion as a molecular determinant, leading to the spatial patterning and segmentation arising from threshold responses to local morphogens [71, 357]. While the bicoid gradient in drosophila embryos is among one of the most studied developmental events [89], spatial organizers have also been established within more complex species, such as the Spemann organizer in Xenopus [114] and Hensens node in the chick [137], which are the sources of many morphogenic signals, analogous to that of the node and anterior visceral endoderm in mammalian development [24, 26]. Originating from localized subpopulations, growth factors, including agonists (BMPs, Wnts) and antagonists (Noggin, Chordin, Frizzled, Axin, Dkk) are responsible for axis asymmetry, boundary formation and tissue divergence *in utero* [375, 190, 370]. While the identity of such signals has been established across several organisms, questions remain regarding the molecular mechanisms responsible for the initiation and regulation of gradients. In the context of embryonic morphogenesis, computational approaches proven powerful for interrogating factors contributing to the fidelity of gradients and boundaries, including the complex kinetics of morphogen synthesis, diffusion, and degradation

[281], across a range of embryonic size scales corresponding to different species [122].

Pluripotent embryonic stem cells (ESCs) derived from the inner cell mass of the embryonic blastocyst [209, 323, 96] respond to similar embryonic morphogenic cues, including biochemical and biophysical exogenous stimuli. Directed differentiation approaches commonly implement growth factors, including BMPs, Activin, and Wnts, to direct cell fate in monolayers via conserved embryonic developmental pathways [228]. However, recent striking examples of self organization and tissue morphogenesis leading to organoid formation within three-dimensional aggregates of pluripotent stem cells [92, 235, 307, 182, 311, 11, 318], termed embryoid bodies (EBs), have led to questions regarding the regulation of cell fate by the three-dimensional biophysical microenvironment [163]. Specifically, the dynamics of exogenous and paracrine signaling within EBs remains largely undefined. We and others have demonstrated the unique physical characteristics of stem cell spheroids, including tightly packed cells with an outer shell comprised of epithelial tight junctions, and evidence of small molecule transport limitations [51, 278]. However, it remains unclear how the transport dynamics of small molecules and growth factors within EBs compares to other biological systems, including native tissue structures, as well as monolayer cells and 3D constructs *in vitro*.

The objective of this study was to implement a data-driven mathematical approach to quantitatively measure the population dynamics of molecular transport and downstream signaling in parallel with computational interrogations to ultimately inform approaches for manipulating biochemical delivery and understanding parallels with embryonic development. Small molecule and growth factor transport were quantified by measuring uptake and signaling via flow cytometry and implemented in the context of a mathematical model to interrogate the influence of various physical and microenvironmental factors specific to stem cell expansion and differentiation. Overall, we demonstrate that the high density of cells within EBs leads to marked

transport limitations, particularly for small molecules with high uptake rates. In addition, the physiologically relevant BMP4 signaling pathway also exhibited population heterogeneity and signal attenuation. Moreover, a rules-based computational model was employed to further interrogate the effects of phenotypic spatial inhomogeneities on transport during stem cell differentiation. Together, these data indicate important biophysical principles of three-dimensional stem cell derived microtissues, which may inform the development of novel tissue engineering strategies to establish uniform molecular delivery, as well as approaches to engineer biomimetic gradients of exogenous or endogenous cytokines and growth factors.

5.2 Materials and Methods

5.2.1 Embryonic stem cell culture

Murine ESCs (D3 cell line) were expanded on 0.1% gelatin-coated tissue culture polystyrene culture plates in media consisting of Dulbeccos Modified Eagles Medium (DMEM) supplemented with 15% fetal bovine serum (FBS), 100 U/mL penicillin, 100 μg/mL streptomycin, 0.25 μg/mL amphotericin, 2mM L-glutamine, 1x MEM non-essential amino acid solution, 0.1 mM 2-mercaptoethanol, and 10^3 U/mL leukemia inhibitory factor (LIF). ESCs were expanded undifferentiated in the presence of LIF and routinely passaged at 70% confluence.

5.2.2 Embryoid body formation and maintenance

Differentiation of ESCs was initiated via the formation and culture of cells as three dimensional aggregates, termed embryoid bodies (EBs). EBs were formed via forced aggregation of single cells in 400 μm microwells, as previously described [335, 165], with a seeding density of 1000 cells per well in ESC expansion media without LIF. After 24 hours of formation, EBs were transferred into suspension ($\sim$1200 EBs per 10 mL of media) and maintained on a rotary orbital shaker platform at 45 rpm,

in order to support subsequent growth while preventing agglomeration of individual aggregates. EBs were maintained in rotary orbital suspension culture through 7 days of differentiation.

5.2.3 Measurement of embryoid body physical metrics

Phase images were acquired after 2, 4, and 7 days of differentiation using a Nikon TE 2000 inverted microscope equipped with a SpotFlex camera. The cross sectional area of individual EBs was quantified via a custom-written macro in CellProfiler, which iteratively processes images by correcting the background irregularities, including removing single cells and uneven illumination, followed by identification of objects using the Otsu Adaptive method. Several images (5-10) were quantified per plate, with a total of >200 EBs per independent replicate for each condition (n=3). To quantify the yield of cells, EBs from the same stages of differentiation were washed in PBS and dissociated using 0.05% trypsin / 0.53mM EDTA, followed by quantification using a Coulter counter. EBs were also sampled, diluted, and manually counted (3 counts per replicate) in order to verify that agglomeration was limited throughout the culture duration.

5.2.4 Small molecule transport

0.1 μM Calcein AM was supplemented in 2 mL of serum-free media containing either 5x10^5 cells or ~200 EBs, either as trypsin-dissociated single cells or intact EBs. After 15 minutes of incubation, 5 volumes of PBS were added and cells were collected by centrifugation at 200 rcf for 5 minutes. After centrifugation, fluorescence was directly measured via flow cytometry on an Accuri C6 cytometer using a blue laser (excitation: 488 nm) with an attenuated FITC filter (FL1 90%; 530 $\pm$ 15 nm). Following the calcein staining and washing procedures, EBs were dissociated via incubation in 0.05% trypsin/ 0.53 mM EDTA and fluorescence intensity was measured using flow cytometry as described. In all cases, the cell population was identified within the

forward- versus side-scatter plot, and $2x10^4$ events were collected within the cell gate. Subsequent analysis of flow cytometry data was conducted by measuring the mean fluorescent intensity and intensity distributions using FlowJo software. The radial fluorescence profiles were subsequently determined by exporting the raw intensity data collected by the Accuri CFlowPlus software into a custom program in MATLAB, which normalized and binned the intensity as a function of EB radius, for a theoretical EB of size representative of the population average, with the assumption that the intensity decreases with increasing radius, based upon the principles of diffusive mass transfer.

5.2.5 Spheroid diffusion model & parameter case studies

The Thiele modulus (ϕ) was determined at each stage of differentiation by using a nonlinear regression based upon iterative least squares estimation in MATLAB to fit the non-dimensionalized radial fluorescence profiles according to the transport equation for reaction & diffusion in a spherical porous catalyst (Eq. 4):

$$C^* = \frac{1}{r^*}\frac{sinh(r^*\phi)}{sinh(\phi)} \tag{4}$$

where C^* is the nondimensional concentration (C/C_o), r^* is the nondimensional radius (r/R). The effectiveness factor (η) and molecular uptake rate (Q; mol/cell/s) were calculated from the Thiele modulus, based on Eq. 5 & 6:

$$\eta = \frac{2}{\phi}\frac{I_0(\phi)}{I_1(\phi)} \tag{5}$$

$$Q = \frac{CD\phi^2}{\rho R^2} \tag{6}$$

where I_0 and I_1 are Bessel functions of the 0th and 1st order, respectively, C is the bulk concentration (mol/m^3), D is the molecular diffusion coefficient (m^2/s), ρ is the cell density ($cells/\mu m^3$), and R is the spheroid radius (m). To interrogate

comparisons with other physiological systems and microenvironmental changes, the Thiele modulus and effectiveness factor were calculated from Eq. 7 upon varying the effective cell density (ρ) and biochemical concentration (C) and molecular uptake rate (Q), based upon published values. Cell density within EBs was estimated based upon the measured physical parameters (cell and EB counts, as well as EB cross sectional area), assuming population uniformity and spherical nature of aggregates at early stages of differentiation [165].

$$\phi = \left(\frac{\rho Q R^2}{CD} \right)^{1/2} \tag{7}$$

The cell density in physiological tissues was modeled within the range from 5x10^7 to 2x10^8 cells/cm^3 in cartilaginous and hepatic tissues, respectively [123], with a lower range of densities in tissue engineered constructs, ranging from 1x10^6 to 1x10^7 cells/cm^3 [69]. A case study of transport changes upon biomaterial microparticle incorporation (effective cell density change) was constructed based upon published incorporation ratios (1:2, 1:1, 2:1 MP:cells) for microparticles via forced aggregation into spheroids composed of 1000 cells [40] and the volumetric changes in density were calculated for microparticles of varying sizes and assuming spherical packing. Similarly, the molecular uptake rate (2x10^{-22} mol/cell/s) and K_d (1 nM) were interrogated for epidermal growth factor (EGF), as a representative growth factor [123] and compared to the measured uptake of calcein AM, with comparison to oxygen uptake rates (2x10^{-17} to 7x10^{-17} mol/cell/s) as a higher extreme [123, 337]. In all simulations the diffusion coefficient was assumed to be 380 and 20 μm^2/s for small molecules [343] and growth factors [123], respectively.

5.2.6 Growth factor transport

Growth factor transport was assessed in physiological conditions using transcriptional signaling sentinel mESCs that are responsive to regulatory sequences in the BMP signaling pathway. As previously reported [297], the cells harbor an inserted response element within a deletion at -228 bp within the constitutive *Rosa26* locus. The response element for BMP signaling is the IBRE element from the promoter region of the *Smad7* gene, fused to a TATA element and the CFP reporter (-228/IBRE4-TA-CFP). Smad7, which is an inhibitor Smad, or I-Smad, is part of a negative feedback loop and one of the early targets of the BMP signaling pathway [4]. The IBRE element binds protein dimers of Gata-1 -5 or -6 with Smad1 and has been previously demonstrated responsiveness to lower concentrations of BMP compared to other response elements in the Smad7 gene [27]. Cell responsiveness to BMP4 was first validated by plating undifferentiated cells into ESC media (with LIF) either in the presence or absence of BMP4 (10 ng/mL) and incubated for 24 hours prior to collecting and fixing the cells in 10% formalin. The fluorescent profiles were assessed via flow cytometry, and the sentinel cells with and without BMP4 were compared to naive, untransduced D3s as a negative control (Fig. 5-1). To assess transport, equal cell yields, either as EBs or as single cells dissociated from EBs at day 2 of differentiation, were incubated in ESC differentiation media supplemented with 0, 5, 10 or 20 ng/mL recombinant BMP4 and incubated overnight. After 24 hours, cells were collected by retrieval of monolayer cells or dissociation of EBs using 0.05% trypsin / 0.53 mM EDTA. Single cells from each culture context were subsequently fixed in 10% formalin and washed with PBS prior to analysis via flow cytometry. The CFP signal within the signaling sentinels was assessed using a BD LSR II flow cytometer equipped with a 405 nm violet laser with a 450/50 nm filter. Flow cytometry analysis was conducted using FlowJo software, with the cells identified via the forward (FSC-A) and side scatter (SSC-A) profiles, with doublets removed from the SSC-W vs. SSC-H profile.

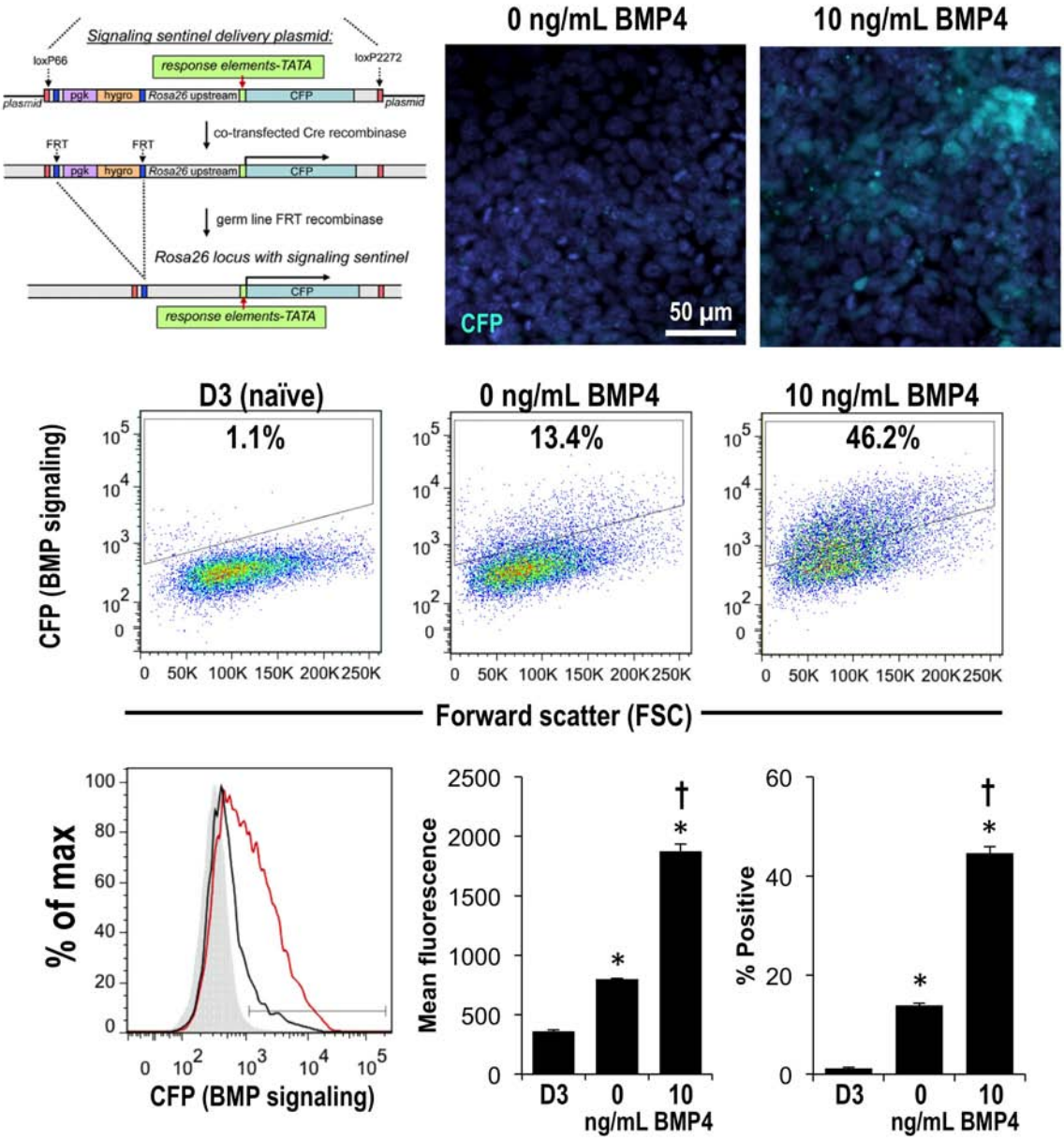

Figure 5-1: BMP sentinel signaling cell validation. Sentinel signaling cells exhibited increases in the mean fluorescence and percent of positive cells, in a dose-dependent manner, with approximately 14% of cells positive in basal differentiation conditions (with serum but without supplementation of BMP4; 0 ng/mL BMP4) and an increase to 45% positive cells with the addition of 10 ng/mL BMP4. * = $p<0.001$ compared to naive cells (untransduced D3s). † = $p<0.001$ compared to signaling sentinels without BMP4 (0 ng/mL). The schematic representation of sentinel signaling cell construction was reproduced from [297].

5.2.7 Computational spatial diffusion model

Transport was further studied in the context of spatial changes in stem cell phenotype during EB differentiation using a previously described computational framework [349]. Briefly, EBs were modeled using a custom C# physics simulation which assumes the cells to be rigid spheres connected by springs. The kinetics of the simulations were fit to experimental observations of cell growth and division was assumed to be symmetrical, with both daughter cells exhibiting the same phenotype. The loss of pluripotency was subsequently modeled in Python, based upon the previously validated competing feedback mechanism (Eq. 8):

$$P(x) = \frac{1}{1 + e^{\gamma - \beta}} \tag{8}$$

where β is the number of differentiated neighboring nodes and γ is the number of undifferentiated neighboring nodes. The phenotypic patterns at discrete time steps were then paired with the steady-state diffusion-reaction equation (Eq. 9), with the boundary conditions based upon a specified bulk concentration ($C=C_{o(r=R)}$) and spherical symmetry ($[dC/dr]_{r=0} = 0$) in order to calculate transport phenomena as a function of radius (Eq. 10).

$$D\left(\frac{d^2C}{dr^2} + \frac{2}{r}\frac{dC}{dr}\right) - Q = 0 \tag{9}$$

$$C_o - C = \frac{Q}{3D}\left(\frac{R^2 - r^2}{2}\right) \tag{10}$$

To simulate changes in receptor expression upon differentiation, the consumption rate (Q) was varied within the population of differentiated cells, in order to represent increased and decreased sensitivity upon regulation of receptor expression accompanying cell fate changes.

5.2.8 Statistical analysis

All experiments were conducted with replicate data are represented as the mean of n=3 independent replicates ± standard error. Prior to statistical analysis, all data were pre-processed using a box-cox power transform, in order to normalize data according to a Gaussian distribution. Statistical tests were conducted between groups and time points using one-way or two-way ANOVA, combined with either a post-hoc Tukey or Mann-Whitney U test for comparison of individual samples, depending on the results from Levenes equality of variances test.

5.3 Results

5.3.1 Changes in microtissue characteristics during embryoid body differentiation

Consistent with previous reports [165], embryoid bodies formed via forced aggregation and maintained in rotary orbital suspension culture exhibited uniform formation, size and morphology (Fig. 5-2 A), thereby providing robust and reproducible control of population homogeneity during the course of differentiation. Specifically, EBs maintained spherical ultrastructure, with no significant changes in the yield over the 7 days of differentiation (Fig. 5-2 B), indicating that individual EBs remained distinct and did not exhibit evidence of agglomeration. In addition, the cell yield ($p<0.001$) and EB size ($p<0.001$) both increased over the course of differentiation (Fig. 5-2 B), resulting in >7 fold increase in the number of cells per EB during after 7 days (Table 1); however, interestingly, the cell density significantly decreased between days 2 and 7 of differentiation ($p = 0.006$; Table 1), which indicates biophysical changes in the EB microenvironment due to morphogenesis and remodeling that occur concomitant with cell fate changes. Together, the control enabled through this platform and the analysis of biophysical cellular properties in parallel with transport assays

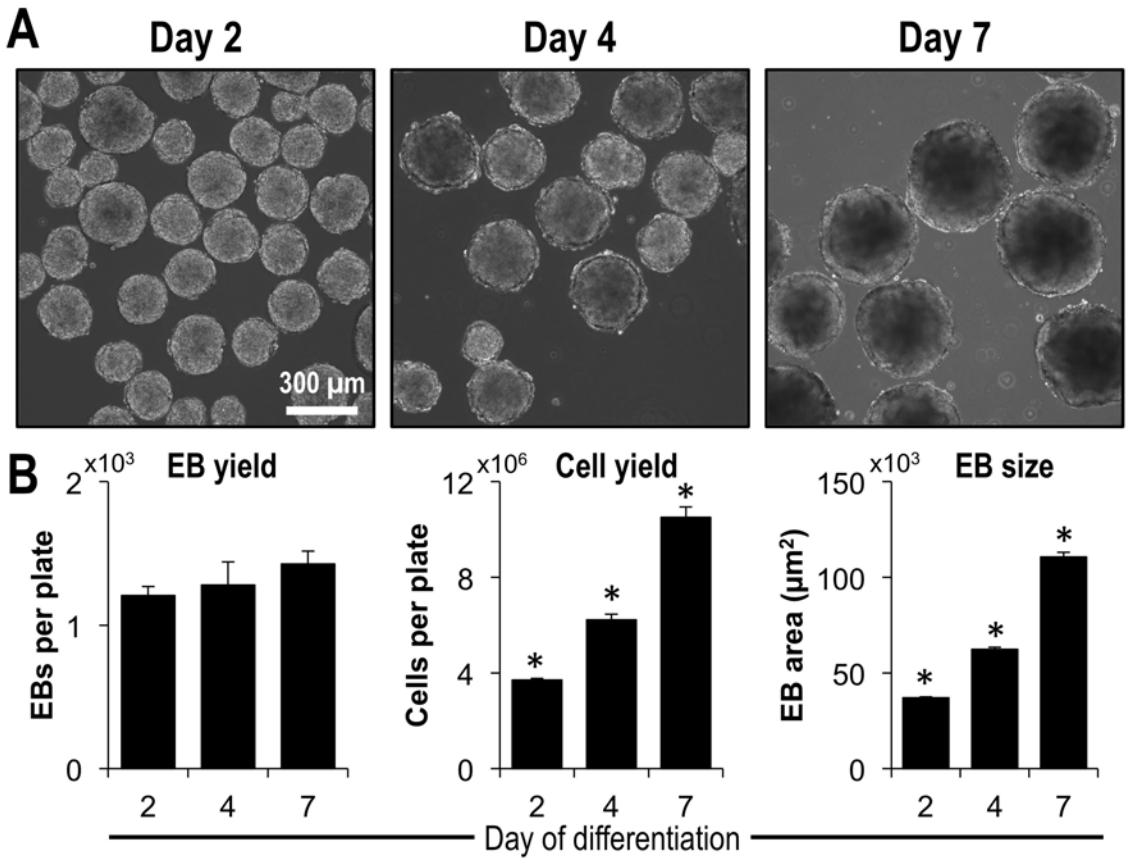

Figure 5-2: EB biophysical characteristics. (A) EB populations exhibit characteristic uniform round morphology during the course of differentiation, with changes in the size and ultrastructure during by day 7 of differentiation. (B) While the yield of EBs did not change statistically during the course of differentiation, the overall cell yield and EB size were both significantly increased at each stage of differentiation. * = $p<0.05$ compared to all other days of differentiation. Scale bar in (A) = 300 μm.

enables the development of novel quantitative models for understanding morphogen dynamics in stem cell spheroids.

5.3.2 Attenuation of small molecule transport in embryoid bodies compared to single cells

Based upon the common practice of adapting monolayer culture conditions to three-dimensional spheroid formats, the transport profiles were first compared between single cells and EBs incubated in calcein AM (0.1 μM), a fluorescent hydrophobic small molecule. In all experiments, the single cells were derived from dissociated

Table 1: Biophysical characteristics of EBs during differentiation

Day	Cells per EB	EB diameter (μm)	Cell density (cells/μm^3 x10^{-3})
2	3089 ± 163	217 ± 1.3	0.58 ± 0.04
4	5015 ± 626	282 ± 2.3	0.43 ± 0.06
7	7439 ± 642	375 ± 4.2	0.27 ± 0.03

EBs at the same stage of differentiation and an equivalent total number of cells were stained in each format (Fig. 5-3 A). At all stages of differentiation, the fluorescence profile of cells derived from embryoid bodies was distinct from that of both naive, unstained cells, as well as calcein AM stained single cells (Fig. 5-3 B). The fluorescence profile of EB-derived cells exhibited significantly decreased mean fluorescence intensity ($p<0.001$), with an increased coefficient of variance (CV; $p<0.006$ at days 2 and 7); the more spread distributions and decreased fluorescence (Fig. 5-3 C) together indicate that exogenous delivery of small molecules may result in increased heterogeneity within EBs compared to monolayer cultures.

5.3.3 Increasing heterogeneity in small molecule uptake during EB differentiation

In contrast to the previous experiment, the EB number was, instead, maintained constant, in order to compare the changes in EB transport over the course of differentiation, analogous to standard *in vitro* feeding and supplementation regimens, which traditionally do not vary the concentration over time, despite increased cell yields (Fig. 5-4 A). During the course of differentiation, the fluorescence intensity significantly decreased ($p<0.001$), while the CV increased at day 7 ($p=0.007$ compared to day 2; $p=0.03$ compared to day 4), indicating an overall decrease in the number of stained cells, with an increased population heterogeneity over time (Fig. 5-4 B). Assuming spherical reaction-diffusion kinetics, the raw flow cytometry fluorescence profiles were plotted along the radius of the EB, with the highest intensity cells at the exterior and lowest at the interior (Fig. 5-4 C). Analysis of the data-driven spatial

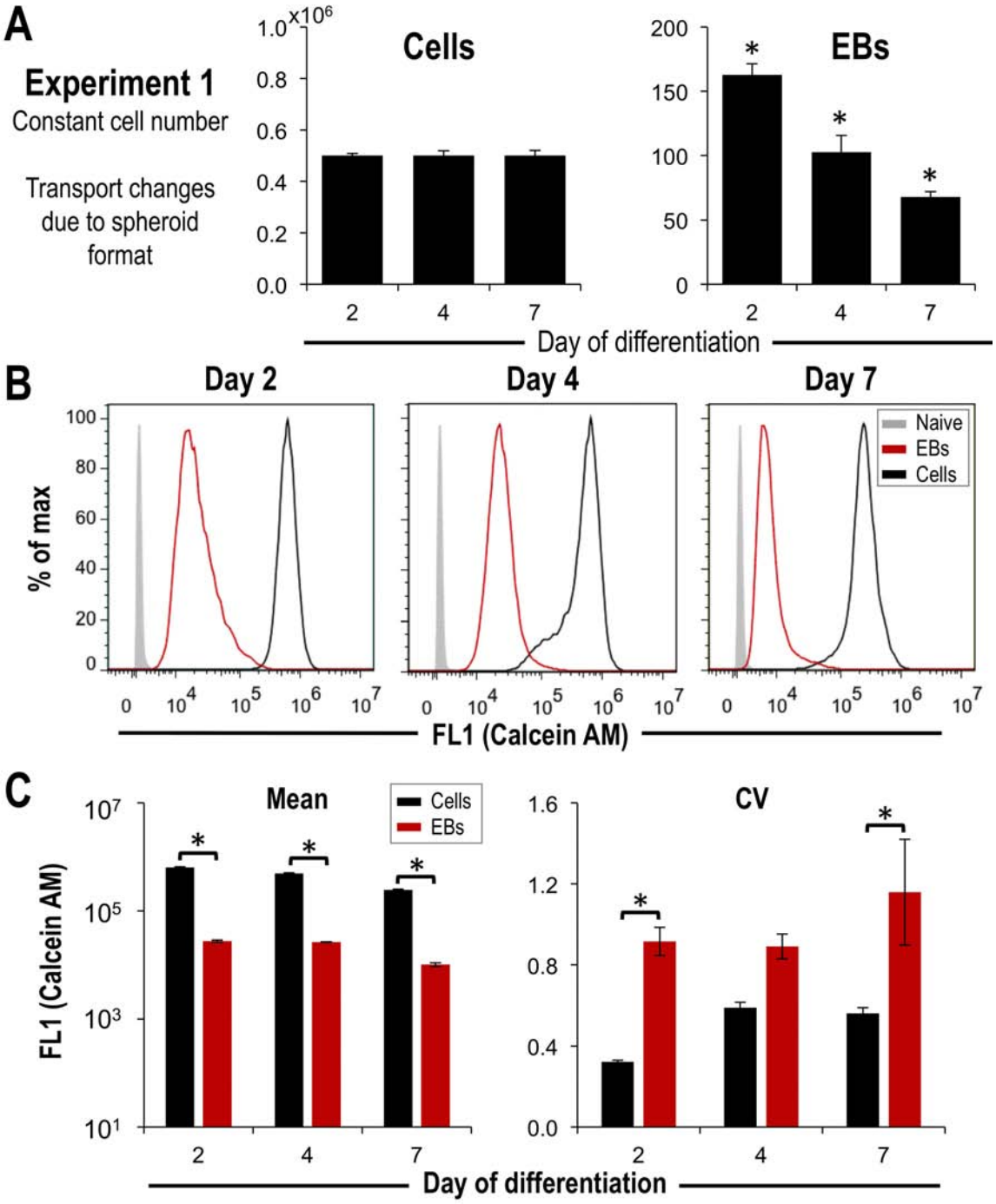

Figure 5-3: Transport limitations due to spheroid culture format. (A) To assess changes in transport between spheroids and cells cultured in a traditional monolayer format, the same number of cells (corresponding to a decreasing number of EBs) was incubated with calcein AM (0.1 μM) in the two contexts after days 2, 4 and 7 of differentiation. (B) The cells from dissociated EBs (red) exhibited unique dye uptake profiles compared to those in monolayer (black), (C) with overall decreases in the mean fluorescence and increased coefficient of variance (CV). * = $p<0.05$ compared to (A) all other days of differentiation or (C) denoted comparison.

model indicated that the fluorescence intensity was significantly attenuated within the first cell layers of the EB (D_{90} ~10-13 μm; Fig. 5-5). The corresponding region of highly stained cells at the exterior of the EB led to an increase ($p<0.05$) in the total number of stained cells over time; however, due to the geometrical changes in EBs during the course of differentiation (Fig. 5-5 B), the highly stained cells represented a decreasing ($p<0.001$) fraction of the total cells over time (Fig. 5-4 D), consistent with the measured population averages. Together, these data suggest that supplementation of culture conditions with a constant small molecule morphogen concentration results in decreasing intensity and increasing spatial heterogeneity during the course of stem cell spheroid differentiation.

5.3.4 Mathematical model of small molecule and growth factor distribution in stem cell spheroids

In order to relate the measured fluorescence profiles to engineering parameters, the radial distributions were fit to determine two dimensionless constants: (1) the Thiele modulus (ϕ), which describes the ratio of diffusion time to reaction time in a system and (2) the effectiveness factor (η), which quantifies the ratio of internal reaction compared to reaction in the bulk media. The Thiele modulus in EBs ranged from 32.8 to 44.6 (Fig. 5-6 A) during the course of differentiation, which indicated significantly decreased transport (Fig. 5-6 B) at day 7 compared to earlier time points ($p=0.001$ compared to day 2; $p=0.004$ compared to day 4). The calculated Thiele modulus corresponded to low effectiveness factors (<1), further supporting the restricted transport in the experimental system. In addition, the calculated uptake rate for calcein AM also increased after 7 days of differentiation ($p=0.007$), which may have contributed to the increase in Thiele modulus.

As the cell density within EBs (~10^8 cells/cm^3) was measured as orders of magnitude above that reported for native tissues (~10^7 cells/cm^3) and scaffold-based

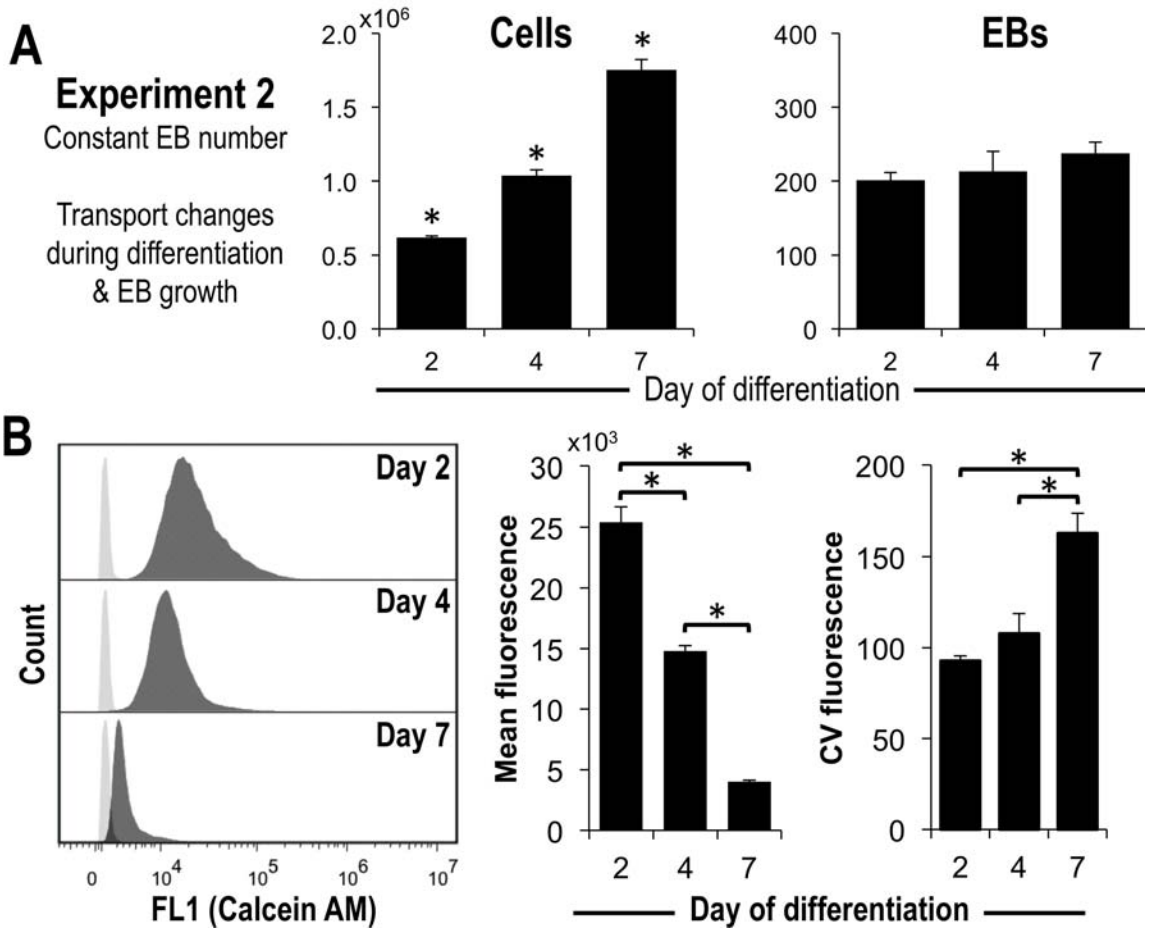

Figure 5-4: Transport limitations during EB differentiation. (A) To assess the changes in transport within spheroid populations over the course of time, the same total number of EBs (corresponding to an increasing number of cells) were incubated with calcein AM (0.1 μM) after days 2, 4 and 7 of differentiation. (B) The cells from dissociated EBs (black) exhibited unique dye uptake profiles at each stage of differentiation, with decreasing fluorescence and increasing coefficient of variance (CV). * = $p<0.05$ compared to (A) all other days of differentiation or (B) denoted comparison.

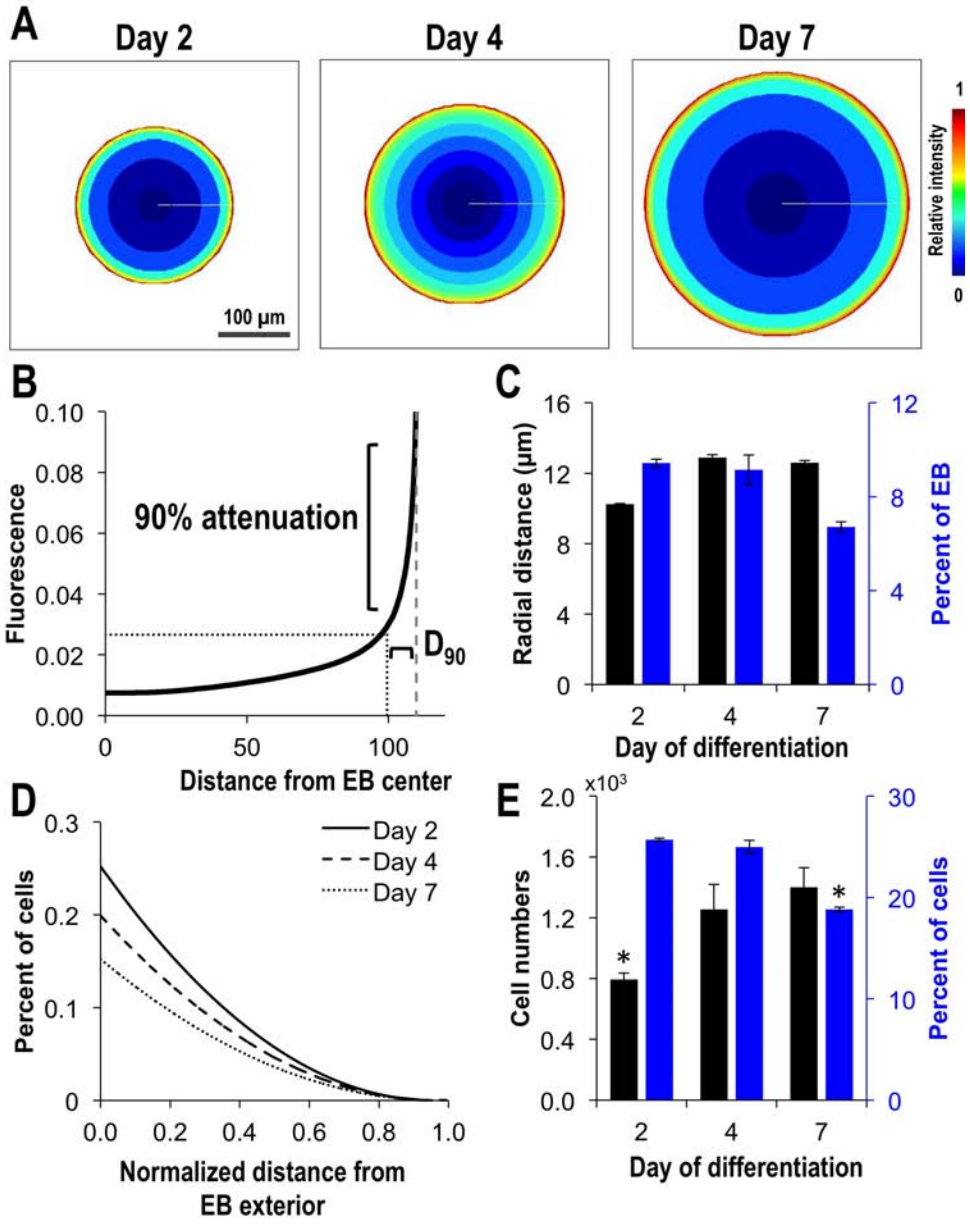

Figure 5-5: Spatial transport limitations arise from spheroid geometry. (A) When the profiles were spatially mapped using a computational approach, the attenuation of fluorescence (B,C) occurred within the first cell layers of the EB. (D,E) While the number of highly stained cells increased over time, the radial changes in relative EB proportions at each stage of differentiation led to a decreasing proportion of stained cells within the EB. * = $p<0.05$ compared to (A,D) all other days of differentiation or (B) denoted comparison. Scale bar in (C) = 100 μm.

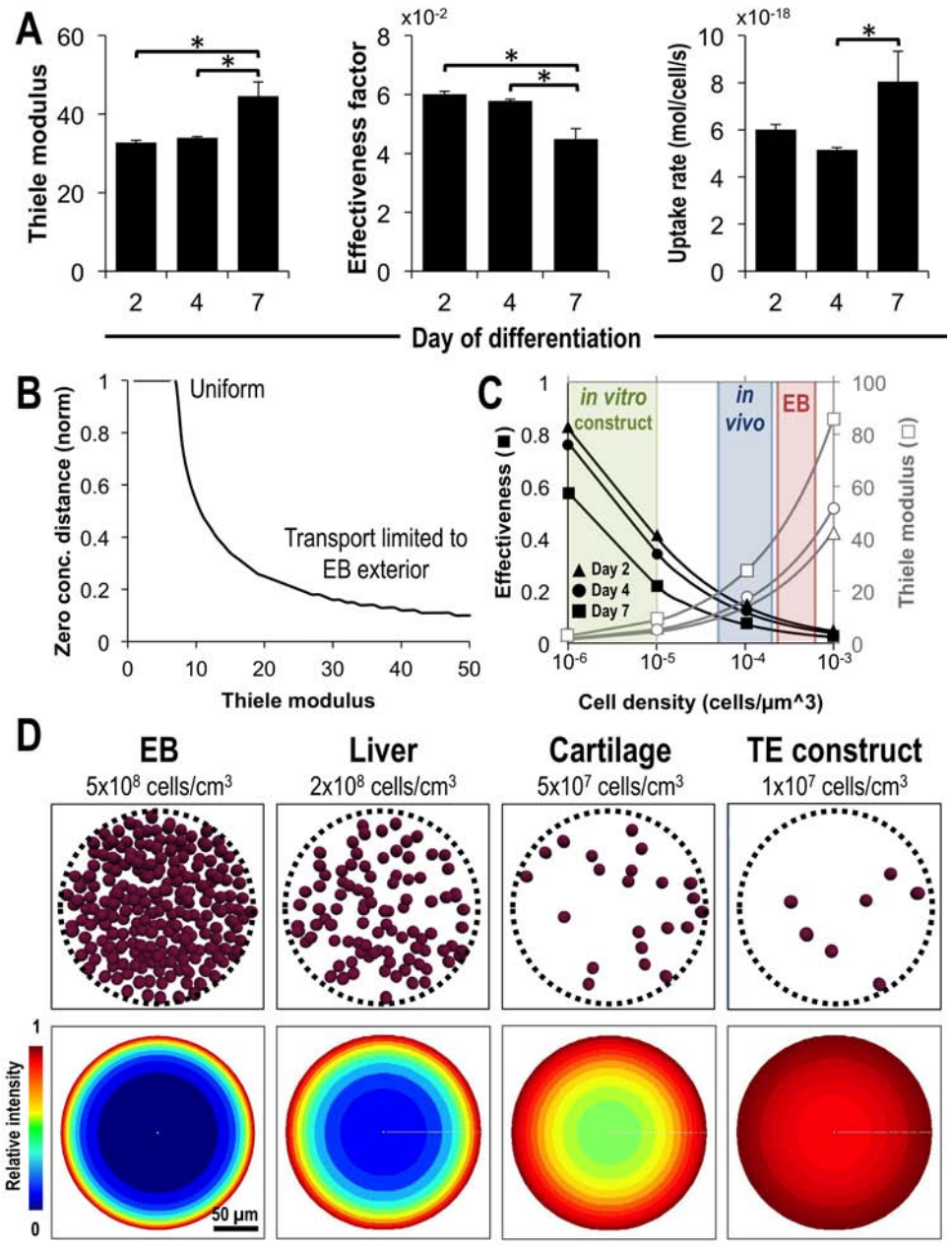

Figure 5-6: Influence of cell density on spheroid transport characteristics. (A) Chemical engineering parameters, including the Thiele modulus, effectiveness factor, and biochemical uptake rate upon treatment with calcein AM were altered as a function of differentiation stage in EBs, (B) leading to parameters indicative of a large central zone consisting of zero concentration at the center of EBs. (C) The Thiele modulus and effectiveness factors were increased and decreased, respectively, as a function of cell density, with tissue engineered constructs (green) and native tissues (blue) exhibiting densities characteristic of decreased transport limitations compared to EBs (red), resulting in (D) dramatically different spatial concentration profiles within computationally derived spheroids of the same size and biochemical conditions. Scale bar in (D) = 50 μm.

culture platforms ($\sim 10^6$ cells/cm^3), a comparison of the Thiele modulus and effectiveness factor was calculated across microtissues of different cellular compositions. Increasing cell density over several orders of magnitude led to an increase in the Thiele modulus and reciprocal decrease in effectiveness factor, which highlights the increased transport limitations in EBs compared to *in vivo* tissues and *in vitro* tissue engineered constructs, simply due to changes in cell density (Fig. 5-6 C). In a simulation maintaining constant microtissue size, small molecule concentration, uptake rate, and physical properties while simply varying the cell density, there was an apparent distinction between the radial profiles, both in terms of concentration and spatial attenuation of morphogen (Fig. 5-6 D).

Similar to tissue engineering approaches which seed cells onto scaffolds, biomaterials have also been implemented within the context of stem cell spheroids in the form of microparticles composed of synthetic or natural polymers [41, 51]. While microparticles have traditionally served as point sources for local morphogen release inside of EBs, unloaded microparticles may also alter transport by creating void regions, thereby altering the effective cell density. Based on volumetric void space calculated using previously measured rates of incorporation for gelatin microparticles into stem cell aggregates [40], the effective cell density for stem cell aggregates decreased with increased microparticle incorporation (Fig. 5-7 A). Moreover, when microparticle diameter approached that of the cells (~ 15 μm), the effective density within the spheroid approached the density of *in vivo* tissues at high incorporation ratios (2:1 MP:cell). Similar to previous simulations of cell density, increasing microparticle incorporation (and thus decreasing effective density) decreased the spatial heterogeneity and the magnitude of morphogen attenuation within the spheroid (Fig. 5-7 B&C). Together, these mathematical simulations highlight the biophysical transport properties within stem cell spheroids as a result of high cell density and demonstrate principles by which tissue engineering approaches may alter transport

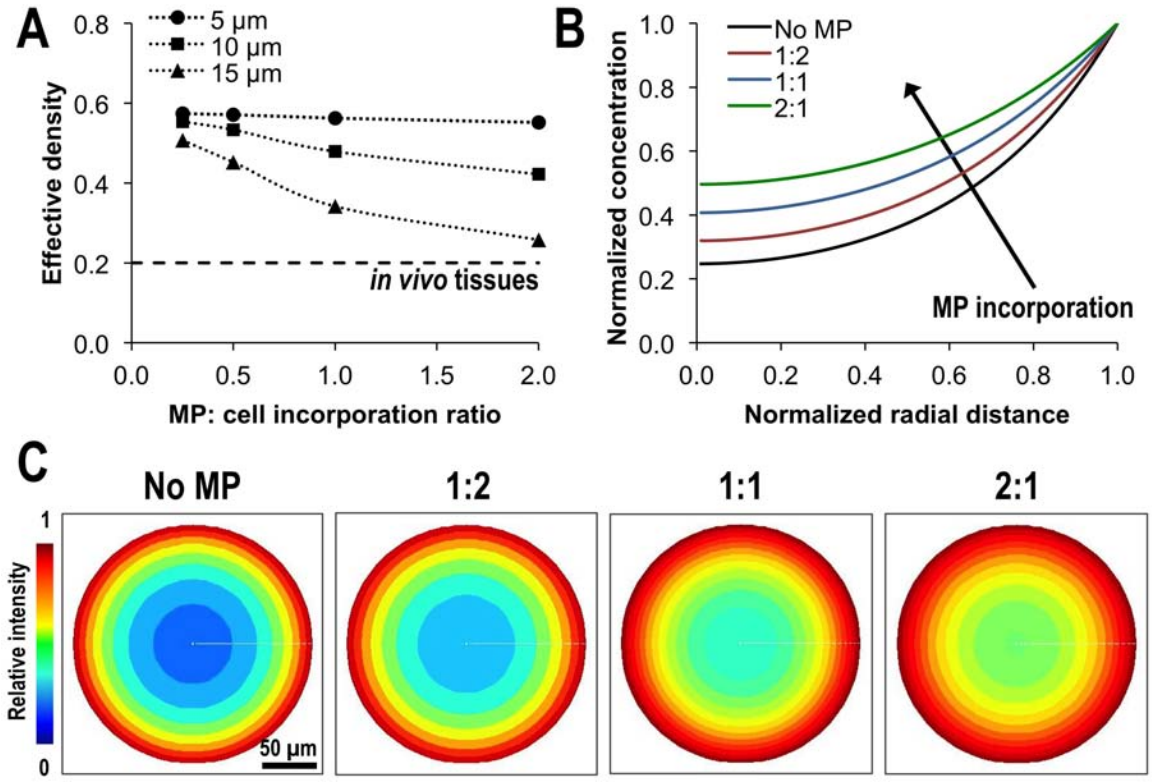

Figure 5-7: Impact of microparticle incorporation on aggregate density and transport. (A) The effective cell density in spheroids with incorporated biomaterials was decreased as a function of both the microparticle size (circle = 5 μm; square = 10 μm; triangle = 15 μm) and the incorporation ratio. (B,C) Upon incorporation of microparticles approximating the size of individual cells (15 μm), the spatial concentration profiles suggested decreasing transport limitations with increasing incorporation (effectively decreasing spheroid density) within MP:cell ratios of 1:2 (red), 1:1 (blue) and 2:1 (green). Scale bar in (C) = 50 μm.

via simple microenvironmental perturbations.

While the measured data and mathematical simulations provide context for small molecule uptake into stem cell spheroids, questions remain regarding other classes of physiologically relevant morphogens, including growth factors. To interrogate the changes in transport under different biochemical contexts, engineering parameters were calculated by varying the cellular uptake rate, which varies based upon the mode of morphogen interaction with cells. Consistent with known relations, the Thiele modulus increased as a function of uptake rate, with a reciprocal decrease in

effectiveness factor (Fig. 5-8 A). Therefore, for molecules with high uptake rates, such as oxygen, the transport is increasingly restricted, whereas growth factors may exhibit a decreased propensity to exhibit gradients and transport limitations. However, further simulations using relevant uptake and physical parameters for growth factors [123] also indicated that sufficiently high concentrations are required to decrease the Thiele modulus and increase the effectiveness factor in EBs (Fig. 5-8 B). For example, the radial profile of EBs supplemented with epidermal growth factor (EGF) at a concentration corresponding to 10 K_d (10 nM) demonstrated 60% attenuation at the center of the EB. While *in vitro* cultures are often supplemented in the range of ~10 K_d [292], these simulations highlight the need for supraphysiological concentration (>50 K_d) in order to maintain biochemical homogeneity throughout EBs.

5.3.5 Growth factor signaling in aggregates of ESCs

In addition to the kinetics of small molecule uptake within spheroid structures, growth factor signaling was assessed using a novel enabling technology, previously described by Serup et al, which employs recombinase mediated cassette exchange to substitute regions within the Rosa26 gene with a response element for the BMP signaling pathway in mESCs [297]. Therefore, upon incubation of cells, either in monolayer or as EBs, with BMP4 at various concentrations, the downstream signaling activation was assessed indirectly via the corresponding CFP fluorescence profile. This system provides a physiologically relevant method of assessing the effect of exogenous growth factor addition within cultures (Fig. 5-9). As with the small molecule uptake and fluorescence, growth factor signaling within monolayer cultures from day 2 of differentiation was accentuated compared to the signaling within EBs of the same differentiation stage, across a range of BMP4 concentrations (5-20 ng/mL). Both conditions exhibited low basal activity when unstimulated, which was not statically increased over naive cells; in addition, both monolayer and EB cultures exhibited a

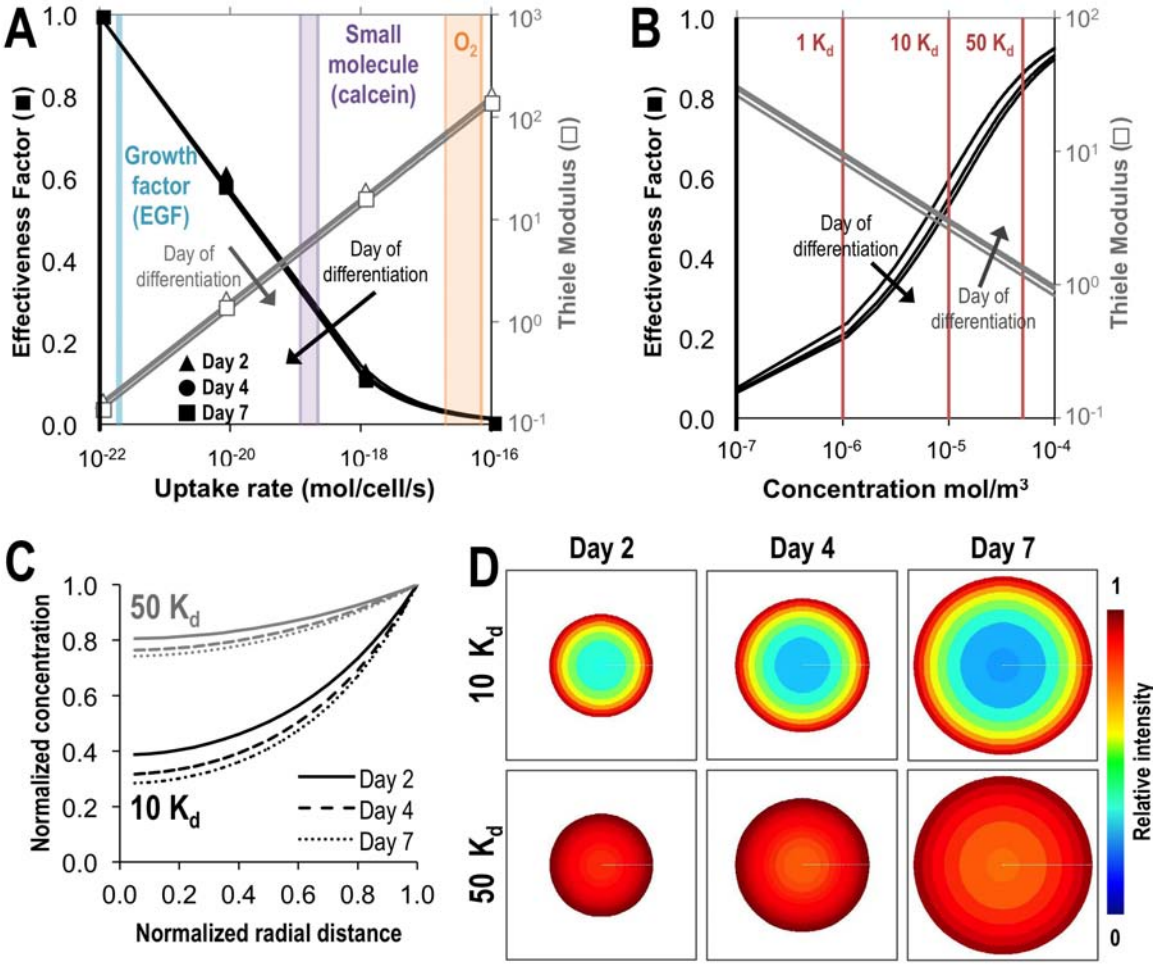

Figure 5-8: Transport profiles with varying molecular characteristics. (A) The Thiele modulus and effectiveness factor were increased and decreased, respectively, as a function of cellular uptake rate, with the uptake rates for growth factors (blue) suggesting decreased transport limitations compared to small molecules (purple) and oxygen (orange). (B) Conversely, the Thiele modulus was decreased as a function of biochemical concentration, with (C,D) decreased spatial heterogeneity upon increasing from 10-fold to 50-fold increases in the growth factor dissociation constant (K_d). Scale bar in (D) = 100 μm.

significant response compared to nave cells all concentrations ($p<0.01$). However, even at concentrations as low as 5 ng/mL, 14.5% of monolayer cells were CFP+, compared to only 4.5% of cells from EBs ($p=0.003$). Interestingly, the coefficient of variance was significantly increased at lower BMP concentrations, but decreased with the addition of 20 ng/mL BMP4, suggesting a decrease in heterogeneity with increasing morphogen concentrations, consistent with the mathematical results (Fig. 5-8).

5.3.6 Computational dynamics of growth factor distribution during with phenotypic transitions

While the sentinel signaling cells provide an approach to assess downstream signaling activation upon exogenous growth factor stimulation, direct comparison of the biochemical transport during the course of time remains difficult due to dynamic changes in cell phenotype, which alters the responsiveness to biochemical signals. For example, upon differentiation, cells may either increase or decrease cell surface receptor presentation, leading to increased or decreased uptake rates, respectively. Moreover, the response to various pathways is altered temporally as cells proceed down various differentiation trajectories. We have previously established a rules-based computational platform capable of recapitulating spatial patterns of early differentiation due to competing feedback from the intercellular communication of neighboring cells [349]. To assess growth factor transport as a function of differentiation, the model was used to generate representative patterns of undifferentiated and differentiated cells from transitional stages (Fig. 5-10). The differentiated cells either maintained the same uptake rates as the undifferentiated cells or exhibited increased of decreased uptake. Overall, these data suggest that the influence of the differentiated cells is not apparent at early stages, but dominates later stages of differentiation. Moreover, while the transport patterns remain largely reminiscent of spherical diffusive transport profiles, the patterns of differentiation also lead to spatial heterogeneity, particularly in the

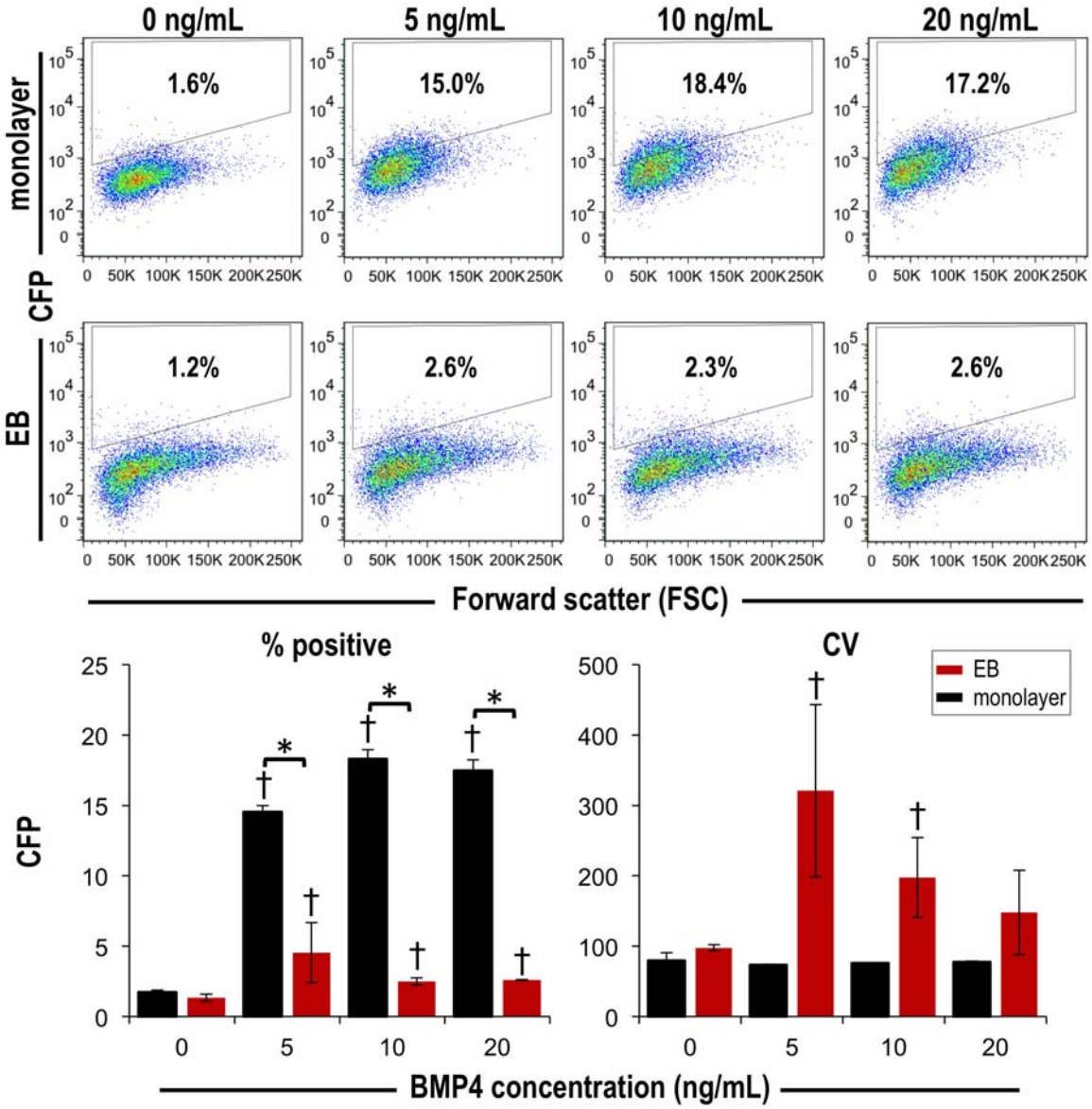

Figure 5-9: Attenuation of growth factor signaling in spheroids. Forward scatter (FSC) versus CFP fluorescence profiles for monolayer (top) and spheroid (bottom) cultures, across a range of BMP4 concentrations, including 0, 5, 10 and 20 ng/mL. The denoted gate was established based upon 1% in naive, untransduced D3s. Cells cultured in monolayer demonstrated increased proportions of CFP+ cells, with a decreased coefficient of variance. † = $p \leq 0.01$ compared to nave cells (untransduced D3s). * = $p < 0.005$ compared to denoted comparison.

transitional stages whereby approximately half of the cells are differentiated. Together, these data indicate that changes in the molecular identity of differentiating cells may dynamically alter growth factor signaling within spheroids, leading to increases and decreases in the transport limitations characteristic of specific growth factors.

5.4 Discussion

This study elucidates the dynamics of diffusive transport during stem cell differentiation and highlights characteristics of stem cell aggregates that lead to transport limitations. The analysis of both small molecule uptake and growth factor signaling via quantitative, single cell metrics provided a foundation for mathematically probing a larger experimental space by varying individual parameters such as cell density, biochemical characteristics (uptake, concentration), and cell phenotype. As stem cell aggregates pose unique challenges due to dynamic changes in cell identity and aggregate size, as well as exquisite sensitivity to both microenvironmental and biochemical cues, this study provides a foundation for understanding the role of exogenous morphogens during differentiation. Together, these data highlight the stark transport limitations in stem cell spheroids, thereby suggesting an increasing role of endogenous factors in the regional patterning and morphogenesis that occur within differentiating structures and organoids and ultimately highlighting individual parameters, which may be exploited through engineering approaches to modulate the delivery of exogenous biochemical cues.

The transport within spheroids has long been an area scientific interest, particularly in the context of oxygen transport [337], as the high oxygen uptake rates lead to hypoxic conditions, which can cause necrosis [347] and decreased growth rates [46]. Interestingly, Wartenburg et al measured a 10 fold increase in the diffusion coefficient

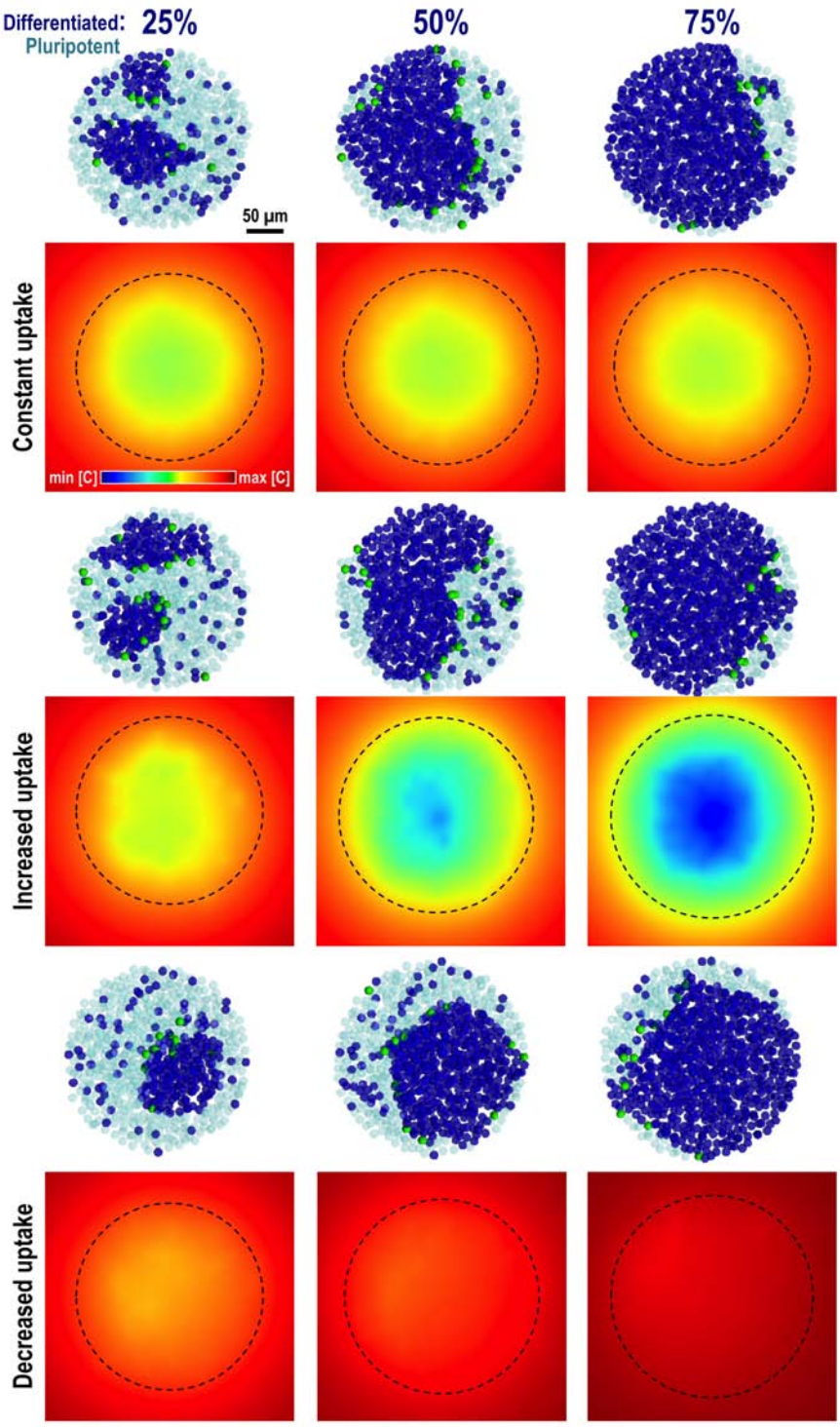

Figure 5-10: Spatial heterogeneity in growth factor transport due to phenotypic transitions. EBs consisting of undifferentiated (cyan) and differentiated (blue) cells from representative transitional stages of differentiation, consisting of 25, 50 and 75% differentiated cells, were developed using a computational algorithm. The transport was modeled in the instances where: all cells exhibited constant uptake, differentiated cells exhibited 10-fold increased sensitivity to the soluble morphogen, and differentiated cells exhibited 10-fold decreased sensitivity.

within vascularized EBs compared to early stage, avascular spheroids [347]; similar to the incorporation of microparticles, modeled herein, the development of voids within the spheroid structure highlight opportunities for engineering spheroids with altered diffusive transport kinetics via incorporation of internal structures via guidance of biological phenomena or integration of novel biomaterial structures. Moreover, the increased diffusive transport within vascularized EBs has implications for the role of exogenous morphogens during the course of time and in the context of directed differentiation protocols toward different germ lineages, particularly within spheroids composed of tightly packed, epithelial structures which remain avascular, even at later stages of differentiation.

In addition, regions of tumor formation *in vivo* also rely primarily on diffusion [296], due to the lack of lymphatics, which has prompted parallel studies of tumor spheroids [313], which exhibit similar dense cellular organization and avascular characteristics, analogous to stem cell aggregates. Multicellular tumor spheroids have provided valuable insight into cancer biology, as they recapitulate aspects of *in vivo* pathology, including cellular heterogeneity [369], morphology [60], cell growth kinetics [132, 109], and drug resistance [348, 330], more accurately compared to the same cells in monolayer cultures, thus underscoring the context dependence of responses to environmental cues. In addition, the density within cellular aggregates comprised of other stem and progenitor cell types (i.e. MSC spheroids, neurospheres, cardiospheres) [20, 17, 30, 82] dictates similar consideration in the experimental design, as the in biochemical milieu will likely be distinct from that of cells in monolayer or other scaffold-based 3D formats.

In contrast to cancer therapeutics, which largely rely on the transport of small molecule drugs, embryonic development and stem cell differentiated occurs via the integrated effects of a wide range of different morphogens [228]. For example, retinoic acid, which is secreted by Hensens node in chick development [136], is a hydrophobic

small molecule (300 Da) that is membrane permeable and does not depend on extracellular receptor binding for downstream signaling [261]. Therefore, the transport characteristics of small molecule dyes such as calcein AM (995 Da) may more accurately recapitulate the spatial transport characteristics of retinoic acid. In contrast, growth factors exhibit a wide range of molecular sizes and signaling is dependent upon receptor presentation, which dramatically alters the availability, analogous to molecular consumption or uptake rates. As the cell surface identity of cells is dynamically altered during the course of stem cell differentiation [289], the changes in receptor distribution are expected to alter the transport characteristics of stem cell spheroids, both due to spatial and temporal changes in cell fate (Fig. 9). While growth factor signaling has previously been difficult to characterize quantitatively, the novel technology [297] implemented herein provides a proof-of-concept for understanding BMP4 signaling in spheroids; in combination with imaging platforms [135], signaling reporter cells may be amenable to further elucidating the spatiotemporal kinetics of signaling in real time during differentiation.

In addition to direct changes in receptor availability upon phenotypic changes, cell fate also alters the metabolic and proliferative properties of the differentiated cells [135, 205], which may also change the efficacy of delivered morphogens. For example, the responsiveness of tumor cells to cancer therapeutics is altered spatially [147], and hypothesized to originate due to the metabolic and hypoxic state of cells at the center of the tumor [85]. The oxygen transport in spheroids has been computationally [337] and experimentally [346, 278] studied in various contexts, with reports of hypoxic regions, particularly at the center of large EBs. Therefore, regions of hypoxia within EBs may also lead to spatial heterogeneity due to increased signaling via the HIF pathway [50], and may therefore alter the response to exogenous morphogens and the profile of endogenously secreted morphogens as a function of differentiation stage. Moreover, extracellular matrix molecules [105], such as glycosaminoglycans,

alter transport via steric hindrance as well as through binding of growth factors, which alters the availability and diffusion coefficient of molecules within multicellular spheroids [239, 152]. In addition, one parameter not accounted for in this model is the internalization and degradation of molecules. While such dynamics depend upon receptor availability and ligand concentration, the dynamic changes in response to exogenous molecules may also contribute to spatial changes in the diffusive transport profile, particularly at high concentrations [123]; in addition, as typical media replenishment regimens are on the order of several days, the steady state transport may be altered over time due to degradation of supplemented morphogens. This phenomenon highlights the possibility that endogenous molecules may play increasing roles at distinct stages of differentiation, depending on the timing and precision of the supplementation regimen, which may ultimately alter the differentiation trajectories and/or the inter-experimental variability either within or across laboratories.

The results presented demonstrate the attenuated small molecule and growth factor signaling within spheroids, highlighting the need for increased concentrations and/or alternative delivery modalities. These results have direct implications for the adaptation of protocols developed in monolayer, and highlight the increased role of paracrine signaling in spheroids. Therefore, in the context of current techniques for organoid differentiation and morphogenesis, it is likely that the signals dictating patterning and interior structure formation are derived from paracrine signals derived from various populations within the spheroid. However, there may also be an essential role for the exogenous milieu in directing differentiation via the exterior cells [39, 164]. For example, EB differentiation in the presence of serum has been well characterized to occur via specification of the exterior cells toward the endoderm lineage [95]; moreover, the endoderm cells further direct differentiation within the spheroid toward cardiac fates [22], analogous to similar signaling roles in embryonic development [293]. In addition, polarity has been postulated to play a role in the spatial

context for embryonic development [341], which highlights possible innate differences in the cells at the exterior and interior of spheroids.

The stark transport characteristics of EBs also highlight opportunities to develop engineering approaches amenable to altering the exogenous delivery to impart spatially precise gradient or present localized morphogen delivery. Therefore, the increasing implementation of stem cell spheroids within microfluidic platforms [368] is a promising to route to impart controlled culture conditions and is easily amenable to gradient formation [63] and fluidic convection [162]. In addition to the physical and structural role for microparticles in modulating the effective cell density within spheroids, morphogen delivery via microparticles also provides a method for local exogenous presentation of growth factors and small molecules in the interior of cell aggregates [41, 51]. With the advent of new approaches to precisely control biochemical loading and release [185], it may be possible to create a more homogeneous biochemical context, analogous to differentiation of stem cells in monolayer or to direct patterning via precise, localized point sources of morphogen secretion [124], in order to recapitulate the activity of organizing centers in development.

Ultimately, the biophysical characteristics of stem cell aggregates, including high cellular density, minimal ECM deposition, and embryonic-like biophysical characteristics (Chapter 4), paired with the high metabolic demand of stem cells and complexity arising from divergent differentiation trajectories, contribute to unique transport profiles accompanying the initiation and differentiation of stem cell-derived microtissues and highlight routes to harness or modulate the exogenous gradients for the development of tissue engineered constructs or patterning of organoid structures.

CHAPTER VI

DEVELOPMENT OF A BIOREACTOR PLATFORM FOR CONVECTIVE TRANSPORT IN STEM CELL AGGREGATES

6.1 Introduction

The growing interest in the clinical promise of stem cells has prompted parallel strategies to engineer scalable manufacturing platforms for the implementation of stem cell expansion and differentiation schemes within bioprocess development pipelines. Interestingly, the culture of pluripotent embryonic stem cells (ESCs) as three-dimensional spheroids, traditionally implemented as a route to induce differentiation [146], is easily amenable to traditional scalable bioreactor platforms, across different volume scales [377, 47, 104]. Such large volume mixed configurations such as spinner flasks, rotating wall vessels (RWV), and slow turning lateral vessels (STLV) enable batch processing, with increased control of the physiochemical parameters of the culture environment [42] via automation and monitoring [291, 21], thus allowing increased reproducibility within and between lots of the biological product. Moreover, the stem cell spheroids, termed embryoid bodies (EBs), enable parallel processing of individual microtissues within a single reactor volume; however, in contrast to traditional tissue engineering strategies which employ fixed scaffolds within the reactor [32], microtissues freely move with the fluid flow [282], thereby complicating the analysis of hydrodynamic parameters such as fluid shear and transport within stem cell spheroids [166]. In addition, stem cells pose distinct requirements due to the extreme sensitivity to biophysical and microenvironmental perturbations [52, 282, 165], as well as heterogeneity stemming from the three-dimensional microtissue structure [39]. While

stem cell expansion and differentiation within platforms adapted from other industries have provided a proof-of-concept for the feasibility of implementation in scalable bioprocesses, the increased understanding of stem cell biology motivates parallel tailored approaches for engineering novel platforms to direct three-dimensional stem cell differentiation.

Routes to direct stem cell differentiation have traditionally relied on conserved signaling pathways studied in embryonic development and morphogenesis, and therefore largely focus on the delivery of biochemical cues, such as growth factors and small molecules, to alter stem cell fate in a temporally sensitive manner [228]. However, within stem cell spheroids, the biochemical context is also spatially altered, due to diffusive transport limitations [278, 51], thereby resulting in spatially heterogeneous signals, which may ultimately impact cell fate. Therefore, understanding and controlling transport within stem cell spheroids has implications for directing stem cell differentiation and patterning. In analogous avascular microtissues, low velocity extracellular fluid flow improves viability of large tissue constructs [271, 75, 76] and has been implicated in morphogenesis and remodeling. For example, implementation of interstitial flow *in vitro* [35] directs blood and capillary formation [294, 130, 131], ECM deposition [267] and as well as cell alignment [240], and migration [264], likely due to the development of morphogen gradients and proteolytic remodeling. Moreover, at velocities in the range of interstitial transport (0.1-1 μm/s) [123], the local shear stresses have been measured on the order of 10^{-2} - 10^{-3} dyn/cm^2 [257], suggesting that interstitial transport may be amenable to overcoming transport limitations in avascular tissues, without imparting high shear forces.

The objective of this study, therefore, was to engineer a novel bioreactor platform to impart convective transport, based on the design constraints specific to stem cell biology and spheroid differentiation. A custom bioreactor was designed and fabricated in order to impart controlled convection by altering the pressure drop across

aggregates immobilized within individual fluidic microwells. Interestingly, while EBs were immobilized with high specificity, there was no significant evidence of increased dye uptake upon forced convection via perfusion. To inform the parameters for a computational fluid dynamics (CFD) model of fluid transport in stem cell spheroids, the bioreactor platform was instead employed as a novel route to directly measure fluidic resistance and permeability within EBs. Overall, while EBs exhibited a range of permeability ($\sim 10^7$ cm^2) conducive to fluidic transport at low velocities with minimal stress (<1 dyn/cm^2), CFD modeling suggested that the mismatch in bulk and EB permeability within the bioreactor design resulted in non-uniform flow within the EB. Together, these data suggest a computational proof-of-concept for the implementation of low velocity fluidic convection by matching bulk permeability with that of stem cell spheroids as a novel route to deliver morphogens and engineer gradients to manufacture three-dimensional microtissues amenable to implementation as clinical regenerative therapeutics.

6.2 Materials and Methods

6.2.1 Bioreactor fabrication and assembly

A perfusion bioreactor was custom designed using SolidWorks and fabricated via stereolithography using a Viper SLA system (FineLine Prototyping), which is ideal for manufacturing fine details, with a minimum feature size of 0.004 inches. The bulk bioreactor material was a Somos 9120 resin, which is a UV cured photopolymer. The parts underwent standard finishing by sanding to remove SLA artifacts prior to assembly. The internal features of the bioreactor were created from a 500 μm thick sheet of polyethyl ethyl ketone (PEEK), with holes created via laser drilling. The array was specified with 110 holes of 80 μm diameter, with 750 μm spacing between the holes. The final bioreactor platform was assembled via standard hardware and

using polydimethylsiloxane (PDMS) to create an air- and water-tight seal.

6.2.2 Bioreactor operation and validation

The bioreactor design implemented threaded input ports for cross flow and EB seeding, as well as output ports for the cross flow and perfusion. The tubing configuration was set up such that the two outputs were driven independently by individual syringe pumps (KD scientific), with working flow rates in the range of μL/min. Initial filling of the channels was accomplished via subsequent washes with ethanol and PBS in order to ensure removal of all bubbles from the system. In addition, three-way valves were implemented within the tubing upstream of the device input in order to avoid bubble entry while switching solutions.

The validation of cross flow and residence time was accomplished using dye injected into the system at a series of flow rates. The videos of dye flow through the device were collected using a digital camera and were analyzed via a custom written MATLAB code, whereby the image analysis was conducted across samples from various locations in the chamber, and iterated over the course of time. The normalized concentration was plotted as a function of time, and the residence time was calculated as the difference between the curves at opposite ends of the channel.

6.2.3 Embryoid body formation & culture

Murine embryonic stem cells (D3 cell line) were expanded undifferentiated in Dulbeccos Modified Eagles Medium (DMEM) containing fetal bovine serum (FBS; 15%), L-glutamine (2 mM), penicillin (100 U/mL), streptomycin (100 μg/mL), amphotericin (0.25 μg/mL), non-essential amino acids (1x), β-mercaptoethanol (0.1 mM) and leukemia inhibitory factor (LIF; 1000 U/mL). Media was replenished every other day and cells were routinely passaged at 70% confluence.

Embryoid bodies were formed via forced aggregation of undifferentiated ESCs into 400 μm diameter agarose microwells, with 1000 cells per well. After 24 hours

of formation, spheroids were removed from the microwells and transferred into bulk suspension in 100 mm petri dishes on a rotary orbital shaker. EBs were maintained by exchanging 90% of the media every other day through day 7 of differentiation. EB formation was accomplished using complete ESC media without LIF, as previously described, and were subsequently differentiated in either the same serum containing media or a chemically defined serum-free media containing N2 and B27 supplements.

6.2.4 Mathematical modeling of oxygen concentration & fluid shear

The steady state oxygen concentrations within the bioreactor channel were mathematically assessed using standard models for transport and consumption within a well-mixed volume. The oxygen consumption rate was assumed to be $4\text{x}10^{-17}$ mol/cell/s, based on previous reports in stem cells [337], and were assumed to remain constant during the course of differentiation. The number of cells within the system was assumed to increase based on previously measured growth kinetics, with ~7 fold increase over the course of differentiation. The total number of cells was modeled based on the previously measured metric of cells per EB, assuming 100% seeding efficiency within the perfusion array. Curves of oxygen concentration as a function of flow rate were constructed for each day of differentiation and the minimum flow rates were established, defined as the rate at which oxygen concentration was maintained at 90% of the bulk concentration at steady state. The wall shear due to fluid movement was calculated across the same range of fluid flow conditions, according to the standard equation for parallel plate geometries (Eq. 11):

$$\tau = \frac{6Q\mu}{bh^2} \tag{11}$$

where Q (m^3/s) is the volumetric flow rate, μ (Pa·s) is the fluid viscosity, b (m) is the chamber width, and h (m) is the chamber height.

6.2.5 Small molecule transport

The transport within EBs was characterized via fluorescent dye distribution in EBs, using calcein AM (0.1 μM) in DMEM. In all cases, EBs were immobilized in the microwell array using DMEM alone, as previously described. Media containing calcein AM was then flowed through the channel at an exchange range of 200 μL/min for 10 minutes (total volume of 2 mL), followed by washing with DMEM at the same flow rate for 20 minutes. In addition to the cross-flow delivery of calcein AM, perfusion flow was imparted at rates of 10 and 50 μL/min. In each case, the cross flow rate was decreased to 190 and 150 μL/min, respectively, in order to conserve the total molar quantity of calcein AM delivered to the EBs over the course of the experiment. After washing, EBs were collected from the outlet, dissociated using 0.05% trypsin / 0.53 mM EDTA, and suspended in PBS. The fluorescent intensity profiles within the cell populations were assessed via flow cytometry using an Accuri C6 cytometer with an attenuated FITC filter (FL1 90%; 530 15 nm). Subsequent analysis was conducted with FlowJo software.

6.2.6 Measurement of EB permeability

EB permeability was assessed directly within the perfusion bioreactor configuration by measuring the pressure drop across EBs. EBs were immobilized within the microwells by adding a large excess of spheroids within the bioreactor volume. The flow configuration was modified to include a series of two pressure transducers upstream of the inlet and downstream of the perfusion outlet. The pressure drop was recorded as a function of flow rate, across a range of relevant perfusion flow rates (50-500 μL/min). Baseline measurements without EBs were recorded in order to determine the baseline resistance of the empty reactor volume and subsequent measurements of EBs were then normalized by subtracting the empty baseline. The slope of the resultant curve (pressure vs. flow rate) was then used to define the fluidic resistance

(Pa/μL/min). Permeability was calculated using Darcys Law (Eq. 12):

$$\kappa = \frac{Q}{\Delta P}\frac{\mu \Delta L}{A} \tag{12}$$

where ΔP/Q (Pa·s/m^3) was the slope of the curve, μ (Pa·s) is the fluid viscosity, ΔL (m) is the diameter of the EB, and A (m^2) is the cross sectional area of flow through the series of 110 holes (80 μm diameter). The diameter and cellular composition of EBs was characterized in parallel using morphometric analysis of phase images and coulter counter metrics, respectively.

6.2.7 Computational fluid dynamics

To model the perfusion flow within EBs, a simplified geometry was developed in COMSOL, consisting of an EB immobilized over a single microwell with single inlet and outlet. The model employed coupled fluidic and solid mechanics physics modules in order to assess the transport as well as physical changes in EB ultrastructure under perfusion conditions. Within the free and porous media flow model, the bulk media was approximated to have the same properties as water, with the EB modeled as a porous media of defined properties (Table 2). The permeability and mechanical characteristics were based upon previously measured values; the porosity was based on the previously validated assumption of spherical packing within EBs [349] and the remaining geometries were based upon constraints from the bioreactor design. The fluid was driven by laminar outflow at defined velocities from 1-100 μm/s, with laminar inflow assuming atmospheric pressure. The secondary solid mechanics module employed the solution for pressure drop in response to fluid flow as the boundary condition for determining the stress and deformation on the spheroid, with the EB modeled as a linear viscoelastic material. A stationary solver was used to determine the solutions within a physics-controlled mesh consisting of 63131 elements. Based upon the 2D solution, a vertical 1D cut line was created corresponding to the length

of the EB along the center of microwell outlet and the pressure drop was calculated as the pressure difference across the EB length. The minimum and average calculations for stress and deformation were calculated over the domain corresponding to the EB area.

Table 2: Computational fluid dynamics model biophysical parameters

Parameter	Value	Reference
Permeability	1x10^{-11} m^2	Measured
Porosity	0.25	Spherical packing
Young's modulus	200 Pa	Measured
Poisson's ratio	0.45	Measured
Outlet diameter	80 μm	Design constraint
Chamber height	800 μm	Design constraint
Velocity (output)	1-100 μm^2/s	Independent variable

6.2.8 Statistical analysis

All experimental analyses were conducted with n=3 replicates, and represented as the mean ± standard error. Prior to statistical analysis, all data were pre-processed using a box-cox power transform, in order to normalize data according to a Gaussian distribution. Statistical tests were conducted between groups and time points using one-way ANOVA, combined with either a post-hoc Tukey test for comparison of individual samples.

6.3 Results

6.3.1 Design constraints & principles of operation

The central objective of this project was to design a novel bioreactor platform to enable convection within stem cell spheroids. The design criteria were developed based on engineering (Table 3) and biological (Table 4) constraints, which together accomplish the two major goals of: (1) supporting standard spheroid culture conditions, while simultaneously (2) imparting convection through spheroids. Specifically, the simple parallel plate channel design (Fig. 6-1 A) enables laminar flow, with well-mixed concentrations via a series of pillars at the input and output, in order to permit exchange of media, waste, nutrients, analogous to bulk media exchange in standard *in vitro* cultures. Moreover, in addition to supporting cell viability via media exchange, the parallel plate flow configuration also enables morphogen supplementation and removal, in order to direct differentiation via biochemical cues with high temporal sensitivity. Within the channel design, a laser-drilled grid is housed above the perfusion outlet. The polyether ether ketone (PEEK) grid serves the dual purposes of enabling immobilization of spheroids within microwells (110 wells per channel; 80 μm diameter) and ensuring that all flow exiting the perfusion outlet occurs through the microwells, and thus through the immobilized EBs. By arraying the spheroids with fixed well spacing (750 μm), the device design enables independent culture of EBs, and avoids agglomeration that can lead to size heterogeneity [165] and increased transport limitations. Moreover, the fluid convection constrained through the microwells decreases the cross sectional area for flow, and thus decreases the overall magnitude of velocity required within the system. Finally, when assembled, the device can be maintained as a closed-loop, with separate modes of operation for: (1) EB seeding, (2), cross flow, and (3) perfusion flow, each of which has independent control via input/output ports and syringe pumps (Fig. 6-1 B). A port at the top of the channel enables direct EB input to the channel volume; upon deposition into the channel,

the perfusion flow is employed to capture the spheroids over microwells, while any free spheroids are removed via cross flow. During the culture duration, the cross and perfusion flows are operated separately via downstream syringe pumps, in order to modulate the delivery and/or transport kinetics of the system. EBs can be retrieved by simply ceasing perfusion flow and collecting the fluid volume from the cross flow channel outlet.

Table 3: Engineering constraints for perfusion bioreactor design

Specification	Rationale	Implementation
Low Reynold's number flow	Laminar flow	Parallel plate geometry
Well mixed	Uniform concentration throughout chamber	Pillars at input and output
Closed loop	Sterility; minimal manipulation	Integrated seeding and cross flow
Perfusion control	Preferential flow through spheroids	Laser drilled holes in rigid substrate
Temporal control	Modulation of biochemical culture conditions	Independent cross flow magnitude
Real-time monitoring	Validation of design and operation	Optical access; in line pressure sensors

6.3.2 Exchange of nutrients, waste, and supplements

In order to enable flexibility in terms of exchange kinetics, the parallel plate flow channel was designed with a small volume (∼0.5 mL). In addition to the channel size, the small number of immobilized EBs enables the implementation of low velocity

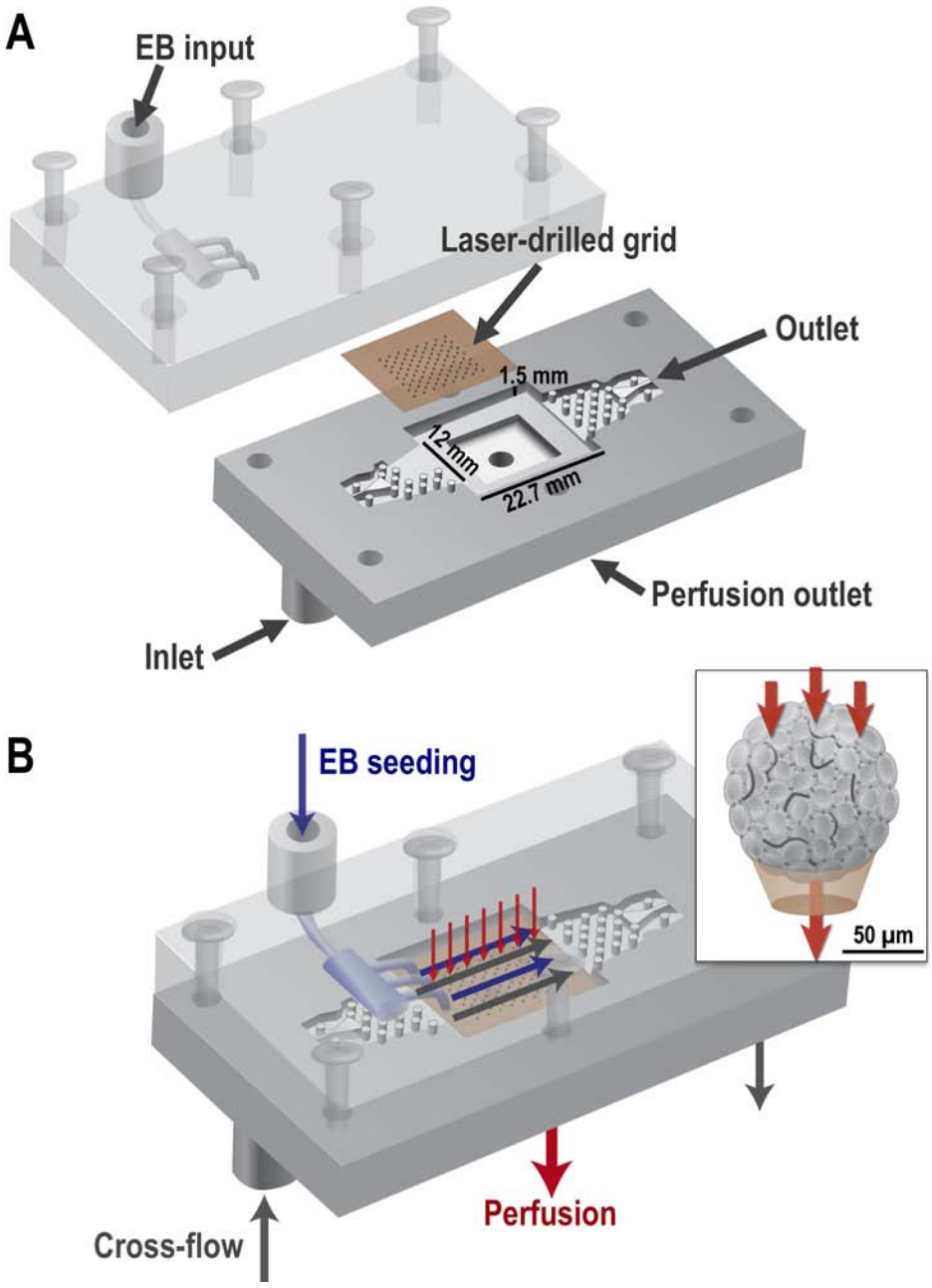

Figure 6-1: Bioreactor design and operation. (A) The perfusion bioreactor consists of an assembly of three pieces: (1) a lid containing the inlet port for EBs, (2) the main body of the bioreactor with parallel channel geometry, cross flow inlet and outlet and perfusion outlet, and (3) a laser drilled grid amenable to arraying immobilized EBs, which is housed above the perfusion outlet. (B) The assembled bioreactor operates in three independent modes, by enabling EB seeding (blue), providing cross flow of media and morphogens (gray), and perfusion through the microwells (red; inset). Bioreactor drawn to scale, based upon SolidWorks drawing, with relevant length scales denoted. Scale bar in (B) = 50 μm.

Table 4: Biological constraints for perfusion bioreactor design

Specification	Rationale	Implementation
Limit EB agglomeration	Culture uniformity & reproducibility	Immobilization in individual wells
Limit EB agglomeration	EB growth during differentiation	Fixed well spacing (750 μm)
Limit shear & EB deformation	Minimize secondary effects on phenotype	Low magnitude perfusion and cross flow rates
Maintain oxygen concentration	Maintain cell viability & metabolic profiles	Cross flow delivery of fresh media
Supplementation of morphogens	Direct stem cell differentiation	Amenable to addition via cross flow

flow in order to provide adequate oxygen and nutrient transport (Fig. 6-2 A). Based on known growth kinetics and molecular consumption rates of oxygen, the average concentration was calculated across a range of flow rates, assuming well-mixed conditions within the channel (Fig. 6-2 B). Particularly at early stages of differentiation with smaller EBs ($\sim$1700 cells/EB), flow rates as low as 50 μL/min would maintain adequate oxygenation within the channel volume. However, by 7 days of differentiation ($\sim$14,000 cells/EB), a minimum exchange of 350 μL/min would be required. Although the increase in cell yield during differentiation necessitates a $>$7 fold increase in the fluid exchange, the magnitude of flow rates remains low, with fluid shear below $\ll$1 dyn/cm^2 (Fig. 6-2 C). Therefore, the parallel plate bioreactor design is amenable to providing adequate oxygenation while imparting minimal fluid shear on EBs.

In addition to functionality in terms of media replenishment, the cross flow design

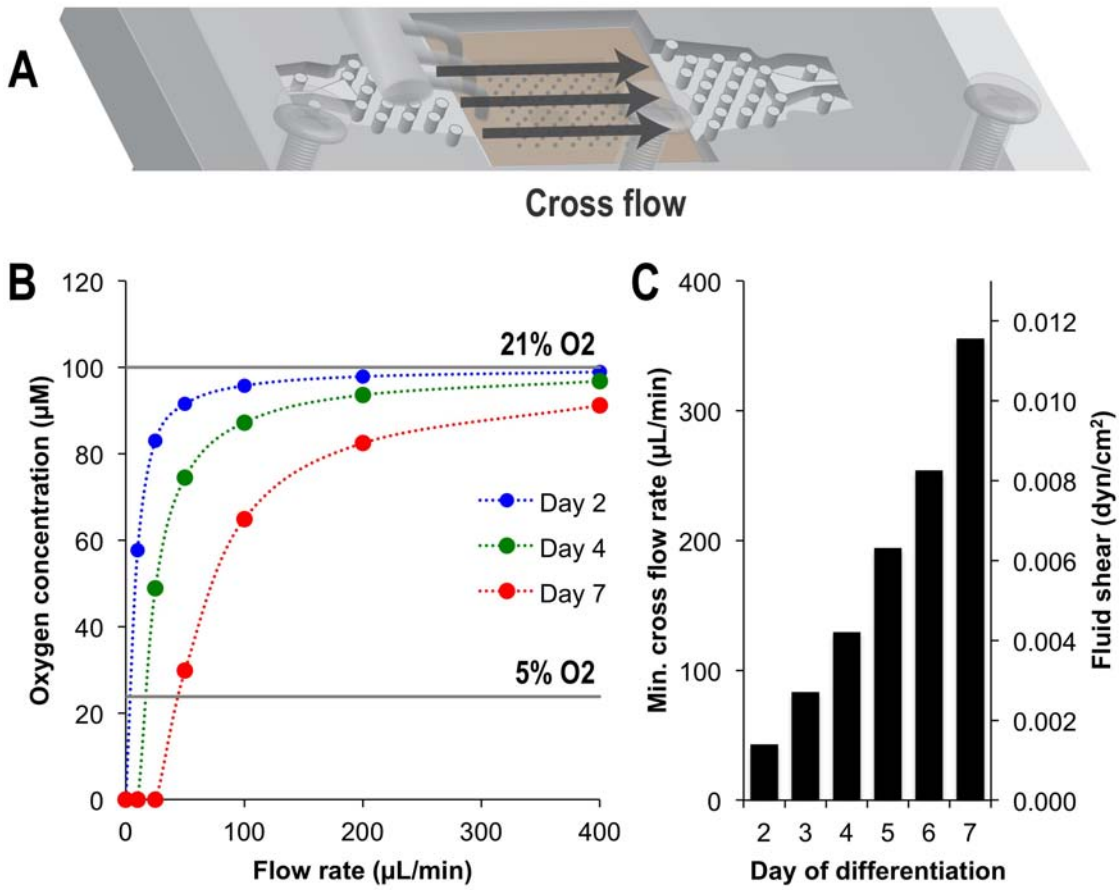

Figure 6-2: Oxygen exchange via laminar cross flow. (A) Schematic representation of the bioreactor cross flow. (B) The oxygen concentration was mathematically calculated across a range of flow rates, based upon standard mass balance equations with known rates of ESC oxygen consumption and EB sizes after days 2 (blue), 4 (green) and 7 (red) of differentiation. The concentrations for standard *in vitro* culture concentrations at atmospheric (21% O2) and low or hypoxic (5% O2) oxygen levels are denoted for reference. (C) Based upon calculated oxygen concentration curves, the flow rate corresponding to 90% of atmospheric oxygen (90 μM) was determined as the minimum flow rate for each day of differentiation. Moreover, the fluid shear stress arising due to cross flow within the parallel chamber was calculated for the minimum flow rates corresponding to each day of differentiation.

within the parallel plate chamber also enables temporal control of the biochemical microenvironment, including additional and removal of supplements such as growth factors or other morphogens. While the exchange time varies depending on the application and cross flow velocity, there is a rapid transition in concentration, on the order of minutes, within the range of expected cross flow rates (Fig. 6-3 A). For example, while the expected cross flow rates varied from 50-350 μL/min during the course of EB culture, the corresponding exchange times range from 27 to 3 minutes, respectively (Fig. 6-3 B). Moreover, the fast temporal dynamics of media exchange also enables rapid swapping of media compositions; by implementing a manual or automated valve system, it is possible to continuously alter the biochemical concentration on the order of minutes. While the temporal dynamics of morphogen addition to stem cell culture has been identified as a critical determinant of cell fate, the features implemented within the perfusion bioreactor platform are amenable to more systematically perturbing the temporal experimental space.

6.3.3 Embryoid body immobilization

In addition to the spatiotemporal control of the biochemical composition enabled by the parallel plate cross flow design, the bioreactor also integrates a novel, laser-drilled grid microwell configuration for EB immobilization and perfusion. The array of 110 wells was first validated for the capacity to immobilize an array of EBs. The seeding procedure was developed such that a large excess ($\sim$10 fold) of EBs were added to the chamber volume via an input port at the top of the bioreactor design (Fig. 5-2) while simultaneously imparting a pressure drop through the microwells via suction at the perfusion outlet. Subsequently, the remainder of EBs were removed from the chamber via the cross flow, using 30% Percoll, in order to increase the EB buoyancy and facilitate entry into the cross flow stream. Upon further washing with media to remove the Percoll, the seeding was assessed via two metrics: 1) efficiency, or the

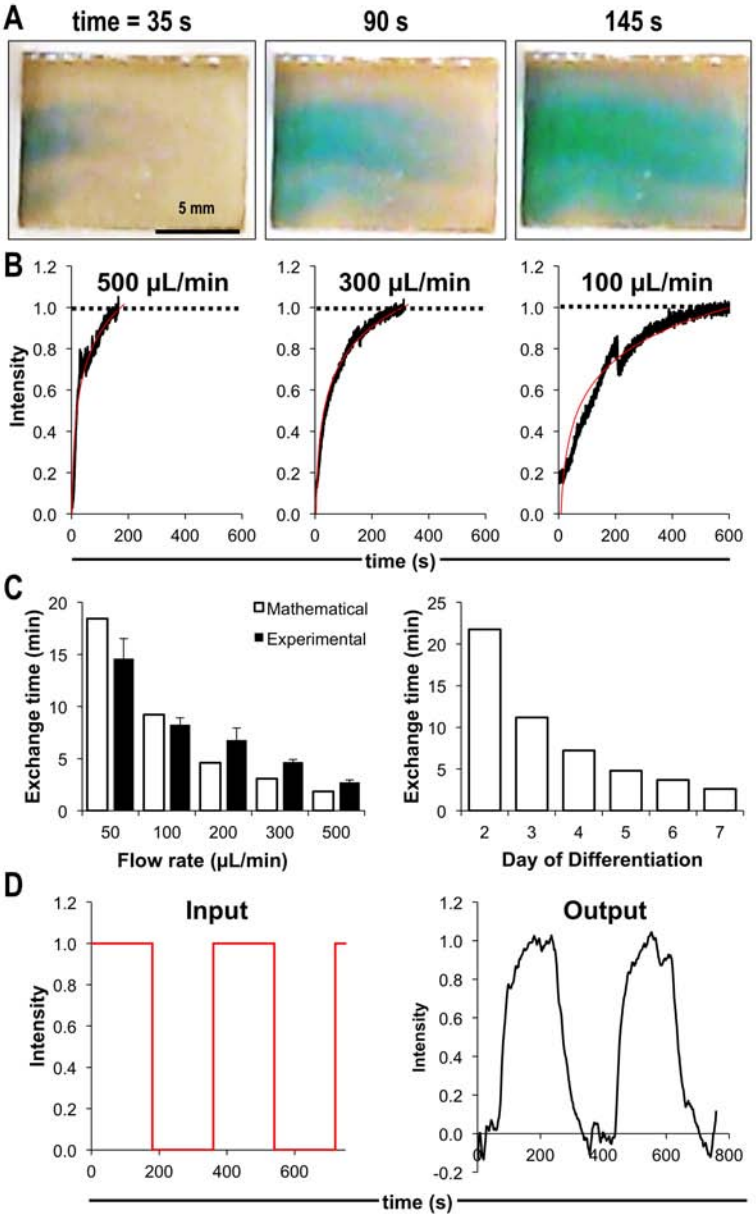

Figure 6-3: Biochemical exchange via laminar cross flow. (A) Dye entry into the bioreactor channel exhibits characteristics of laminar flow, and occurs over the course of minutes at a flow rate of 200 μL/min. (B) When varying the flow rates within a relevant range for EB culture, the channel reaches equilibrium via curves of logarithmic character (red lines), with equilibrium reached more quickly at higher cross flow rates. (C) Experimental measurements and mathematical calculations for the exchange time, defined as the time to reach 90% equilibrium, were consistent across a range of flow rates, and corresponded to exchange times in EBs (based upon minimum flow rates denoted in Fig. 2) <25 minutes. (D) The flow characteristics and fast exchange rates of the platform are also amenable to oscillatory control of concentration within the bioreactor on the order of minutes, by simply changing the input solution. Scale bar in (A) = 5 mm.

percentage of microwells containing immobilized EBs, and 2) specificity, or the percent of EBs remaining in the bioreactor which were properly immobilized over wells (Fig. 6-4). The second metric is particularly important, as EBs remaining on the solid PEEK grid area would not undergo convective perfusion. Under the established seeding procedure, the efficiency of seeding varied between ∼50-90% within individual channels of the bioreactor; however, the overall seeding procedure was reproducible, with no statistical differences between individual seeding trials. Upon visual inspection of dye efflux from the microwells, it was clear that some of the wells were blocked, due to the small cross sectional area. Moreover, a qualitative estimate of free holes demonstrated that there was a difference between channels, with channels 1 and 3 exhibiting ∼70-80% microwells freely permeable to convection, whereas channels 2 and 4 exhibited low instances of clogged microwells, with ∼90-100% open. Therefore, it is likely that the seeding efficiency discrepancies can be explained by relative variability between channels and that all channels exhibit high seeding efficiency, as a percentage of open microwells (∼80-90%). Moreover, the specificity remained high within all channels and across individual trials, indicating that, although all wells were not necessarily filled, the majority (∼90%) of EBs within the bioreactor grid region were immobilized within microwells. Together, these data suggest that the majority of EBs seeded within the bioreactor are immobilized within the microwells, and therefore would undergo perfusion upon implementation of a pressure drop across the microwells.

6.3.4 Convective transport within stem cell aggregates

As previous work indicated striking transport limitations of small molecules dyes within diffusive transport regimes (Chapter 5), the transport of calcein AM was studied in the context of bioreactor delivery and perfusion of EBs after days 2 (Fig. 6-5) and 4 (Fig. 6-6) of differentiation. As previously established, the formation of EBs

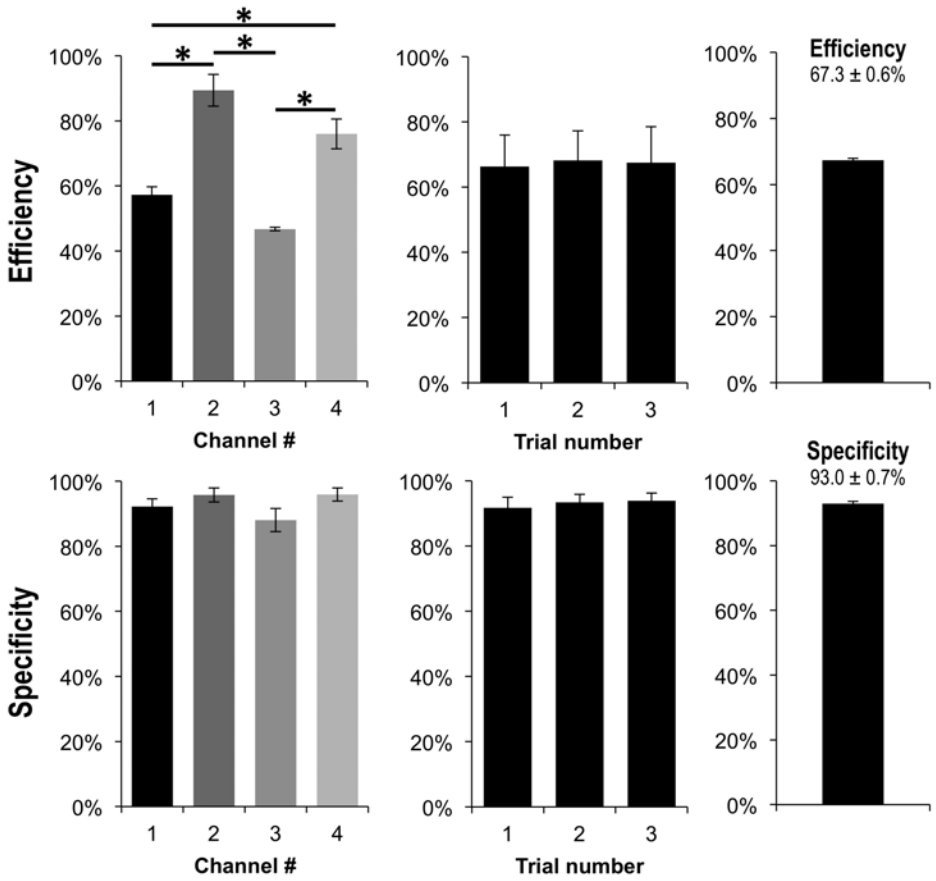

Figure 6-4: EB immobilization within perfusion microwell arrays. Quantification of efficiency and specificity of EB seeding within the perfusion bioreactor microwell array, both as a comparison across individual channels and seeding trials. n = 3 independent trials for n=4 bioreactor channels; * = $p<0.05$ within indicated comparison.

via forced aggregation followed by culture in rotary orbital suspension enables the maintenance of relatively homogeneous, size-controlled populations (Chapter 3). After 2 days of differentiation, EBs exhibit a narrow distribution in terms of EB cross sectional area, with an average diameter of 250.7 μm, whereas EBs were slightly larger (296.9 μm) by day 4 of differentiation. Therefore, both populations were studied, as the transport limitations were expected to be more pronounced in larger EBs. Consistent with purely diffusive transport studies (Chapter 5), the delivery of 0.1 μM calcein AM via cross flow (200 μL/min, total volume of 2 mL) led to EBs exhibiting similar transport limitations, as denoted by a small shift, yet substantial overlap, in fluorescence intensity profile, compared to unstained cells. Therefore, the fluorescence profile of EBs under perfusion was hypothesized to exhibit a more pronounced shift, approaching that of cells stained as a single cell suspension (Chapter 5, Fig. 5-3). However, upon perfusion of EBs at 50 μL/min and a conserved mass flow rate of calcein delivery (200 μL/min), EBs exhibited similar fluorescence intensity profiles compared to those maintained in the absence of perfusion, and did not exhibit statistically significant changes in terms of the median and coefficient of variance of fluorescence or the percentage of positive cells. Moreover, EBs maintained under the same conditions at day 4 of differentiation exhibited similar results, with comparable fluorescence profiles in the presence and absence of perfusion.

6.3.5 Measurement of EB permeability

Although the growth characteristics, size and morphology of EBs have been well characterized during the course of differentiation (Fig. 6-7 A; Chapter 3), relatively little is known regarding the biophysical characteristics of the three dimensional microenvironment; therefore, the bioreactor platform was also employed as a novel approach for directly measuring the fluidic properties of stem cell spheroids. The fluidic resistance of EBs, defined as the change in pressure over a range of flow rates, was

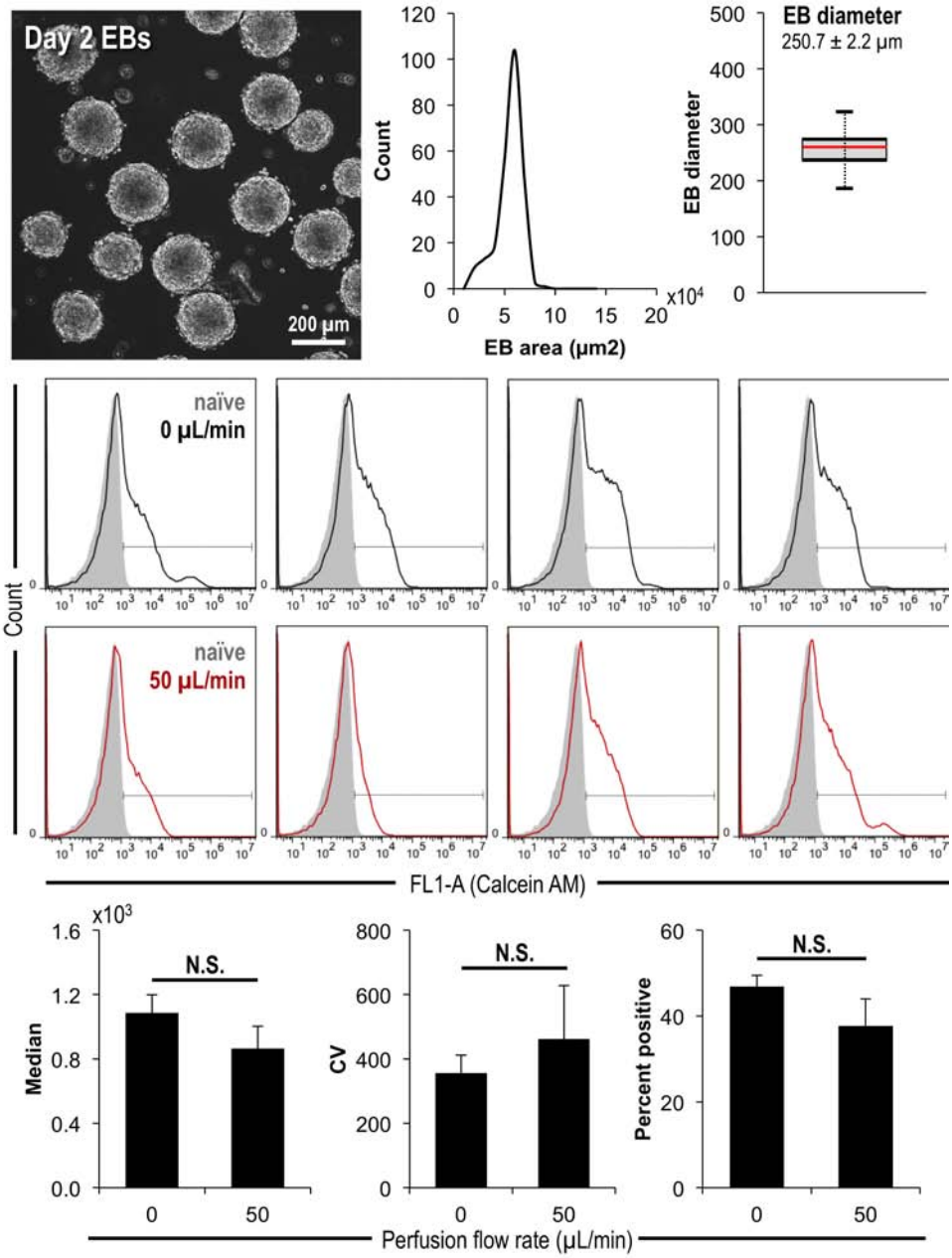

Figure 6-5: Convective small molecule transport within day 2 EBs. EBs after day 2 of differentiation exhibited spherical morphology with a narrow size distribution. The fluorescence profiles after staining with calcein AM exhibited a shift compared to unstained EBs (gray), both without perfusion (black) and after perfusion at 50 μL/min (red). However, the median, coefficient of variance (CV) and percent of positive cells were not statically different when comparing perfused EBs to those maintained without perfusion.

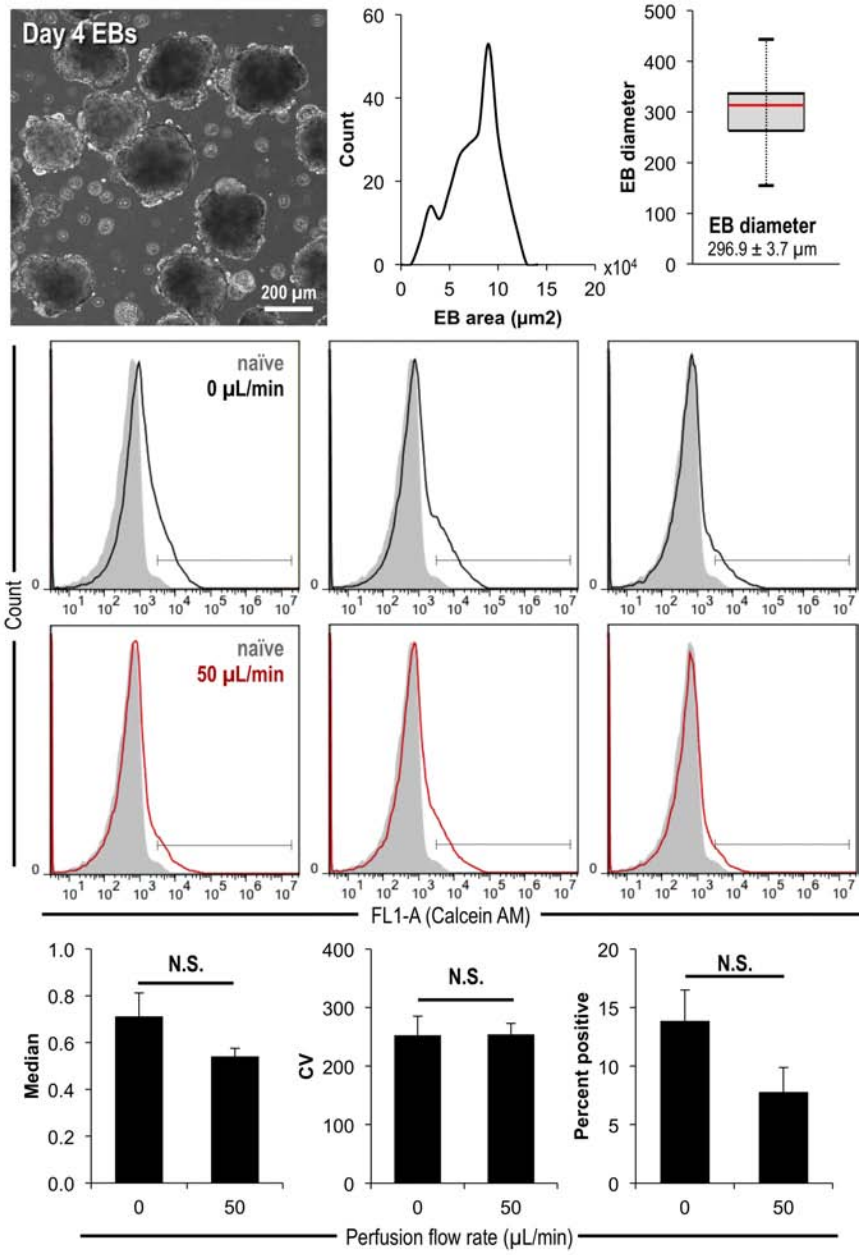

Figure 6-6: Convective small molecule transport within day 4 EBs. EBs after day 4 of differentiation exhibited changes in morphology and size coincident with differentiation, resulting in a wider distribution and overall larger EBs. The fluorescence profiles after staining with calcein AM exhibited a shift compared to unstained EBs (gray), both without perfusion (black) and after perfusion at 50 μL/min (red). However, the median, coefficient of variance (CV) and percent of positive cells were not statically different when comparing perfused EBs to those maintained without perfusion.

calculated by measuring the pressure drop across the perfusion outlet in the presence of immobilized EBs. Between days 2 and 7 of differentiation, the resistance of EBs to fluid flow significantly increased ($p<0.05$ compared to days 2 and 3), with an apparent transition between days 3 and 4 of differentiation (Fig. 6-7 B&C). Reciprocally, the permeability of EBs decreased during the course of differentiation; however, EBs remained more permeable to fluid flow compared to tissue engineered constructs or native tissues (Fig. 6-7 D). In addition, the number of cells per EB was directly correlated ($p=0.01$) with the resistance, whereas the cell size exhibited a significant inverse correlation ($p<0.001$) with resistance, thereby demonstrating that morphogenic changes that occur during differentiation are related to changes in the fluidic properties of EBs. Together, the measurement of EB permeability provides a basis for further understanding diffusive and convective transport in stem cell spheroids.

6.3.6 CFD analysis of perfusion flow within EB microwells

To more throughly dissect the mechanisms underlying convective transport in the bioreactor platform developed herein, computational fluid dynamics (CFD) modeling was employed to inform spatially aspects of the fluid flow within the bioreactor platform, based upon measured biophysical characteristics (transport, mechanical), as well as the geometric design constraints. CFD is an advantageous approach for providing preliminary assessments of fluid dynamics, as the solvers employ numerical algorithms to determine approximations for parameters that can not be solved analytically; while such approaches are subject to caveats such as spatial discretization associated with finite element methods and insufficient convergence, CFD modeling provides a relatively rapid and cost-efficient method to study variations in geometrical and fluidic parameters [246]. In the model employed herein, the solutions have been verified to ensure conservation of mass across several different cross sections of the bioreactor. However, the numerical solutions and conclusions presented herein

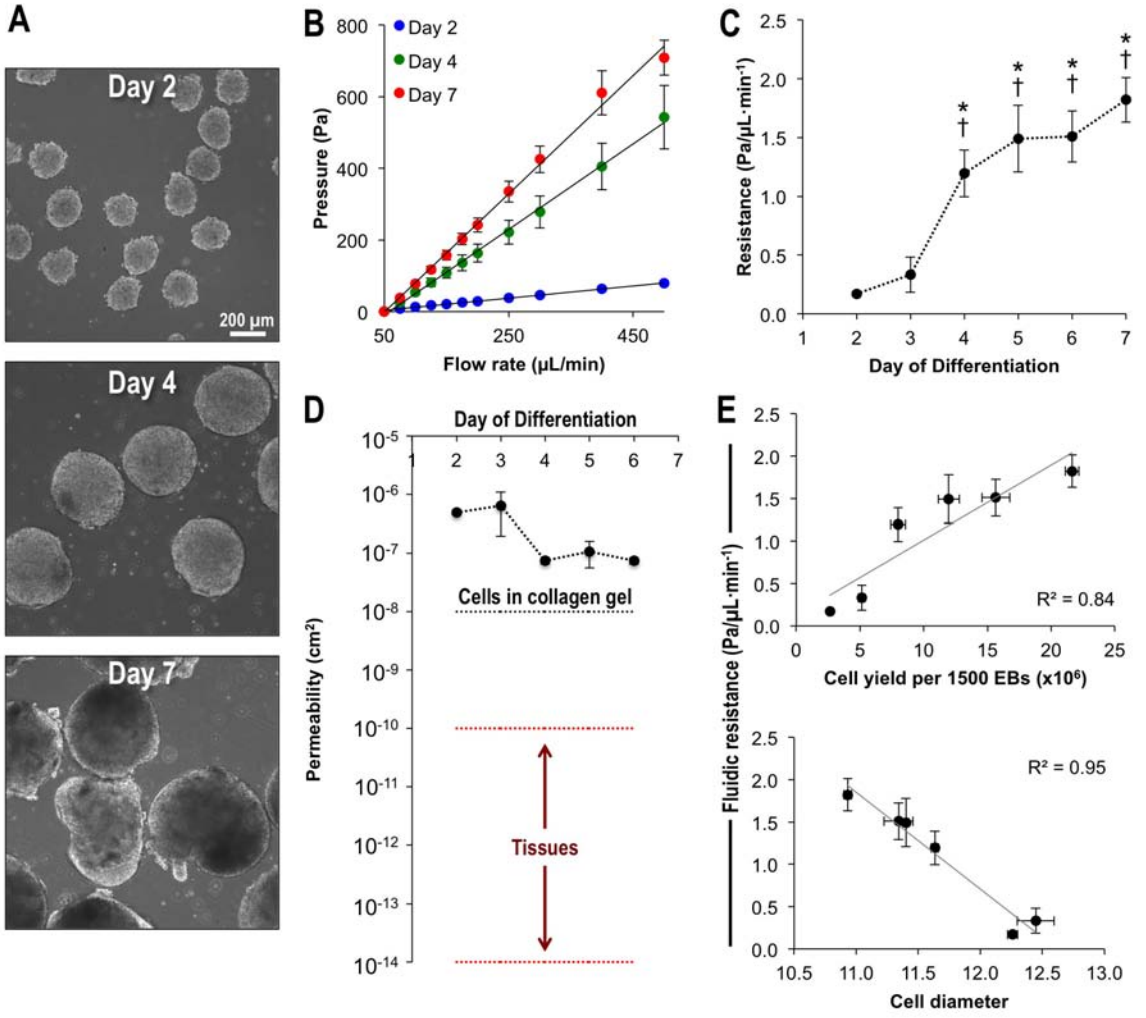

Figure 6-7: Measurement of EB permeability. (A) Representative EBs exhibit changes in size and morphological characteristics during the course of differentiation, thus motivating the analysis of biophysical characteristics, such as permeability. (B) The pressure drop across EBs in the perfusion bioreactor was measured at days 2 (blue), 4 (green) and 7 (red) of differentiation and (C) the slope of the relative curves was used to calculate the resistance during the course of differentiation. (D) Known geometrical characteristics of the bioreactor and EBs were then used to calculate the permeability, and compared to previously reported characteristics of other microtissue and native tissues. The fluidic resistance was also directly compared with physical characteristics of EBs, including the cellular composition (cells per EB) and the average cell size, both of which were significantly correlated with resistance. (C) $p < 0.05$ compared to: * day 2, † day 4 of differentiation. Scale bar in (A) = 200 μm.

should also be validated by experimental approaches such as particle image velocimetry (PIV).

Across several relevant orders of magnitude for permeability, the model predicted flow through the EB, approximated as a spherical porous material, to varying extents (Fig. 6-8 A), with increasing spatial heterogeneity arising coincident with increasing resistance (decreasing permeability). Specifically, at high permeabilities (10^{-6} 10^{-7} cm^2), the velocity profiles exhibited uniform flow within the EB; however, as the permeability decreased, the velocity profiles were not uniform and exhibited increased flow within the bottom portion of the spheroid, adjacent to the the microwell edges. While EBs exhibit relatively low fluidic resistance (Fig. 5-5), the CFD profiles within spheroids of increasing resistance suggest that much of the flow may circumvent the EB, with even more stark implications for imparting fluidic convection in more mature tissues which exhibit further decreased permeability. In addition, as expected, the pressure drop across the spheroid increased with increasing resistance, with magnitudes on the order of 1 Pa (Fig. 6-8 B). Although localized regions of stress were apparent at the contact region between the EB and the microwell (Fig. 6-8 C), the average stress across EBs under a relevant range of perfusion velocities did not exceed 1 N/m^2 (10 dyn/cm^2), with the stress at interstitial flow rates as low as 0.05 N/m^2 (0.5 dyn/cm^2). In addition, the spheroid formation in response to fluidic pressure drop remained low, with maximum deformation less than 1 μm (Fig. 6-8 D). Together, these data suggest that across the range of experimental perfusion velocities, EBs are not expected to undergo appreciable stress or deformation, thereby enabling analysis of the direct effects of fluid convection and biochemical transport.

One additional complicating factor highlighted by the experimental data is that of incomplete seeding, which may potentially result in relative changes in resistance within regions exhibiting open microwells, thereby leading to increased flow through open microwells and reciprocal decreases in flow through adjacent EBs. Consistent

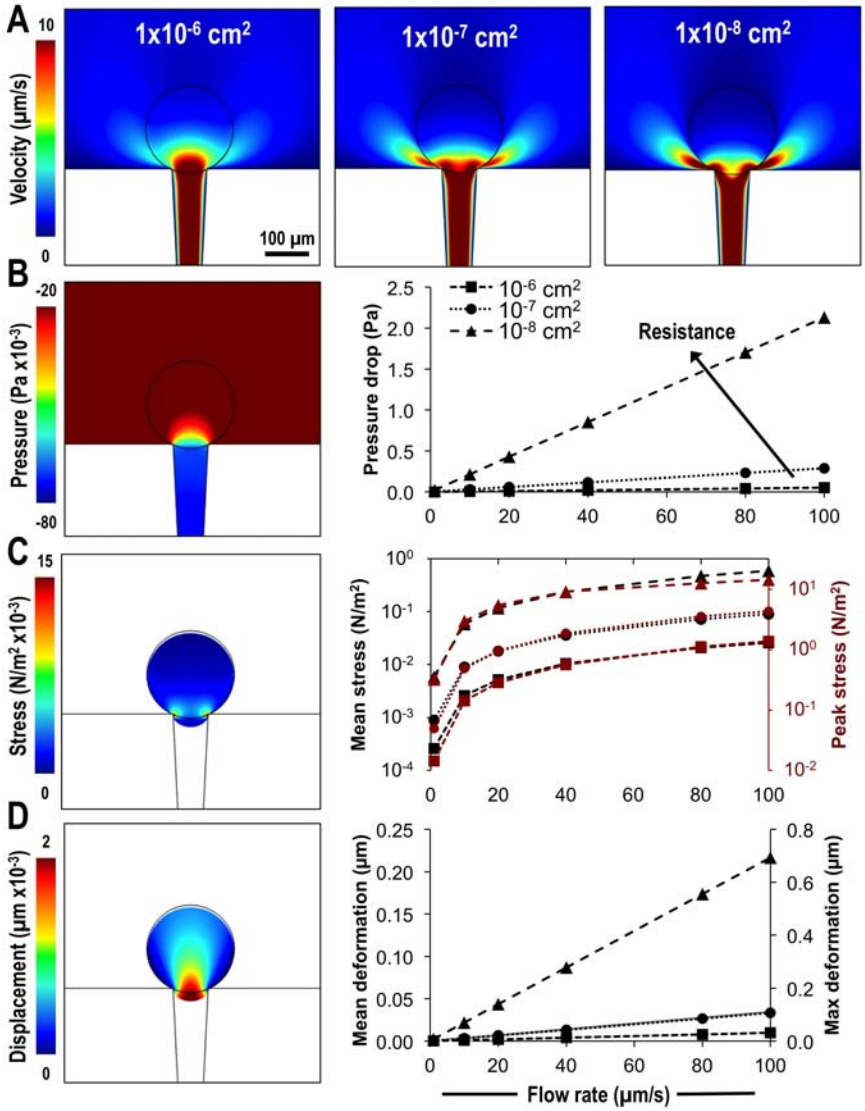

Figure 6-8: Computational fluid dynamic model of microwell perfusion of EBs. (A) A simple model was constructed in COMSOL, consisting of an EB immobilized above a single perfusion well, with the EB approximated as a porous material of known properties (Table 1). The velocity profiles through the EB are depicted for a range of characteristic permeabilities (square = 10^6 cm^2, circle = 10^7 cm^2, triangle = 10^8 cm^2). (B) The pressure drop across the EB also increases as a function of flow rate, as well as the inherent fluidic resistance of the EB. (C) Localized regions of Von Mises stress were apparent at the interface between the EB and the microwell; however, the average stress remained low (<1 N/m^2) within EBs across a range of flow rates. (D) Although solid mechanics physics were used to model EB deformation within the microwell region, based upon previously measured mechanical properties (Chapter 4), the deformation remained less than 1 μm within the relevant perfusion flow rates. All images represent outlet velocities of 20 μm/s. Scale bar in (A) = 100 μm.

with such hypotheses, CFD analysis suggested that wells without EBs were expected to exhibit increased flow velocities and those with EBs immobilized exhibit a decreased velocity; however, the relative magnitude of change is relatively low, particularly based on the high seeding efficiency within the bioreactor design; with seeding efficiencies on the order of ∼80%, the CFD model suggests that there would only be ∼20-30% decrease in velocity through EBs. At the relatively high flow rate tested experimentally (50 μL/min), a 20-30% change would likely not explain the lack of transport through EBs under perfusion. In addition, effectively blocking the open holes by increasing bulk permeability (i.e.immobilizing EBs within hydrogel in the bioreactor volume) would minimize this effect, but only for instances where the bulk is closely matched with EB permeability, thereby suggesting an approach whereby controlling the bulk properties may alleviate heterogeneity due to seeding variability.

In addition, as the CFD analysis highlighted the EB permeability and spherical geometry as potential factors contributing to the lack of perfusion throughout the EBs experimentally, the bulk resistance was also explored as a parameter amenable to controlling the flow patterns around and within EBs. Interestingly, within a specific range of permeabilities, CFD analysis suggested that altering the bulk material resulted in more uniform flow through spheroid. Specifically, the flow pattern observed upon perfusion in liquid media results in a very high maximum velocity within the EB, at the region adjacent to the microwell opening, and relatively low average velocity throughout the EB. At the point where the bulk permeability matches that of the EB, the maximum velocity decreases, which suggested a decrease in the previously modeled flow through the bottom of EBs. Moreover, at the same point, the average velocity through EBs increased, resulting in more homogeneous flow throughout. Interestingly, at high bulk permeabilities, the velocity profiles within EBs was disrupted, suggesting an ideal scenario whereby the bulk is closely matched with EB permeability.

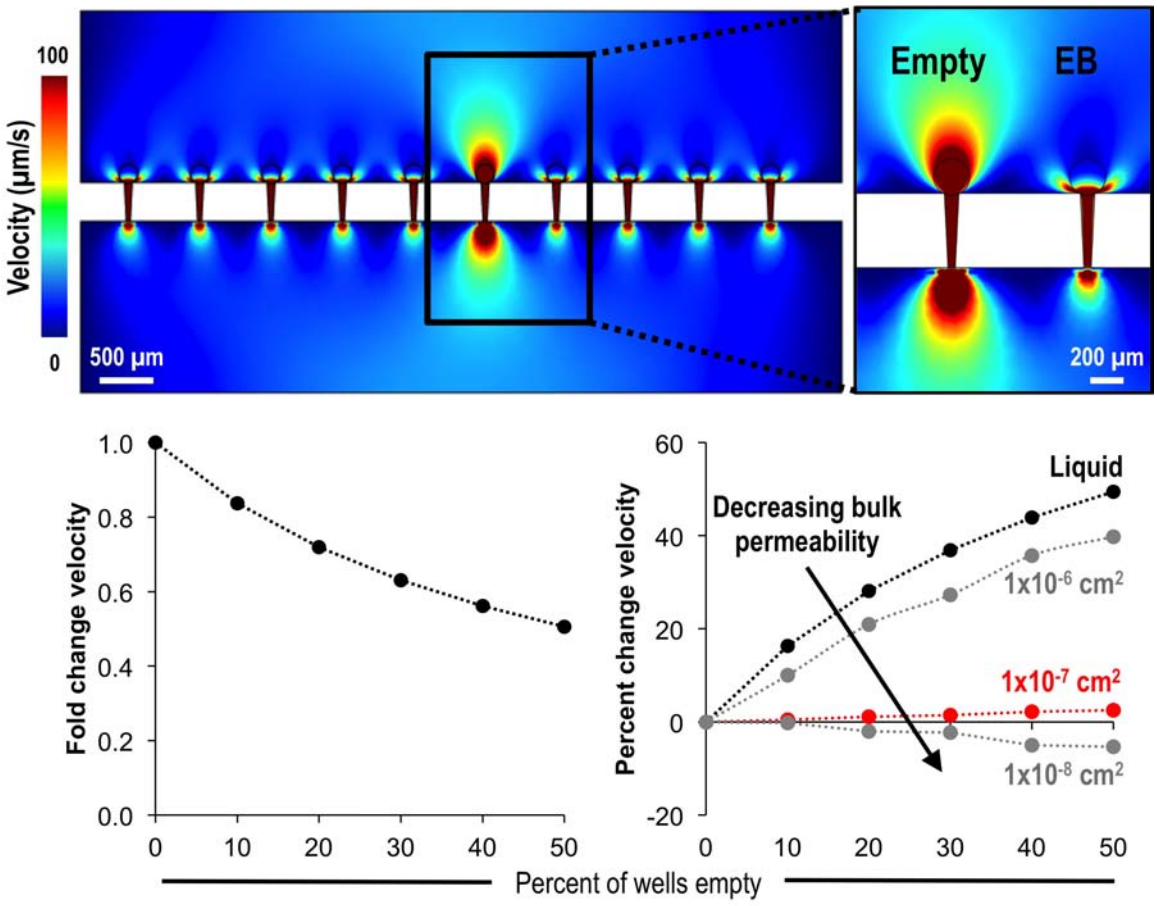

Figure 6-9: CFD analysis of the relative changes in perfusion flow rate due to seeding variability. An expanded Images and analysis based upon 10 connected perfusion microwells with a common outlet (bottom) was created to assess relative magnitude and spatial changes in velocity in response to empty microwells. Empty microwells exhibit increased flow velocities, compared to those through microwells containing immobilized EBs, with the relative magnitude of decrease related to the fraction of holes empty. In addition, altering the bulk permeability across several orders of magnitude, including those matched with EBs (red), alters the relative change in velocity in response to empty microwells. outlet velocities of 20 μm/s. Scale bar = 200 μm

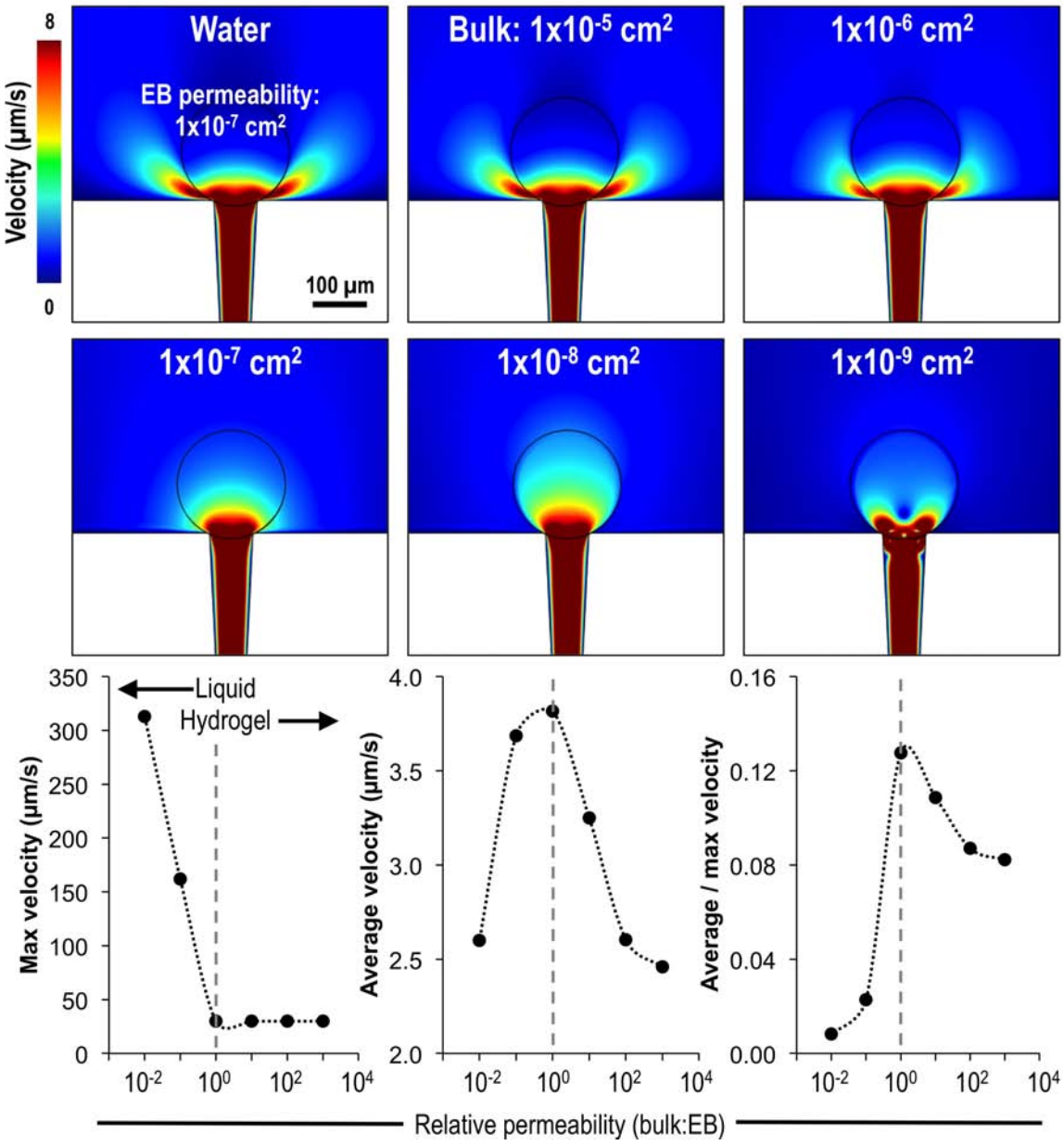

Figure 6-10: Fluid flow patterns in response to changes in bulk permeability. Modulation of the bulk permeability across several orders of magnitude ($10^{-}5$ - $10^{-}9$ cm^2) alters the flow patterns around and within EBs. The maximum velocity is decreased, with a peak in average velocity within EBs at the point where the bulk permeability is matched with the EB permeability (dashed line; $10^{-}7$ cm^2. Scale bar = 100 μm.

6.4 Discussion

Together, the data presented highlight a novel route for imparting convective transport within high-density aggregates of stem cells, as an approach to control the biochemical milieu and ultimately engineer the spatiotemporal kinetics of differentiation. The development of a bioreactor platform has enabled the measurement permeability in stem cell spheroids, a previously unknown biophysical property. Moreover, the understanding of EB ultrastructure gained through these approaches, in combination with previous work, informs the rational design of a bioreactor platform for microfluidic perfusion of stem cell aggregates. Ultimately, the increased control of biochemical transport will create opportunities to understand and perturb three-dimensional morphogenesis and patterning concomitant with *in vitro* organoid development.

The central motivation for the design and implementation of micron-scale flow within stem cell spheroids is derived from physiological phenomena, whereby biochemical transport to avascular regions occurs via low velocity, interstitial flow [277, 316]. A common hypothesis is that the steady state size of spheroids *in vitro* is controlled by the transport of nutrients and morphogens, with transport limitations restricting further growth [346]. Therefore, avascular microtissue structures, such as stem cell and tumor spheroids and tissue engineered constructs, may be amenable to controlled growth and/or differentiation via implementation of a low magnitude pressure drop to drive fluidic convection, analogous to interstitial flow. Interstitial flow has been extensively studied *in vivo*, with velocities measured on the order of 10^{-1} -10^{2} μm/s. In the bioreactor platform developed and described herein, the corresponding mass flow rates have been calculated on the order of 10^{-3} - 10^{0} μL/min, which equates to volumes on the order of $\sim$5 μL - 5 mL over 24 hours. While the lower range of flow rates are not expected to provide sufficient oxygenation, the implementation of a low velocity cross flow, on the order of 10^{2} μL/min or $\sim 10^{2}$ μm/s is amenable to delivery

of biochemical morphogens and nutrients, with removal of waste. Together, the platform described is amenable to implementing fluidic convection on the same order of magnitude as interstitial flow, as a novel technology to modulate the metabolic and biochemical context of high density stem cell spheroids.

In the context of tissue engineering, analogous approaches for imparting convection within larger constructs have been developed and tested, and range on size scales over several orders of magnitude. For example, the device developed herein is based upon a model system that was designed to impart a pressure drop across neural constructs (500-750 μm thickness) comprised of cells embedded in Matrigel [76, 75]. Similarly, cardiac tissue constructs (1.5 mm thickness) have been cultured within a perfused flow loop, with evidence that the configuration supports increased cell viability of explants on the order of millimeters [270, 269]. Interestingly, one commonality between existing systems is the use of a hydrogel structure to embed cells or tissues [264, 35], which has traditionally been a central tenet of tissue engineering. However, the size scale and traditionally scaffold-free culture of stem cell spheroids prompted additional design constraints to address the parallel processing of many individual units.

The data presented describe fluidic resistance, inversely proportional to permeability, as a novel metric to characterize the EB biophysical structure. Interestingly, EB permeability was calculated to be orders of magnitude greater than that of porous, cell seeded hydrogel constructs [241] or native tissues [189]. Previous work has identified the structural components of EBs as largely comprised of cell-cell adhesions and cell-intrinsic tension via cytoskeletal elements (Chapter 4), with minimal ECM deposition [230], particularly at early stages of differentiation. EBs have also been previously reported to exhibit epithelial-like morphology and a characteristic shell formation at the exterior [51], with evidence that the EB ultrastructure leads to diffusive transport limitations for small molecules [278], as well as growth factors (Chapter 5).

However, the transport characteristics have also been mathematically linked to the high cell density and uptake rates, rather than physical restrictions.

Previous measurements of the interstitial space within tumor spheroids reported 1 μm spaces between cells, with the interstitial volume constituting $\sim$16% of the total spheroid volume [8]. In contrast, while the pore size remains similar [259], the void fraction within spheroids is much lower than that of hydrogels, which are typically comprised of >90% water when swollen [258]. In hydrogels comprised of hydrophilic monomers, the permeability can be controlled by cross-linking density. In addition, decreasing permeability serves as a route to protect the specimen against mechanical forces, as the permeability is modulated when the specimen is subjected to either a fluidic pressure drop or maintained in compression [153]. Therefore, while hydrogels and spheroids exhibit different structural characteristics, the permeability may be tuned such that the bulk properties of the system exhibit similar permeabilities compared to that of spheroids. Ultimately, the increased understanding of EB permeability permits the incorporation of additional design constraints for the development of next generation convective bioreactors.

While stem cell spheroids are traditionally expanded and differentiated in the absence of biomaterial scaffolds, encapsulation of aggregates within polymer beads has been extensively explored in the context of physical protection from hydrodynamic mixing as well as for *in vivo*, immunologically shielded cellular therapies [354, 353]. Such approaches typically employ natural polymers, such as alginate, due to its rapid and reversible cross-linking via divalent cations. Other thermally reversible natural polymers, such as Matrigel, fibrin, or collagen, have been explored for their utility in 3D stem cell differentiation; however, as Matrigel is derived from basement membrane of sarcoma cells, the presentation of ECM molecules and adhesive moieties may drastically alter the trajectory of stem cell differentiation [263] and disrupt the spheroid

structure by promoting migration into the gel. Therefore, as a relatively inert material with respect to cellular interactions, alginates are ideal for the encapsulation of stem cell aggregates. While encapsulation typically yields spherical droplets, which may lead to similar convective velocity profiles as exhibited computationally by EBs alone, it is also possible to create bulk gels from alginates [174]. Moreover, purified forms of alginate are readily available with different molecular weights and ratios of the two anionic monomers, which together are amenable to engineering a wide range of gel properties [169, 354].

Microfluidic platforms have been implemented to array individual spheroids [312] or tissue structures [62] for real-time monitoring of morphogenic events. However, in such platforms, the design may limit precise control of the exogenous and endogenous biochemical concentrations, as the array is often immobilized along a single, long channel. Therefore, factors secreted by EB populations may affect those downstream, and, reciprocally, uptake of morphogens may deplete the concentration upstream in the device. The system developed is somewhat analogous to a packed bed bioreactor design, albeit at much smaller scale, with the implementation of a single layer of EBs within a common reservoir; while the spacing between spheroids in this particular prototype remains large (750 μm between wells), the modular nature of the bioreactor enables the simple integration of different grid designs. The controlled bulk media delivery and removal, in this context, is a particularly interesting variable, which has not been systematically studied in the context of three-dimensional stem cell differentiation. For example, Csaszar et al., demonstrated that hematopoietic stem cell (HSC) expansion is hindered by negative feedback, which leads to the secretion of endogenous inhibitory factors; simple perfusion or fed-batch media supplementation strategies greatly reduced the concentration of such factors, leading to increased HSC expansion [72]. Similarly, the role of autocrine factors in ESC self-renewal and differentiation has been increasingly appreciated through systematic studies of media

perfusion in microfluidic platforms [265, 33, 162, 221]. While large volume bioreactor platforms have enabled the controlled physiochemical environments and media perfusion of EBs [21], the capacity to immobilize EBs within a small volume, parallel-plate flow configuration enables the systematic study of multiple parameters in parallel, including the delivery, removal, and recycling of media components, across a range of time scales.

Together, the design parameters identified through this study motivate the development of a novel bioreactor for the parallel processing of individual aggregates within a bulk hydrogel, in order to control both the extracellular milieu via media recycling, as well as the intra-EB milieu via modulation of the biochemical transport dynamics. Ultimately, such culture platforms will allow systematic variation of hydrodynamic parameters, biochemical composition, and EB ultrastructure in order to develop novel approaches for directing stem cell differentiation.

CHAPTER VII

FUTURE CONSIDERATIONS

Current approaches to direct stem cell differentiation focus on systematically understanding the relative influences of microenvironmental perturbations and simultaneously engineering platforms aimed at recapitulating physicochemical aspects of tissue morphogenesis. Together, the data presented collectively identify the biophysical basis for stem cell differentiation as three-dimensional spheroids, including biomechanical and transport properties, which are distinct from those of adult tissues or tissue engineered constructs. This thesis provides a basis for developing novel approaches to control the spatiotemporal dynamics of stem cell signaling and morphogenic remodeling to direct the differentiation of stem cells, in order to ultimately develop functional microtissues for *in vitro* screening and regenerative medicine technologies.

7.1 Controlling EB ultrastructure & ECM composition to direct downstream signaling and morphogenesis

The studies presented in this dissertation collectively highlight the important role of EB formation and composition on subsequent morphogenesis and differentiation. Specifically, controlling the kinetics of aggregation and the subsequent EB size dramatically decreased intra- and inter-experimental variability (Chapter 3). Moreover, the spheroid aggregation kinetics were linked to β-catenin signaling and cardiomyocyte differentiation (Appendix A). Interestingly, recent studies have demonstrated the role of altering surface area, and thus endoderm composition, on cardiogenic differentiation [22]; therefore, the role of β-catenin should be further studied in EBs of varying sizes. In addition, although the studies presented in this dissertation

have significantly contributed to systematically controlling the size and decoupling aggregation kinetics, opportunities also remain to study the opposite to control aggregation, independent of EB size. In the studies presented, the EB formation and size were coordinately regulated, with those undergoing rapid aggregation - and increased β-catenin signaling - also resulting in larger EBs. As β-catenin signaling is implicated downstream of E-cadherin, the polarity of cells within the spheroid likely influences Wnt pathway activation via β-catenin; therefore, the size the EBs, and the corresponding surface area to volume ratio, likely modulate β-catenin activity as well. Although studies are increasingly moving to high throughput forced aggregation formation techniques which result in rapid aggregation within hanging drop, microwells or multi-well plate formats, it remains unclear whether such techniques bias differentiation toward certain trajectories. Therefore, future studies should systematically investigate and develop novel aggregation methods, in order to inform directed differentiation approaches from the initial stage of spheroid formation.

In addition, the aforementioned link between β-catenin signaling and cardiac differentiation (Appendix A) motivates further study of the signaling pathway in the context of mesoderm differentiation. Consistent with our results, Wnt signaling has been previously characterized to exhibit biphasic regulation during cardiogenesis, with a requirement for Wnt signaling during early mesoderm specification, followed by a later decrease, implicated in the maturation of cardiac lineages. Conversely, continued activation of Wnt signaling following mesoderm specification leads to hemangioblast differentiation and maturation of cell fates along the hematopoietic lineages. In our studies, we demonstrate that supplementation of BMP4 in a basal, serum-free media results in mesoderm differentiation and phenotypic analyses suggest the differentiated phenotypes may be more indicative of a trajectory along the hematopoietic lineages, rather than cardiac (Chapter 4). Interestingly, opposing roles of the Wnt and BMP4 pathways have been established, with Noggin (BMP4 antagonist) downstream of the

Wnt signaling. Therefore, the further analysis of the spatiotemporal context for Wnt signaling in BMP4-mediated mesoderm differentiation may elucidate synergistic and antagonistic signaling contexts responsible for hematopoiesis.

These data also establish a three-dimensional morphogenesis characteristic of an epithelial-to-mesenchymal transition (EMT) accompanying mesoderm differentiation via supplementation of serum-free media with BMP4 (Chapter 4). Interestingly, such phenomena have not been reported in monolayer cultures, highlighting the possibility to direct distinct cell fate decisions and organization in 3D. As waves of EMT are well characterized during embryonic development [322], particularly during the early cell fate decisions that constitute primitive streak formation and migration, this platform may serve as an *in vitro* functional assay, amenable to screening the effects of biochemical or environmental stimuli on early embryonic development. While these data demonstrate changes in the extracellular milieu via changes in the glycosaminoglycan (GAG) presentation and composition accompanying EMT, future work should continue to address the influence of GAGs and other ECM molecules on the patterning and differentiation of mesodermal populations. For example, hyaluronan (HA) has been correlated with tumor invasiveness [29] and loss of one of the hyaluronan synthase isoforms (HAS-2) results in inhibition of EMT and abnormal cardiac development during embryonic development, which can be rescued via soluble HA [45]. Consistent with these results, HAS-2 gene expression is significantly increased during differentiation toward mesoderm lineages (Chapter 4). Similarly, in addition to its role in mesoderm differentiation (Appendix A), accumulation of nuclear β-catenin, indicative of active Wnt signaling, is implicated in tumor metastasis via remodeling of E-cadherin and subsequent EMT [37]. Therefore, more robust EMT and/or mesoderm differentiation may be attained by altering the biochemical, cell adhesive and extracellular milieu. Routes to locally enrich the GAG composition within the 3D spheroid structure include the integration of biomaterials to directly present various

GAG species or to present a binding motif (i.e. HA-binding protein) amenable to retaining endogenously secreted HA molecules. Moreover, manipulating cell adhesions or actomyosin contractility (Chapter 4) may be sufficient to initiate EMT [83]. While biochemical cues are classically thought to initiate EMT, a pool of β-catenin becomes available following cadherin internalization [139]; therefore, engineering selective substrates or imparting regions of increased tension may also provide biophysical cues to physically disrupt adhesions and incite downstream signaling via β-catenin, leading to the appearance of classical mesenchymal morphologies and associated functional changes. Together, the data presented throughout this thesis highlight the interconnected nature of matrix, adhesions, cell contractility, and downstream signaling, which together coordinately regulate mesoderm differentiation and morphogenesis.

7.2 Characterization and perturbation of EB structural components as a route to direct patterning

Owing to such crosstalk between biophysical cues and downstream signaling, dynamic changes in local biophysical characteristics, including ECM composition and adhesive signature of cells may also be responsible or permissive for patterning and cell fate. This work demonstrates that stem cell spheroids differentiated toward divergent fates, including those comprised largely cells from endoderm and mesoderm lineages, exhibit distinct patterns of mechanical stiffness and viscoelasticity, with mesodermal cells stiffening during differentiation and mesenchymal morphogenesis (Chapter 4). While these data suggest that unique profiles may be characteristic of different stages of differentiation and phenotypic lineages, questions remain regarding the biophysical profiles of other lineages and in spheroids with unique morphological characteristics. Future studies should continue to verify the validity of the biophysical assay as a means to both understand and perturb the structure and differentiation state of stem cell spheroids. In particular, as many of the recently reported organoid structures rely

on the use of exogenous matrix (i.e. Matrigel), it would be interesting to probe the dynamic changes in biophysical characteristics as those structures are formed and as they undergo changes in multicellular organization, including invagination and evagination of structures [285]. In addition, structural characteristics of organoids may identify underlying mechanisms relevant to *in vitro* patterning, which will ultimately inform engineering approaches to perturb the microenvironment.

While these studies provide a foundation for understanding the structural components within stem cell spheroids, questions remain regarding the specific structural elements. For example, a recent report identified the intracellular distribution of myosin isoforms as a key regulator of symmetric and asymmetric division in hematopoietic stem cells [300]. While the bulk mechanical properties characterized through these studies identify the actomyosin cytoskeleton as a central mediator of microtissue stiffness, the cell-scale mechanical properties, particularly the specific elements and molecular distribution contributing to dynamic morphogenic changes, remain largely unknown in the context of stem cell spheroids. While traditional methods, such as atomic force microscopy, are not easily amenable to measuring local changes inside of aggregates, the advent of novel technologies for assessing [48] and modeling [250] local tension will enable future work to address such questions. In addition to the understanding of cellular contractility, explored herein, there are likely several other mechanisms underlying the biophysical changes in microtissue architecture during differentiation. For example, the nuclear structure has previously been correlated with tissue stiffness, with lamin expression being influenced by matrix stiffness [317]. However, there is no currently available method for acute (i.e. small molecule) knockdown of lamin-A expression or structural integrity. Perturbation of EBs using approaches such as siRNA and shRNA knockdown of lamin would likely result in widespread changes in the differentiation trajectories and therefore would confound the analysis. Therefore, future studies should systematically interrogate nuclear changes during

3D ESC differentiation. Similarly, the relative contribution of adhesions is not easily studied in the context of stem cell spheroids, as simple disruption via blocking antibodies or ion chelation results in aggregate disassembly. Therefore, additional methods, such as laser ablation, should be explored to more systematically perturb elements of the physical structure. Biomaterial incorporation may also be amenable to perturbing local cellular tension and adhesive profiles, as MSC spheroids exhibited an increase in bulk stiffness upon incorporation of gelatin microparticles [15]. While spheroids comprised of ESCs in the same context did not exhibit increased stiffness, it would be interesting to explore the presentation of alternative molecules, such as cadherins.

As studies presented herein also identified the cellular composition (Chapter 3) and aggregation kinetics (Appendix A) as critical determinants of cell fate, questions also remain regarding the biophysical characteristics in various differentiation contexts. For example, the E-cadherin expression and distribution was dynamically modulated within culture conditions that influenced the aggregation kinetics; therefore, it is likely that associated structural elements may also be modulated in a context dependent fashion, upon simple environmental perturbations such as mixing conditions. Therefore, future studies should continue to study the biophysical cues associated with β-catenin signaling and EB formation. Similarly, EB size affects cell polarity by modulating the number of cells exposed at the exterior boundary; systematically testing the biophysical properties of EBs of varying sizes may, therefore, provide insight into the contribution of the exterior cells in maintaining the structural integrity of the spheroid. Similarly, changes in microtissue shape have been previously shown to pattern EMT within regions of high stress Gomez:2010gb. Therefore, these data together motivate the development engineering approaches to perturb the spheroidal nature of stem cell aggregates, as a novel biophysical route to induce morphogenesis via EMT, and identify both signaling (Wnt/β-catenin) and biophysical metrics for

characterizing subsequent changes in morphogenesis and cell fate.

7.3 Spatiotemporal delivery and retention of exogenous and endogenous biochemical morphogens

In addition to the physical cues presented within the microtissue structure via cell-cell contacts and multicellular organization, the biochemical milieu is also a critical determinant of cell fate. This study has identified important transport properties of stem cell spheroids (Chapter 5), which likely contribute to complexity and heterogeneity within individual aggregates. Specifically, the high cell density inherent within cellular aggregates leads to transport limitations, particularly for biochemical compositions at concentrations typically employed for monolayer differentiation. Moreover, as differentiation protocols are increasingly moving toward using small molecule inhibitors as pathway antagonists, these data highlight the additional barriers associated with the increased uptake rate of such molecules. However, the transport limitations within spheroids also afford opportunities to further understand the role of endogenous signaling within stem cell populations. As the exogenously delivered factors are largely constrained to the exterior of EBs, the patterning and organization occurring within the center of EBs is likely directed primarily by cell-secreted signals or those presented locally within the microenvironment. This is particularly interesting in the context of organoid morphogenesis, as the protocols rely on EBs that are much larger than those traditionally employed, suggesting that the biomimetic structures emerging within organoids may be a result of self-organization and self-directed differentiation. The transport characteristics of spheroids also highlights a new paradigm, whereby approaches may focus on directing the differentiation of the exterior cells toward populations known to secrete signals of interest or those which are responsible for patterning adjacent structures during embryonic development (i.e. direct endoderm differentiation to influence mesoderm differentiation).

While the secretome of stem cell populations has been of widespread interest, with recent advances in labeling of endogenous molecules for mass spectrometry analysis, the heterogeneity within differentiated populations poses additional challenges for identifying the source(s) of specific secreted morphogens. Therefore, novel reporters, such as the sentinel signaling cells, are transformative technologies, which may enable the spatiotemporal analysis of pathway activation. Similarly, in situ hybridization, traditionally used to characterize developmental signals, enable systematic assessment of spatial signaling within EBs. Ideally, the analysis of the spatiotemporal context for multiple pathways simultaneously will enable the derivation of systems biology computational approaches to model network regulation at the multicellular scale. More robust models created via the aforementioned experimental approaches may also enable additional parameters to be defined, including the relative uptake rates for different types of molecules and the role of dynamic feedback in pathway regulation and stem cell differentiation.

In addition, while these studies highlight a role for microparticles in modulating the physical structure of stem cell spheroids, the localized release of morphogens from microparticles should also be modeled and experimentally measured within stem cell aggregates, in order to define the transport characteristics upon localized release. The increased understanding of microparticle delivery may, therefore, enable the development of engineering approaches to more homogeneously deliver morphogens or to create point sources amenable to impacting small, localized populations. For example, the incorporation of GAG species, as previously characterized in endodermal and mesodermal microenvironments (Chapter 4), may also exert secondary effects through the local binding and presentation of growth factors. Therefore, the platform for assessing transport established herein may also be implemented in the context of studying transport in the presence of endogenous and exogenous matrices. In the

context of BMP4-mediated mesodermal differentiation, the histological staining patterns suggest a decrease in sulfated GAGs, with an increase in non-sulfated species, such as HA. Therefore, based upon the BMP binding capacity of sulfated GAGs, the transport of BMP4 may be less restricted within later stage, mesodermal spheroids compared to those at early stages, which exhibit robust safranin-O staining, indicative of sulfated GAG expression. Similarly, BMP signaling upon incorporation of exogenous sulfated GAGs, such as heparin, should be assessed to determine the extent to which transport of soluble morphogens is further limited and the spatial extent of gradients are created by sequestration in the ECM.

In addition to biomaterial approaches, manipulation of transport is also increasingly being explored via microfluidics [111], as the implementation of convective fluid flow is easily amenable to creating gradients or altering delivery in a precisely spatially controlled manner. While all of the studies presented herein demonstrate transport in the context of diffusion, as is standard in most traditional cultures of stem cell spheroids, the transport profiles within convective culture platforms, including rotary orbital suspension and bioreactor cultures, should be further studied. The data presented herein demonstrate that rotary orbital suspension cultures both implement convective mixing and maintain spheroids as homogeneous, individual aggregates by inhibiting agglomeration (Chapter 3). Therefore, the combination of size control and mixing may alter biochemical transport. While the convective nature of scalable bioreactor platforms has traditionally been implemented to maintain well-mixed conditions through the bulk media volume, the movement of spheroids may also influence the dynamics of morphogen transport. While previous work has characterized the fluid shear profile within mixed bioreactor platforms [282], it is difficult to assess the influence of fluid mixing on individual spheroids, as the fluid dynamics are altered as a function of the spatial position in the dish and the EBs are free to move, rather than being fixed, in contrast to traditional tissue engineering approaches [32].

Therefore, while fluid mixing may increase transport within the spheroid structure, substantial fluidic convection within the aggregate is not likely.

7.4 Fluidic convection to manipulate the biochemical milieu and harness the secretome of differentiating ESCs

To address such complexity, a novel culture platform has been developed to immobilize spheroids within a convective context, which is amenable to increasing transport through the aggregate structure (Chapter 6). Similar to rotary orbital suspension (Chapter 3), the implementation of a microwell array, via laser-drilled holes, enables the maintenance of individual spheroids, in order to maintain control of size without agglomeration. The subsequent operation of perfused fluidic convection via the application of a pressure drop across the immobilized EBs then enables modulation of the transport profile. The platform developed herein is also amenable to implementation in parallel with secondary approaches for increasing transport, including biological of biomaterial-based methods for increasing EB permeability. For example, the use of enzymatic agents, such as collagenase, or non-enzymatic chelating agents, such as EDTA, are amenable to dissociating or perturbing the ECM or cell-cell adhesions to increase transport [278]. The introduction of such agents is particularly ideal in the perfusion bioreactor platform, as the fast exchange kinetics enable solutions to be introduced and washed out in a rapid or pulsatile manner, such that the EB structure would not be completely disrupted. Similarly, the introduction of physical conduits for fluid flow, as in the incorporation of microparticles or other biomaterial constructs, may permit fluid access to increase transport while minimizing detrimental fluid shear within the spheroid volume.

The perfusion bioreactor platform developed through this thesis enables a wide range of opportunities for studying, perturbing, and controlling and the EB microenvironment by directly employing the novel features and through parallel operation

with additional enabling stem cell technologies. For example, the implementation of perfusion via microfluidics provides opportunities for parallelization of different culture platforms for independent control, screening, and monitoring in high throughput. In combination with technologies such as the sentinel signaling cells and imaging platforms, microfluidic perfusion would enable real time tracking of population dynamics. In addition, the convective transport afforded through perfusion may also be amenable to combination with other means of spatial control, including microparticles to release or sequester morphogens. By tuning the flow parameters and transport characteristics in such platforms, it may be possible to develop and maintain morphogen gradients, in order to direct regional patterning and emulate aspects of embryonic development. In addition, the culture of larger aggregates or assemblies of aggregates may also facilitate gradient formation.

The controlled perfusion also creates opportunities for identifying fluidic parameters permissive for directing the differentiation of specific cell phenotypes. For examples, increased fluid velocities may also be explored for applications aimed at directing vasculogenesis or cardiogenesis, analogous to the role of fluid shear in the initiation of primitive hematopoietic and cardiac events. Similarly, pulsatile flow may be executed within the platform, in order to provide durations of increased transport while also permitting a residence time for molecules within the spheroid structure. This tactic may be especially applicable in contexts aimed to maintain endogenously secreted molecules, as constant perfusion flow will likely remove factors secreted by the cells.

Finally, the forced convection through spheroids also provides opportunities for capturing the perfusate. The comparison of the perfusate with the bulk media may enable more quantitative characterization of relative uptake over time, which will inform the development of more robust computational approaches to assess transport (Chapter 5), as discussed previously. Moreover, as the perfused volume is relatively small and not diluted by the bulk media, the perfusion of EBs may serve as a novel

route to concentrate the secretome of EBs for subsequent analysis of the temporal profile of morphogen secretion. In addition, the concentrated EB secretome may be amenable to use as a therapeutic, due to the wide range of morphogens involved in regeneration and self-renewal. Therefore, in addition to the primary functionality of delivering nutrients, growth factors, and other morphogens within differentiating spheroids, the mode of perfusion operation is also amenable to secondary questions and applications for capturing and analyzing the EB milieu.

To date, many approaches have been developed or proposed as means to precisely control the biophysical characteristics of stem cell aggregates, including high throughput platforms to control the spheroid size and homogeneity, microfluidic approaches to increase the precision and profile of molecular transport, and biomaterial techniques to deliver, present, and/or sequester inductive cues (physical, chemical) in a highly efficient and spatiotemporally controlled manner. However, as has been underscored throughout, the impact of biophysical cues are manifested through multiparametric, synergistic responses to simple perturbations. Therefore, opportunities remain to develop experimental and mathematical approaches to understand the complex interrelationship between cellular composition (adhesions, remodeling) and physical characteristics (mechanics, transport), particularly as a function of space and time during morphogenesis. Ongoing efforts should focus on establishing advanced mathematical models to simulate the dynamic changes within the EB structure as the function of time (differentiation state, phenotype) and developing sensitive experimental tools to sample and control the microenvironment within aggregates. Such advances will elucidate the relative influences of various biophysical factors in mediating developmental dynamics and ultimately inform engineering approaches to perturb and control stem cell morphogenesis to guide the formation of tissue-specific microtissues amenable to screening and therapeutic applications.

APPENDIX A

TEMPORAL MODULATION OF β-CATENIN SIGNALING BY MULTICELLULAR AGGREGATION KINETICS IMPACTS EMBRYONIC STEM CELL CARDIOMYOGENESIS[1]

A.1 Introduction

Pluripotent embryonic stem cells (ESCs) are a promising cell source for therapies aimed to treat degenerative and chronic diseases in which native tissues are damaged beyond their endogenous capacity for repair. Elucidating the mechanisms regulating ESC fate decisions will significantly aid in the development of directed differentiation approaches, in order to produce large quantities of differentiated cells for regenerative therapies. Differentiation of ESCs is commonly initiated by the spontaneous aggregation of cells via E-cadherin, a Ca^{2+} dependent homophilic adhesion molecule [183]. The resulting multicellular aggregates, termed embryoid bodies (EBs), recapitulate morphogenic events similar to those of pre-implantation stage embryos, including differentiation into cell phenotypes comprising the three germ lineages (ectoderm, endoderm and mesoderm) [146, 88]. Although EBs often lack the spatial organization to directly mimic the regulation of tightly controlled spatiotemporal signaling exhibited *in vivo*, ESCs maintain the capacity to respond to similar molecular cues, thus motivating the analysis of developmentally relevant signaling pathways in the context of stem cell differentiation [156].

---

[1]Modified from: MA Kinney, CY Sargent, and TC McDevitt. (2013). *Temporal Modulation of β-Catenin Signaling by Multicellular Aggregation Kinetics Impacts Embryonic Stem Cell Cardiomyogenesis.* Stem Cells Dev, 22(19), 26652677. doi:10.1089/scd.2013.0007

Transcriptional activation induced by the β-catenin signaling pathway controls cell fate decisions during early embryonic development, aiding in the regulation of embryonic patterning and axis formation [367], primitive streak formation [218], and mesoderm differentiation [125]. Similarly, in ESCs, β-catenin signaling is required for the maintenance of pluripotency [287, 158], and mesoderm differentiation [196], as well as self-organization and axis formation within EBs [321]. Two main pools of β-catenin are present within cells [121]: 1) β-catenin sequestered at the cell membrane within adherens junctions, specifically as a mediator between cadherins and the actin cytoskeleton [159, 1, 360], and 2) stabilized cytoplasmic β-catenin, which mediates transcription upon destabilization and translocation to the nucleus [133, 25]. Canonical Wnt signaling is a well-studied pathway, which is involved in the initiation of β-catenin-regulated transcription [65]. In the absence of Wnt, cytoplasmic β-catenin is phosphorylated by the glycogen synthase kinase 3β (GSK3β)/adenomatous poliposis coli (APC)/Axin complex and is targeted for ubiquitination [367, 336, 126, 248]. Upon Wnt binding to members of the seven-transmembrane Frizzled receptor family, the Frizzled receptor heterodimerizes with low-density lipoprotein receptor-related protein 5 and/or 6 (LRP5/6) [66], which in turn causes the disruption of the GSK3β/APC/Axin complex [206], resulting in the accumulation of stabilized, cytoplasmic β-catenin [226, 170]. The cytoplasmic stabilization of dephosphorylated β-catenin permits translocation of β-catenin to the nucleus, where it acts as a transcriptional co-activator with T-cell factor/lymphoid enhancer-binding factor (TCF/LEF) transcription factors [25] to regulate the transcription of target genes involved in a wide range of cellular processes, including cardiac specification and morphogenesis during embryonic development [141, 195] and ESC differentiation [194, 232, 251]. Thus, β-catenin is a central component in cell-cell interactions and gene transcription, both of which are key factors regulating embryonic and ESC morphogenesis.

Although the presence of Wnt ligands and the destabilization of the GSK3β/APC/Axin complex are required to permit the transcriptional activity of β-catenin, the temporal onset and duration of signaling may also be modulated by the presence of E-cadherin adhesions between cells, which sequester β-catenin at the membrane [238, 208]. Studies have illustrated the potential for cross-talk between β-catenin associated with E-cadherin and its availability to participate in signaling and transcriptional activities [151]; therefore, the intercellular adhesion events mitigating initial EB formation may also regulate downstream β-catenin regulated transcription, thus potentially modulating the cardiomyogenic potential of the ESC population.

The formation and maintenance of EBs in rotary orbital suspension culture produces increased yields of homogeneous EB populations (Chapter 3; [52, 282, 283]) and is a relatively facile technique to modulate ESC aggregation kinetics by simply varying the orbital mixing speed [282]. Interestingly, previous studies demonstrated that the extent of cardiomyogenic differentiation in rotary cultures was modulated by the orbital speed, with the conditions promoting accelerated EB formation kinetics also exhibiting increased cardiomyocyte differentiation [282]. Therefore, the control of ESC aggregation afforded by the rotary orbital suspension culture platform enables a systematic study of aggregation-induced modulation of β-catenin signaling kinetics and the associated regulation of cardiomyocyte differentiation.

The objective of the present study was to investigate the dynamics of β-catenin transcriptional activity in response to modulation of ESC aggregation kinetics during EB formation. β-catenin protein expression and localization were assessed via immunostaining for total and dephosphorylated β-catenin isoforms and immunoblotting of cytoplasmic and nuclear protein fractions, in conjunction with analysis of transcriptional activity using stably transduced luciferase TCF/LEF reporter mouse ESCs. Additionally, gene expression of downstream targets of β-catenin signaling and

cardiomyocyte differentiation were analyzed to determine the relationship between β-catenin protein expression, localization, Wnt/β-catenin pathway signaling dynamics, and differentiated phenotypes. The findings of this work demonstrate that the dynamics of ESC aggregation during multicellular assembly via cadherins modulates the β-catenin signaling pathway and alters cardiomyogenic gene transcription in ESCs.

A.2 Materials and Methods

A.2.1 Embryonic Stem Cell Culture

Murine ESCs (D3 cell line) were cultured on 0.1% gelatin-coated tissue culture-treated plates (Corning). Culture media consisted of Dulbeccos modified Eagles medium (DMEM) supplemented with 15% fetal bovine serum (Hyclone), 100 U/mL penicillin, 100 μg/mL streptomycin and 0.25 μg/mL amphotericin (Mediatech), 2mM L-glutamine (Mediatech), 1x MEM nonessential amino acid solution (Mediatech), 0.1 mM β-mercaptoethanol (Fisher), and 10^3 U/mL of leukemia inhibitory factor (LIF; ESGRO, Chemicon). Cultures were re-fed with fresh media every other day, and passaged at approximately 70% confluence.

A.2.2 Embryoid Body Formation and Culture

Embryoid bodies were formed, as described previously, by inoculating a single-suspension of ESCs at 2 x 10^5 cells/mL into 100 mm bacteriological grade polystyrene Petri dishes with 10 mL ESC media without LIF [51]. Dishes were incubated at 37C with 5% CO2 either statically or placed on rotary orbital shakers (Lab-Line Lab Rotator, Barnstead International) at 25, 40, or 55 rpm to impart hydrodynamic conditions Sargent:2010ct. 90% of media was exchanged every two days by collecting the EBs via gravity sedimentation and re-suspending the cultures in fresh media.

A.2.3 Whole-mount Embryoid Body Immunostaining

Embryoid bodies were collected by sedimentation at days 1, 2, 4, and 7 of differentiation, rinsed 3x with PBS, and formalin (4% formaldehyde) fixed at room temperature for 45 minutes with rotation. EBs were then rinsed 3x (5 minutes with rotation) in EB wash/block buffer (2% BSA/0.1% Tween-20 in PBS) and permeabilized in 0.05% Triton X-100 and 2% BSA solution for 1 hour at 4C with rotation. EBs were blocked in wash/block buffer for 2 hours at 4C with rotation. After permeabilization and blocking, EBs were incubated with polyclonal rabbit anti-β-catenin (Millipore, 1:200) and monoclonal mouse anti-active β-catenin (Millipore, 1:50) specific to dephosphorylated Ser-33 and Thr-41 [336] (anti-aβC, Millipore, 1:50) or with monoclonal rat anti-E-cadherin (Sigma, 1:200) at 4C overnight with rotation, rinsed in wash buffer, and incubated with secondary antibodies (Alex Fluor 488 anti-rabbit and Alexa Fluor 546 anti-mouse, Invitrogen, 1:200) for 4 hours at 4C with rotation. EBs were rinsed, counterstained with Hoechst (1:100) and imaged with a multiphoton laser scanning confocal microscope (Zeiss LSM 510 NLO).

A.2.4 Quantification of Immunostaining

The relative intensity of expression of E-cadherin, β-catenin, and aβC was quantified with CellProfiler image analysis software [54] using a custom-written script. Briefly, the outlines of individual cells were determined based on primary identification of nuclei followed by expansion of the bounded region to determine cell boundaries. The intensity of staining for E-cadherin, β-catenin, and aβC was then determined on a per cell basis, with approximately 50-100 cells per EB. The total expression levels for each experimental condition were calculated from the average of at least three individual representative EBs.

A.2.5 Luciferase Transduction

Lentiviral transduction of mESCs with a luciferase TCF/LEF reporter construct (Cignal TCF/LEF luciferase reporter; SA Biosciences) was performed to generate stably transduced puromycin resistant clones that expressed luciferase in response to β-catenin signaling. ESCs were plated at 50,000 cells/well on 0.1% gelatin-coated tissue culture treated 6-well dishes (Corning) and cultured for 24 hours prior to the introduction of Cignal Lenti vectors. Stable transduction of D3 ESCs was accomplished by incubating cells with Cignal Lenti TCF/LEF vectors at Multiplicity of Infection (MOI) levels (3, 10, or 25) for 24 hours in the presence of 1 μg/mL polybrene (Sigma). ESCs were incubated with lentivirus particles for 24 hours, and after an additional 72 hours, transduced cells were selected using 3 μg/mL of puromycin (Sigma); concentration was determined from a kill curve using 0.5 3.0 μg/mL. After transduction and selection, individual colonies were chosen using cloning rings and 0.05% trypsin-EDTA, and plated onto 0.1% gelatin-coated tissue culture treated 100 mm dishes. The selected clones were maintained in ESC media supplemented with 3 μg/mL puromycin for an additional 2 weeks and assessed for luciferase expression via anti-luciferase immunostaining, luciferase activity (with and without LiCl treatment), and alkaline phosphatase activity.

A.2.6 ESC Immunostaining

Transduced clones and naive D3s were cultured on 0.1% gelatin-adsorbed tissue culture treated polystyrene 6-well dishes. At ~70% confluence, cells were rinsed 3x with PBS, formalin fixed in the wells for 10 minutes, and rinsed again with PBS. At ~70% confluence, ESCs were fixed with formalin (4% formaldehyde), rinsed with PBS, permeabilized and blocked with 0.05% Triton X-100/2% BSA/PBS solution for 1 hour at room temperature. ESCs were then incubated overnight at 4C with polyclonal rabbit anti-β-catenin (Millipore, 1:200), monoclonal rat anti-E-cadherin (Sigma, 1:200)

[336], monoclonal mouse anti-luciferase (Santa Cruz Biotech, 1:50) or polyclonal goat anti Oct-4 (Santa Cruz Biotech, 1:100). Cells were rinsed with PBS 3x, and then incubated with Alexa Fluor conjugated secondary antibodies (Invitrogen, 1:200) for 2 hours at room, counterstained with Hoechst (10 μg/mL), mounted and cover-slipped. To assess alkaline phosphatase activity, ESCs were stained using the Vector Red alkaline Phosphatase Substrate kit (Vector Laboratories). Briefly, cells were incubated in Vector Red substrate in 100 mM Tris-HCl buffer to allow color development for 30 minutes at room temperature while protected from light. Following color development, cells were rinsed with Tris-HCl buffer and water, mounted and cover-slipped. Images were acquired with a Nikon TE 2000 inverted microscope (Nikon Inc.) with a SpotFlex camera (Diagnostic Instruments) or an EVOS fl inverted microscope (Advanced Microscopy Group).

A.2.7 Luciferase Activity Quantification

ESCs were cultured with or without the addition of LiCl (25 mM) for 24 hours to disrupt the GSK3β/APC/Axin complex and inhibit the phosphorylation of β-catenin, ultimately resulting in increased TCF/LEF activity within transduced cells [10]. Luciferase activity was quantified using the Luciferase Assay System (Promega), according to manufacturers instructions. Briefly, ESCs or EBs were rinsed 3x in PBS, lysed with rotation at 4C for 10 minutes, vortexed for 5 seconds, and centrifuged at 10,000 rcf for 5 minutes. The supernatant was collected and transferred to a pre-chilled microcentrifuge tube. Twenty microliters of the cell lysate was added to 100 μL of Luciferase Assay Reagent and luminescence was detected using a Femtomaster FB12 luminometer (Zylux Corporation). Relative light units (RLUs) were normalized to μg of DNA per sample as determined by Quant-It PicoGreen assay (Invitrogen).

A.2.8 Protein Fractionation

EBs were collected at days 2 and 4 of differentiation for Western blot analysis. The NE-PER cell fractionation kit (Pierce) was used to separate the cytoplasmic and nuclear fractions of undifferentiated cells and differentiating EBs. Briefly, cells and EBs were lysed using CER I reagent supplemented with 500x protease inhibitor cocktail (Calbiochem) and 50x phosphatase inhibitor cocktail (Calbiochem), followed by addition of the CER II reagent. After centrifugation at 16,000 rcf, the cytoplasmic supernatant fraction was collected. The remaining nuclear pellet was incubated in the NER reagent containing 500x protease and 50x phosphatase inhibitors, and centrifuged at 16,000 rcf for 10 minutes followed by collection of the supernatant containing the nuclear fraction.

A.2.9 Western Blotting

Sample protein concentration was determined using the BCA Protein Quantification kit (Pierce); equal amounts of protein per sample (10 μg for cytoplasmic fractions; 35 μg for nuclear fractions) were mixed with loading buffer (0.1 M Tris-HCl containing SDS, glycerol, biomophenol blue, and β-mercaptoethanol), incubated at 95C for 5 minutes, and loaded in 4-15% Mini-PROTEAN TGX gels (Bio-Rad). Vertical electrophoresis was performed using the Mini-PROTEAN Treta Cell (Bio-Rad) system with SDS/PAGE running buffer (Tris base/glycine/SDS solution) at 200V for 30 minutes. A protein ladder (Precision Plus Protein Kaleidoscope, 10-250 kDa, Bio-Rad) was also loaded into each gel as a molecular weight reference.

Following SDS/PAGE separation, protein was transferred to a nitrocellulose membrane (Bio-rad) via semi dry transfer (Trans-Blot SD, Bio-Rad) at 25V for 20 minutes. Membranes were then blocked in near infrared blocking medium (Rockland Immunochemicals) for 1 hour and subsequently incubated with primary antibodies for β-catenin (polyclonal rabbit anti-β-catenin; Millipore; 1:400) and loading controls for

cytoplasmic (polyclonal rabbit anti-GAPDH; Pierce; 1:400) and nuclear (monoclonal mouse anti-TATA binding protein, TBP; Abcam; 1:2000) fractions overnight at 4C. Primary antibody incubation was followed washes in 0.01% Tween-20/PBS solution, and membranes were incubated with IR secondary antibodies (680 anti-mouse and anti-rabbit, LiCor Biosciences, 1:2000), followed by washes in PBS/0.1% Tween-20 solution. Blots were imaged using the Odyssey Infrared imager (LiCor Biosciences).

A.2.10 Quantitative PCR

Expression of Wnt pathway agonists and antagonists, as well as cardiogenic genes were assessed via quantitative PCR from EBs formed with different aggregation kinetics, as well as for those supplemented with Wnt inhibitors (5 μM Inhibitor of Wnt Production-4, IWP-4; Stemgent) during the first 4 days of differentiation [194]. RNA was extracted from undifferentiated ESCs and from EBs using the RNeasy Mini kit (Qiagen Incorporated, Valencia, CA). Reverse transcription for complementary DNA synthesis was performed from 1 μg RNA using the iScript cDNA synthesis kit (Bio-Rad, Hercules, CA), and quantitative PCR was performed with SYBR green technology on the MyiQ cycler (Bio-Rad). Primer sequences and annealing temperatures are listed in Table 5 for *Wnt-1*, *Wnt-3a*, *Dickkopf-1* (*Dkk-1*), *Brachyury T* (*B-T*), *mesoderm posterior 1* (*Mesp-1*), *myocyte enhancer factor-2c* (*Mef-2c*), *Nkx2.5*, *α-myosin heavy chain* (*α-MHC*), *myosin light chain-2 ventricle* (*MLC-2v*), and *18S ribosome*. Each primer set was designed with either Beacon Designer software (Invitrogen, Carlsbad, CA) (*B-T*, *Mesp-1*, *Mef-2c*, *α-MHC*, and *MLC-2v*) or the Integrated DNA technologies INC design website (www.idtdna.com) (*Wnt11*, *Wnt3a*, *Dkk-1*, *Nkx2.5*) and validated with appropriate cell controls. In order to account for variability in expression of housekeeping genes, absolute gene expression concentrations were calculated against standard curves and represented per μg of total RNA.

Table 5: Primer sequences and annealing temperatures

Gene	Forward	Reverse	Temp.
Wnt 11	AGG GTG AGG ACA GAC GTC TTG AAA	TGG CTG TGC TGT AAG AAT GTC CCT	57.9 C
Wnt3a	GTC TTC TGC CTG GAA CTT TGC GTT	TGT CTA AAT CCA GTG GTG GGT GGA	57.0 C
Dkk1	GCG GCA GCT GTC CGG TTC TT	GAG AAC TCC CGG CGC CAC AC	58.0 C
B-T	GAC TCC AGC CTT CCT TCC	CAC ACC ACT GAC GCA CAC	56.5 C
Mesp1	GAC CCA TCG TTC CTG TAC	CTG AAG AGC GGA GAT GAG	56.5 C
Mef2c	CCC AAT CTT CTG CCA CTG	GGT TGC CGT ATC CAT TCC	57.0 C
Nkx2.5	ATG CCC TGT CCC TCA GAT TTC ACA	AAG TGG GAT GGA TCG GAG AAA GGT	60.5 C
α-MHC	GGT CCA CAT TCT TCA GGA TTC TC	GCG TTC CTT CTC TGA CTT TCG	58.0 C
MLC-2v	GAC CAT TCT CAA CGC ATT CAA G	CTT CTC CGT GGG TAA TGA TGT G	56.5 C

A.2.11 Statistical Analysis

Experimental conditions were examined with triplicate samples for a minimum of two independent experiments and the data values presented reflect the mean value standard error. One- or two-way analysis of variance were performed to determine statistical significance ($p \leq 0.05$) between experimental groups and time points, and where significant, was followed by post-hoc Tukey analysis to define statistical differences ($p \leq 0.05$) between specific experimental variables.

A.3 Results

A.3.1 Spatial localization of E-cadherin and association with β-catenin in ESCs

Previous studies have demonstrated that the Wnt signaling pathway is an important regulator of pluripotency, and that nuclear accumulation of β-catenin via treatment using a GSK-3 inhibitor aids in maintenance of ESC self-renewal [287]. Consistent with published reports, undifferentiated mESC colonies expressed β-catenin, which was co-localized with E-cadherin at the plasma membrane, as well as expressed within the cytoplasm and nucleus (Fig. A-1). The spatial distribution of both proteins was similar throughout the majority of cells in the colony, with the exception of cells exhibiting pyknotic nuclei, which demonstrated disrupted patterns of both β-catenin and E-cadherin. Additionally, cells at the perimeter of colonies expressed decreased β-catenin at the membrane, concurrent with decreases in E-cadherin in regions lacking intercellular connections. Overall, the spatial localization of β-catenin and E-cadherin indicates the existence of both molecules during undifferentiated expansion prior to EB formation, as well as the localization of β-catenin both at the membrane (localized with E-cadherin) and in the cytoplasm and nucleus.

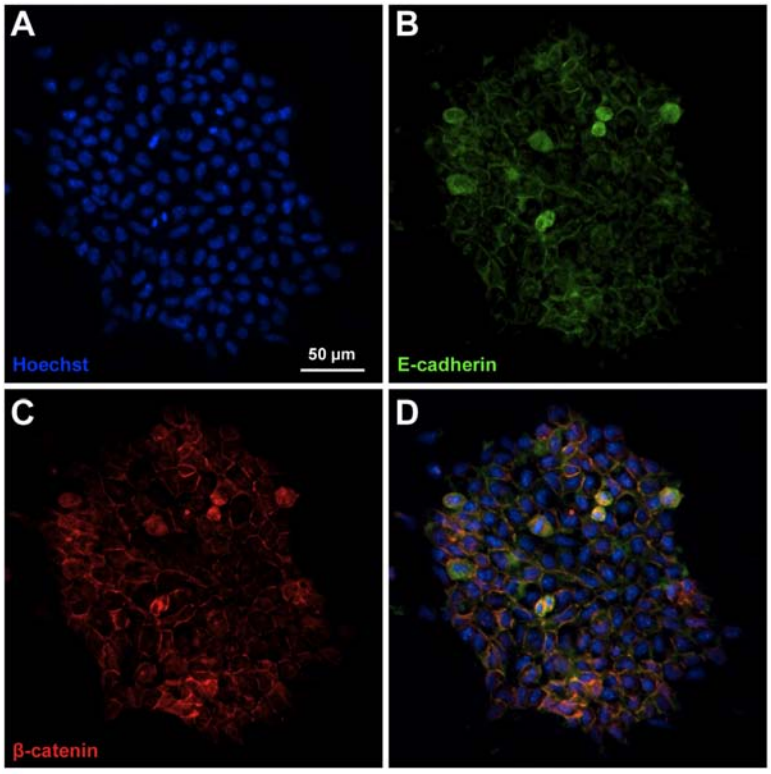

Figure A-1: β-catenin and E-cadherin expression patterns within ESCs. Localization of (A) nuclei, (B) E-cadherin, and (C) β-catenin in undifferentiated ESCs demonstrates expression primarily at the cell membrane between adjacent cells (D). Green = E-cadherin, red = β-catenin, blue = nuclei. Scale bar = 50 μm.

A.3.2 Temporal and spatial expression of E-cadherin in response to EB formation kinetics

Upon aggregation and continued differentiation of EBs in rotary orbital suspension culture, E-cadherin was localized to the cell membrane at sites of intercellular connections, and was relatively homogeneously expressed throughout by most cells in the EB (Fig. A-2). Altering the kinetics of cell-cell aggregation via changes in rotary orbital speed [282] suggested the modulation of E-cadherin expression during the course of differentiation. Specifically, the delayed aggregation kinetics of EBs formed at 55 rpm led to significantly decreased E-cadherin expression after 1 day (Fig. A-2 D), compared to 25 rpm rotary orbital conditions, which support more rapid EB formation (Fig. A-2 B). Additionally, while the expression of E-cadherin appeared to decrease over 4 days of differentiation at 25 rpm (Fig. A-2 L), cultures maintained at 40 and 55 rpm (Fig. A-2 M&N) exhibited significantly increased expression of E-cadherin at the cell membrane. Taken together, β-catenin was co-localized with E-cadherin in undifferentiated ESCs, and upon EB formation, E-cadherin localization was temporally modulated in response to altered cell association kinetics.

A.3.3 Temporal and spatial expression of β-catenin in response to EB formation kinetics

Based on the temporal modulation of E-cadherin and its established association with β-catenin, the spatial patterns of total (β-catenin+, red in Fig. A-3) and dephosphorylated, transcriptionally active β-catenin (aβC+, green in Fig. A-3) were assessed within EBs maintained in different culture conditions during the first 7 days of differentiation. Overall, static EBs exhibited significantly increased expression of β-catenin at early and late time points, compared to rotary conditions (Fig. A-3 A&E). Moreover, EBs maintained in static conditions exhibited nuclear expression of aβC at day 2 of differentiation (Fig. A-3 A, inset), accompanied by intercellular β-catenin expression at the cell membrane. Conversely, EBs from rotary orbital suspension cultures

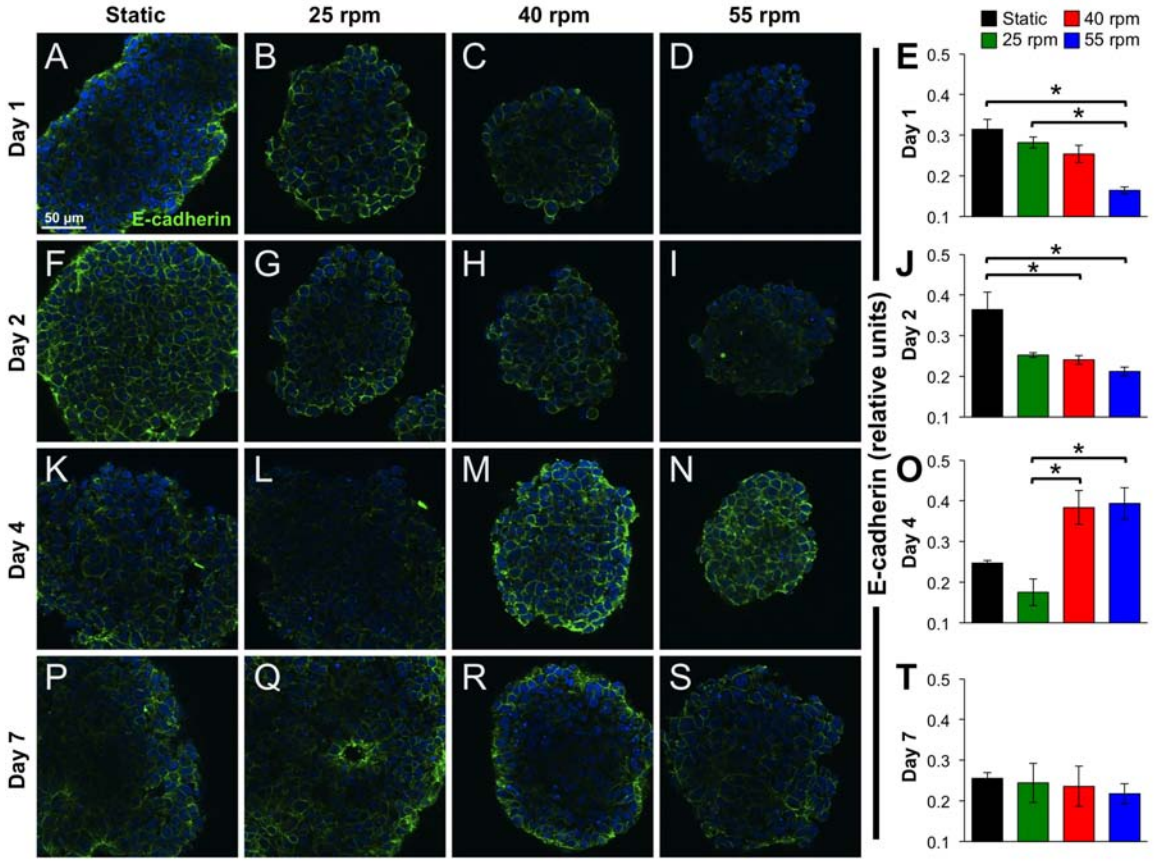

Figure A-2: E-cadherin expression patterns during EB differentiation. Static (A,F,K,P) and rotary EBs at 25 (B,G,L,Q), 40 (C,H,M,R), and 55 rpm (D,I,N,S) were stained for E-cadherin+ cells at days 1 (A-D), 2 (F-I), 4 (K-N), and 7 (P-S) of differentiation. Quantification of the staining patterns of E-cadherin (E,J,O,T), suggesting that E-cadherin expression within EBs was dynamically modulated during differentiation as a result of changes in ESC aggregation kinetics. Scale bar = 50 μm. Green = E-cadherin, blue = nuclei. n=3, * = p$\leq$0.05.

exhibited more homogeneous expression patterns of β-catenin and aβC over time, in which β-catenin was distinctly located either within the nucleus or at the cell membrane (Fig. A-3 B-D, H-J, N-P). After 2 days of differentiation, significantly decreased expression of β-catenin and aβC were observed within rotary EBs (Fig. A-3 B&C, inset), and aβC appeared to be sequestered at the cell membrane (Fig. A-3 B-D). However, at day 4 of differentiation, aβC expression appeared to increase within 25 and 40 rpm EBs and altered localization of aβC was suggested by the appearance of aβC+ nuclei, which was distinct from aβC previously observed at the cell membrane (Fig. A-3 H&I). In general, 55 rpm EBs exhibited little dephosphorylated β-catenin, and the majority of β-catenin expression was restricted to the cell membrane at days 2 and 4 of differentiation (Fig. A-3 D&J). After 7 days of differentiation, expression of β-catenin was significantly decreased in all rotary conditions compared to static EBs, and little to no nuclear staining of β-catenin was observed in EBs from any of the culture conditions (Fig. A-3 M-P), suggesting that β-catenin transcriptional activity was diminished. Overall, patterns of β-catenin expression within differentiating EBs indicated that ESC aggregation modulates both the expression patterns and phosphorylation state of β-catenin.

Interestingly, comparison of the dynamic expression patterns of E-cadherin (Fig. A-2) and β-catenin (Fig. A-3) over time revealed significant correlations, including a positive correlation ($p=0.01$) between E-cadherin and aβC after 2 days of differentiation and a negative correlation ($p=0.03$) between E-cadherin and total β-catenin expression after 4 days of differentiation (Table 6). Together, such results suggest an interplay between intercellular adhesions and β-catenin, with increased early expression of E-cadherin, followed by decreased E-cadherin levels supporting increased expression of aβC and total β-catenin, respectively.

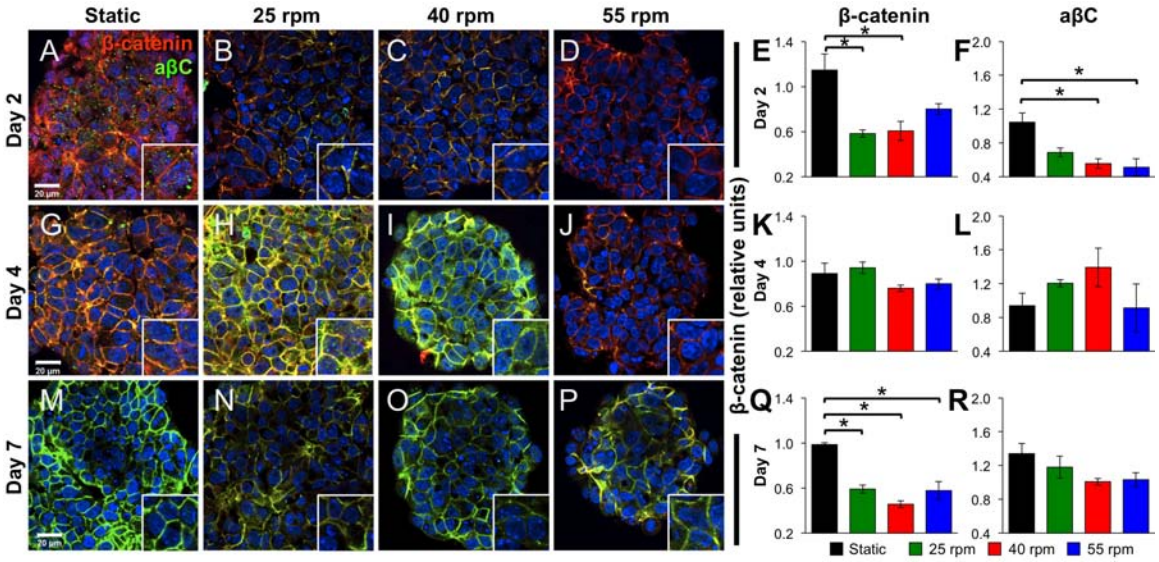

Figure A-3: Expression and phosphorylation state of β-catenin within EBs. Static (A,G,M) and rotary EBs at 25 (B,H,N), 40 (C,I,O), and 55 rpm (D,J,P) were stained for β-catenin+ and aβC+ cells at days 2 (A-D), 4 (G-J), and 7 (M-P) of differentiation. Quantification of the expression of β-catenin (E,K,Q) and aβC (F,L,R) indicated differences in β-catenin phosphorylation and location during differentiation. Scale bar = 20 μm. Red = β-catenin, green = aβC, yellow = β-catenin/aβC overlay, blue = nuclei. n=3, * = p$\leq$0.05.

Table 6: Correlation of E-cadherin and β-catenin expression dynamics

Day	Protein Expression		Pearson's r	p-value
2	E-cadherin	Total B-catenin	0.80	0.20
2	E-cadherin	Active B-catenin	0.99	0.01
4	E-cadherin	Total B-catenin	-0.97	0.03
4	E-cadherin	Active B-catenin	0.03	0.97
7	E-cadherin	Total B-catenin	0.67	0.33
7	E-cadherin	Active B-catenin	0.85	0.15

A.3.4 β-catenin cellular localization in response to EB formation kinetics

The intracellular localization of total β-catenin was further examined by Western blot analysis of cytoplasmic (Fig. A-4 A) and nuclear (Fig. A-4 B) protein fractions from EBs cultured in static or rotary (25, 40, and 55 rpm) conditions at days 2 and 4 of differentiation. EBs from all conditions expressed total β-catenin in both the cytoplasm and nucleus at all time points examined (Fig. A-4 A&B). Overall, the expression of β-catenin in the cytoplasm remained relatively constant across all conditions at both time points examined (Fig. A-4 A). In contrast, nuclear fractions suggested differences in the β-catenin expression across different EB formation conditions. Specifically, EBs maintained at 25 rpm appeared to exhibit increased nuclear expression of total β-catenin at both days 2 and 4 of differentiation compared to other rotary conditions (Fig. A-4 B), which was consistent with the increased expression of aβC noted by immunofluorescence in 25 rpm EBs at day 4 of differentiation (Fig. A-3 F). Taken together, these data suggest the dynamic regulation of β-catenin protein expression, phosphorylation state, and localization during the initial stages of differentiation in response to intercellular adhesion kinetics.

A.3.5 TCF/LEF activity in response to ESC aggregation kinetics

To quantitatively assess β-catenin transcriptional activity with high temporal resolution during the initial stages of EB differentiation, ESCs were transduced with a TCF/LEF-luciferase lentivirus. Transduced cells retained a typical undifferentiated

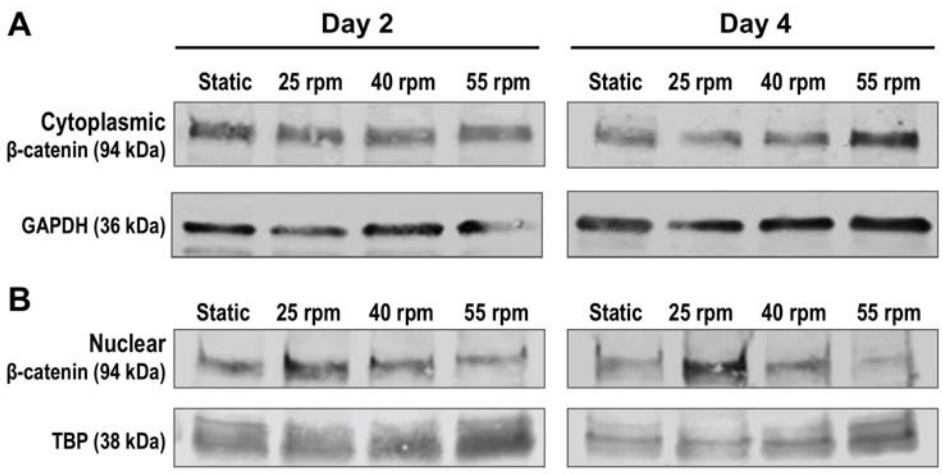

Figure A-4: β-catenin cellular localization. Although cytoplasmic (A) expression of β-catenin was similar among culture conditions, nuclear (B) β-catenin exhibited changes in expression among static and rotary (25, 40, 55 rpm) EBs after days 2 and 4 of differentiation.

morphological appearance at all MOI levels examined (Fig. A-5 A-C); however, only ESCs transduced with 10 and 25 MOI survived after puromycin treatment (Fig. A-5 D-F). Stably transduced clones were characterized based upon morphological appearance, doubling time, pluripotency (alkaline phosphatase activity, and Oct-4 protein expression), luciferase expression, and the capacity to form embryoid bodies (Fig. A-6), all of which supported the maintenance of the pluripotent ESC phenotype. The clones that exhibited the greatest dynamic range in luciferase activity in response to LiCl treatment were selected for additional analyses (Fig. A-6 G). Importantly, transduced ESCs formed and maintained EBs that were similar in size and appearance to EBs formed from naive ESCs [282] at various rotary speeds (25, 40 and 55 rpm) and in static conditions (Fig. A-6 H), indicating the capacity to quantitatively assess β-catenin transcriptional activity in response to ESC aggregation kinetics.

EBs cultured under all conditions exhibited transient β-catenin transcriptional activity during the first 2-6 days of differentiation (Fig. A-7). After 2 days of EB differentiation, static and 25 rpm EBs exhibited the highest levels of luciferase activity,

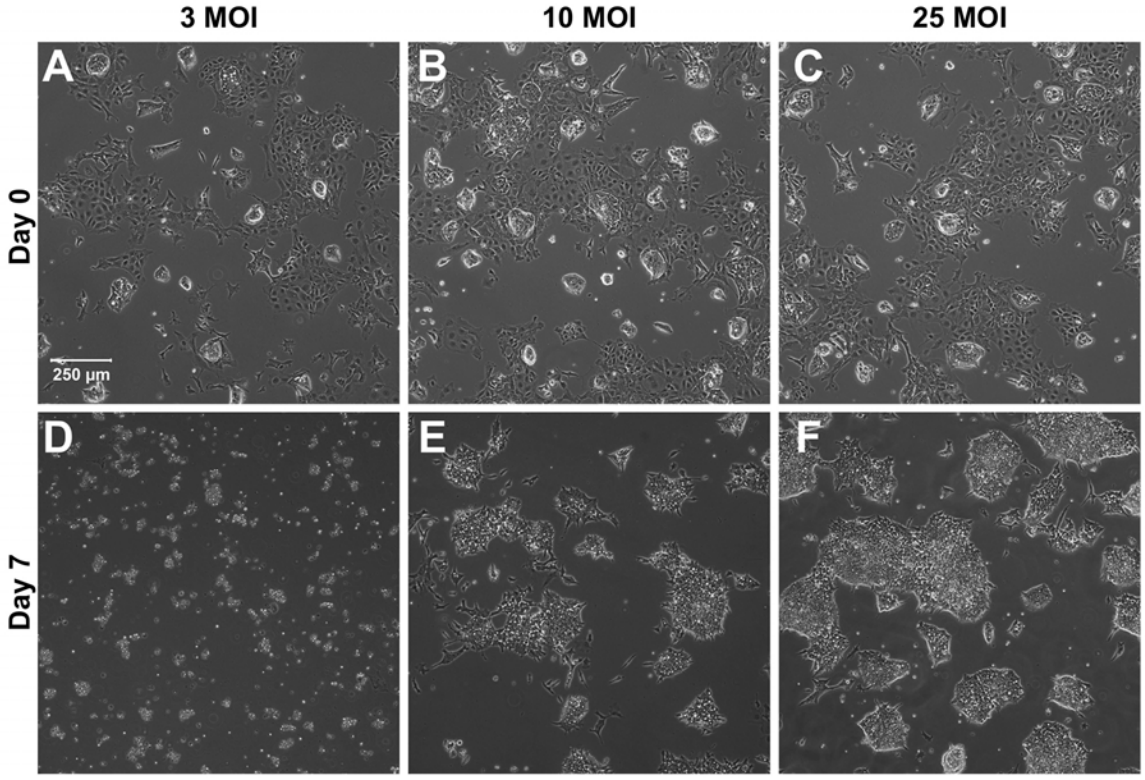

Figure A-5: ESC transduction. ESCs were incubated with lentiviral particles containing the luciferase TCF/LEF reporter construct for 24 hours at 3 (A), 10 (B), and 25 (C) MOI. Selection with puromycin resulted in no transduced colonies from 3 MOI (D), but colonies from 10 MOI (E) and 25 MOI (F) remained after 1 week of puromycin treatment (3 μg/mL). Scale bar = 250 μm

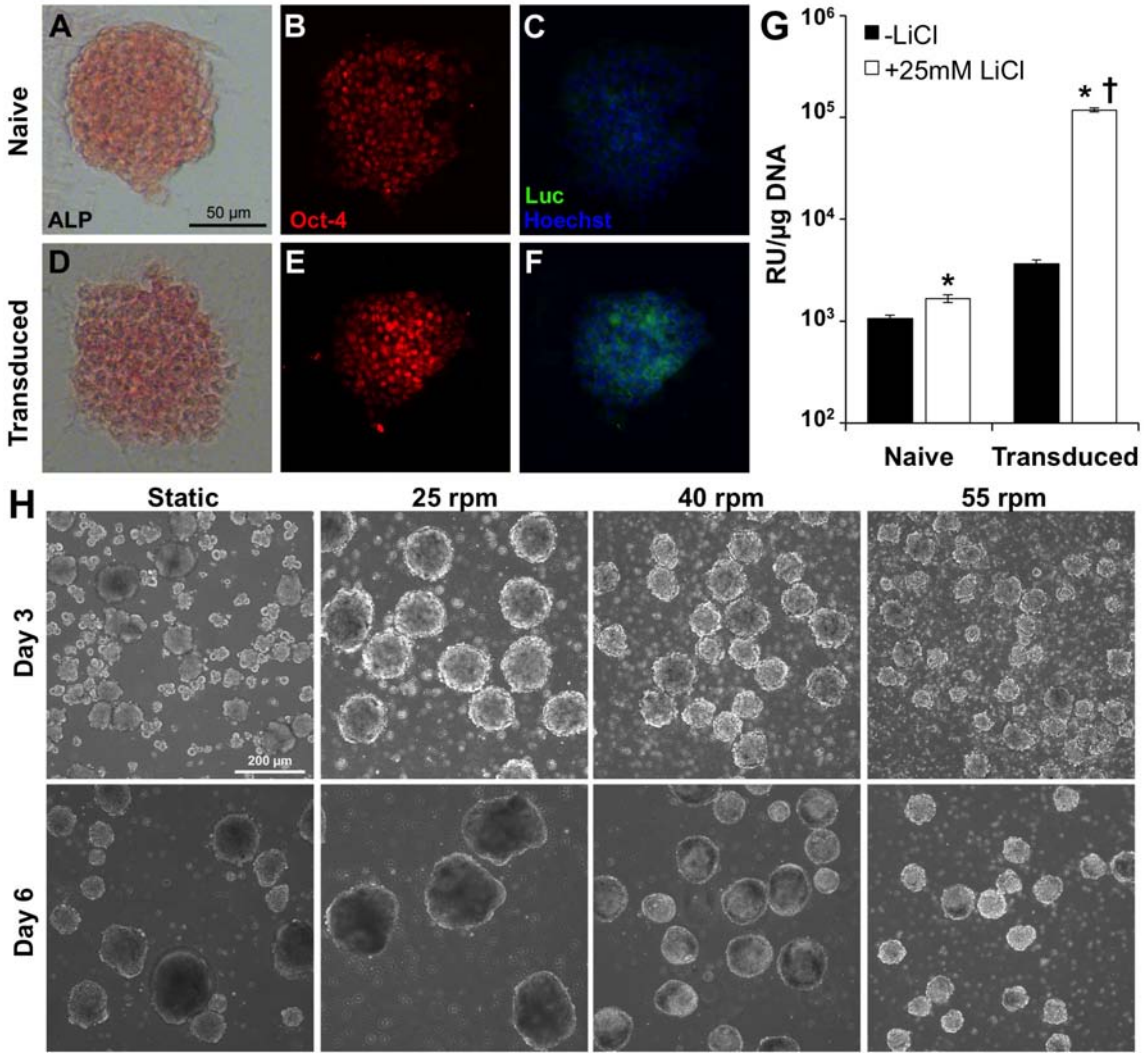

Figure A-6: TCF/LEF activity and pluripotent phenotype of transduced ESCs. Naive and transduced mESCs expressed alkaline phosphatase (A&D) and Oct-4 (B&E); however, only transduced cells expressed luciferase (C&F). Transduced cells expressed a higher baseline level of luciferase activity compared to naive cells and also exhibited increased activity upon stimulation with LiCl (25 mM) (G). In addition, transduced ESCs were capable of formation and differentiation as EBs in rotary and static culture conditions (H). Scale bar = 50 μm. n=3, P $\leq$ 0.05: * compared to naive +/- LiCl, † compared to -LiCl.

compared to 40 and 55 rpm ($p \leq 0.05$). By day 3, EBs from all rotary conditions exhibited increased β-catenin transcriptional activity compared to static cultures ($p \leq 0.001$, 25 rpm; $p \leq 0.01$, 40 rpm; $p \leq 0.05$, 55 rpm), with the β-catenin transcription in 25 rpm EBs statistically increased compared to the other two rotary conditions ($p \leq 0.05$). Whereas EBs cultured in rotary orbital suspension increased transcription activity between days 2 and 3 of differentiation, statically cultured EBs exhibited decreased TCF/LEF activity over the same time course (Fig. A-7). Within 6 days of differentiation, all cultures exhibited decreased β-catenin transcription, below the initial levels at day 2, though static EBs maintained an increased level of TCF/LEF activity compared to any of the rotary orbital culture conditions ($p \leq 0.001$) (Fig. A-7). Overall, the TCF/LEF transcriptional activity was most active within the first 3 days of EB differentiation and increasing the EB aggregation kinetics via rotary orbital conditions (25 rpm) enhanced the peak β-catenin transcriptional activity between days 2-4 of differentiation, consistent with immunofluorescence and Western blot, which together reflected increased β-catenin protein expression and nuclear localization.

A.3.6 Temporal dynamics of β-catenin-target gene expression

Since β-catenin expression, phosphorylation state, localization, and transcriptional activity were modulated by ESC aggregation kinetics, the downstream expression of β-catenin-target genes was examined. The expression patterns of canonical and non-canonical Wnt genes (*Wnt3a* and *Wnt11*, respectively) exhibited similar temporal expression (Fig. A-8 A,B). After 2 days of differentiation, EBs from all culture conditions expressed similar levels of both Wnt11 and Wnt3a; however, after 4 days of differentiation, 25 rpm EBs significantly decreased *Wnt11* expression compared to static and 55 rpm ($p \leq 0.05$, static; $p \leq 0.01$, 55 rpm), accompanied by a decrease in *Wnt3a* expression compared to 55 rpm ($p \leq 0.05$). At day 6 of differentiation, 40 rpm

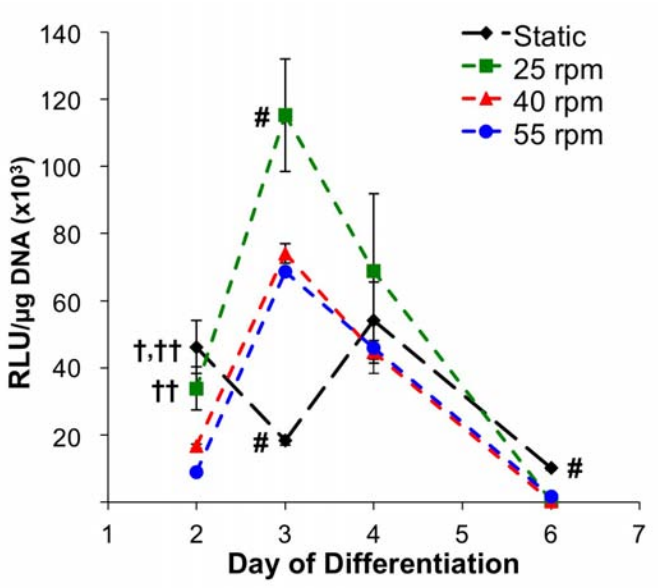

Figure A-7: TCF/LEF activity in differentiating EBs. TCF/LEF-mediated luciferase activity was transiently increased by rotary orbital culture compared to static EBs, with a peak in expression after 3 days of differentiation; within rotary conditions, EBs maintained at 25 rpm yielded the largest increase in luciferase activity. $p \leq 0.05$, # = compared to all other conditions, * = compared to static, † = compared to 40 rpm, and †† = compared to 55 rpm.

EBs exhibited increased *Wnt11* and *Wnt3a* expression levels compared to all other conditions ($p \leq 0.05$) (Fig. A-8 A,B). Interestingly, expression of *Dkk-1*, a canonical Wnt inhibitor, increased in 25 rpm EBs at days 4 and 8 compared to static and 55 rpm EBs ($p \leq 0.05$) (Fig. A-8 A,B,C). Moreover, *Dkk-1* expression increased in all rotary conditions compared to static culture at day 4 of differentiation ($p \leq 0.001$, 25 rpm; $p \leq 0.01$, 40 rpm; $p \leq 0.05$, 55 rpm) (Fig. A-8 C).

Expression of *Brachyury-T* (*B-T*), an early marker associated with primitive streak formation and mesoderm differentiation, was increased significantly after 2 days of differentiation within 25 rpm EBs compared to all other culture conditions ($p \leq 0.05$), followed by increased expression at day 4 in all rotary conditions compared to static culture ($p \leq 0.01$). *Mesoderm posterior 1* (*Mesp-1*), a direct target of TCF/LEF regulated transcription [81], which is also implicated in early mesoderm differentiation within ESCs [196], exhibited increased expression in 25 rpm conditions at day 4 of differentiation compared to all other culture conditions ($p \leq 0.001$).

Temporally controlled Wnt/β-catenin signaling has been implicated in the specification of mesoderm cells toward cardiac progenitors and subsequent cardiomyocyte maturation [177, 195, 231]. *Nkx2.5*, an early marker of cardiomyocyte progenitors, exhibited increased expression at early time points in all rotary orbital culture conditions compared to static (Fig. A-8 G,H). After 6 days of differentiation, *Nkx2.5* expression was greater in all rotary conditions compared to static culture ($p \leq 0.005$, 25 rpm; $p \leq 0.001$, 40 rpm; $p \leq 0.05$, 55 rpm) and *Nkx2.5* continued to exhibit increased expression in 25 rpm EBs compared to all other culture conditions after 10 days of differentiation ($p \leq 0.005$). Likewise, 25 rpm EBs expressed increased levels of *myocyte enhancer 2c* (*Mef-2c*) after 10 days of differentiation compared to all other conditions ($p \leq 0.005$, static; $p \leq 0.01$, 40 & 55 rpm).

Expression of sarcomeric muscle related genes *α-myosin heavy chain* (*α-MHC*) and *myosin light chain 2 ventricle* (*MLC-2v*), phenotypic markers of more mature

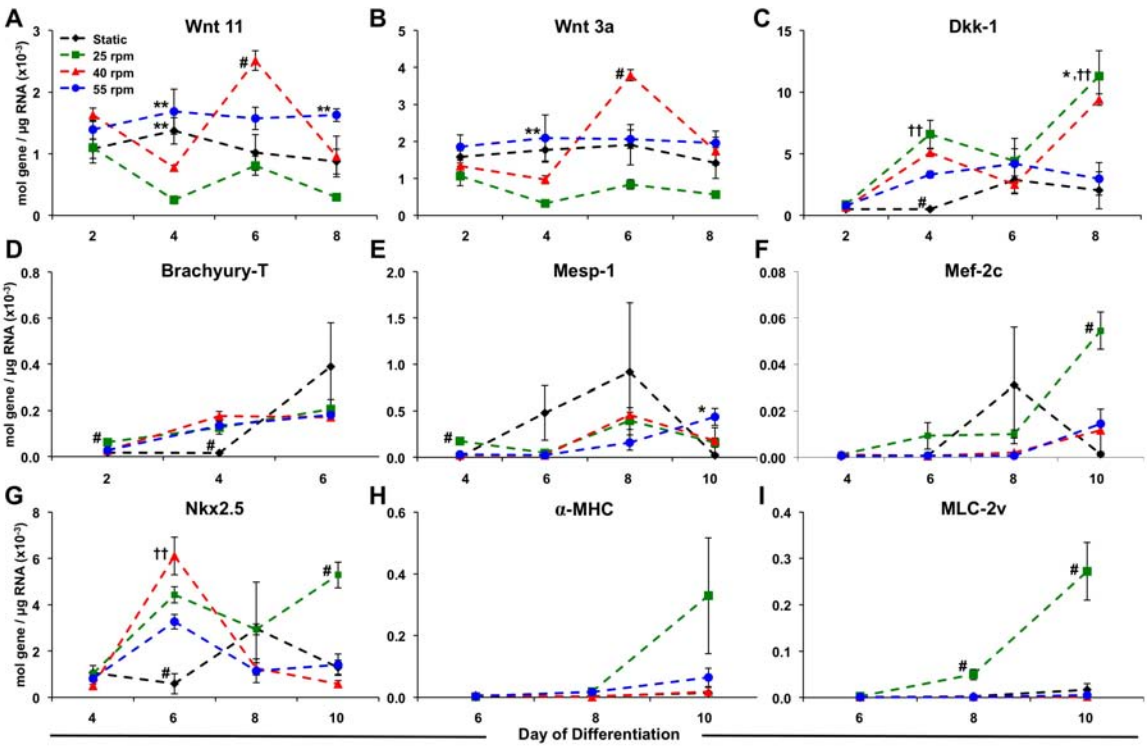

Figure A-8: Expression of β-catenin-target cardiomyogenic genes. qPCR analysis of RNA from static and rotary EBs (25, 40, 55 rpm) was performed at day 2, 4, 6, 8, and 10 of differentiation. Expression levels of non-canonical and canonical Wnts (A,B) was similar, but was modulated by culture condition, with 25 rpm rotary conditions exhibiting decreased levels of both *Wnt11* and *Wnt3*. In contrast, Wnt inhibitor *Dkk-1* expression was increased within rotary EBs compared to static EBs (C), also corresponding to increased mesoderm-related gene expression within rotary conditions compared to static (D,E). Additionally, early cardiomyogenic markers *Mef-2c* and *Nkx2.5* were increased by rotary orbital culture (F,G), with 25 rpm conditions resulting in increased expression of sarcomeric muscle genes *α-MHC* and *MLC-2v* (H,I). n=3, $p \leq 0.05$, # = compared to all other conditions, * = compared to static, ** = compared to 25 rpm, † = compared to 40 rpm, and †† = compared to 55 rpm.

cardiomyocytes, were observed by day 10 of differentiation within EBs maintained at 25 rpm (Fig. A-8 H,I). *MLC-2v* expression was significantly increased within 25 rpm EBs compared to other culture conditions ($p \leq 0.05$, static; $p \leq 0.01$, 40 & 55 rpm) as early as day 8 of differentiation compared to other culture conditions, and continued to exhibit increased expression after 10 days of differentiation ($p \leq 0.005$) (Fig. A-8 I). Together, the targets of the Wnt/β-catenin pathway (*Mesp-1*, *Mef-2c*) exhibited increased expression at early stages of differentiation (day 4), followed by increased expression of Wnt and β-catenin inhibitors (*Dkk-1*, *Nkx2.5*) and cardiomyogenic gene transcription in response to accelerated aggregation kinetics within 25 rpm rotary orbital cultures.

A.3.7 Regulation of cardiomyogenic gene transcription by Wnt/β-catenin signaling

To establish a more mechanistic link between the observed regulation of β-catenin signaling and cardiomyogenic gene transcription, 25 rpm EBs were supplemented with inhibitors of canonical Wnt/β-catenin signaling (IWP-4; 5 μM) during the initial 4 days of differentiation (Fig. A-9 A). As expected, the pluripotency marker *Oct-4* was significantly decreased compared to ESCs and expression of genes related to endoderm (*Foxa2*) and ectoderm (*Nestin*) lineages were significantly increased compared to ESCs; however, Wnt inhibition did not significantly affect the expression of genes related to pluripotency, endoderm, or ectoderm differentiation. In contrast, inhibition of Wnt signaling significantly abrogated the previously observed increase in cardiomyogenic genes α-*MHC* and *MLC-2v*, thus indicating the role of canonical Wnt/β-catenin signaling in mediating the cardiomyogenic gene transcription downstream of intercellular aggregation at 25 rpm. The results of this study suggest that the dynamic interplay between E-cadherin-mediated cellular adhesion and Wnt signaling leads to nuclear accumulation and TCF/LEF transcriptional activation via dephosphorylated, β-catenin (aβC), thereby inducing downstream cardiomyogenic

gene expression (Fig. A-9 B).

A.4 Discussion

In this study, β-catenin expression, localization and transcriptional activity, as well as cardiomyogenic gene transcription were assessed in response to changes in ESC aggregation kinetics. Overall, rotary orbital culture increased β-catenin-regulated transcription and cardiomyogenic gene expression compared to static culture conditions. The spatiotemporal location and phosphorylation state of β-catenin was modulated by rotary orbital speed, with slower rotary speeds (faster ESC aggregation kinetics) resulting in increased accumulation of nuclear, dephosphorylated β-catenin at early time points (Fig. A-3 and Fig. A-4). Additionally, gene transcription downstream of β-catenin was increased initially by slower rotary speeds, evidenced by increased TCF/LEF activity and the expression of *Mesp-1* and *Mef-2c* (Fig. A-8). Moreover, inhibition of Wnt signaling significantly decreased cardiomyogenic gene transcription. Overall, this study illustrates that β-catenin signaling and downstream cardiomyogenic gene transcription are enhanced within culture conditions that promote increased multicellular aggregation kinetics.

Recent studies have illustrated that activation of the β-catenin pathway can play both inductive and repressive roles in cardiomyogenesis, depending on the temporal onset and duration of transcriptional activity [231, 194, 334]. Early activation of β-catenin within differentiating ESCs has been linked to increased mesoderm differentiation and proliferation of Mesp-1+, Isl-1+, and Mef-2c+ cardiomyocyte progenitor cells [196, 231, 251, 334, 178, 268]. However, persistent β-catenin signaling (i.e. beyond day 4 of differentiation) inhibits subsequent cardiomyocyte maturation [231, 334]; conversely, inhibition of β-catenin signaling through natural (eg. Dkk-1) or small molecule Wnt inhibitors at later stages of differentiation (day 4+) increases

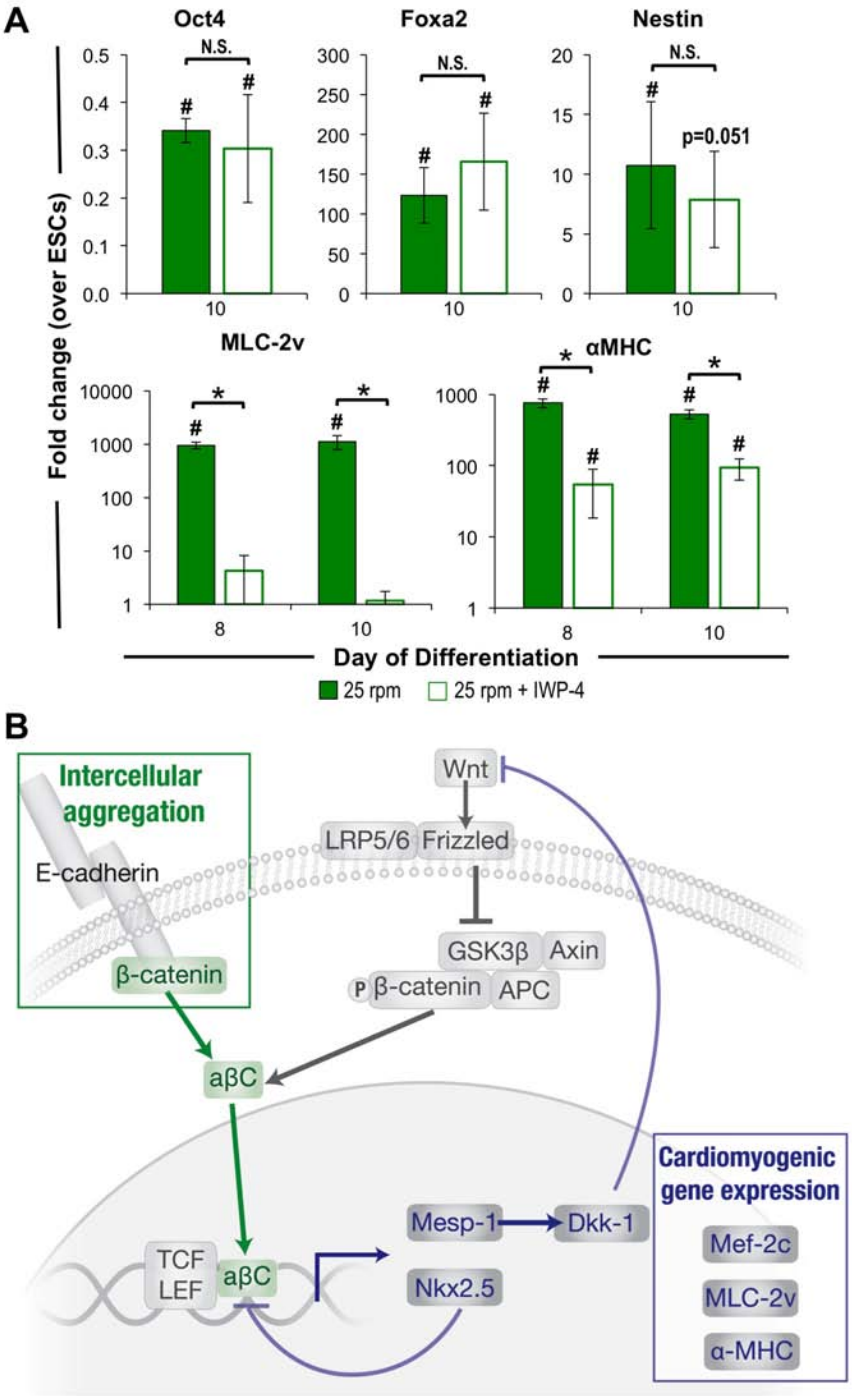

Figure A-9: Influence of canonical Wnt/β-catenin signaling in aggregation-mediated cardiogenic gene transcription. Expression of genes related to pluripotency (*Oct-4*), endoderm (*Foxa2*), and ectoderm (*Nestin*) phenotypes were not altered by inhibition of Wnt signaling via treatment with IWP-4 during the first 4 days of differentiation at 25 rpm; however, cardiomyogenic markers α-*MHC* and *MLC-2v* were significantly decreased upon Wnt inhibition (A). The proposed model depicting Wnt/β-catenin-mediated increase in cardiomyogenic gene transcription resulting from intercellular adhesion of ESCs (B). n=3, * = $p \leq 0.05$

mature cardiomyocyte development within EBs [272, 344, 352, 194]. A similar biphasic regulation of β-catenin activity and inhibitor expression was observed in this study in response to accelerated cellular adhesion kinetics. Nuclear total β-catenin expression was modulated by ESC aggregation kinetics (Fig 4 B), with increased expression of signaling active β-catenin within 25 rpm rotary conditions at early time points of differentiation (days 2 and 4, Fig. A-3), significantly increased TCF/LEF activation at day 3 of differentiation (Fig. A-4 C), and increased *Mesp-1* and *Mef-2c* expression (day 4) compared to other conditions (Fig. A-8). Subsequently, expression of β-catenin signaling inhibitors Dkk-1 and Nkx2.5 [274] was also increased within the same rotary orbital condition, concomitant with decreased Wnt expression levels (days 4-6). The increase in *Dkk-1* expression may be related to increased *Mesp-1* expression within 25 rpm rotary conditions, as *Mesp-1* is a transcription factor capable of directly increasing *Dkk-1* expression [81]. Thus, the expression of *Mesp-1*, *Dkk-1*, and *Nkx2.5* at later stages of differentiation supports the maturation of cardiomyocyte progenitors, as evidenced by increased expression of *MLC-2v* in 25 rpm rotary conditions (Fig. A-8 I). Consistent with our previous results [282, 283], rotary orbital culture promoted cardiomyogenic gene transcription in a speed-dependent manner, and the results from this study suggest that β-catenin signaling may be implicated in the regulation of mesoderm differentiation and maturation of cardiomyocyte progenitors (Fig. A-9) in response to changes in early ESC aggregation kinetics.

Until recently, the membrane associated and nuclear signaling roles of β-catenin have been largely studied independently; however, increasing evidence suggests that the two processes may be intimately coordinated through competition for the total pool of available β-catenin in the cell [238, 151]. Studies using recombinant forms of β-catenin indicate that the binding domains of β-catenin which mediate interactions with cadherins, TCF/LEF and APC are mutually exclusive [249]. The loss of

E-cadherin expression is correlated with invasive phenotypes during cancer progression and is exhibited concomitant with upregulation of the Wnt/β-catenin signaling, suggesting the possible interplay between E-cadherin expression and β-catenin transcriptional activation [121, 115, 252, 148, 233, 120]. In the undifferentiated state, ESCs largely express β-catenin at the plasma membrane, presumably bound to E-cadherin, with little nuclear localization and signaling (Fig. A-1) [10]. Moreover, the culture of ESCs in a three-dimensional microwell format increased E-cadherin expression and subsequently increased Wnt signaling upon EB formation, suggesting a link between intercellular adhesions, Wnt signaling, and cardiogenesis in ESCs [14]. Similarly, in this study, E-cadherin was dynamically regulated, including significant correlations between E-cadherin (Fig. A-2) and β-catenin (Fig. A-3) expression over time (Table 6), concurrent with increased TCF/LEF transcriptional activity (Fig. A-7). The regulation of intercellular adhesions in EBs is consistent with changes during embryonic development, whereby E-cadherin is down-regulated as cells traverse the primitive streak and β-catenin signaling is increased to promote axis formation and mesoderm differentiation [43, 44, 64, 128, 129, 18]. It is likely that similar interrelated signaling between cadherins and β-catenin may enable the pool of cadherin-bound β-catenin to become available for nuclear translocation and signaling upon remodeling of cadherins following EB formation. Although the direct relationship between cadherin and TCF/LEF mediated regulation of the β-catenin pool remains unclear [36, 207, 151], evidence from this study suggests a correlation between E-cadherin and β-catenin signaling during EB formation and ESC differentiation.

Rotary orbital suspension culture has previously demonstrated the modulation of EB formation kinetics across a range of mixing conditions, with slower speeds resulting in increased EB formation kinetics [52, 282]. The changes in β-catenin transcriptional activity as a function of rotary speed, in conjunction with changes in E-cadherin expression, indicate that cell association kinetics during EB formation can impact the

subsequent pathway activation and ESC differentiation. β-catenin transcriptional activity was significantly increased at early stages of differentiation in EBs that exhibit faster cell association kinetics during EB formation at slower rotary speeds. Studies indicate that mixed culture conditions also modulate EB size, which may be partially responsible for changes in ESC differentiation [282]. Mesoderm induction in different sized EBs, however, is thought to result from paracrine actions of endoderm cells at the exterior of EBs [22], which do not arise until later stages of differentiation. In the context of this study, the initial cell specification resulting from changes in β-catenin signaling at early time points (days 2-4) is likely independent of signaling from divergent cell populations. The observed changes in cell aggregation kinetics due to rotary orbital suspension culture conditions may also be modulated across a range of suspension culture formats [166]; β-catenin transcriptional activity may be implicated in the modulation of cardiogenic differentiation as a function of bioreactor configuration, mixing speed, and cell density [146, 298]. Hanging drop cultures exhibit an increased endogenous propensity to differentiate toward mesoderm lineages and develop functional cardiomyocytes compared to other formats [283, 366]. In contrast to suspension cultures, which rely on the random collision of cells in larger volume suspensions to form EBs, hanging drop cultures force ESC aggregation in small volumes to more precisely control EB size, which likely results in faster association kinetics compared to suspension cultures. The increased cardiac differentiation yielded by hanging drops, therefore, is consistent with the observed increase in cardiomyogenic gene transcription in response to slower rotary speed and faster aggregation kinetics. Many recently developed technologies for spheroid formation may also alter the formation kinetics, by controlling aggregation within microwells or on micropatterned surfaces [219, 335, 253]; EBs formed via forced aggregation exhibited increased homogeneity and endogenous differentiation capacities across a similar range of rotary

conditions examined in this study (Chapter 3). Thus, techniques to control intercellular adhesion dynamics may impact the differentiation capacity of stem and progenitor cells to either aid or hinder directed differentiation protocols, depending on the application. The results from this study, coupled with the developing understanding of the complex relationship between E-cadherin and β-catenin, highlight the important roles of β-catenin signaling in ESCs, which may be modulated by increasing cell association kinetics during EB formation to enhance cardiomyogenic differentiation.

REFERENCES

[1] Aberle, H., Schwartz, H., and Kemler, R., "Cadherin-catenin complex: Protein interactions and their implications for cadherin function," *J Cell Biochem*, vol. 61, no. 4, pp. 514–523, 1996.

[2] Adamo, L., Naveiras, O., Wenzel, P. L., McKinney-Freeman, S., Mack, P. J., Gracia-Sancho, J., Suchy-Dicey, A., Yoshimoto, M., Lensch, M. W., Yoder, M. C., García-Cardeña, G., and Daley, G. Q., "Biomechanical forces promote embryonic haematopoiesis.," *Nature*, vol. 459, pp. 1131–1135, June 2009.

[3] Aegerter-Wilmsen, T., Aegerter, C. M., Hafen, E., and Basler, K., "Model for the regulation of size in the wing imaginal disc of Drosophila.," *Mech Dev*, vol. 124, pp. 318–326, Apr. 2007.

[4] Afrakhte, M., Morén, A., Jossan, S., Itoh, S., Sampath, K., Westermark, B., Heldin, C. H., Heldin, N. E., and ten Dijke, P., "Induction of inhibitory Smad6 and Smad7 mRNA by TGF-beta family members.," *Biochem Biophys Res Commun*, vol. 249, pp. 505–511, Aug. 1998.

[5] Ahsan, T. and Nerem, R. M., "Fluid shear stress promotes an endothelial-like phenotype during the early differentiation of embryonic stem cells.," *Tissue Eng Part A*, vol. 16, pp. 3547–3553, Nov. 2010.

[6] Ahuja, P., Sdek, P., and MacLellan, W. R., "Cardiac myocyte cell cycle control in development, disease, and regeneration," *Physiol Rev*, vol. 87, pp. 521–544, Apr. 2007.

[7] Akins, R. E., Rockwood, D., Robinson, K. G., Sandusky, D., Rabolt, J., and Pizarro, C., "Three-dimensional culture alters primary cardiac cell phenotype.," *Tissue Eng Part A*, vol. 16, pp. 629–641, Feb. 2010.

[8] Albanese, A., Lam, A. K., Sykes, E. A., Rocheleau, J. V., and Chan, W. C. W., "Tumour-on-a-chip provides an optical window into nanoparticle tissue transport.," *Nat Commun*, vol. 4, p. 2718, 2013.

[9] Anderson, D., Levenberg, S., and Langer, R., "Nanoliter-scale synthesis of arrayed biomaterials and application to human embryonic stem cells," *Nat Biotechnol*, vol. 22, no. 7, pp. 863–866, 2004.

[10] Anton, R., Kestler, H. A., and Kühl, M., "Beta-catenin signaling contributes to stemness and regulates early differentiation in murine embryonic stem cells," *FEBS Lett*, vol. 581, pp. 5247–5254, Nov. 2007.

[11] Antonica, F., Kasprzyk, D. F., Opitz, R., Iacovino, M., Liao, X.-H., Dumitrescu, A. M., Refetoff, S., Peremans, K., Manto, M., Kyba, M., and Costagliola, S., "Generation of functional thyroid from embryonic stem cells.," *Nature*, vol. 491, pp. 66–71, Nov. 2012.

[12] Assmus, B., Schächinger, V., Teupe, C., Britten, M., Lehmann, R., Döbert, N., Grünwald, F., Aicher, A., Urbich, C., Martin, H., Hoelzer, D., Dimmeler, S., and Zeiher, A. M., "Transplantation of Progenitor Cells and Regeneration Enhancement in Acute Myocardial Infarction (TOPCARE-AMI)," *Circulation*, vol. 106, pp. 3009–3017, Dec. 2002.

[13] Aubert, J., Dunstan, H., Chambers, I., and Smith, A., "Functional gene screening in embryonic stem cells implicates Wnt antagonism in neural differentiation," *Nat Biotechnol*, vol. 20, pp. 1240–1245, Dec. 2002.

[14] Azarin, S. M., Lian, X., Larson, E. A., Popelka, H. M., De Pablo, J. J., and Palecek, S. P., "Modulation of Wnt/β-catenin signaling in human embryonic stem cells using a 3-D microwell array.," *Biomaterials*, vol. 33, pp. 2041–2049, Mar. 2012.

[15] Baraniak, P. R., Cooke, M. T., Saeed, R., Kinney, M. A., Fridley, K. M., and McDevitt, T. C., "Stiffening of human mesenchymal stem cell spheroid microenvironments induced by incorporation of gelatin microparticles.," *J Mech Behav Biomed Mater*, vol. 11, pp. 63–71, July 2012.

[16] Baraniak, P. R. and McDevitt, T. C., "Stem cell paracrine actions and tissue regeneration.," *Regen Med*, vol. 5, pp. 121–143, Jan. 2010.

[17] Baraniak, P. R. and McDevitt, T. C., "Scaffold-free culture of mesenchymal stem cell spheroids in suspension preserves multilineage potential.," *Cell Tissue Res*, vol. 347, pp. 701–711, Mar. 2012.

[18] Barker, N., Hurlstone, A., Musisi, H., Miles, A., Bienz, M., and Clevers, H., "The chromatin remodelling factor Brg-1 interacts with beta-catenin to promote target gene activation," *EMBO J*, vol. 20, pp. 4935–4943, Sept. 2001.

[19] Barrett, K., Leptin, M., and Settleman, J., "The Rho GTPase and a putative RhoGEF mediate a signaling pathway for the cell shape changes in Drosophila gastrulation.," *Cell*, vol. 91, pp. 905–915, Dec. 1997.

[20] Bartosh, T. J., Ylöstalo, J. H., Mohammadipoor, A., Bazhanov, N., Coble, K., Claypool, K., Lee, R. H., Choi, H., and Prockop, D. J., "Aggregation of human mesenchymal stromal cells (MSCs) into 3D spheroids enhances their antiinflammatory properties.," *Proc Natl Acad Sci USA*, vol. 107, pp. 13724–13729, Aug. 2010.

[21] Bauwens, C., Yin, T., Dang, S., Peerani, R., and Zandstra, P. W., "Development of a perfusion fed bioreactor for embryonic stem cell-derived cardiomyocyte generation: oxygen-mediated enhancement of cardiomyocyte output.," *Biotechnol Bioeng*, vol. 90, pp. 452–461, May 2005.

[22] Bauwens, C. L., Song, H., Thavandiran, N., Ungrin, M., Masse, S., Nanthakumar, K., Seguin, C., and Zandstra, P. W., "Geometric control of cardiomyogenic induction in human pluripotent stem cells.," *Tissue Eng Part A*, vol. 17, pp. 1901–1909, Aug. 2011.

[23] Bauwens, C. L., Peerani, R., Niebruegge, S., Woodhouse, K. A., Kumacheva, E., Husain, M., and Zandstra, P. W., "Control of human embryonic stem cell colony and aggregate size heterogeneity influences differentiation trajectories.," *Stem Cells*, vol. 26, pp. 2300–2310, Sept. 2008.

[24] Beddington, R. S., "Induction of a second neural axis by the mouse node.," *Development*, vol. 120, pp. 613–620, Mar. 1994.

[25] Behrens, J., von Kries, J. P., Kühl, M., Bruhn, L., Wedlich, D., Grosschedl, R., and Birchmeier, W., "Functional interaction of beta-catenin with the transcription factor LEF-1.," *Nature*, vol. 382, pp. 638–642, Aug. 1996.

[26] Belo, J. A., Bouwmeester, T., Leyns, L., Kertesz, N., Gallo, M., Follettie, M., and De Robertis, E. M., "Cerberus-like is a secreted factor with neutralizing activity expressed in the anterior primitive endoderm of the mouse gastrula.," *Mech Dev*, vol. 68, pp. 45–57, Nov. 1997.

[27] Benchabane, H. and Wrana, J. L., "GATA- and Smad1-dependent enhancers in the Smad7 gene differentially interpret bone morphogenetic protein concentrations.," *Mol Cell Biol*, vol. 23, pp. 6646–6661, Sept. 2003.

[28] Bernardo, A. S., Cho, C. H.-H., Mason, S., Docherty, H. M., Pedersen, R. A., Vallier, L., and Docherty, K., "Biphasic induction of Pdx1 in mouse and human embryonic stem cells can mimic development of pancreatic beta-cells," *Stem Cells*, vol. 27, pp. 341–351, Feb. 2009.

[29] Bertrand, P., Girard, N., Delpech, B., Duval, C., d'Anjou, J., and Dauce, J. P., "Hyaluronan (hyaluronic acid) and hyaluronectin in the extracellular matrix of human breast carcinomas: comparison between invasive and non-invasive areas.," *Int J Cancer*, vol. 52, pp. 1–6, Aug. 1992.

[30] Bez, A., Corsini, E., Curti, D., Biggiogera, M., Colombo, A., Nicosia, R. F., Pagano, S. F., and Parati, E. A., "Neurosphere and neurosphere-forming cells: morphological and ultrastructural characterization.," *Brain Res*, vol. 993, pp. 18–29, Dec. 2003.

[31] Bhowmick, N. A., Ghiassi, M., Bakin, A., Aakre, M., Lundquist, C. A., Engel, M. E., Arteaga, C. L., and Moses, H. L., "Transforming growth factor-beta1 mediates epithelial to mesenchymal transdifferentiation through a RhoA-dependent mechanism.," *Mol Biol Cell*, vol. 12, pp. 27–36, Jan. 2001.

[32] Bilgen, B., Sucosky, P., Neitzel, G. P., and Barabino, G. A., "Flow characterization of a wavy-walled bioreactor for cartilage tissue engineering.," *Biotechnol Bioeng*, vol. 95, pp. 1009–1022, Dec. 2006.

[33] Blagovic, K., Kim, L. Y., and Voldman, J., "Microfluidic perfusion for regulating diffusible signaling in stem cells," *PLoS ONE*, vol. 6, no. 8, p. e22892, 2011.

[34] Boheler, K. R., Czyz, J., Tweedie, D., Yang, H.-T., Anisimov, S. V., and Wobus, A. M., "Differentiation of pluripotent embryonic stem cells into cardiomyocytes," *Circ Res*, vol. 91, pp. 189–201, Aug. 2002.

[35] Bonvin, C., Overney, J., Shieh, A. C., Dixon, J. B., and Swartz, M. A., "A multichamber fluidic device for 3D cultures under interstitial flow with live imaging: development, characterization, and applications," *Biotechnol Bioeng*, vol. 105, pp. 982–991, Apr. 2010.

[36] Bonvini, P., An, W. G., Rosolen, A., Nguyen, P., Trepel, J., Garcia de Herreros, A., Dunach, M., and Neckers, L. M., "Geldanamycin abrogates ErbB2 association with proteasome-resistant beta-catenin in melanoma cells, increases beta-catenin-E-cadherin association, and decreases beta-catenin-sensitive transcription," *Cancer Res*, vol. 61, pp. 1671–1677, Feb. 2001.

[37] Brabletz, T., Jung, A., Reu, S., Porzner, M., Hlubek, F., Kunz-Schughart, L. A., Knuechel, R., and Kirchner, T., "Variable beta-catenin expression in colorectal cancers indicates tumor progression driven by the tumor environment.," *Proc Natl Acad Sci USA*, vol. 98, pp. 10356–10361, Aug. 2001.

[38] Braga, V. M., Del Maschio, A., Machesky, L., and Dejana, E., "Regulation of cadherin function by Rho and Rac: modulation by junction maturation and cellular context.," *Mol Biol Cell*, vol. 10, pp. 9–22, Jan. 1999.

[39] Bratt-Leal, A. M., Carpenedo, R. L., and McDevitt, T. C., "Engineering the embryoid body microenvironment to direct embryonic stem cell differentiation.," *Biotechnology Progress*, vol. 25, pp. 43–51, Jan. 2009.

[40] Bratt-Leal, A. M., Carpenedo, R. L., Ungrin, M. D., Zandstra, P. W., and McDevitt, T. C., "Incorporation of biomaterials in multicellular aggregates modulates pluripotent stem cell differentiation.," *Biomaterials*, vol. 32, pp. 48–56, Jan. 2011.

[41] Bratt-Leal, A. M., Nguyen, A. H., Hammersmith, K. A., Singh, A., and McDevitt, T. C., "A microparticle approach to morphogen delivery within pluripotent stem cell aggregates.," *Biomaterials*, vol. 34, pp. 7227–7235, Oct. 2013.

[42] Bueno, E. M., Bilgen, B., Carrier, R. L., and Barabino, G. A., "Increased rate of chondrocyte aggregation in a wavy-walled bioreactor.," *Biotechnol Bioeng*, vol. 88, pp. 767–777, Dec. 2004.

[43] Burdsal, C. A., Damsky, C. H., and Pedersen, R. A., "The role of E-cadherin and integrins in mesoderm differentiation and migration at the mammalian primitive streak.," *Development*, vol. 118, pp. 829–844, July 1993.

[44] Cadigan, K. M. and Nusse, R., "Wnt signaling: a common theme in animal development," *Genes Dev*, vol. 11, pp. 3286–3305, Dec. 1997.

[45] Camenisch, T. D., Schroeder, J. A., Bradley, J., Klewer, S. E., and McDonald, J. A., "Heart-valve mesenchyme formation is dependent on hyaluronan-augmented activation of ErbB2-ErbB3 receptors.," *Nat Med*, vol. 8, pp. 850–855, Aug. 2002.

[46] Cameron, C. M., Harding, F., Hu, W.-S., and Kaufman, D. S., "Activation of hypoxic response in human embryonic stem cell-derived embryoid bodies.," *Exp Biol Med*, vol. 233, pp. 1044–1057, Aug. 2008.

[47] Cameron, C. M., Hu, W.-S., and Kaufman, D. S., "Improved development of human embryonic stem cell-derived embryoid bodies by stirred vessel cultivation.," *Biotechnol Bioeng*, vol. 94, pp. 938–948, Aug. 2006.

[48] Campàs, O., Mammoto, T., Hasso, S., Sperling, R. A., O'Connell, D., Bischof, A. G., Maas, R., Weitz, D. A., Mahadevan, L., and Ingber, D. E., "Quantifying cell-generated mechanical forces within living embryonic tissues.," *Nat Methods*, Dec. 2013.

[49] Cano, A., Pérez-Moreno, M. A., Rodrigo, I., Locascio, A., Blanco, M. J., del Barrio, M. G., Portillo, F., and Nieto, M. A., "The transcription factor snail controls epithelial-mesenchymal transitions by repressing E-cadherin expression.," *Nat Cell Biol*, vol. 2, pp. 76–83, Feb. 2000.

[50] Carmeliet, P., Dor, Y., Herbert, J. M., Fukumura, D., Brusselmans, K., Dewerchin, M., Neeman, M., Bono, F., Abramovitch, R., Maxwell, P., Koch, C. J., Ratcliffe, P., Moons, L., Jain, R. K., Collen, D., Keshert, E., and Keshet, E., "Role of HIF-1alpha in hypoxia-mediated apoptosis, cell proliferation and tumour angiogenesis.," *Nature*, vol. 394, pp. 485–490, July 1998.

[51] Carpenedo, R. L., Bratt-Leal, A. M., Marklein, R. A., Seaman, S. A., Bowen, N. J., McDonald, J. F., and McDevitt, T. C., "Homogeneous and organized differentiation within embryoid bodies induced by microsphere-mediated delivery of small molecules.," *Biomaterials*, vol. 30, pp. 2507–2515, May 2009.

[52] Carpenedo, R. L., Sargent, C. Y., and McDevitt, T. C., "Rotary suspension culture enhances the efficiency, yield, and homogeneity of embryoid body differentiation.," *Stem Cells*, vol. 25, pp. 2224–2234, Sept. 2007.

[53] Carpenedo, R. L., Seaman, S. A., and McDevitt, T. C., "Microsphere size effects on embryoid body incorporation and embryonic stem cell differentiation.," *J Biomed Mater Res A*, vol. 94, pp. 466–475, Aug. 2010.

[54] Carpenter, A. E., Jones, T. R., Lamprecht, M. R., Clarke, C., Kang, I. H., Friman, O., Guertin, D. A., Chang, J. H., Lindquist, R. A., Moffat, J., Golland, P., and Sabatini, D. M., "CellProfiler: image analysis software for identifying and quantifying cell phenotypes.," *Genome Biol*, vol. 7, no. 10, p. R100, 2006.

[55] Champeris Tsaniras, S. and Jones, P. M., "Generating pancreatic beta-cells from embryonic stem cells by manipulating signaling pathways," *J Endocrinol*, vol. 206, pp. 13–26, July 2010.

[56] Chang, T. T. and Hughes-Fulford, M., "Monolayer and spheroid culture of human liver hepatocellular carcinoma cell line cells demonstrate distinct global gene expression patterns and functional phenotypes.," *Tissue Eng Part A*, vol. 15, pp. 559–567, Mar. 2009.

[57] Chary, S. R. and Jain, R. K., "Direct measurement of interstitial convection and diffusion of albumin in normal and neoplastic tissues by fluorescence photobleaching," *Proc Natl Acad Sci USA*, vol. 86, pp. 5385–5389, July 1989.

[58] Chen, S., Lewallen, M., and Xie, T., "Adhesion in the stem cell niche: biological roles and regulation.," *Development*, vol. 140, pp. 255–265, Jan. 2013.

[59] Chen, Y., Li, X., Eswarakumar, V. P., Seger, R., and Lonai, P., "Fibroblast growth factor (FGF) signaling through PI 3-kinase and Akt/PKB is required for embryoid body differentiation," *Oncogene*, vol. 19, pp. 3750–3756, Aug. 2000.

[60] Cheng, G., Tse, J., Jain, R. K., and Munn, L. L., "Micro-environmental mechanical stress controls tumor spheroid size and morphology by suppressing proliferation and inducing apoptosis in cancer cells.," *PLoS ONE*, vol. 4, no. 2, p. e4632, 2009.

[61] Cho, S. K., Webber, T. D., Carlyle, J. R., Nakano, T., Lewis, S. M., and Zúñiga-Pflücker, J. C., "Functional characterization of B lymphocytes

generated in vitro from embryonic stem cells," *Proc Natl Acad Sci USA*, vol. 96, pp. 9797–9802, Aug. 1999.

[62] Chung, K., Kim, Y., Kanodia, J. S., Gong, E., Shvartsman, S. Y., and Lu, H., "A microfluidic array for large-scale ordering and orientation of embryos," *Nat Methods*, vol. 8, pp. 171–176, Dec. 2010.

[63] Cimetta, E., Cannizzaro, C., James, R., Biechele, T., Moon, R. T., Elvassore, N., and Vunjak-Novakovic, G., "Microfluidic device generating stable concentration gradients for long term cell culture: application to Wnt3a regulation of β-catenin signaling.," *Lab Chip*, vol. 10, pp. 3277–3283, Dec. 2010.

[64] Ciruna, B. and Rossant, J., "FGF signaling regulates mesoderm cell fate specification and morphogenetic movement at the primitive streak.," *Dev Cell*, vol. 1, pp. 37–49, July 2001.

[65] Clevers, H., "Wnt/beta-catenin signaling in development and disease," *Cell*, vol. 127, pp. 469–480, Nov. 2006.

[66] Cong, F., Schweizer, L., and Varmus, H., "Wnt signals across the plasma membrane to activate the beta-catenin pathway by forming oligomers containing its receptors, Frizzled and LRP.," *Development*, vol. 131, pp. 5103–5115, Oct. 2004.

[67] Constantinescu, D., Gray, H. L., Sammak, P. J., Schatten, G. P., and Csoka, A. B., "Lamin A/C expression is a marker of mouse and human embryonic stem cell differentiation.," *Stem Cells*, vol. 24, pp. 177–185, Jan. 2006.

[68] Cormier, J. T., zur Nieden, N. I., Rancourt, D. E., and Kallos, M. S., "Expansion of undifferentiated murine embryonic stem cells as aggregates in suspension culture bioreactors.," *Tissue Eng*, vol. 12, pp. 3233–3245, Nov. 2006.

[69] Corstorphine, L. and Sefton, M. V., "Effectiveness factor and diffusion limitations in collagen gel modules containing HepG2 cells.," *J Tissue Eng Regen Med*, vol. 5, pp. 119–129, Feb. 2011.

[70] Coucouvanis, E. and Martin, G. R., "Signals for death and survival: a two-step mechanism for cavitation in the vertebrate embryo," *Cell*, vol. 83, pp. 279–287, Oct. 1995.

[71] Crick, F., "Diffusion in embryogenesis.," *Nature*, vol. 225, pp. 420–422, Jan. 1970.

[72] Csaszar, E., Kirouac, D. C., Yu, M., Wang, W., Qiao, W., Cooke, M. P., Boitano, A. E., Ito, C., and Zandstra, P. W., "Rapid expansion of human hematopoietic stem cells by automated control of inhibitory feedback signaling.," *Cell Stem Cell*, vol. 10, pp. 218–229, Feb. 2012.

[73] Cukierman, E., Pankov, R., Stevens, D. R., and Yamada, K. M., "Taking cell-matrix adhesions to the third dimension.," *Science*, vol. 294, pp. 1708–1712, Nov. 2001.

[74] Cullen, D. K., Stabenfeldt, S. E., Simon, C. M., Tate, C. C., and LaPlaca, M. C., "In vitro neural injury model for optimization of tissue-engineered constructs.," *J Neurosci Res*, vol. 85, pp. 3642–3651, Dec. 2007.

[75] Cullen, D. K., Vukasinovic, J., Glezer, A., and LaPlaca, M. C., "High cell density three-dimensional neural co-cultures require continuous medium perfusion for survival.," *Conf Proc IEEE Eng Med Biol Soc*, vol. 1, pp. 636–639, 2006.

[76] Cullen, D. K., Vukasinovic, J., Glezer, A., and LaPlaca, M. C., "Microfluidic engineered high cell density three-dimensional neural cultures.," *J. Neural Eng*, vol. 4, pp. 159–172, June 2007.

[77] Dafni, H., Israely, T., Bhujwalla, Z. M., Benjamin, L. E., and Neeman, M., "Overexpression of vascular endothelial growth factor 165 drives peritumor interstitial convection and induces lymphatic drain: magnetic resonance imaging, confocal microscopy, and histological tracking of triple-labeled albumin," *Cancer Res*, vol. 62, pp. 6731–6739, Nov. 2002.

[78] Dahl, K. N., Ribeiro, A. J. S., and Lammerding, J., "Nuclear shape, mechanics, and mechanotransduction.," *Circ Res*, vol. 102, pp. 1307–1318, June 2008.

[79] Dang, S. M., Kyba, M., Perlingeiro, R., Daley, G. Q., and Zandstra, P. W., "Efficiency of embryoid body formation and hematopoietic development from embryonic stem cells in different culture systems.," *Biotechnol Bioeng*, vol. 78, pp. 442–453, May 2002.

[80] Dasgupta, A., Hughey, R., Lancin, P., Larue, L., and Moghe, P. V., "E-cadherin synergistically induces hepatospecific phenotype and maturation of embryonic stem cells in conjunction with hepatotrophic factors," *Biotechnol Bioeng*, vol. 92, pp. 257–266, Nov. 2005.

[81] David, R., Brenner, C., Stieber, J., Schwarz, F., Brunner, S., Vollmer, M., Mentele, E., Müller-Höcker, J., Kitajima, S., Lickert, H., Rupp, R., and Franz, W.-M., "MesP1 drives vertebrate cardiovascular differentiation through Dkk-1-mediated blockade of Wnt-signalling," *Nat Cell Biol*, vol. 10, pp. 338–345, Mar. 2008.

[82] Davis, D. R., Zhang, Y., Smith, R. R., Cheng, K., Terrovitis, J., Malliaras, K., Li, T.-S., White, A., Makkar, R., and Marbán, E., "Validation of the cardiosphere method to culture cardiac progenitor cells from myocardial tissue.," *PLoS ONE*, vol. 4, no. 9, p. e7195, 2009.

[83] de Rooij, J., Kerstens, A., Danuser, G., Schwartz, M. A., and Waterman-Storer, C. M., "Integrin-dependent actomyosin contraction regulates epithelial cell scattering.," *J Cell Biol*, vol. 171, pp. 153–164, Oct. 2005.

[84] Desbordes, S. C., Placantonakis, D. G., Ciro, A., Socci, N. D., Lee, G., Djaballah, H., and Studer, L., "High-throughput screening assay for the identification of compounds regulating self-renewal and differentiation in human embryonic stem cells," *Cell Stem Cell*, vol. 2, pp. 602–612, June 2008.

[85] Dewhirst, M. W., Cao, Y., and Moeller, B., "Cycling hypoxia and free radicals regulate angiogenesis and radiotherapy response.," *Nat Rev Cancer*, vol. 8, pp. 425–437, June 2008.

[86] Discher, D. E., Janmey, P., and Wang, Y.-L., "Tissue cells feel and respond to the stiffness of their substrate.," *Science*, vol. 310, pp. 1139–1143, Nov. 2005.

[87] Discher, D. E., Mooney, D. J., and Zandstra, P. W., "Growth factors, matrices, and forces combine and control stem cells.," *Science*, vol. 324, pp. 1673–1677, June 2009.

[88] Doetschman, T. C., Eistetter, H., Katz, M., Schmidt, W., and Kemler, R., "The in vitro development of blastocyst-derived embryonic stem cell lines: formation of visceral yolk sac, blood islands and myocardium.," *J Embryol Exp Morphol*, vol. 87, pp. 27–45, June 1985.

[89] Driever, W. and Nüsslein-Volhard, C., "A gradient of bicoid protein in Drosophila embryos.," *Cell*, vol. 54, pp. 83–93, July 1988.

[90] DuFort, C. C., Paszek, M. J., and Weaver, V. M., "Balancing forces: architectural control of mechanotransduction.," *Nat Rev Mol Cell Biol*, vol. 12, pp. 308–319, May 2011.

[91] Dvash, T., Mayshar, Y., Darr, H., McElhaney, M., Barker, D., Yanuka, O., Kotkow, K. J., Rubin, L. L., Benvenisty, N., and Eiges, R., "Temporal gene expression during differentiation of human embryonic stem cells and embryoid bodies," *Hum Reprod*, vol. 19, pp. 2875–2883, Dec. 2004.

[92] Eiraku, M., Takata, N., Ishibashi, H., Kawada, M., Sakakura, E., Okuda, S., Sekiguchi, K., Adachi, T., and Sasai, Y., "Self-organizing optic-cup morphogenesis in three-dimensional culture," *Nature*, vol. 472, pp. 51–56, Apr. 2011.

[93] Engler, A. J., Sen, S., Sweeney, H. L., and Discher, D. E., "Matrix elasticity directs stem cell lineage specification," *Cell*, vol. 126, pp. 677–689, Aug. 2006.

[94] Erbs, S., Linke, A., Schächinger, V., Assmus, B., Thiele, H., Diederich, K.-W., Hoffmann, C., Dimmeler, S., Tonn, T., Hambrecht, R., Zeiher, A. M., and Schuler, G., "Restoration of microvascular function in the infarct-related artery by intracoronary transplantation of bone marrow progenitor cells in patients with acute myocardial infarction: the Doppler Substudy of the Reinfusion of Enriched Progenitor Cells and Infarct Remodeling in Acute Myocardial Infarction (REPAIR-AMI) trial," *Circulation*, vol. 116, pp. 366–374, July 2007.

[95] Esner, M., Pachernik, J., Hampl, A., and Dvorak, P., "Targeted disruption of fibroblast growth factor receptor-1 blocks maturation of visceral endoderm and cavitation in mouse embryoid bodies," *Int J Dev Biol*, vol. 46, pp. 817–825, Sept. 2002.

[96] Evans, M. J. and Kaufman, M. H., "Establishment in culture of pluripotential cells from mouse embryos.," *Nature*, vol. 292, pp. 154–156, July 1981.

[97] Farhadifar, R., Röper, J.-C., Aigouy, B., Eaton, S., and Jülicher, F., "The influence of cell mechanics, cell-cell interactions, and proliferation on epithelial packing.," *Curr Biol*, vol. 17, pp. 2095–2104, Dec. 2007.

[98] Ferreira, L., Squier, T., Park, H., Choe, H., Kohane, D., and Langer, R., "Human embryoid bodies containing nano-and microparticulate delivery vehicles," *Adv Mater*, vol. 20, no. 12, pp. 2285–2291, 2008.

[99] Fijnvandraat, A. C., van Ginneken, A. C. G., de Boer, P. A. J., Ruijter, J. M., Christoffels, V. M., Moorman, A. F. M., and Lekanne Deprez, R. H., "Cardiomyocytes derived from embryonic stem cells resemble cardiomyocytes of the embryonic heart tube," *Cardiovasc Res*, vol. 58, pp. 399–409, May 2003.

[100] Finley, K. R., Tennessen, J., and Shawlot, W., "The mouse secreted frizzled-related protein 5 gene is expressed in the anterior visceral endoderm and foregut endoderm during early post-implantation development," *Gene Expr Patterns*, vol. 3, pp. 681–684, Oct. 2003.

[101] Flaim, C. J., Chien, S., and Bhatia, S. N., "An extracellular matrix microarray for probing cellular differentiation," *Nat Methods*, vol. 2, pp. 119–125, Feb. 2005.

[102] Fletcher, D. A. and Mullins, R. D., "Cell mechanics and the cytoskeleton.," *Nature*, vol. 463, pp. 485–492, Jan. 2010.

[103] Foe, V. E. and Alberts, B. M., "Studies of nuclear and cytoplasmic behaviour during the five mitotic cycles that precede gastrulation in Drosophila embryogenesis.," *J Cell Sci*, vol. 61, pp. 31–70, May 1983.

[104] Fok, E. Y. L. and Zandstra, P. W., "Shear-controlled single-step mouse embryonic stem cell expansion and embryoid body-based differentiation.," *Stem Cells*, vol. 23, pp. 1333–1342, Oct. 2005.

[105] Folkman, J., Klagsbrun, M., Sasse, J., Wadzinski, M., Ingber, D., and Vlodavsky, I., "A heparin-binding angiogenic protein–basic fibroblast growth factor–is stored within basement membrane.," *Am J Pathol*, vol. 130, pp. 393–400, Feb. 1988.

[106] Fox, V., Gokhale, P. J., Walsh, J. R., Matin, M., Jones, M., and Andrews, P. W., "Cell-cell signaling through NOTCH regulates human embryonic stem cell proliferation," *Stem Cells*, vol. 26, pp. 715–723, Mar. 2008.

[107] Franke, J. D., Montague, R. A., and Kiehart, D. P., "Nonmuscle myosin II generates forces that transmit tension and drive contraction in multiple tissues during dorsal closure.," *Curr Biol*, vol. 15, pp. 2208–2221, Dec. 2005.

[108] Franke, R. P., Gräfe, M., Schnittler, H., Seiffge, D., Mittermayer, C., and Drenckhahn, D., "Induction of human vascular endothelial stress fibres by fluid shear stress.," *Nature*, vol. 307, pp. 648–649, Feb. 1984.

[109] Freyer, J. P. and Sutherland, R. M., "Proliferative and clonogenic heterogeneity of cells from EMT6/Ro multicellular spheroids induced by the glucose and oxygen supply.," *Cancer Res*, vol. 46, pp. 3513–3520, July 1986.

[110] Fridley, K. M., Fernandez, I., Li, M.-T. A., Kettlewell, R. B., and Roy, K., "Unique differentiation profile of mouse embryonic stem cells in rotary and stirred tank bioreactors.," *Tissue Eng Part A*, vol. 16, pp. 3285–3298, Nov. 2010.

[111] Fridley, K. M., Kinney, M. A., and McDevitt, T. C., "Hydrodynamic modulation of pluripotent stem cells.," *Stem Cell Res Ther*, vol. 3, p. 45, Nov. 2012.

[112] Fu, J., Wang, Y.-K., Yang, M. T., Desai, R. A., Yu, X., Liu, Z., and Chen, C. S., "Mechanical regulation of cell function with geometrically modulated elastomeric substrates.," *Nat Methods*, vol. 7, pp. 733–736, Sept. 2010.

[113] Fuchs, E., Tumbar, T., and Guasch, G., "Socializing with the neighbors: stem cells and their niche.," *Cell*, vol. 116, pp. 769–778, Mar. 2004.

[114] Garcia-Fernàndez, J., D'Aniello, S., and Escrivà, H., "Organizing chordates with an organizer.," *Bioessays*, vol. 29, pp. 619–624, July 2007.

[115] Gavard, J. and Mège, R.-M., "Once upon a time there was beta-catenin in cadherin-mediated signalling," *Biol Cell*, vol. 97, pp. 921–926, Dec. 2005.

[116] Geladi, P. and Kowalski, B. R., "Partial least-squares regression: a tutorial," *Anal Chim Acta*, vol. 185, pp. 1–17, Jan. 1986.

[117] Gerecht-Nir, S., Cohen, S., and Itskovitz-Eldor, J., "Bioreactor cultivation enhances the efficiency of human embryoid body (hEB) formation and differentiation.," *Biotechnol Bioeng*, vol. 86, pp. 493–502, June 2004.

[118] Gomez, E. W., Chen, Q. K., Gjorevski, N., and Nelson, C. M., "Tissue geometry patterns epithelial-mesenchymal transition via intercellular mechanotransduction," *J Cell Biochem*, vol. 110, pp. 44–51, May 2010.

[119] González-Cruz, R. D., Fonseca, V. C., and Darling, E. M., "Cellular mechanical properties reflect the differentiation potential of adipose-derived mesenchymal stem cells.," *Proc Natl Acad Sci USA*, vol. 109, pp. E1523–9, June 2012.

[120] Gottardi, C. J., Wong, E., and Gumbiner, B. M., "E-cadherin suppresses cellular transformation by inhibiting beta-catenin signaling in an adhesion-independent manner," *J Cell Biol*, vol. 153, pp. 1049–1060, May 2001.

[121] Gottardi, C. J. and Gumbiner, B. M., "Distinct molecular forms of beta-catenin are targeted to adhesive or transcriptional complexes," *J Cell Biol*, vol. 167, pp. 339–349, Oct. 2004.

[122] Gregor, T., Bialek, W., de Ruyter van Steveninck, R. R., Tank, D. W., and Wieschaus, E. F., "Diffusion and scaling during early embryonic pattern formation.," *Proc Natl Acad Sci USA*, vol. 102, pp. 18403–18407, Dec. 2005.

[123] Griffith, L. G. and Swartz, M. A., "Capturing complex 3D tissue physiology in vitro.," *Nat Rev Mol Cell Biol*, vol. 7, pp. 211–224, Mar. 2006.

[124] Habib, S. J., Chen, B.-C., Tsai, F.-C., Anastassiadis, K., Meyer, T., Betzig, E., and Nusse, R., "A localized Wnt signal orients asymmetric stem cell division in vitro.," *Science*, vol. 339, pp. 1445–1448, Mar. 2013.

[125] Haegel, H., Larue, L., Ohsugi, M., Fedorov, L., Herrenknecht, K., and Kemler, R., "Lack of beta-catenin affects mouse development at gastrulation.," *Development*, vol. 121, pp. 3529–3537, Nov. 1995.

[126] Hart, M. J., de los Santos, R., Albert, I. N., Rubinfeld, B., and Polakis, P., "Downregulation of beta-catenin by human Axin and its association with the APC tumor suppressor, beta-catenin and GSK3 beta.," *Curr Biol*, vol. 8, pp. 573–581, May 1998.

[127] Hayot, C., Debeir, O., Van Ham, P., Van Damme, M., Kiss, R., and Decaestecker, C., "Characterization of the activities of actin-affecting drugs on tumor cell migration.," *Toxicol Appl Pharmacol*, vol. 211, pp. 30–40, Feb. 2006.

[128] Hecht, A., Litterst, C. M., Huber, O., and Kemler, R., "Functional characterization of multiple transactivating elements in beta-catenin, some of which interact with the TATA-binding protein in vitro," *J Biol Chem*, vol. 274, pp. 18017–18025, June 1999.

[129] Hecht, A., Vleminckx, K., Stemmler, M. P., van Roy, F., and Kemler, R., "The p300/CBP acetyltransferases function as transcriptional coactivators of beta-catenin in vertebrates," *EMBO J*, vol. 19, pp. 1839–1850, Apr. 2000.

[130] Helm, C.-L. E., Fleury, M. E., Zisch, A. H., Boschetti, F., and Swartz, M. A., "Synergy between interstitial flow and VEGF directs capillary morphogenesis in vitro through a gradient amplification mechanism," *Proc Natl Acad Sci USA*, vol. 102, pp. 15779–15784, Nov. 2005.

[131] Helm, C.-L. E., Zisch, A., and Swartz, M. A., "Engineered blood and lymphatic capillaries in 3-D VEGF-fibrin-collagen matrices with interstitial flow," *Biotechnol Bioeng*, vol. 96, no. 1, pp. 167–176, 2007.

[132] Helmlinger, G., Netti, P. A., Lichtenbeld, H. C., Melder, R. J., and Jain, R. K., "Solid stress inhibits the growth of multicellular tumor spheroids.," *Nat Biotechnol*, vol. 15, pp. 778–783, Aug. 1997.

[133] Henderson, B. R., "Nuclear-cytoplasmic shuttling of APC regulates beta-catenin subcellular localization and turnover.," *Nat Cell Biol*, vol. 2, pp. 653–660, Sept. 2000.

[134] Heng, J.-C. D., Feng, B., Han, J., Jiang, J., Kraus, P., Ng, J.-H., Orlov, Y. L., Huss, M., Yang, L., Lufkin, T., Lim, B., and Ng, H.-H., "The nuclear receptor Nr5a2 can replace Oct4 in the reprogramming of murine somatic cells to pluripotent cells.," *Cell Stem Cell*, vol. 6, pp. 167–174, Feb. 2010.

[135] Höckendorf, B., Thumberger, T., and Wittbrodt, J., "Quantitative analysis of embryogenesis: a perspective for light sheet microscopy.," *Dev Cell*, vol. 23, pp. 1111–1120, Dec. 2012.

[136] Hogan, B. L., Thaller, C., and Eichele, G., "Evidence that Hensen's node is a site of retinoic acid synthesis.," *Nature*, vol. 359, pp. 237–241, Sept. 1992.

[137] Hornbruch, A. and Wolpert, L., "Positional signalling by Hensen's node when grafted to the chick limb bud.," *J Embryol Exp Morphol*, vol. 94, pp. 257–265, June 1986.

[138] Hove, J. R., Köster, R. W., Forouhar, A. S., Acevedo-Bolton, G., Fraser, S. E., and Gharib, M., "Intracardiac fluid forces are an essential epigenetic factor for embryonic cardiogenesis.," *Nature*, vol. 421, pp. 172–177, Jan. 2003.

[139] Howard, S., Deroo, T., Fujita, Y., and Itasaki, N., "A positive role of cadherin in Wnt/β-catenin signalling during epithelial-mesenchymal transition.," *PLoS ONE*, vol. 6, no. 8, p. e23899, 2011.

[140] Hufnagel, L., Teleman, A. A., Rouault, H., Cohen, S. M., and Shraiman, B. I., "On the mechanism of wing size determination in fly development.," *Proc Natl Acad Sci USA*, vol. 104, pp. 3835–3840, Mar. 2007.

[141] Hurlstone, A. F. L., Haramis, A.-P. G., Wienholds, E., Begthel, H., Korving, J., Van Eeden, F., Cuppen, E., Zivkovic, D., Plasterk, R. H. A., and Clevers, H., "The Wnt/beta-catenin pathway regulates cardiac valve formation.," *Nature*, vol. 425, pp. 633–637, Oct. 2003.

[142] Hwang, Y.-S., Chung, B. G., Ortmann, D., Hattori, N., Moeller, H.-C., and Khademhosseini, A., "Microwell-mediated control of embryoid body size regulates embryonic stem cell fate via differential expression of WNT5a and WNT11.," *Proc Natl Acad Sci USA*, vol. 106, pp. 16978–16983, Oct. 2009.

[143] Ingber, D. E., "Tensegrity: the architectural basis of cellular mechanotransduction.," *Annu Rev Physiol*, vol. 59, pp. 575–599, 1997.

[144] Ingber, D. E., "Cellular mechanotransduction: putting all the pieces together again.," *FASEB J*, vol. 20, pp. 811–827, May 2006.

[145] Ishizaki, T., Uehata, M., Tamechika, I., Keel, J., Nonomura, K., Maekawa, M., and Narumiya, S., "Pharmacological properties of Y-27632, a specific inhibitor of rho-associated kinases.," *Mol Pharmacol*, vol. 57, pp. 976–983, May 2000.

[146] Itskovitz-Eldor, J., Schuldiner, M., Karsenti, D., Eden, A., Yanuka, O., Amit, M., Soreq, H., and Benvenisty, N., "Differentiation of human embryonic stem cells into embryoid bodies compromising the three embryonic germ layers.," *Mol Med*, vol. 6, pp. 88–95, Feb. 2000.

[147] Jackson, T. L. and Byrne, H. M., "A mathematical model to study the effects of drug resistance and vasculature on the response of solid tumors to chemotherapy.," *Math Biosci*, vol. 164, pp. 17–38, Mar. 2000.

[148] Jamora, C. and Fuchs, E., "Intercellular adhesion, signalling and the cytoskeleton," *Nat Cell Biol*, vol. 4, pp. E101–8, Apr. 2002.

[149] Jing, D., Parikh, A., Canty, J. M., and Tzanakakis, E. S., "Stem cells for heart cell therapies," *Tissue Eng Part B Rev*, vol. 14, pp. 393–406, Dec. 2008.

[150] Johansson, B. M. and Wiles, M. V., "Evidence for involvement of activin A and bone morphogenetic protein 4 in mammalian mesoderm and hematopoietic development.," *Mol Cell Biol*, vol. 15, pp. 141–151, Jan. 1995.

[151] Kam, Y. and Quaranta, V., "Cadherin-bound beta-catenin feeds into the Wnt pathway upon adherens junctions dissociation: evidence for an intersection between beta-catenin pools," *PLoS ONE*, vol. 4, no. 2, p. e4580, 2009.

[152] Kappler, J., Hegener, O., Baader, S. L., Franken, S., Gieselmann, V., Häberlein, H., and Rauch, U., "Transport of a hyaluronan-binding protein in brain tissue.," *Matrix Biol*, vol. 28, pp. 396–405, Sept. 2009.

[153] Kapur, V., Charkoudian, J. C., Kessler, S. B., and Anderson, J. L., "Hydrodynamic permeability of hydrogels stabilized within porous membranes," *Ind Eng Chem Res*, vol. 35, no. 9, pp. 3179–3185, 1996.

[154] Kehat, I., Kenyagin-Karsenti, D., Snir, M., Segev, H., Amit, M., Gepstein, A., Livne, E., Binah, O., Itskovitz-Eldor, J., and Gepstein, L., "Human embryonic stem cells can differentiate into myocytes with structural and functional properties of cardiomyocytes.," *J Clin Invest*, vol. 108, pp. 407–414, Aug. 2001.

[155] Kehat, I., Khimovich, L., Caspi, O., Gepstein, A., Shofti, R., Arbel, G., Huber, I., Satin, J., Itskovitz-Eldor, J., and Gepstein, L., "Electromechanical integration of cardiomyocytes derived from human embryonic stem cells," *Nat Biotechnol*, vol. 22, pp. 1282–1289, Oct. 2004.

[156] Keller, G., "Embryonic stem cell differentiation: emergence of a new era in biology and medicine," *Genes Dev*, vol. 19, no. 10, pp. 1129–1155, 2005.

[157] Keller, R., Davidson, L. A., and Shook, D. R., "How we are shaped: the biomechanics of gastrulation," *Differentiation*, vol. 71, pp. 171–205, Apr. 2003.

[158] Kelly, K. F., Ng, D. Y., Jayakumaran, G., Wood, G. A., Koide, H., and Doble, B. W., "β-catenin enhances Oct-4 activity and reinforces pluripotency through a TCF-independent mechanism," *Cell Stem Cell*, vol. 8, pp. 214–227, Feb. 2011.

[159] Kemler, R., "From cadherins to catenins: cytoplasmic protein interactions and regulation of cell adhesion.," *Trends Genet.*, vol. 9, pp. 317–321, Sept. 1993.

[160] Kemp, C., Willems, E., Abdo, S., Lambiv, L., and Leyns, L., "Expression of all Wnt genes and their secreted antagonists during mouse blastocyst and postimplantation development," *Dev Dyn*, vol. 233, pp. 1064–1075, July 2005.

[161] Kim, H. Y. and Davidson, L. A., "Punctuated actin contractions during convergent extension and their permissive regulation by the non-canonical Wnt-signaling pathway.," *J Cell Sci*, vol. 124, pp. 635–646, Feb. 2011.

[162] Kim, L., Vahey, M. D., Lee, H.-Y., and Voldman, J., "Microfluidic arrays for logarithmically perfused embryonic stem cell culture.," *Lab Chip*, vol. 6, pp. 394–406, Mar. 2006.

[163] Kinney, M. A., Hookway, T. A., Wang, Y., and McDevitt, T. C., "Engineering three-dimensional stem cell morphogenesis for the development of tissue models and scalable regenerative therapeutics.," *Ann Biomed Eng*, vol. 42, pp. 352–367, Feb. 2014.

[164] Kinney, M. A. and McDevitt, T. C., "Emerging strategies for spatiotemporal control of stem cell fate and morphogenesis.," *Trends Biotechnol*, vol. 31, pp. 78–84, Feb. 2013.

[165] Kinney, M. A., Saeed, R., and McDevitt, T. C., "Systematic analysis of embryonic stem cell differentiation in hydrodynamic environments with controlled embryoid body size.," *Integr Biol*, vol. 4, pp. 641–650, June 2012.

[166] Kinney, M. A., Sargent, C. Y., and McDevitt, T. C., "The multiparametric effects of hydrodynamic environments on stem cell culture.," *Tissue Eng Part B Rev*, vol. 17, pp. 249–262, Aug. 2011.

[167] Kinney, M. A., Sargent, C. Y., and McDevitt, T. C., "Temporal modulation of β-catenin signaling by multicellular aggregation kinetics impacts embryonic stem cell cardiomyogenesis.," *Stem Cells Dev*, vol. 22, pp. 2665–2677, Oct. 2013.

[168] Kirouac, D. C. and Zandstra, P. W., "The systematic production of cells for cell therapies," *Cell Stem Cell*, vol. 3, pp. 369–381, Oct. 2008.

[169] Kong, H. J., Kaigler, D., Kim, K., and Mooney, D. J., "Controlling rigidity and degradation of alginate hydrogels via molecular weight distribution," *Biomacromolecules*, vol. 5, no. 5, pp. 1720–1727, 2004.

[170] Korinek, V., Barker, N., Morin, P. J., van Wichen, D., de Weger, R., Kinzler, K. W., Vogelstein, B., and Clevers, H., "Constitutive transcriptional activation by a beta-catenin-Tcf complex in APC-/- colon carcinoma.," *Science*, vol. 275, pp. 1784–1787, Mar. 1997.

[171] Kovacs, E. M., Goodwin, M., Ali, R. G., Paterson, A. D., and Yap, A. S., "Cadherin-directed actin assembly: E-cadherin physically associates with the Arp2/3 complex to direct actin assembly in nascent adhesive contacts.," *Curr Biol*, vol. 12, pp. 379–382, Mar. 2002.

[172] Krtolica, A., Genbacev, O., Escobedo, C., Zdravkovic, T., Nordstrom, A., Vabuena, D., Nath, A., Simon, C., Mostov, K., and Fisher, S. J., "Disruption of apical-basal polarity of human embryonic stem cells enhances hematoendothelial differentiation," *Stem Cells*, vol. 25, pp. 2215–2223, Sept. 2007.

[173] Kubo, A., Shinozaki, K., Shannon, J. M., Kouskoff, V., Kennedy, M., Woo, S., Fehling, H. J., and Keller, G., "Development of definitive endoderm from embryonic stem cells in culture," *Development*, vol. 131, pp. 1651–1662, Apr. 2004.

[174] Kuo, C. K. and Ma, P. X., "Ionically crosslinked alginate hydrogels as scaffolds for tissue engineering: part 1. Structure, gelation rate and mechanical properties.," *Biomaterials*, vol. 22, pp. 511–521, Mar. 2001.

[175] Kurosawa, H., "Methods for inducing embryoid body formation: in vitro differentiation system of embryonic stem cells.," *J Biosci Bioeng*, vol. 103, pp. 389–398, May 2007.

[176] Kurosawa, H., Imamura, T., Koike, M., Sasaki, K., and Amano, Y., "A simple method for forming embryoid body from mouse embryonic stem cells," *J Biosci Bioeng*, vol. 96, no. 4, pp. 409–411, 2003.

[177] Kwon, C., Arnold, J., Hsiao, E. C., Taketo, M. M., Conklin, B. R., and Srivastava, D., "Canonical Wnt signaling is a positive regulator of mammalian cardiac progenitors," *Proc Natl Acad Sci USA*, vol. 104, pp. 10894–10899, June 2007.

[178] Kwon, C., Qian, L., Cheng, P., Nigam, V., Arnold, J., and Srivastava, D., "A regulatory pathway involving Notch1/beta-catenin/Isl1 determines cardiac progenitor cell fate," *Nat Cell Biol*, vol. 11, pp. 951–957, Aug. 2009.

[179] Laflamme, M. A., Chen, K. Y., Naumova, A. V., Muskheli, V., Fugate, J. A., Dupras, S. K., Reinecke, H., Xu, C., Hassanipour, M., Police, S., O'Sullivan, C., Collins, L., Chen, Y., Minami, E., Gill, E. A., Ueno, S., Yuan, C., Gold, J., and Murry, C. E., "Cardiomyocytes derived from human embryonic stem cells in pro-survival factors enhance function of infarcted rat hearts.," *Nat Biotechnol*, vol. 25, pp. 1015–1024, Sept. 2007.

[180] Laflamme, M. A., Gold, J., Xu, C., Hassanipour, M., Rosler, E., Police, S., Muskheli, V., and Murry, C. E., "Formation of human myocardium in the rat heart from human embryonic stem cells," *Am J Pathol*, vol. 167, pp. 663–671, Sept. 2005.

[181] Lammerding, J., Schulze, P. C., Takahashi, T., Kozlov, S., Sullivan, T., Kamm, R. D., Stewart, C. L., and Lee, R. T., "Lamin A/C deficiency causes defective nuclear mechanics and mechanotransduction.," *J Clin Invest*, vol. 113, pp. 370–378, Feb. 2004.

[182] Lancaster, M. A., Renner, M., Martin, C.-A., Wenzel, D., Bicknell, L. S., Hurles, M. E., Homfray, T., Penninger, J. M., Jackson, A. P., and Knoblich, J. A., "Cerebral organoids model human brain development and microcephaly.," *Nature*, vol. 501, pp. 373–379, Sept. 2013.

[183] Larue, L., Antos, C., Butz, S., Huber, O., Delmas, V., Dominis, M., and Kemler, R., "A role for cadherins in tissue formation," *Development*, vol. 122, pp. 3185–3194, Oct. 1996.

[184] Lawson, K. A., Meneses, J. J., and Pedersen, R. A., "Clonal analysis of epiblast fate during germ layer formation in the mouse embryo," *Development*, vol. 113, pp. 891–911, Nov. 1991.

[185] Lee, K., Silva, E. A., and Mooney, D. J., "Growth factor delivery-based tissue engineering: general approaches and a review of recent developments.," *J R Soc Interface*, vol. 8, pp. 153–170, Feb. 2011.

[186] Leistner, D. M., Fischer-Rasokat, U., Honold, J., Seeger, F. H., Schächinger, V., Lehmann, R., Martin, H., Burck, I., Urbich, C., Dimmeler, S., Zeiher, A. M., and Assmus, B., "Transplantation of progenitor cells and regeneration enhancement in acute myocardial infarction (TOPCARE-AMI): final 5-year results suggest long-term safety and efficacy.," *Clin Res Cardiol*, vol. 100, pp. 925–934, Oct. 2011.

[187] Levenberg, S., Rouwkema, J., Macdonald, M., Garfein, E. S., Kohane, D. S., Darland, D. C., Marini, R., van Blitterswijk, C. A., Mulligan, R. C., D'Amore, P. A., and Langer, R., "Engineering vascularized skeletal muscle tissue," *Nat Biotechnol*, vol. 23, pp. 879–884, July 2005.

[188] Levesque, M. J. and Nerem, R. M., "The elongation and orientation of cultured endothelial cells in response to shear stress.," *J Biomech Eng*, vol. 107, pp. 341–347, Nov. 1985.

[189] Levick, J. R., "Flow through interstitium and other fibrous matrices.," *Q J Exp Physiol*, vol. 72, pp. 409–437, Oct. 1987.

[190] Leyns, L., Bouwmeester, T., Kim, S. H., Piccolo, S., and De Robertis, E. M., "Frzb-1 is a secreted antagonist of Wnt signaling expressed in the Spemann organizer.," *Cell*, vol. 88, pp. 747–756, Mar. 1997.

[191] Li, F., Lü, S., Vida, L., Thomson, J. A., and Honig, G. R., "Bone morphogenetic protein 4 induces efficient hematopoietic differentiation of rhesus monkey embryonic stem cells in vitro.," *Blood*, vol. 98, pp. 335–342, July 2001.

[192] Li, L. and Neaves, W. B., "Normal stem cells and cancer stem cells: the niche matters.," *Cancer Res*, vol. 66, pp. 4553–4557, May 2006.

[193] Li, X., Chen, Y., Schéele, S., Arman, E., Haffner-Krausz, R., Ekblom, P., and Lonai, P., "Fibroblast growth factor signaling and basement membrane assembly are connected during epithelial morphogenesis of the embryoid body," *J Cell Biol*, vol. 153, pp. 811–822, May 2001.

[194] Lian, X., Hsiao, C., Wilson, G., Zhu, K., Hazeltine, L. B., Azarin, S. M., Raval, K. K., Zhang, J., Kamp, T. J., and Palecek, S. P., "Robust cardiomyocyte differentiation from human pluripotent stem cells via temporal modulation of canonical Wnt signaling.," *Proc Natl Acad Sci USA*, vol. 109, pp. E1848–57, July 2012.

[195] Lin, L., Cui, L., Zhou, W., Dufort, D., Zhang, X., Cai, C.-L., Bu, L., Yang, L., Martin, J., Kemler, R., Rosenfeld, M. G., Chen, J., and Evans, S. M., "Beta-catenin directly regulates Islet1 expression in cardiovascular progenitors and is required for multiple aspects of cardiogenesis.," *Proc Natl Acad Sci USA*, vol. 104, pp. 9313–9318, May 2007.

[196] Lindsley, R. C., Gill, J. G., Kyba, M., Murphy, T. L., and Murphy, K. M., "Canonical Wnt signaling is required for development of embryonic stem cell-derived mesoderm.," *Development*, vol. 133, pp. 3787–3796, Oct. 2006.

[197] Liu, H., Lin, J., and Roy, K., "Effect of 3D scaffold and dynamic culture condition on the global gene expression profile of mouse embryonic stem cells.," *Biomaterials*, vol. 27, pp. 5978–5989, Dec. 2006.

[198] Liu, Z., Tan, J. L., Cohen, D. M., Yang, M. T., Sniadecki, N. J., Ruiz, S. A., Nelson, C. M., and Chen, C. S., "Mechanical tugging force regulates the size of cell-cell junctions.," *Proc Natl Acad Sci USA*, vol. 107, pp. 9944–9949, June 2010.

[199] Lock, L. T. and Tzanakakis, E. S., "Stem/Progenitor cell sources of insulin-producing cells for the treatment of diabetes," *Tissue Eng*, vol. 13, pp. 1399–1412, July 2007.

[200] Lopez, A. D., Mathers, C. D., Ezzati, M., Jamison, D. T., and Murray, C. J. L., "Global and regional burden of disease and risk factors, 2001: systematic analysis of population health data," *Lancet*, vol. 367, pp. 1747–1757, May 2006.

[201] Lutolf, M. P. and Hubbell, J. A., "Synthetic biomaterials as instructive extracellular microenvironments for morphogenesis in tissue engineering.," *Nat Biotechnol*, vol. 23, pp. 47–55, Jan. 2005.

[202] Maekawa, M., Ishizaki, T., Boku, S., Watanabe, N., Fujita, A., Iwamatsu, A., Obinata, T., Ohashi, K., Mizuno, K., and Narumiya, S., "Signaling from Rho to the actin cytoskeleton through protein kinases ROCK and LIM-kinase.," *Science*, vol. 285, pp. 895–898, Aug. 1999.

[203] Mahoney, M. J. and Saltzman, W. M., "Transplantation of brain cells assembled around a programmable synthetic microenvironment," *Nat Biotechnol*, vol. 19, pp. 934–939, Oct. 2001.

[204] Maltsev, V. A., Rohwedel, J., Hescheler, J., and Wobus, A. M., "Embryonic stem cells differentiate in vitro into cardiomyocytes representing sinusnodal, atrial and ventricular cell types," *Mech Dev*, vol. 44, pp. 41–50, Nov. 1993.

[205] Mandal, S., Lindgren, A. G., Srivastava, A. S., Clark, A. T., and Banerjee, U., "Mitochondrial function controls proliferation and early differentiation potential of embryonic stem cells.," *Stem Cells*, vol. 29, pp. 486–495, Mar. 2011.

[206] Mao, J., Wang, J., Liu, B., Pan, W., Farr, G. H., Flynn, C., Yuan, H., Takada, S., Kimelman, D., Li, L., and Wu, D., "Low-density lipoprotein receptor-related protein-5 binds to Axin and regulates the canonical Wnt signaling pathway.," *Mol Cell*, vol. 7, pp. 801–809, Apr. 2001.

[207] Marambaud, P., Shioi, J., Serban, G., Georgakopoulos, A., Sarner, S., Nagy, V., Baki, L., Wen, P., Efthimiopoulos, S., Shao, Z., Wisniewski, T., and Robakis, N. K., "A presenilin-1/gamma-secretase cleavage releases the E-cadherin intracellular domain and regulates disassembly of adherens junctions," *EMBO J*, vol. 21, pp. 1948–1956, Apr. 2002.

[208] Maretzky, T., Reiss, K., Ludwig, A., Buchholz, J., Scholz, F., Proksch, E., de Strooper, B., Hartmann, D., and Saftig, P., "ADAM10 mediates E-cadherin shedding and regulates epithelial cell-cell adhesion, migration, and beta-catenin translocation.," *Proc Natl Acad Sci USA*, vol. 102, pp. 9182–9187, June 2005.

[209] Martin, G. R., "Isolation of a pluripotent cell line from early mouse embryos cultured in medium conditioned by teratocarcinoma stem cells.," *Proc Natl Acad Sci USA*, vol. 78, pp. 7634–7638, Dec. 1981.

[210] Masszi, A., Di Ciano, C., Sirokmány, G., Arthur, W. T., Rotstein, O. D., Wang, J., McCulloch, C. A. G., Rosivall, L., Mucsi, I., and Kapus, A., "Central role for Rho in TGF-beta1-induced alpha-smooth muscle actin expression during epithelial-mesenchymal transition.," *Am J Physiol Renal Physiol*, vol. 284, pp. F911–24, May 2003.

[211] Masumura, T., Yamamoto, K., Shimizu, N., Obi, S., and Ando, J., "Shear stress increases expression of the arterial endothelial marker ephrinB2 in murine ES cells via the VEGF-Notch signaling pathways.," *Arterioscler Thromb Vasc Biol*, vol. 29, pp. 2125–2131, Dec. 2009.

[212] Mathur, A. B., Collinsworth, A. M., Reichert, W. M., Kraus, W. E., and Truskey, G. A., "Endothelial, cardiac muscle and skeletal muscle exhibit different viscous and elastic properties as determined by atomic force microscopy.," *J Biomech*, vol. 34, pp. 1545–1553, Dec. 2001.

[213] Matthews, B. D., Overby, D. R., Mannix, R., and Ingber, D. E., "Cellular adaptation to mechanical stress: role of integrins, Rho, cytoskeletal tension and mechanosensitive ion channels," *J Cell Sci*, vol. 119, pp. 508–518, Feb. 2006.

[214] Mazumdar, J., O'Brien, W. T., Johnson, R. S., LaManna, J. C., Chavez, J. C., Klein, P. S., and Simon, M. C., "O2 regulates stem cells through Wnt/β-catenin signalling," *Nat Cell Biol*, vol. 12, pp. 1007–1013, Oct. 2010.

[215] McBeath, R., Pirone, D. M., Nelson, C. M., Bhadriraju, K., and Chen, C. S., "Cell shape, cytoskeletal tension, and RhoA regulate stem cell lineage commitment.," *Dev Cell*, vol. 6, pp. 483–495, Apr. 2004.

[216] McNeish, J., "Embryonic stem cells in drug discovery.," *Nat Rev Drug Discov*, vol. 3, pp. 70–80, Jan. 2004.

[217] Moeller, H.-C., Mian, M. K., Shrivastava, S., Chung, B. G., and Khademhosseini, A., "A microwell array system for stem cell culture," *Biomaterials*, vol. 29, pp. 752–763, Feb. 2008.

[218] Mohamed, O. A., Clarke, H. J., and Dufort, D., "Beta-catenin signaling marks the prospective site of primitive streak formation in the mouse embryo.," *Dev Dyn*, vol. 231, pp. 416–424, Oct. 2004.

[219] Mohr, J. C., De Pablo, J. J., and Palecek, S. P., "3-D microwell culture of human embryonic stem cells," *Biomaterials*, vol. 27, pp. 6032–6042, Dec. 2006.

[220] Mohr, J. C., Zhang, J., Azarin, S. M., Soerens, A. G., De Pablo, J. J., Thomson, J. A., Lyons, G. E., Palecek, S. P., and Kamp, T. J., "The microwell control of embryoid body size in order to regulate cardiac differentiation of human embryonic stem cells.," *Biomaterials*, vol. 31, pp. 1885–1893, Mar. 2010.

[221] Moledina, F., Clarke, G., Oskooei, A., Onishi, K., Günther, A., and Zandstra, P. W., "Predictive microfluidic control of regulatory ligand trajectories in individual pluripotent cells.," *Proc Natl Acad Sci USA*, Feb. 2012.

[222] Morrison, S. J. and Spradling, A. C., "Stem cells and niches: mechanisms that promote stem cell maintenance throughout life.," *Cell*, vol. 132, pp. 598–611, Feb. 2008.

[223] Mow, V. C., Holmes, M. H., and Lai, W. M., "Fluid transport and mechanical properties of articular cartilage: a review," *J Biomech*, vol. 17, no. 5, pp. 377–394, 1984.

[224] Mummery, C., Ward, D., van den Brink, C. E., Bird, S. D., Doevendans, P. A., Opthof, T., Brutel de la Riviere, A., Tertoolen, L., van der Heyden, M., and Pera, M., "Cardiomyocyte differentiation of mouse and human embryonic stem cells," *J Anat*, vol. 200, pp. 233–242, Mar. 2002.

[225] Mummery, C., Ward-van Oostwaard, D., Doevendans, P., Spijker, R., van den Brink, S., Hassink, R., van der Heyden, M., Opthof, T., Pera, M., de la Riviere, A., Passier, R., and Tertoolen, L., "Differentiation of human embryonic stem cells to cardiomyocytes: role of coculture with visceral endoderm-like cells," *Circulation*, vol. 107, pp. 2733–2740, June 2003.

[226] Munemitsu, S., Albert, I., Souza, B., Rubinfeld, B., and Polakis, P., "Regulation of intracellular beta-catenin levels by the adenomatous polyposis coli (APC) tumor-suppressor protein.," *Proc Natl Acad Sci USA*, vol. 92, pp. 3046–3050, Mar. 1995.

[227] Murray, P. and Edgar, D., "Regulation of programmed cell death by basement membranes in embryonic development," *J Cell Biol*, vol. 150, pp. 1215–1221, Sept. 2000.

[228] Murry, C. E. and Keller, G., "Differentiation of embryonic stem cells to clinically relevant populations: lessons from embryonic development," *Cell*, vol. 132, pp. 661–680, Feb. 2008.

[229] Murry, C. E., Reinecke, H., and Pabon, L. M., "Regeneration gaps: observations on stem cells and cardiac repair," *J Am Coll Cardiol*, vol. 47, pp. 1777–1785, May 2006.

[230] Nair, R., Ngangan, A. V., Kemp, M. L., and McDevitt, T. C., "Gene expression signatures of extracellular matrix and growth factors during embryonic stem cell differentiation.," *PLoS ONE*, vol. 7, no. 10, p. e42580, 2012.

[231] Naito, A. T., Shiojima, I., Akazawa, H., Hidaka, K., Morisaki, T., Kikuchi, A., and Komuro, I., "Developmental stage-specific biphasic roles of Wnt/beta-catenin signaling in cardiomyogenesis and hematopoiesis," *Proc Natl Acad Sci USA*, vol. 103, pp. 19812–19817, Dec. 2006.

[232] Nakamura, T., Sano, M., Songyang, Z., and Schneider, M. D., "A Wnt- and beta -catenin-dependent pathway for mammalian cardiac myogenesis.," *Proc Natl Acad Sci USA*, vol. 100, pp. 5834–5839, May 2003.

[233] Nakanishi, Y., Ochiai, A., Akimoto, S., Kato, H., Watanabe, H., Tachimori, Y., Yamamoto, S., and Hirohashi, S., "Expression of E-cadherin, alpha-catenin, beta-catenin and plakoglobin in esophageal carcinomas and its prognostic significance: immunohistochemical analysis of 96 lesions.," *Oncology*, vol. 54, pp. 158–165, Feb. 1997.

[234] Nakano, T., Kodama, H., and Honjo, T., "Generation of lymphohematopoietic cells from embryonic stem cells in culture," *Science*, vol. 265, pp. 1098–1101, Aug. 1994.

[235] Nakano, T., Ando, S., Takata, N., Kawada, M., Muguruma, K., Sekiguchi, K., Saito, K., Yonemura, S., Eiraku, M., and Sasai, Y., "Self-formation of optic cups and storable stratified neural retina from human ESCs.," *Cell Stem Cell*, vol. 10, pp. 771–785, June 2012.

[236] Nakayama, T. and Inoue, N., "Neural stem sphere method: induction of neural stem cells and neurons by astrocyte-derived factors in embryonic stem cells in vitro," *Methods Mol Biol*, vol. 330, pp. 1–13, 2006.

[237] Nelson, C. M., Jean, R. P., Tan, J. L., Liu, W. F., Sniadecki, N. J., Spector, A. A., and Chen, C. S., "Emergent patterns of growth controlled by multicellular form and mechanics.," *Proc Natl Acad Sci USA*, vol. 102, pp. 11594–11599, Aug. 2005.

[238] Nelson, W. J. and Nusse, R., "Convergence of Wnt, beta-catenin, and cadherin pathways," *Science*, vol. 303, pp. 1483–1487, Mar. 2004.

[239] Netti, P. A., Berk, D. A., Swartz, M. A., Grodzinsky, A. J., and Jain, R. K., "Role of extracellular matrix assembly in interstitial transport in solid tumors," *Cancer Res*, vol. 60, pp. 2497–2503, May 2000.

[240] Ng, C. P., Helm, C.-L. E., and Swartz, M. A., "Interstitial flow differentially stimulates blood and lymphatic endothelial cell morphogenesis in vitro," *Microvasc Res*, vol. 68, pp. 258–264, Nov. 2004.

[241] Ng, C. P. and Swartz, M. A., "Fibroblast alignment under interstitial fluid flow using a novel 3-D tissue culture model," *Am J Physiol Heart Circ Physiol*, vol. 284, pp. H1771–7, May 2003.

[242] Ng, E. S., Davis, R. P., Azzola, L., Stanley, E. G., and Elefanty, A. G., "Forced aggregation of defined numbers of human embryonic stem cells into embryoid bodies fosters robust, reproducible hematopoietic differentiation," *Blood*, vol. 106, pp. 1601–1603, Sept. 2005.

[243] Niebruegge, S., Bauwens, C. L., Peerani, R., Thavandiran, N., Masse, S., Sevaptisidis, E., Nanthakumar, K., Woodhouse, K., Husain, M., Kumacheva, E., and Zandstra, P. W., "Generation of human embryonic stem cell-derived mesoderm and cardiac cells using size-specified aggregates in an oxygen-controlled bioreactor.," *Biotechnol Bioeng*, vol. 102, pp. 493–507, Feb. 2009.

[244] North, T. E., Goessling, W., Peeters, M., Li, P., Ceol, C., Lord, A. M., Weber, G. J., Harris, J., Cutting, C. C., Huang, P., Dzierzak, E., and Zon, L. I., "Hematopoietic stem cell development is dependent on blood flow," *Cell*, vol. 137, pp. 736–748, May 2009.

[245] Nostro, M. C., Cheng, X., Keller, G. M., and Gadue, P., "Wnt, activin, and BMP signaling regulate distinct stages in the developmental pathway

from embryonic stem cells to blood," *Cell Stem Cell*, vol. 2, pp. 60–71, Jan. 2008.

[246] Oberkampf, W. L. and Trucano, T. G., "Verification and validation in computational fluid dynamics," *Progress in Aerospace Sciences*, 2002.

[247] Ofek, G., Willard, V. P., Koay, E. J., Hu, J. C., Lin, P., and Athanasiou, K. A., "Mechanical characterization of differentiated human embryonic stem cells.," *J Biomech Eng*, vol. 131, p. 061011, June 2009.

[248] Orford, K., Crockett, C., Jensen, J. P., Weissman, A. M., and Byers, S. W., "Serine phosphorylation-regulated ubiquitination and degradation of beta-catenin.," *J Biol Chem*, vol. 272, pp. 24735–24738, Oct. 1997.

[249] Orsulic, S., Huber, O., Aberle, H., Arnold, S., and Kemler, R., "E-cadherin binding prevents beta-catenin nuclear localization and beta-catenin/LEF-1-mediated transactivation.," *J Cell Sci*, vol. 112 (Pt 8), pp. 1237–1245, Apr. 1999.

[250] Osterfield, M., Du, X., Schüpbach, T., Wieschaus, E., and Shvartsman, S. Y., "Three-dimensional epithelial morphogenesis in the developing Drosophila egg.," *Dev Cell*, vol. 24, pp. 400–410, Feb. 2013.

[251] Paige, S. L., Osugi, T., Afanasiev, O. K., Pabon, L., Reinecke, H., and Murry, C. E., "Endogenous Wnt/beta-catenin signaling is required for cardiac differentiation in human embryonic stem cells.," *PLoS ONE*, vol. 5, no. 6, p. e11134, 2010.

[252] Pálmer, H. G., González-Sancho, J. M., Espada, J., Berciano, M. T., Puig, I., Baulida, J., Quintanilla, M., Cano, A., de Herreros, A. G., Lafarga, M., and Muñoz, A., "Vitamin D(3) promotes the differentiation of colon carcinoma cells by the induction of E-cadherin and the inhibition of beta-catenin signaling.," *J Cell Biol*, vol. 154, pp. 369–387, July 2001.

[253] Park, J., Cho, C. H., Parashurama, N., Li, Y., Berthiaume, F., Toner, M., Tilles, A. W., and Yarmush, M. L., "Microfabrication-based modulation of embryonic stem cell differentiation.," *Lab Chip*, vol. 7, pp. 1018–1028, Aug. 2007.

[254] Park, K.-Y., Li, W. A., and Platt, M. O., "Patient specific proteolytic activity of monocyte-derived macrophages and osteoclasts predicted with temporal kinase activation states during differentiation.," *Integr Biol*, vol. 4, pp. 1459–1469, Nov. 2012.

[255] Paszek, M. J., Boettiger, D., Weaver, V. M., and Hammer, D. A., "Integrin clustering is driven by mechanical resistance from the glycocalyx and the substrate.," *PLoS Comput Biol*, vol. 5, p. e1000604, Dec. 2009.

[256] Paszek, M. J., Zahir, N., Johnson, K. R., Lakins, J. N., Rozenberg, G. I., Gefen, A., Reinhart-King, C. A., Margulies, S. S., Dembo, M., Boettiger, D., Hammer, D. A., and Weaver, V. M., "Tensional homeostasis and the malignant phenotype.," *Cancer Cell*, vol. 8, pp. 241–254, Sept. 2005.

[257] Pedersen, J. A., Boschetti, F., and Swartz, M. A., "Effects of extracellular fiber architecture on cell membrane shear stress in a 3D fibrous matrix," *J Biomech*, vol. 40, no. 7, pp. 1484–1492, 2007.

[258] Pedersen, J. A., Lichter, S., and Swartz, M. A., "Cells in 3D matrices under interstitial flow: effects of extracellular matrix alignment on cell shear stress and drag forces," *J Biomech*, vol. 43, pp. 900–905, Mar. 2010.

[259] Pedersen, J. A. and Swartz, M. A., "Mechanobiology in the third dimension.," *Ann Biomed Eng*, vol. 33, pp. 1469–1490, Nov. 2005.

[260] Pera, M. F., Andrade, J., Houssami, S., Reubinoff, B., Trounson, A., Stanley, E. G., Ward-van Oostwaard, D., and Mummery, C., "Regulation of human embryonic stem cell differentiation by BMP-2 and its antagonist noggin," *J Cell Sci*, vol. 117, pp. 1269–1280, Mar. 2004.

[261] Petkovich, M., Brand, N. J., Krust, A., and Chambon, P., "A human retinoic acid receptor which belongs to the family of nuclear receptors.," *Nature*, vol. 330, pp. 444–450, Dec. 1987.

[262] Pfaffl, M. W., "A new mathematical model for relative quantification in real-time RT-PCR.," *Nucleic Acids Res*, vol. 29, p. e45, May 2001.

[263] Philp, D., Chen, S. S., Fitzgerald, W., Orenstein, J., Margolis, L., and Kleinman, H. K., "Complex extracellular matrices promote tissue-specific stem cell differentiation.," *Stem Cells*, vol. 23, pp. 288–296, Feb. 2005.

[264] Polacheck, W. J., Charest, J. L., and Kamm, R. D., "Interstitial flow influences direction of tumor cell migration through competing mechanisms.," *Proc Natl Acad Sci USA*, vol. 108, pp. 11115–11120, July 2011.

[265] Przybyla, L. M. and Voldman, J., "Attenuation of extrinsic signaling reveals the importance of matrix remodeling on maintenance of embryonic stem cell self-renewal.," *Proc Natl Acad Sci USA*, vol. 109, pp. 835–840, Jan. 2012.

[266] Purpura, K. A., Morin, J., and Zandstra, P. W., "Analysis of the temporal and concentration-dependent effects of BMP-4, VEGF, and TPO on development of embryonic stem cell-derived mesoderm and blood progenitors in a defined, serum-free media.," *Exp Hematol*, vol. 36, pp. 1186–1198, Sept. 2008.

[267] Quinn, T. M., Grodzinsky, A. J., Buschmann, M. D., Kim, Y. J., and Hunziker, E. B., "Mechanical compression alters proteoglycan deposition and

matrix deformation around individual cells in cartilage explants," *J Cell Sci*, vol. 111 (Pt 5), pp. 573–583, Mar. 1998.

[268] Qyang, Y., Martin-Puig, S., Chiravuri, M., Chen, S., Xu, H., Bu, L., Jiang, X., Lin, L., Granger, A., Moretti, A., Caron, L., Wu, X., Clarke, J., Taketo, M. M., Laugwitz, K.-L., Moon, R. T., Gruber, P., Evans, S. M., Ding, S., and Chien, K. R., "The renewal and differentiation of Isl1+ cardiovascular progenitors are controlled by a Wnt/beta-catenin pathway," *Cell Stem Cell*, vol. 1, pp. 165–179, Aug. 2007.

[269] Radisic, M., Marsano, A., Maidhof, R., Wang, Y., and Vunjak-Novakovic, G., "Cardiac tissue engineering using perfusion bioreactor systems.," *Nat Protoc*, vol. 3, no. 4, pp. 719–738, 2008.

[270] Radisic, M., Yang, L., Boublik, J., Cohen, R. J., Langer, R., Freed, L. E., and Vunjak-Novakovic, G., "Medium perfusion enables engineering of compact and contractile cardiac tissue.," *Am J Physiol Heart Circ Physiol*, vol. 286, pp. H507–16, Feb. 2004.

[271] Rambani, K., Vukasinovic, J., Glezer, A., and Potter, S. M., "Culturing thick brain slices: an interstitial 3D microperfusion system for enhanced viability," *J Neurosci Methods*, vol. 180, pp. 243–254, June 2009.

[272] Ren, Y., Lee, M. Y., Schliffke, S., Paavola, J., Amos, P. J., Ge, X., Ye, M., Zhu, S., Senyei, G., Lum, L., Ehrlich, B. E., and Qyang, Y., "Small molecule Wnt inhibitors enhance the efficiency of BMP-4-directed cardiac differentiation of human pluripotent stem cells.," *J Mol Cell Cardiol*, vol. 51, pp. 280–287, Sept. 2011.

[273] Reubinoff, B. E., Pera, M. F., Fong, C. Y., Trounson, A., and Bongso, A., "Embryonic stem cell lines from human blastocysts: somatic differentiation in vitro.," *Nat Biotechnol*, vol. 18, pp. 399–404, Apr. 2000.

[274] Riazi, A. M., Takeuchi, J. K., Hornberger, L. K., Zaidi, S. H., Amini, F., Coles, J., Bruneau, B. G., and Van Arsdell, G. S., "NKX2-5 regulates the expression of beta-catenin and GATA4 in ventricular myocytes.," *PLoS ONE*, vol. 4, no. 5, p. e5698, 2009.

[275] Rivera-Pérez, J. A. and Magnuson, T., "Primitive streak formation in mice is preceded by localized activation of Brachyury and Wnt3," *Dev Biol*, vol. 288, pp. 363–371, Dec. 2005.

[276] Ruiz, S. A. and Chen, C. S., "Emergence of patterned stem cell differentiation within multicellular structures," *Stem Cells*, vol. 26, pp. 2921–2927, Nov. 2008.

[277] Rutkowski, J. M. and Swartz, M. A., "A driving force for change: interstitial flow as a morphoregulator," *Trends Cell Biol*, vol. 17, no. 1, pp. 44–50, 2007.

[278] Sachlos, E. and Auguste, D. T., "Embryoid body morphology influences diffusive transport of inductive biochemicals: a strategy for stem cell differentiation," *Biomaterials*, vol. 29, pp. 4471–4480, Dec. 2008.

[279] Saha, K., Keung, A. J., Irwin, E. F., Li, Y., Little, L., Schaffer, D. V., and Healy, K. E., "Substrate modulus directs neural stem cell behavior.," *Biophys J*, vol. 95, pp. 4426–4438, Nov. 2008.

[280] Sahai, E. and Marshall, C. J., "ROCK and Dia have opposing effects on adherens junctions downstream of Rho," *Nat Cell Biol*, vol. 4, pp. 408–415, June 2002.

[281] Sample, C. and Shvartsman, S. Y., "Multiscale modeling of diffusion in the early Drosophila embryo.," *Proc Natl Acad Sci USA*, vol. 107, pp. 10092–10096, June 2010.

[282] Sargent, C. Y., Berguig, G. Y., Kinney, M. A., Hiatt, L. A., Carpenedo, R. L., Berson, R. E., and McDevitt, T. C., "Hydrodynamic modulation of embryonic stem cell differentiation by rotary orbital suspension culture.," *Biotechnol Bioeng*, vol. 105, pp. 611–626, Feb. 2010.

[283] Sargent, C. Y., Berguig, G. Y., and McDevitt, T. C., "Cardiomyogenic differentiation of embryoid bodies is promoted by rotary orbital suspension culture.," *Tissue Eng Part A*, vol. 15, pp. 331–342, Feb. 2009.

[284] Sasai, Y., "Generation of dopaminergic neurons from embryonic stem cells," *J Neurol*, vol. 249 Suppl 2, pp. II41–4, Sept. 2002.

[285] Sasai, Y., "Cytosystems dynamics in self-organization of tissue architecture.," *Nature*, vol. 493, pp. 318–326, Jan. 2013.

[286] Sasai, Y., "Next-Generation Regenerative Medicine: Organogenesis from Stem Cells in 3D Culture.," *Cell Stem Cell*, vol. 12, pp. 520–530, May 2013.

[287] Sato, N., Meijer, L., Skaltsounis, L., Greengard, P., and Brivanlou, A. H., "Maintenance of pluripotency in human and mouse embryonic stem cells through activation of Wnt signaling by a pharmacological GSK-3-specific inhibitor.," *Nat Med*, vol. 10, pp. 55–63, Jan. 2004.

[288] Scadden, D. T., "The stem-cell niche as an entity of action.," *Nature*, vol. 441, pp. 1075–1079, June 2006.

[289] Schmitt, R. M., Bruyns, E., and Snodgrass, H. R., "Hematopoietic development of embryonic stem cells in vitro: cytokine and receptor gene expression.," *Genes Dev*, vol. 5, pp. 728–740, May 1991.

[290] Schmitt, T. M., de Pooter, R. F., Gronski, M. A., Cho, S. K., Ohashi, P. S., and Zúñiga-Pflücker, J. C., "Induction of T cell development and establishment of T cell competence from embryonic stem cells differentiated in vitro," *Nat Immunol*, vol. 5, pp. 410–417, Apr. 2004.

[291] Schroeder, M., Niebruegge, S., Werner, A., Willbold, E., Burg, M., Ruediger, M., Field, L. J., Lehmann, J., and Zweigerdt, R., "Differentiation and lineage selection of mouse embryonic stem cells in a stirred bench scale bioreactor with automated process control.," *Biotechnol Bioeng*, vol. 92, pp. 920–933, Dec. 2005.

[292] Schuldiner, M., Yanuka, O., Itskovitz-Eldor, J., Melton, D. A., and Benvenisty, N., "Effects of eight growth factors on the differentiation of cells derived from human embryonic stem cells.," *Proc Natl Acad Sci USA*, vol. 97, pp. 11307–11312, Oct. 2000.

[293] Schultheiss, T. M., Burch, J. B., and Lassar, A. B., "A role for bone morphogenetic proteins in the induction of cardiac myogenesis.," *Genes Dev*, vol. 11, pp. 451–462, Feb. 1997.

[294] Semino, C. E., Kamm, R. D., and Lauffenburger, D. A., "Autocrine EGF receptor activation mediates endothelial cell migration and vascular morphogenesis induced by VEGF under interstitial flow," *Exp Cell Res*, vol. 312, pp. 289–298, Feb. 2006.

[295] Sen, A., Kallos, M. S., and Behie, L. A., "Effects of hydrodynamics on cultures of mammalian neural stem cell aggregates in suspension bioreactors," *Ind Eng Chem Res*, vol. 40, no. 23, pp. 5350–5357, 2001.

[296] Serganova, I., Doubrovin, M., Vider, J., Ponomarev, V., Soghomonyan, S., Beresten, T., Ageyeva, L., Serganov, A., Cai, S., Balatoni, J., Blasberg, R., and Gelovani, J., "Molecular imaging of temporal dynamics and spatial heterogeneity of hypoxia-inducible factor-1 signal transduction activity in tumors in living mice.," *Cancer Res*, vol. 64, pp. 6101–6108, Sept. 2004.

[297] Serup, P., Gustavsen, C., Klein, T., Potter, L. A., Lin, R., Mullapudi, N., Wandzioch, E., Hines, A., Davis, A., Bruun, C., Engberg, N., Petersen, D. R., Peterslund, J. M. L., Macdonald, R. J., Grapin-Botton, A., Magnuson, M. A., and Zaret, K. S., "Partial promoter substitutions generating transcriptional sentinels of diverse signaling pathways in embryonic stem cells and mice.," *Dis Model Mech*, vol. 5, pp. 956–966, Nov. 2012.

[298] Shafa, M., Krawetz, R., Zhang, Y., Rattner, J. B., Godollei, A., Duff, H. J., and Rancourt, D. E., "Impact of stirred suspension bioreactor culture on the differentiation of murine embryonic stem cells into cardiomyocytes.," *BMC Cell Biol*, vol. 12, p. 53, 2011.

[299] Shi, Y., Hou, L., Tang, F., Jiang, W., Wang, P., Ding, M., and Deng, H., "Inducing embryonic stem cells to differentiate into pancreatic beta cells by a novel three-step approach with activin A and all-trans retinoic acid," *Stem Cells*, vol. 23, pp. 656–662, May 2005.

[300] Shin, J.-W., Buxboim, A., Spinler, K. R., Swift, J., Christian, D. A., Hunter, C. A., Léon, C., Gachet, C., Dingal, P. C. D. P., Ivanovska, I. L., Rehfeldt, F., Chasis, J. A., and Discher, D. E., "Contractile forces sustain and polarize hematopoiesis from stem and progenitor cells.," *Cell Stem Cell*, vol. 14, pp. 81–93, Jan. 2014.

[301] Shraiman, B. I., "Mechanical feedback as a possible regulator of tissue growth.," *Proc Natl Acad Sci USA*, vol. 102, pp. 3318–3323, Mar. 2005.

[302] Shukla, S., Nair, R., Rolle, M. W., Braun, K. R., Chan, C. K., Johnson, P. Y., Wight, T. N., and McDevitt, T. C., "Synthesis and organization of hyaluronan and versican by embryonic stem cells undergoing embryoid body differentiation.," *J Histochem Cytochem*, vol. 58, pp. 345–358, Apr. 2010.

[303] Simon, M. C. and Keith, B., "The role of oxygen availability in embryonic development and stem cell function," *Nat Rev Mol Cell Biol*, vol. 9, pp. 285–296, Apr. 2008.

[304] Sims, J. R., Karp, S., and Ingber, D. E., "Altering the cellular mechanical force balance results in integrated changes in cell, cytoskeletal and nuclear shape.," *J Cell Sci*, vol. 103 (Pt 4), pp. 1215–1222, Dec. 1992.

[305] Smyth, N., Vatansever, H. S., Murray, P., Meyer, M., Frie, C., Paulsson, M., and Edgar, D., "Absence of basement membranes after targeting the LAMC1 gene results in embryonic lethality due to failure of endoderm differentiation," *J Cell Biol*, vol. 144, pp. 151–160, Jan. 1999.

[306] Solorio, L. D., Fu, A. S., Hernández-Irizarry, R., and Alsberg, E., "Chondrogenic differentiation of human mesenchymal stem cell aggregates via controlled release of TGF-beta1 from incorporated polymer microspheres," *J Biomed Mater Res A*, vol. 92, pp. 1139–1144, Mar. 2010.

[307] Spence, J. R., Mayhew, C. N., Rankin, S. A., Kuhar, M. F., Vallance, J. E., Tolle, K., Hoskins, E. E., Kalinichenko, V. V., Wells, S. I., Zorn, A. M., Shroyer, N. F., and Wells, J. M., "Directed differentiation of human pluripotent stem cells into intestinal tissue in vitro.," *Nature*, vol. 470, pp. 105–109, Feb. 2011.

[308] Stainier, D. Y., Fouquet, B., Chen, J. N., Warren, K. S., Weinstein, B. M., Meiler, S. E., Mohideen, M. A., Neuhauss, S. C., Solnica-Krezel, L., Schier, A. F., Zwartkruis, F., Stemple, D. L., Malicki, J., Driever, W., and Fishman, M. C., "Mutations affecting the formation and function of the cardiovascular system in the zebrafish embryo," *Development*, vol. 123, pp. 285–292, Dec. 1996.

[309] Strauer, B. E., Brehm, M., Zeus, T., Köstering, M., Hernandez, A., Sorg, R. V., Kögler, G., and Wernet, P., "Repair of infarcted myocardium by autologous intracoronary mononuclear bone marrow cell transplantation in humans," *Circulation*, vol. 106, pp. 1913–1918, Oct. 2002.

[310] Strübing, C., Ahnert-Hilger, G., Shan, J., Wiedenmann, B., Hescheler, J., and Wobus, A. M., "Differentiation of pluripotent embryonic stem cells into the neuronal lineage in vitro gives rise to mature inhibitory and excitatory neurons," *Mech Dev*, vol. 53, pp. 275–287, Oct. 1995.

[311] Suga, H., Kadoshima, T., Minaguchi, M., Ohgushi, M., Soen, M., Nakano, T., Takata, N., Wataya, T., Muguruma, K., Miyoshi, H., Yonemura, S., Oiso, Y., and Sasai, Y., "Self-formation of functional adenohypophysis in three-dimensional culture.," *Nature*, vol. 480, pp. 57–62, Dec. 2011.

[312] Suri, S., Singh, A., Nguyen, A. H., Bratt-Leal, A. M., McDevitt, T. C., and Lu, H., "Microfluidic-based patterning of embryonic stem cells for in vitro development studies.," *Lab Chip*, vol. 13, pp. 4617–4624, Dec. 2013.

[313] Sutherland, R. M., "Cell and environment interactions in tumor microregions: the multicell spheroid model.," *Science*, vol. 240, pp. 177–184, Apr. 1988.

[314] Svitkina, T. M. and Borisy, G. G., "Arp2/3 complex and actin depolymerizing factor/cofilin in dendritic organization and treadmilling of actin filament array in lamellipodia.," *J Cell Biol*, vol. 145, pp. 1009–1026, May 1999.

[315] Swartz, M. A., Kaipainen, A., Netti, P. A., Brekken, C., Boucher, Y., Grodzinsky, A. J., and Jain, R. K., "Mechanics of interstitial-lymphatic fluid transport: theoretical foundation and experimental validation," *J Biomech*, vol. 32, pp. 1297–1307, Dec. 1999.

[316] Swartz, M. A. and Fleury, M. E., "Interstitial flow and its effects in soft tissues," *Annu Rev Biomed Eng*, vol. 9, pp. 229–256, 2007.

[317] Swift, J., Ivanovska, I. L., Buxboim, A., Harada, T., Dingal, P. C. D. P., Pinter, J., Pajerowski, J. D., Spinler, K. R., Shin, J.-W., Tewari, M., Rehfeldt, F., Speicher, D. W., and Discher, D. E., "Nuclear lamin-A scales with tissue stiffness and enhances matrix-directed differentiation.," *Science*, vol. 341, p. 1240104, Aug. 2013.

[318] Takebe, T., Sekine, K., Enomura, M., Koike, H., Kimura, M., Ogaeri, T., Zhang, R.-R., Ueno, Y., Zheng, Y.-W., Koike, N., Aoyama, S., Adachi, Y., and Taniguchi, H., "Vascularized and functional human liver from an iPSC-derived organ bud transplant.," *Nature*, vol. 499, pp. 481–484, July 2013.

[319] Tam, P. P. L. and Loebel, D. A. F., "Gene function in mouse embryogenesis: get set for gastrulation," *Nat Rev Genet*, vol. 8, pp. 368–381, May 2007.

[320] Taylor, D. A., Atkins, B. Z., Hungspreugs, P., Jones, T. R., Reedy, M. C., Hutcheson, K. A., Glower, D. D., and Kraus, W. E., "Regenerating functional myocardium: improved performance after skeletal myoblast transplantation," *Nat Med*, vol. 4, pp. 929–933, Aug. 1998.

[321] ten Berge, D., Koole, W., Fuerer, C., Fish, M., Eroglu, E., and Nusse, R., "Wnt signaling mediates self-organization and axis formation in embryoid bodies," *Cell Stem Cell*, vol. 3, pp. 508–518, Nov. 2008.

[322] Thiery, J. P., Acloque, H., Huang, R. Y. J., and Nieto, M. A., "Epithelial-mesenchymal transitions in development and disease.," *Cell*, vol. 139, pp. 871–890, Nov. 2009.

[323] Thomson, J. A., Itskovitz-Eldor, J., Shapiro, S. S., Waknitz, M. A., Swiergiel, J. J., Marshall, V. S., and Jones, J. M., "Embryonic stem cell lines derived from human blastocysts.," *Science*, vol. 282, pp. 1145–1147, Nov. 1998.

[324] Thomson, J. A., Kalishman, J., Golos, T. G., Durning, M., Harris, C. P., Becker, R. A., and Hearn, J. P., "Isolation of a primate embryonic stem cell line.," *Proc Natl Acad Sci USA*, vol. 92, pp. 7844–7848, Aug. 1995.

[325] Thomson, J. A., Kalishman, J., Golos, T. G., Durning, M., Harris, C. P., and Hearn, J. P., "Pluripotent cell lines derived from common marmoset (Callithrix jacchus) blastocysts.," *Biol Reprod*, vol. 55, pp. 254–259, Aug. 1996.

[326] Toma, C., Pittenger, M. F., Cahill, K. S., Byrne, B. J., and Kessler, P. D., "Human mesenchymal stem cells differentiate to a cardiomyocyte phenotype in the adult murine heart," *Circulation*, vol. 105, no. 1, pp. 93–98, 2002.

[327] Torisawa, Y.-s., Chueh, B.-h., Huh, D., Ramamurthy, P., Roth, T. M., Barald, K. F., and Takayama, S., "Efficient formation of uniform-sized embryoid bodies using a compartmentalized microchannel device.," *Lab Chip*, vol. 7, pp. 770–776, June 2007.

[328] Toyooka, Y., Tsunekawa, N., Akasu, R., and Noce, T., "Embryonic stem cells can form germ cells in vitro," *Proc Natl Acad Sci USA*, vol. 100, pp. 11457–11462, Sept. 2003.

[329] Trappmann, B., Gautrot, J. E., Connelly, J. T., Strange, D. G. T., Li, Y., Oyen, M. L., Cohen Stuart, M. A., Boehm, H., Li, B., Vogel, V., Spatz, J. P., Watt, F. M., and Huck, W. T. S., "Extracellular-matrix tethering regulates stem-cell fate.," *Nat Mater*, vol. 11, pp. 642–649, July 2012.

[330] Trédan, O., Galmarini, C. M., Patel, K., and Tannock, I. F., "Drug resistance and the solid tumor microenvironment.," *J Natl Cancer Inst*, vol. 99, pp. 1441–1454, Oct. 2007.

[331] Treiser, M. D., Yang, E. H., Gordonov, S., Cohen, D. M., Androulakis, I. P., Kohn, J., Chen, C. S., and Moghe, P. V., "Cytoskeleton-based forecasting of stem cell lineage fates.," *Proc Natl Acad Sci USA*, vol. 107, pp. 610–615, Jan. 2010.

[332] Tung, Y.-C., Hsiao, A. Y., Allen, S. G., Torisawa, Y.-s., Ho, M., and Takayama, S., "High-throughput 3D spheroid culture and drug testing using a 384 hanging drop array.," *Analyst*, vol. 136, pp. 473–478, Feb. 2011.

[333] Tzanakakis, E. S., Hess, D. J., Sielaff, T. D., and Hu, W. S., "Extracorporeal tissue engineered liver-assist devices," *Annu Rev Biomed Eng*, vol. 2, pp. 607–632, 2000.

[334] Ueno, S., Weidinger, G., Osugi, T., Kohn, A. D., Golob, J. L., Pabon, L., Reinecke, H., Moon, R. T., and Murry, C. E., "Biphasic role for Wnt/beta-catenin signaling in cardiac specification in zebrafish and embryonic stem cells," *Proc Natl Acad Sci USA*, vol. 104, pp. 9685–9690, June 2007.

[335] Ungrin, M. D., Joshi, C., Nica, A., Bauwens, C., and Zandstra, P. W., "Reproducible, ultra high-throughput formation of multicellular organization from single cell suspension-derived human embryonic stem cell aggregates.," *PLoS ONE*, vol. 3, no. 2, p. e1565, 2008.

[336] van Noort, M., Meeldijk, J., van der Zee, R., Destree, O., and Clevers, H., "Wnt signaling controls the phosphorylation status of beta-catenin," *J Biol Chem*, vol. 277, pp. 17901–17905, May 2002.

[337] Van Winkle, A. P., Gates, I. D., and Kallos, M. S., "Mass transfer limitations in embryoid bodies during human embryonic stem cell differentiation.," *Cells Tissues Organs*, vol. 196, no. 1, pp. 34–47, 2012.

[338] Vandesompele, J., De Preter, K., Pattyn, F., Poppe, B., Van Roy, N., De Paepe, A., and Speleman, F., "Accurate normalization of real-time quantitative RT-PCR data by geometric averaging of multiple internal control genes.," *Genome Biol*, vol. 3, p. RESEARCH0034, June 2002.

[339] von Dassow, M., Strother, J. A., and Davidson, L. A., "Surprisingly simple mechanical behavior of a complex embryonic tissue.," *PLoS ONE*, vol. 5, no. 12, p. e15359, 2010.

[340] Wakatsuki, T., Schwab, B., Thompson, N. C., and Elson, E. L., "Effects of cytochalasin D and latrunculin B on mechanical properties of cells.," *J Cell Sci*, vol. 114, pp. 1025–1036, Mar. 2001.

[341] Wallingford, J. B., Fraser, S. E., and Harland, R. M., "Convergent extension: the molecular control of polarized cell movement during embryonic development.," *Dev Cell*, vol. 2, pp. 695–706, June 2002.

[342] Wan, Y. J., Wu, T. C., Chung, A. E., and Damjanov, I., "Monoclonal antibodies to laminin reveal the heterogeneity of basement membranes in the developing and adult mouse tissues," *J Cell Biol*, vol. 98, pp. 971–979, Mar. 1984.

[343] Wang, F., Wang, H., Wang, J., Wang, H.-Y., Rummel, P. L., Garimella, S. V., and Lu, C., "Microfluidic delivery of small molecules into mammalian cells based on hydrodynamic focusing.," *Biotechnol Bioeng*, vol. 100, pp. 150–158, May 2008.

[344] Wang, H., Hao, J., and Hong, C. C., "Cardiac induction of embryonic stem cells by a small molecule inhibitor of Wnt/β-catenin signaling.," *ACS Chem. Biol.*, vol. 6, pp. 192–197, Feb. 2011.

[345] Wang, H., Riha, G. M., Yan, S., Li, M., Chai, H., Yang, H., Yao, Q., and Chen, C., "Shear stress induces endothelial differentiation from a murine embryonic mesenchymal progenitor cell line.," *Arterioscler Thromb Vasc Biol*, vol. 25, pp. 1817–1823, Sept. 2005.

[346] Wartenberg, M., Dönmez, F., Ling, F. C., Acker, H., Hescheler, J., and Sauer, H., "Tumor-induced angiogenesis studied in confrontation cultures of multicellular tumor spheroids and embryoid bodies grown from pluripotent embryonic stem cells.," *FASEB J*, vol. 15, pp. 995–1005, Apr. 2001.

[347] Wartenberg, M., Günther, J., Hescheler, J., and Sauer, H., "The embryoid body as a novel in vitro assay system for antiangiogenic agents.," *Lab Invest*, vol. 78, pp. 1301–1314, Oct. 1998.

[348] West, G. W., Weichselbaum, R., and Little, J. B., "Limited penetration of methotrexate into human osteosarcoma spheroids as a proposed model for solid tumor resistance to adjuvant chemotherapy.," *Cancer Res*, vol. 40, pp. 3665–3668, Oct. 1980.

[349] White, D. E., Kinney, M. A., McDevitt, T. C., and Kemp, M. L., "Spatial Pattern Dynamics of 3D Stem Cell Loss of Pluripotency via Rules-Based Computational Modeling," *PLoS Comput Biol*, vol. 9, p. e1002952, Mar. 2013.

[350] Wiese, C., Kania, G., Rolletschek, A., Blyszczuk, P., and Wobus, A. M., "Pluripotency: capacity for in vitro differentiation of undifferentiated embryonic stem cells," *Methods Mol Biol*, vol. 325, pp. 181–205, 2006.

[351] Wiles, M. V. and Keller, G., "Multiple hematopoietic lineages develop from embryonic stem (ES) cells in culture," *Development*, vol. 111, pp. 259–267, Feb. 1991.

[352] Willems, E., Spiering, S., Davidovics, H., Lanier, M., Xia, Z., Dawson, M., Cashman, J., and Mercola, M., "Small-molecule inhibitors of the Wnt pathway potently promote cardiomyocytes from human embryonic stem cell-derived mesoderm.," *Circ Res*, vol. 109, pp. 360–364, Aug. 2011.

[353] Wilson, J. L. and McDevitt, T. C., "Stem cell microencapsulation for phenotypic control, bioprocessing, and transplantation.," *Biotechnol Bioeng*, vol. 110, pp. 667–682, Mar. 2013.

[354] Wilson, J. L., Najia, M. A., Saeed, R., and McDevitt, T. C., "Alginate encapsulation parameters influence the differentiation of microencapsulated embryonic stem cell aggregates.," *Biotechnol Bioeng*, vol. 111, pp. 618–631, Mar. 2014.

[355] Wobus, A. M., Kaomei, G., Shan, J., Wellner, M. C., Rohwedel, J., Guanju, J., Fleischmann, B., Katus, H. A., Hescheler, J., and Franz, W. M., "Retinoic acid accelerates embryonic stem cell-derived cardiac differentiation and enhances development of ventricular cardiomyocytes," *J Mol Cell Cardiol*, vol. 29, pp. 1525–1539, June 1997.

[356] Wobus, A. M., Wallukat, G., and Hescheler, J., "Pluripotent mouse embryonic stem cells are able to differentiate into cardiomyocytes expressing chronotropic responses to adrenergic and cholinergic agents and Ca2+ channel blockers," *Differentiation*, vol. 48, pp. 173–182, Dec. 1991.

[357] Wolpert, L., "Positional information and the spatial pattern of cellular differentiation.," *J Theor Biol*, vol. 25, pp. 1–47, Oct. 1969.

[358] Woods, A. and Beier, F., "RhoA/ROCK signaling regulates chondrogenesis in a context-dependent manner.," *J Biol Chem*, vol. 281, pp. 13134–13140, May 2006.

[359] Wozniak, M. A. and Chen, C. S., "Mechanotransduction in development: a growing role for contractility.," *Nat Rev Mol Cell Biol*, vol. 10, pp. 34–43, Jan. 2009.

[360] Yamada, S., Pokutta, S., Drees, F., Weis, W. I., and Nelson, W. J., "Deconstructing the cadherin-catenin-actin complex.," *Cell*, vol. 123, pp. 889–901, Dec. 2005.

[361] Yamamoto, K., Sokabe, T., Watabe, T., Miyazono, K., Yamashita, J. K., Obi, S., Ohura, N., Matsushita, A., Kamiya, A., and Ando, J., "Fluid shear stress induces differentiation of Flk-1-positive embryonic stem cells into vascular endothelial cells in vitro.," *Am J Physiol Heart Circ Physiol*, vol. 288, pp. H1915–24, Apr. 2005.

[362] Yang, L., Soonpaa, M. H., Adler, E. D., Roepke, T. K., Kattman, S. J., Kennedy, M., Henckaerts, E., Bonham, K., Abbott, G. W.,

Linden, R. M., Field, L. J., and Keller, G. M., "Human cardiovascular progenitor cells develop from a KDR+ embryonic-stem-cell-derived population," *Nature*, vol. 453, pp. 524–528, May 2008.

[363] Yeung, T., Georges, P. C., Flanagan, L. A., Marg, B., Ortiz, M., Funaki, M., Zahir, N., Ming, W., Weaver, V., and Janmey, P. A., "Effects of substrate stiffness on cell morphology, cytoskeletal structure, and adhesion.," *Cell Motil Cytoskeleton*, vol. 60, pp. 24–34, Jan. 2005.

[364] Ying, Q.-L. and Smith, A. G., "Defined conditions for neural commitment and differentiation.," *Meth Enzymol*, vol. 365, pp. 327–341, 2003.

[365] Yirme, G., Amit, M., Laevsky, I., Osenberg, S., and Itskovitz-Eldor, J., "Establishing a dynamic process for the formation, propagation, and differentiation of human embryoid bodies.," *Stem Cells Dev*, vol. 17, pp. 1227–1241, Dec. 2008.

[366] Yoon, B. S., Yoo, S. J., Lee, J. E., You, S., Lee, H. T., and Yoon, H. S., "Enhanced differentiation of human embryonic stem cells into cardiomyocytes by combining hanging drop culture and 5-azacytidine treatment," *Differentiation*, vol. 74, pp. 149–159, Apr. 2006.

[367] Yost, C., Torres, M., Miller, J. R., Huang, E., Kimelman, D., and Moon, R. T., "The axis-inducing activity, stability, and subcellular distribution of beta-catenin is regulated in Xenopus embryos by glycogen synthase kinase 3.," *Genes Dev*, vol. 10, pp. 1443–1454, June 1996.

[368] Young, E. W. K. and Beebe, D. J., "Fundamentals of microfluidic cell culture in controlled microenvironments.," *Chem Soc Rev*, vol. 39, pp. 1036–1048, Mar. 2010.

[369] Yu, P., Mustata, M., Peng, L., Turek, J. J., Melloch, M. R., French, P. M. W., and Nolte, D. D., "Holographic optical coherence imaging of rat osteogenic sarcoma tumor spheroids.," *Appl Opt*, vol. 43, pp. 4862–4873, Sept. 2004.

[370] Zeng, L., Fagotto, F., Zhang, T., Hsu, W., Vasicek, T. J., Perry, W. L., Lee, J. J., Tilghman, S. M., Gumbiner, B. M., and Costantini, F., "The mouse Fused locus encodes Axin, an inhibitor of the Wnt signaling pathway that regulates embryonic axis formation.," *Cell*, vol. 90, pp. 181–192, July 1997.

[371] Zeng, L., Xiao, Q., Margariti, A., Zhang, Z., Zampetaki, A., Patel, S., Capogrossi, M. C., Hu, Y., and Xu, Q., "HDAC3 is crucial in shear- and VEGF-induced stem cell differentiation toward endothelial cells.," *J Cell Biol*, vol. 174, pp. 1059–1069, Sept. 2006.

[372] Zhang, P., Li, J., Tan, Z., Wang, C., Liu, T., Chen, L., Yong, J., Jiang, W., Sun, X., Du, L., Ding, M., and Deng, H., "Short-term BMP-4 treatment initiates mesoderm induction in human embryonic stem cells," *Blood*, vol. 111, pp. 1933–1941, Feb. 2008.

[373] Zhou, J., Kim, H. Y., and Davidson, L. A., "Actomyosin stiffens the vertebrate embryo during crucial stages of elongation and neural tube closure.," *Development*, vol. 136, pp. 677–688, Feb. 2009.

[374] Zhou, J., Kim, H. Y., Wang, J. H.-C., and Davidson, L. A., "Macroscopic stiffening of embryonic tissues via microtubules, RhoGEF and the assembly of contractile bundles of actomyosin.," *Development*, vol. 137, pp. 2785–2794, Aug. 2010.

[375] Zimmerman, L. B., De Jesús-Escobar, J. M., and Harland, R. M., "The Spemann organizer signal noggin binds and inactivates bone morphogenetic protein 4.," *Cell*, vol. 86, pp. 599–606, Aug. 1996.

[376] Zweigerdt, R., Burg, M., Willbold, E., Abts, H., and Ruediger, M., "Generation of confluent cardiomyocyte monolayers derived from embryonic stem cells in suspension: a cell source for new therapies and screening strategies.," *Cytotherapy*, vol. 5, no. 5, pp. 399–413, 2003.

[377] Zweigerdt, R., Olmer, R., Singh, H., Haverich, A., and Martin, U., "Scalable expansion of human pluripotent stem cells in suspension culture," *Nat Protoc*, vol. 6, pp. 689–700, May 2011.